Performance and Behavior of Base-Isolated Building Frames Subjected to Near and Far Field Earthquakes

Ph.D. Thesis

Mohit Bhandari

2015RNC9044

NATIONAL CENTER OF DISASTER MITIGATION AND MANAGEMENT

MALAVIYA NATIONAL INSTITUTE OF TECHNOLOGY JAIPUR

December, 2018

Performance and Behavior of Base-Isolated Building Frames Subjected to Near and Far Field Earthquakes

Submitted in

fulfillment of the requirements for the degree

of

DOCTOR OF PHILOSOPHY

By

MOHIT BHANDARI
ID: 2015RNC9044

Under the Supervision of

Prof. S. D. Bharti
(Supervisor)

Prof. M. K. Shrimali
(Supervisor)

NATIONAL CENTER FOR DISASTER MITIGATION AND MANAGEMENT
MALAVIYA NATIONAL INSTITUTE OF TECHNOLOGY JAIPUR
December, 2018

To My Supportive Father,

My Symbol of Strength

Who offered Me Full support in Life

And

My Affectionate Mother,

My Symbol of Patience

Who Taught Me the Life Alphabets…….

DECLARATION

I, **MOHIT BHANDARI**, declare that this thesis titled," **PERFORMANCE AND BEHAVIOR OF BASE-ISOLATED BUILDING FRAMES SUBJECTED TO NEAR AND FAR FIELD EARTHQUAKES**" and the work presented in it, are my own. I confirm that:

- This work was done wholly or mainly while in candidature for a research degree at this university.
- Where any part of this thesis has previously been submitted for a degree or any other qualification at this university or any other institution, this has been clearly stated.
- Where I have consulted the published work of others, this is always clearly attributed.
- Where I have quoted from the work of others, the source is always given. With the exception of such quotations, this thesis is entirely my own work.
- I have acknowledged all main sources of help.
- Where the thesis is based on work done by myself, jointly with others, I have made clear exactly what was done by others and what I have con-tributed myself.

Date:

Mohit Bhandari
(2015RNC9044)

CERTIFICATE

This is to certify that the thesis entitled, **"Performance and Behavior of Base-Isolated Building Frames Subjected to Near and Far Field Earthquakes",** being submitted by **Mr. Mohit Bhandari (2015RNC9044)** is a bonafide research work carried out under my supervision and guidance in fulfillment of the requirement for the award of the degree of **Doctor of Philosophy** in the National Centre for Disaster Mitigation and Management, Malaviya National Institute of Technology, Jaipur, India. The matter embodied in this thesis is original and has not been submitted to any other University or Institute for the award of any other degree.

Place: Jaipur	(S. D. Bharti)	(M. K. Shrimali)
Date:	Professor (Structural Engg.)	Professor (Structural Engg.)
	MNIT Jaipur	MNIT Jaipur

ACKNOWLEDGEMENT

I express my deep sense of gratitude to Professors Dr. S. D. Bharti, Dr. M. K. Shrimali and Dr. T K Datta at MNIT Jaipur, for their invaluable guidance and continuous support throughout the course of my Doctoral Programme. They have been an infinite source of encouragement for me, and their technical prowess nourished this thesis. I express my sincere gratitude towards my friends, Mr. Navdeep Singh, Mr. Karn Verma, Mr. Jitender Singh, Ms. Poonam Shekhawat who always remains available for technical discussions and guidance. They have always been, and will be, a source of inspiration for me, both on technical and personal fronts.

I would also like to express my sincere gratitude towards my teachers, friends, faculty members, and staff members at MNIT Jaipur. Their unending encouragement has been a source of positive energy, which helped me to have a better outlook, not only in terms of technical matters, but also in interpersonal learning and growth. The peer group at MNIT Jaipur, especially, Mr. Vishisht Bhaiya, Mr. Vijay Sharma, Mr. Shashi Narayan, Mr. Sourab, Mrs. Sunita Tolani, Mrs. Pooja Jain, Mr. Kunal Bhisht and Mr. Mahdi Abdeddaim are acknowledged.

I am grateful to my parents and brother for all their love and support. Their trust in me has been the primary driving force and support for this work. No words can describe my gratitude towards my family and friends, who have always been there for me. Their unstinted and constant support has made this cruise enjoyable. At last, I would like to express gratitude towards almighty God, for showering grace on me, by giving an opportunity to pursue this enriching journey.

ABSTRACT

Base isolation is one of the most successful passive control strategies to protect the buildings from the devastating effects of earthquakes. Base isolation proves to be highly effective to cope up with the seismic demands imposed by the far-field earthquakes. However, the effectiveness of base isolation under the effect of near-field earthquakes is still a topic of concern for the entire earthquake engineering community. The presence of high-velocity pulses in the near-field earthquakes are capable of dragging the base-isolated buildings to get into large inelastic excursions. They can impose high displacement demands at the isolation level, which can lead to the complete failure of the isolation system.

The possibility of a large inelastic excursion of both base-isolated building and base isolators is also quite likely at high PGA levels under the far-field earthquakes. This leaves scopes for the investigation of seismic vulnerability of base-isolated buildings under both near-field and far-field earthquakes. Typically, a near-field earthquake is identified with a large amplitude, low frequency, and short duration pulse type ground motion known for its high damage potential and ductility demand due to its whiplash effect. The present study aims at the performance evaluation of base-isolated building frame both under near and far-field earthquakes.

Four different types of studies are conducted, which are separately presented in four different chapters. The inelastic behavior of the base-isolated building frame under both far-field and near-field earthquakes is extensively investigated in the first study. For the study, a high rise (10-storey) building frame is considered. The behavior of the isolated frame is examined with respect to those of the corresponding fixed base building frame. Two levels of earthquakes are assumed for the study, i.e., design level (scaled to have PGA = 0.2g) and extreme level (scaled to have PGA = 0.4g). The nonlinear time history analysis (NTHA) is performed to obtain the structural responses of interest which include maximum storey drift, maximum floor displacement, maximum top floor acceleration, isolator displacement and base shear.

In the second study, the performance of two base-isolated building frames is evaluated using the capacity spectrum method (CSM) and the nonlinear time history analysis (NTHA). Response quantities of interest at different performance points ranging from elastic to plastic state of the structure obtained by the two analyses are compared. In order to make the study comprehensive one, the comparison is made for a large number of response quantities. Five-storey and ten-storey base-isolated building frames with stiff, medium, and flexible lead rubber

bearing (LRB) isolators, which are defined by their effective stiffnesses, are considered for the analysis. Corresponding fixed base frames are also analyzed as references for the comparison purposes. The performance points are obtained by CSM as per ATC-40, which are consistent with peak ground acceleration (PGA) levels ranging from a relatively small to a large value, i.e., from 0.1g to 0.5g at an increment of 0.05g and also, at the collapse point. The ATC-40 response spectrum compatible time histories, which are artificially generated and scaled to aforementioned PGA levels, are used for performing NTHA.

One of the important aspects in performing the pushover analysis is the consideration of the lateral load pattern, which can approximately describe the lateral forces that are going to act on the building during the event of an earthquake. In the third study, the effectiveness of two proposed lateral load patterns (LLPs) to estimate the seismic demands of base-isolated building frames by the pushover analysis (POA) is assessed by comparing their estimates with the benchmark responses obtained by the nonlinear time history analysis (NTHA). An ensemble of five ground motion time-histories, each of far-field and near-field with forward directivity and fling-step effects were employed for NTHA. The consideration of different types of earthquakes makes the comparison more meaningful by bringing in the effect of the type of earthquake on the assessment criterion. Target displacement-based comparison is performed by considering three target displacements, which cater to elastic, elastic to plastic and plastic states on the capacity curve of the building frames. The same two building frames, i.e., a 5-storey and a 10-storey, considered in the second study with the medium type of isolator are considered for the analysis. Two new LLPs are proposed for carrying out POA, including (i) pattern derived from the square root of the sum of squares (SRSS) of first three mode shapes of the base-isolated frame; and (ii) two variants derived from the modification of the uniform force distribution. Apart from them, the conventional LLP, i.e., proportional to the first mode shape is also used in the POA. The response parameters, namely, peak storey displacement, maximum inter-storey drift, the number of plastic hinges, SRSS of plastic hinge rotations, maximum base shear and maximum isolator displacement, are considered for comparison.

With the uncertainty of the seismic demands imposed by the earthquakes on the buildings, it is essential to evaluate the performance of the buildings in the probabilistic terms to get an idea about the vulnerability of the buildings for different types of earthquakes. In the fourth study, the probabilistic seismic risk assessment of a base-isolated building frame under near and far field earthquakes is evaluated by conducting a fragility analysis. For this purpose, a ten-storey base-isolated reinforced concrete frame is considered with lead rubber bearing as the base isolation system. Fragility curves are developed for a suite of far-field and near-field

earthquakes with directivity and fling-step effects for a number of damage measures namely, maximum inter-storey drift ratio (MIDR), maximum roof drift ratio (MRDR), maximum base shear (MBS), maximum absolute top floor acceleration (MTFA), and maximum isolator displacement (MID). Moreover, to study the effect of frequency contents of near-field earthquakes the peak ground velocity (PGV)/peak ground acceleration (PGA) ratio is varied in the near-field earthquakes with directivity effect. The incremental dynamic analysis is performed to construct the fragility curves.

TABLE OF CONTENTS

LIST OF FIGURES

LIST OF TABLES

NOMENCLATURE

Notations	Description
Z	Seismic zone factor (IS-1893:2016)
I	Importance factor of building (IS-1893:2016)
E_c	Modulus of elasticity of concrete
ν_c	Poisson's ratio of concrete
f_b	Bearing force
c_b	Damping of bearing
u_b	Bearing displacement
α_b , γ	Ratio of post to the pre-yielding stiffness of the bearing
k_b, k_1	initial stiffness of the bearing
k_{eff}	Effective or Equivalent stiffness of bearing
k_2	Post-yield stiffness of bearing
F_y	Yield force of bearing
Q	Characteristic strength of bearing
q, D_y	Yield displacement of bearing
D_{max}	Maximum design displacement of bearing
f_z	Restoring force due to lead core
F_y	Yield strength of the bearing
Z	Non-dimensional hysteretic displacement component
T_b	Isolation time period
ξ_b	Damping ratio of bearing
ω_b	Natural frequency of bearing
M_t	Total mass of building
W_t	Total weight of building
q	Yield displacement of bearing
B, τ	Integer constants for shape and size hysteretic loop
A, n	Strengthening coefficients for smoothness of hysteretic loop
G	Shear modulus of rubber
H	Total thickness of rubber layers in bearing
A_r	Area of cross-section of rubber layer

f_{py}	Yield strength of lead core
β_{eff}	Effective damping ratio of bearing
PF_1	Modal participation factor for 1st mode
N	Total number of floors of building
α_1	Modal mass co-efficient for the 1st mode
w_i	Wight of ith level of building
h_i	Height of ith storey
m_i	Mass of ith floor
k_i	Stiffness of ith floor
ϕ_{i1}	Amplitude of 1st mode at level i
V	Base shear of building
V_b	Base shear at isolation level
W	Total dead load plus appropriate percentage of live load
Δ_{roof}	Roof displacement
S_a	Spectral acceleration
S_d	Spectral displacement
T	Natural period of building
P	Trial performance point
a*	Spectral acceleration corresponding to trail performance point
d*	Spectral displacement corresponding to trail performance point
F_i	Lateral force at ith level of building
F_b	Concentrated force at base level of building
D_b	Base displacement
W_b	Base mass of isolated building
P_f	Probability of exceeding a particular damage state
Φ	Standard cumulative probability function
β_{total}	Total uncertainty in estimating the fragility
β_C	Uncertainty in structural capacity
β_D	Uncertainty in seismic demand
a, b	Coefficients of regression analysis

Chapter 1
Introduction

1.1 Introductory Remarks

Base isolation (BI) is one of the effective, widely accepted and implemented passive control techniques to protect the buildings from the damages caused by the earthquakes (Jangid and Datta, 1995; Kelly, 1986; Warn and Ryan, 2012). Under this technique, horizontally flexible devices are interposed between the superstructure and the foundation, which offers the dual advantage of filtering the damaging high-frequency ground motions and also creates a designed and a safe location for seismic energy dissipation. Thus, the buildings are made more flexible in the horizontal direction, resulting in deliberately lengthened fundamental vibration time period that results in a reduction in the seismic responses during earthquakes. Moreover, the bearings have the capability to dissipate energy up to a certain limit. As the bearings are manufactured in a controlled factory environment, they are easily replaceable and have large deformation capacities. The base isolation systems as a strategy for earthquake hazard mitigation is globally proven for more than three decades. With the development of new base isolation devices, its effectiveness has further increased (Warn and Ryan, 2012).

The fundamental difference between a base-isolated building and a conventional fixed-base building is the behavior of the superstructure in the first mode of vibration. Almost entire deformations are concentrated at the bearing level in the base-isolated building, whereas the superstructure remains almost un-deformed as against the cantilever form of deformation of the superstructure in the conventional fixed-base building in the first mode of vibration. Base-isolated structures offer minimum base shear and floor accelerations as minimum energy is pumped into the structure. Though base-isolated structure is expected to remain in the elastic state for design level earthquake, but it can get into the inelastic state upto some extent in regions of high seismicity where the design level earthquake is high (Cardone *et al.*, 2013; Kikuchi *et al.*, 2008; Kilar and Koren, 2009; Ordonez *et al.*, 2003). Further, it can go into the significant inelastic state under extreme level earthquakes. The extent of inelastic excursion that BI structure undergo may depend on the nature and intensity of the earthquake. Recent studies (Mazza and Vulcano, 2009, 2012; Providakis, 2008a; Tavakoli *et al.*, 2014) have shown that even base-isolated buildings can suffer severe damages when excited by the near-field earthquakes as they contain high energy pulses as compared to the far-field earthquakes. Near-field earthquakes are capable of inputting a large amount of energy into the structures with long period pulses enabling fewer cycles of high inelastic deformations of building to dissipate the

energy. They also impart high isolator displacement in the base-isolated buildings which can even cause complete failure of the isolation system.

As a consequence, the performance evaluation of BI buildings under both near and far field earthquakes, like that in the case of fixed base buildings, attracted the attention of many researchers and became a subject of topical interest. The performance evaluation was carried out using both pushover analysis considering different lateral load patterns and nonlinear time history analysis. The primary objectives of the studies were to propose a lateral load pattern for pushover analysis that would be able to capture the inelastic behavior of the BI buildings at different stages of deformation levels. The final goals of the study were, of course, to evolve performance-based design techniques for BI buildings. The past studies were incomprehensive, and therefore, they require further investigations.

These observations have led to considerable research works in the recent years in a number of areas which include: (i) the study of the behavior of BI buildings in far and near-field earthquakes having different levels of PGA; (ii) damage assessment of BI buildings in the probabilistic terms both under far and near-field earthquakes; and (iii) possibility of replacing nonlinear time history analysis (NTHA) by a suitable nonlinear static analysis in the context of performance-based seismic design (PBSD) of BI buildings. For the fixed base (FB) buildings, extensive investigations concerning the aforementioned areas have been carried out. Since the present study concerns on the topics in the above areas, a brief background of the topics including a very short review of the literature is in order. The detailed review of the associated literature is presented in the next chapter.

1.1.1 Near-Field Earthquakes and their Effects on Base-Isolated Buildings

Near-field earthquakes (typically oriented within a distance of 20km-50km) consist of a major portion of fault energy in the form of pulses. Pulses can frequently be seen in acceleration, velocity, and displacement time histories. These pulses tend to have a maximum Fourier Spectrum in limited periods, whereas far-field earthquakes have maximum Fourier Spectrum in the broad range of periods (Iwan, 1994). Near-field earthquakes are associated with two significant effects known as directivity effect and fling step effect (Bray and Rodriguez-Marek, 2004; Somerville, 2005). These effects are based on three main active parameters of near-field ground motions which are rupture mechanism, slip direction of rupture relative to the site and residual ground displacement. If the direction of propagation of rupture is aligned towards the site or having a small angle between them and when the velocity of fault rupture is close to shear wave velocity of the site then it is called as forward directivity effect.

Due to this effect, large amplitude pulses with the long period and short duration having the high ratio of peak ground velocity to peak ground acceleration (v_{PG}/a_{PG}) are generated which are highly destructive in nature (Li and Xie, 2007; Somerville *et al.*, 1997).

Elnashai (2000) conducted the analysis of the damage potential of the Kocaeli (turkey) earthquake of 17th August 1999 for which two full-scale RC structures have been designed, built and tested. Chopra and Chintanapakdee (2001) compared the various aspects of response spectra for the far field and near field ground motions (fault normal component). They also computed the responses of elastic and inelastic single degree of freedom (SDF) systems for both types of ground motions and compared their strength reduction factor, R_y, and the ratio of peak inelastic to elastic deformation. Akkar *et al.* (2005) developed theoretical expressions for estimating the ground storey and maximum inter-storey drift ratios by considering varying beam to column stiffness ratios in frame buildings subjected to near-fault ground motions. Kalkan and Kunnath (2006b) investigated the consequences of well-known characteristics of near-fault ground motions on the seismic response of steel moment frames and effects of high-amplitude pulses on structural demands by considering idealized pulses. Mazza and Vulcano (2010) showed that the effect of near-fault motions largely depends on the ratio between the pulse period of the motion and the fundamental vibration period of the structure. Davoodi *et al.* (2012) studied the influence of near-fault and far-fault earthquakes by considering soil-structure interaction on the maximum response of an SDOF system. Jamnani *et al.* (2013) investigated the displacement demands of an SDOF with different fundamental period values subjected to ground motion with and without fling-step effect. Heydari and Mousavi (2015) conducted an incremental dynamic analysis of a seven-storey concrete building subjected to near-field and far-field ground motions for comparing the structural displacements. Alonso-Rodríguez and Miranda (2015) investigated inter-storey drift and floor acceleration demand in buildings subjected to near-fault ground motions by considering simplified building and ground motion models.

Rao and Jangid (2001) investigated the response of a building supported by sliding isolation systems under near-fault ground motion in two horizontal directions. Jangid and Kelly (2001) studied the effect of isolation damping on the performance of different isolation systems under near-fault ground motions. Ryan and Chopra (2006) conducted the nonlinear response history analysis of an isolated (lead rubber bearing) block subjected to far-field and near-field ground motions, using an advanced bearing model that incorporates the relationship between axial load and bearing response. Jangid (2007) studied analytically the response of base-isolated multi-storey buildings with lead rubber bearings for near-fault ground motions and

derived an optimum value of bearing yield strength for different system parameters. Yang and Zhao (2010) observed that the inter-storey drift and base shear of the base-isolated structure are intensified by the velocity pulses which are created in fling-step effect. Hence, the long period buildings are severely damaged by fling-step effect, causing frightful damage to long-period buildings. Osgooei *et al.* (2015) carried out the time history analyses on a 2-storey reinforced concrete shear wall structure, seismically isolated, using unbonded rectangular fiber reinforced elastomeric isolator (FREI) and with the fixed base, subjected to far-field and near-field earthquakes.

1.1.2 Development of Capacity Spectrum Method for Performance Evaluation of Base-Isolated Buildings

In recent years, performance evaluation of structures using pushover analysis (POA) and capacity spectrum method (CSM) along with selected demand parameters has attracted the attention of researchers in relation to performance-based seismic design (PBSD). For this purpose, various lateral load patterns have been proposed for POA in order to make the predictions of POA close to those of NTHA. Two types of comparison between the predictions of POA and NTHA are reported in the literature. In the first approach, the PGA of the time history of ground motion records is scaled to match the peak top storey displacement obtained by NTHA with the target displacement on the capacity curve. Under this condition, other demand measures obtained by the two methods of analysis are compared. In the second approach, the demand measures obtained by the POA and NTHA are compared at the performance point corresponding to the PGA values of the demand spectrum.

A considerable amount of research has taken place on the application of the pushover analysis to fixed base structures for which estimation of the seismic demands predicted by the POA was compared with that of the NTHA predictions (Bracci *et al.*, 1997; Elnashai, 2001; Kunnath and Kalkan, 2004; Martinelli and Faella, 2015; Mwafy and Elnashai, 2001). The literature on the evaluation of the responses at the performance points in comparison to those of NTHA is relatively less as compared to target displacement matching approach.

In the context of performance-based design, the performance evaluation is done by various methodologies, the most popular ones are capacity spectrum method (CSM) as per ATC-40 (1996), Coefficient method (CM) as per FEMA-356 (2000), modified CM and CSM as per FEMA-440 (2005), N2 method developed by Fajfar and Gaspersic (1996), which is also adopted in EC8. With the advancement in the pushover analysis in the past years, several methods are developed such as, the upper bound pushover analysis (Jan *et al.*, 2004), the

consecutive modal pushover procedure (Poursha *et al.*, 2009), the extended N2 method (Kreslin and Fajfar, 2011), the adaptive modal combination (AMC) procedure (Kalkan and Kunnath, 2006a), the extended adaptive capacity spectrum method (Bhatt and Bento, 2014), the displacement-based adaptive pushover (DAP) (Antoniou and Pinho, 2004b), and the force-based adaptive pushover (Antoniou and Pinho, 2004a).

A number of investigations in reference to the fixed base structures were carried out to improve the pushover analysis by proposing different lateral load patterns to push the structure to an ultimate state (Bento *et al.*, 2004; Kunnath and Kalkan, 2004; Mwafy and Elnashai, 2001). They include lateral load patterns that can be combined to reflect the multi-mode behavior, namely modal pushover analysis (MPA) developed by Chopra and Goel (2002) and method of modal combinations (MMC) proposed by Kunnath (2004).

The investigations on the applicability of the pushover analysis to base-isolated buildings are relatively very less as compared to fixed base buildings. Initially, performance evaluation of the base isolated (BI) buildings was not attempted because of the fact that it is generally anticipated that the BI buildings will remain more or less in the elastic range under the design level earthquakes. While this assumption is valid for ordinary conditions, they are not valid for specific conditions like near-field earthquakes, site conditions leading to high amplification of PGA, near resonating condition with a predominant frequency of ground motion nearer to the fundamental frequency of the structure. However, it has been shown in a number of studies that the BI buildings can go into different stages of inelastic excursion depending upon the nature and intensity of earthquakes (Cardone *et al.*, 2013; Kikuchi *et al.*, 2008; Kilar and Koren, 2009; Ordonez *et al.*, 2003), especially for near-field earthquakes (Mazza and Vulcano, 2010, 2012).

In recent years, a few studies have been conducted for the performance evaluation of BI buildings. Doudoumis *et al.* (2006) compared the pushover analysis with nonlinear time history analysis for four-storey base isolated reinforced concrete building installed with lead rubber bearings (LRB). Providakis (2008b) performed pushover analysis of two 3D steel-concrete composite base-isolated (LRB) buildings with five storey's each. One of the buildings is also provided with V-bracings. The Performance of buildings is evaluated for near-fault ground motions. The N2 method developed by Fajfar (2000) was successfully applied to the base-isolated buildings. Kilar and Koren (2010) evaluated the performance of the 4-storey base-isolated building by the N2 method. They idealized the capacity curve into a tri-linear curve. Three lateral load distributions were considered, namely, the triangular, proportional to the first mode shape, and as proposed by the protective system committee (SEAONC, 1986).

Lead rubber bearings were used in the study and stiffness of the isolators was varied for three protection levels for which soft, normal, and hard isolators were selected. Results are compared with average values of nonlinear dynamic analysis (NLDA) of seven artificial records scaled to 0.35g, 0.525g, and 0.70g.

Koren and Kilar (2011) also applied the extended N2 method (Fajfar *et al.*, 2005) to estimate the torsional effects in the 4-storey base-isolated for different asymmetric conditions which were created by shifting the center of mass and the center of isolation (CI). Asymmetrical 3-D base-isolated (BI) high-rack steel structure was analyzed by the extended N2 method by Kilar *et al.* (2011). Four asymmetric and five symmetric variants of the structure were considered by varying the eccentricity and payload occupancy levels. Faal and Poursha (2017) compared the applicability of the modal pushover analysis (MPA), the extended N2 method and the N2 method with three load distributions in 3-storey and 12-storey steel moment base-isolated frames. Lee *et al.* (2001) proposed a new formula for the vertical distribution of seismic forces on the base-isolated structure. The new formula was derived by combining the fundamental mode shapes of both isolated and fixed base structures and compared with the distributions as regulated in UBC-91 and UBC-97. York and Ryan (2008) developed improved equations to estimate the distribution of seismic forces in the base-isolated structure considering nonlinearity of the isolation system.

1.1.3 Fragility Analysis of Base-Isolated Buildings

The performance evaluation and damage assessment of building frames can be made in a different way, which is considered to be most appropriate if the uncertainty of the earthquake is recognized. It is widely known as fragility analysis. The research on the seismic risk assessment using fragility analysis is less for base-isolated buildings as compared to the fixed base buildings, especially when they are subjected to near-field earthquakes. Mansouri *et al.* (2017) evaluated the seismic performance of 3-storey and 9-storey base-isolated steel buildings installed with lead rubber bearings by developing the fragility curves. Fragility curves were developed by using incremental dynamic analysis for far-fault records and for a number of design time periods and damping ratios of the isolator considering immediate occupancy (IO) and life safety (LS) as two performance levels. Bakhshi and Mostafavi (2014) assessed the performance of 3,7, and 12 storied reinforced concrete moment resisting frames isolated with the lead-rubber bearings. Fragility curves were constructed by conducting nonlinear time history analysis using a suite of far-field and near-field earthquakes and considering the cumulative absolute velocity (CAV) as intensity parameter. Banazadeh *et al.* (2017) compared

the fragility curves for the collapse assessment of a 4-storey steel building, a building isolated with lead rubber bearings (LRB), and a building isolated with natural rubber (NRB) bearing fitted along with a viscous damper (VD) under near and far-fault earthquakes. Castaldo *et al.* (2017a) conducted the seismic reliability analysis and developed fragility curves for two degrees of freedom system (2-DOFS) provided by the friction pendulum system (FPS). The friction coefficients of the FPS and earthquake characteristics were taken as random variables. Castaldo *et al.* (2017b) developed seismic fragility curves for inelastic 2-DOFS with FPS considering a different range of structure and isolation properties.

1.2 Need for the Present Study

It is seen from the available literature, and real earthquake disasters that well designed and constructed fixed base and base-isolated structures for design level earthquakes can be damaged up to a great extent for near-field earthquakes. Although there are a number of studies on the response behavior of base-isolated buildings under near-field earthquakes, more investigations are required to find out the inelastic demands imposed by the near-field earthquakes. This creates a scope to investigate the behavior of base-isolated structures for design level and extreme level earthquakes under near-field earthquakes and also for far-field earthquakes for comparison so that their inelastic demands can be identified and necessary measures can be taken in order to cope up with the excess seismic demands, especially at isolation level.

Further, the studies regarding the performance evaluation of the base-isolated buildings using pushover analysis are less as compared to fixed base frames. There exist a number of gap areas, where more studies are required in respect to the performance evaluation of BI frames. Three gap areas are identified for the present study:

1. Since the comparison of pushover analysis with nonlinear time history analysis was made at a single performance point only near the ultimate state (collapse) for a limited number of responses which did not show how results of both analyses compare at different stages of inelasticity and different performance levels. Therefore, more exhaustive studies are required in this direction which can reveal the difference between two analyses at different states of the structures when it goes from elastic to inelastic excursions.

2. Since most of the studies on the applicability of pushover analysis for BI buildings were not target displacements specific, target displacement (peak top storey displacement) specific comparison of responses between the NTHA and the POA for assessing the

effectiveness of the lateral load patterns of the POA in predicting the nonlinear behavior of the BI building frames is needed. The reason for this is more compelling from the designer's point of view as they can make a good guess of the expected peak top storey displacement of the structure with the help of the expected PGA of ground motion and the ductility of the top storey displacement in fixing the target displacement.

3. Although some studies on the seismic reliability of the base-isolated building frames using fragility analysis have been carried out, they lack in revealing the extent of variation that could occur under near-field earthquakes with directivity and fling step effects. The consideration of these two effects of near-field earthquakes is extremely important as they can input different type of demands into the structures. There is a need for more exhaustive investigations into the probabilistic performance assessment of base-isolated building frames, especially under near-field earthquakes and also by considering different demand measures.

1.3 Objectives of the Study

Considering the requirement for the research on the present topic as highlighted in the Section 1.2, the present study is carried out to fulfill the following objectives:

1. Evaluation of the behavior of base-isolated building frame subjected to near and far field earthquakes by performing nonlinear time history analysis. Under this, specific objectives of the study are:
    a. To study the effect of the two-level concept (design level and extreme level) of the earthquake on base-isolated building for near and far field ground motions.
    b. To study the difference between the response characteristics of base-isolated buildings under near-field ground motions having directivity and fling-step effects both in the linear and non-linear ranges.
    c. To evaluate the ductility demands and the effect of isolator nonlinearity on the responses under near-field earthquakes as compared to the far field ones.

2. Evaluation of the applicability of capacity spectrum method (CSM) for base-isolated frames at different performance points. Under this, specific objectives of the study are:
    a. To investigate the applicability of CSM for BI building frames in predicting the responses at different performance points in comparison to the benchmark responses of NTHA.

b. To investigate the effect of base isolation characteristics on the response parameters of interest by considering three types of isolators namely, flexible, medium, and stiff defined by the equivalent stiffness of isolators. Also, to carry out the same investigation for the fixed base frames in order to typify the differences.

3. Estimation of the inelastic demands of base-isolated frames by performing pushover analysis using two new proposed lateral load patterns. Under this, specific objectives of the study are:

    a. To evaluate the effectiveness of two proposed lateral load patterns (LLPs) for estimating the seismic demands of base-isolated building frames by the pushover analysis (POA) in comparison with the benchmark responses obtained by the (NTHA) at three target displacements which conform to three states of the structure namely, elastic state, elastic-plastic state and plastic state as identified on the capacity curve.
    b. To show the effectiveness of LLPs separately for near and far field earthquakes.

4. Evaluation of the seismic performance of base-isolated frame in the probabilistic term through fragility curves. Under this, specific objectives of the study are:

    a. To show the variation in the probability of exceedances of a specified damage state for near-field (with both directivity and fling-step effects) and far-field earthquakes for the base-isolated frame in the higher limit (10-storey frame).
    b. To indicate the variations in the probability of exceedance with low, medium, and high levels of peak ground acceleration (PGA).
    c. To study the effect of frequency contents of near-field earthquakes denoted by a PGV/PGA ratio on the exceedance probability of damage states in the base-isolated frame.
    d. To find out the most sensitive demand measure which can help in the decision making regarding the design of base-isolated buildings, especially under near-field earthquakes.

1.4 Scope of the Study

The present study makes an attempt to investigate the behavior and performance of base-isolated building frames under near and far-field earthquakes by conducting nonlinear time history analysis, pushover analysis, and fragility analysis. For this purpose, two reinforced

concrete base-isolated building frames, which represent mid-rise and high-rise buildings of 5-stories and 10-stories are considered. The lead rubber bearing isolators are used as the base isolation system. The investigation is conducted by taking into account different demand measures, namely, maximum inter-storey drift, maximum base shear, peak roof displacement, maximum isolator displacement, the maximum number of plastic hinges, and the square root of the sum of squares of plastic hinge rotations.

1.5 Organization of the Thesis

For the fulfillment of the above objectives, the entire work is divided into seven chapters. **Chapter 1** provides the general introduction of the concerned topic of interest, the gap area in the research, and specific objectives to be fulfilled in the present study.

Chapter 2 provides an extensive literature review on the behavior and performance of base-isolated buildings under near and far field earthquakes. The literature review is broadly divided into five sections which includes: (i) characteristics of near-field earthquakes; (ii) effect of near-field earthquakes on the behavior of fixed base buildings; and (iii) effect of near-field earthquakes on the behavior of base-isolated buildings; (iv) performance evaluation of base-isolated building by pushover analysis (POA); and (v) performance evaluation of base-isolated buildings in the probabilistic terms by incremental dynamic analysis and fragility analysis.

In **the Chapter 3**, an investigation is carried out on the effectiveness of base isolation system for seismic hazard mitigation of buildings, especially under near-field effects. For the study, the response is evaluated by performing the nonlinear time history analysis for a ten-storey building frame, both for a fixed base and base-isolated conditions, subjected to near-field ground motions, and the same structure is also subjected to a set of far-field ground motions. The lead rubber bearing isolator is used for the isolation system. The ground motion time histories are scaled for two assumed levels of earthquakes, i.e., design level (scaled to have PGA = 0.2g) and extreme level (scaled to have PGA = 0.4g). Finally, the effect of the post to the pre-yield stiffness of the base isolator on the response behavior of the base-isolated frame is investigated. The selected response parameters for the comparative study are peak values of floor displacement, top floor absolute acceleration, maximum inter-storey drift, number of plastic hinges and base shear.

Chapter 4 aims to investigate the efficacy of the capacity spectrum method (CSM) in the prediction of seismic demands as compared to the benchmark responses of nonlinear time history analysis (NTHA) for base-isolated building frames at different performance points ranging from elastic to plastic state of the structure. In order to make the study a comprehensive

one, the comparison is made for a large number of response quantities. Five-storey and ten-storey base-isolated building frames with stiff, medium, and flexible lead rubber bearing (LRB) isolators are considered for analysis. Corresponding fixed base frames are also analyzed as references for comparison purposes. The performance points are obtained by the CSM as per ATC-40, which are consistent with the peak ground acceleration (PGA) levels ranging from a relatively small to a large value, i.e., from 0.1g to 0.5g at an increment of 0.05g and also, at the collapse point. ATC-40 response spectrum compatible time histories, which are artificially generated and scaled to aforementioned PGA levels, are used for the NTHA. Finally, the responses obtained by CSM and NTHA are compared at different performance points.

Chapter 5 deals with the assessment of the effectiveness of two proposed lateral load patterns (LLPs) to estimate the seismic demands of base-isolated building frames by the pushover analysis (POA) by comparing their estimates with the benchmark responses obtained by the (NTHA). The comparison is made under a suite of earthquakes consisting of an ensemble of five ground motion time-histories, each of far-field and near-field with forward directivity and fling-step effects. The consideration of different types of earthquakes makes the comparison more meaningful by bringing in the effect of the type of earthquake on the assessment criterion. Target displacement-based comparison is performed by considering three target displacements, which cater to elastic, elastic to plastic and plastic states on the capacity curve of the building frames. For this purpose, a mid-rise (5-storey) and a high-rise (10-storey) base-isolated (BI) reinforced concrete building frames are considered for the analysis. Two new LLPs are proposed for the POA which includes: (i) pattern derived from the square root of the sum of squares (SRSS) of first three mode shapes of BI-frame; and (ii) two variants derived from the modification of the uniform force distribution. Apart from them, the conventional LLP, i.e., proportional to the first mode shape is also considered in the POA. The response parameters, namely, peak storey displacement, maximum inter-storey drift, the number of plastic hinges, SRSS of plastic hinge rotations, maximum base shear, and maximum isolator displacement are considered for comparison.

Chapter 6 deals with the probabilistic seismic risk assessment of a base-isolated building frame under near and far field earthquakes by conducting the fragility analysis. For this purpose, a ten-storey base-isolated reinforced concrete frame is considered with lead rubber bearing as the base isolation system. Fragility curves are developed for a suite of far-field and near-field earthquakes with directivity and fling-step effects for a number of damage measures namely, maximum inter-storey drift ratio (MIDR), maximum roof drift ratio (MRDR), maximum base shear (MBS), maximum absolute top floor acceleration (MTFA), and

maximum isolator displacement (MID). Moreover, to study the effect of frequency contents of near-field earthquakes the peak ground velocity (PGV)/peak ground acceleration (PGA) ratio is varied in the near-field earthquake with directivity effect. Two sets of near-field directivity earthquakes are considered, one having a low PGV/PGA ratio, i.e., less than 150 and the other having a high PGV/PGA ratio which is greater than 150. The incremental dynamic analysis is performed to create the fragility curves assuming the different threshold values of damage states namely, non-structural, slight, moderate, and extensive. Finally, the fragility curves of near and far field earthquakes are compared for different cases to estimate the effectiveness of base isolation system and to find out the most sensitive damage measure for design purpose of base-isolated buildings.

Chapter 7 provides the overall summary of the important conclusions drawn from the present study. Recommendations for future work in the field of the behavior of base-isolated buildings under near-field earthquakes are outlined.

Chapter 2
Literature Review

2.1 Introductory Remarks

The literature on the behavior of base-isolated (BI) buildings and the base isolation systems subjected to earthquake ground motions is vast. Relatively, less literature on the performance evaluation of the (BI) buildings exist, especially under near-field earthquakes. Current research in the area of BI buildings focus primarily on the performance evaluation of BI buildings in the context of performance-based design. A number of investigations are being carried out in order to evolve a nonlinear static analysis procedure similar to the fixed base buildings, which can replace the nonlinear time history analysis. Performance evaluation using the capacity spectrum method is the final objective of these studies. Since the response behavior of the structures under near and far field earthquakes is different, the performance evaluation of the BI buildings under near-field earthquakes have attracted the special attention of the researchers. Not only the behavior of BI buildings for near-field earthquakes is taken up as a subject of extensive research, but also its performance evaluation both, probabilistically and deterministically, has formed a major topic of investigation. Since the present study concerns a few topics of the current research, the review of relevant literature pertaining with the current research trend is only presented in this chapter. Literature on the classical topics on BI buildings are excluded here, for which there exists an excellent state of the art reviews. The review is carried out under the following heads:

1. Characteristic of near-field earthquakes.
2. Effect of near-field earthquakes on the behavior of fixed base buildings.
3. Effect of near-field earthquakes on the behavior of base-isolated buildings.
4. Performance evaluation of base-isolated building by pushover analysis (POA).
5. Performance evaluation of base-isolated buildings in the probabilistic terms by incremental dynamic analysis and fragility analysis.

2.2 Characteristics of Near-Field Earthquakes

The state-of-the-art studies were carried out by many researchers to identify the characteristics of near-field earthquakes. Several researchers have made contributions in revealing the different aspects of near-field earthquakes like characteristic, effects on the structures, distinct nature, origin, source mechanism, etc.

Hanks (1975) studied the waveforms of the ground displacement generated by the San Fernando, 1971 earthquake, California. A total number of 234 ground displacement components of strong ground motions recorded at 78 sites were considered in the study. To obtain the displacement data, the double integration of ground motion accelerograms was done for the baseline adjustments and filtering of records. The empirically calculated displacements were compared with those actual displacements at a sufficient number of stations. It was found that the uncertainty in the displacements was of the order of 0.5 cm to 1 cm for 10 – 15 sec period range. The trend in the uncertainties was in accordance with those found in the previous studies. The predicted displacements from the strong ground motions could be used for the aseismic design of structures.

Ambraseys and Menu (1988) derived the empirical equations to predict the permanent displacements induced by the near-field ground motions. The equations were formulated in terms of predominant period, source distance, ground acceleration, critical acceleration ratio. The sensitivity of the proposed equations to predict the displacements was examined for different parameters. It was found that the predominant period of the ground motion highly influences the ground displacements. The decrease in the critical acceleration ratio would increase the displacements in down slopping grounds.

Somerville and Graves (1993) studied the different conditions which could cause the strong near-field ground motions. The authors explain that the long period pulse type motions were caused when the radiation of horizontally polarized shear wave pattern coincides with the direction of the rupture propagation, which is also known as directivity effect. This effect was readily observed in the case of the strike-slip faults which could cause large dynamic ground motion close to the rupture surface. On the contrary, the vertically polarized shear waves in the direction of strike or parallel to the fault could produce small dynamic motions, but exhibit large ground displacements, which is known as a fling-step effect. It was observed from the past earthquake records that the fault-normal component was larger than the fault-parallel component. The conditions that had caused the near-fault motions in the past earthquakes like Imperial Valley 1979, San Fernando 1971, and Loma Prieta 1989 were discussed with regard to the strike-slip and dip-slip faults. The effect of crustal basins on near-field motions was also investigated considering the case of San Fernando and Loma Prieta earthquakes. Finally, it was concluded that the directivity and basin effects highly influence the long period pulse type motions. The authors suggest that for the analysis of long-period structures (natural period > 1sec) it is very important to consider the directivity and basin effect, if applicable at the site.

Somerville *et al.* (1997) conducted an empirical analysis of the near-field ground motions and developed a model by modifying the attenuation relations of strong ground motions. The modified attenuation relations were developed to incorporate the effects of rupture directivity on strong motion amplitudes and durations. Different parameters of ground motions were considered for the modification, which includes, the ratio of strike-normal to strike parallel spectral acceleration, horizontal amplitude, and the duration of acceleration time history spectral acceleration. In specific, the empirical attenuation relations as proposed by the Abrahamson and Silva were used and then proposed modification factors were applied. The brief about the characteristics of a near-field earthquake having rupture directivity effect was discussed with the help of radiation pattern. The case of Landers earthquake 1992, Lucerne record, was taken as a case study. It was concluded that directivity effect was weak for sites with strike-slip faults close to the epicenter and is strong around the dip-slip faults which were located directly upside on the hypocenter. The rupture directivity effect caused the spatial variations in the amplitude and duration of earthquakes near the faults. The developed model can be used for the probabilistic seismic hazard analysis.

Malhotra (1999) studied the response characteristics of three recorded and one synthetically generated near-field earthquakes with the help of elastic response spectra. It was observed that the acceleration sensitive region of near-field earthquake was quite wide and highly affects the response of the structure: (i) it reduces the flexibility of the wide range of structures, as greater number of structures will fall in wide acceleration region and behave in a stiff manner; (ii) it increases the base shear and inter-storey drift as wide acceleration region attracts high-rise buildings which lead to the larger responses caused by the excitation of higher modes; (iii) it reduces the effect of supplemental damping; and (iv) it increases the ductility demands. The response spectra of the considered near-field earthquakes were also compared with the UBC-1997 spectrum. It was found that UBC spectrum was less conservative in the velocity sensitive region in comparison to the acceleration sensitive region and highly conservative in the displacement sensitive region. Hence, UBC spectrum is unsuitable for highly flexible structures. It was recommended in the study that the response spectrum given in the building codes must be defined in terms of PGA, PGV, and PGD values.

Huang and Chen (2000) studied the characteristics and the velocity waveform patterns of near-field ground motion with respect to the Chelungpu rupture of Chi-Chi 1999 earthquake. The velocity time histories of various hanging wall stations and footwall stations near to Chelungpu fault were compared. The study revealed that the TCU 068 and TCU 052 stations were measured with the highest peak ground velocity (PGV) levels of the order of 383 cm/sec,

and 254 cm/sec; the peak ground displacement (PGD) is noted of the order of 10 m for TCU 068, and 8 m for TCU 052. These offsets were higher as compared to those for the past earthquakes like for lander 1992 earthquake; the PGD is only 250 cm. The drift spectra of TCU 052 and TCU 062 was compared with that of near-field records of Northridge 1994 and Kobe 1995 earthquakes. It was found that both TCU 052 and TCU 068 exhibits high drift demands of 2.5% and 5% on the structures having their period longer than 3.5 sec, which shows high destructive nature of the ground motions recorded at TCU 068 and TCU 052 stations of the Chi-Chi earthquake.

Loh *et al.* (2000) investigated the characteristics and damage potential of the Chi-Chi 1999 earthquake with the help of near-field ground motion data recorded around the Chelungpu rupture fault. The authors report the length of the rupture surface of the Chelungpa fault was 105 km which produced the earthquake of magnitude-7.3 at a focal depth of 7.5 km. This earthquake produced the largest ever vertical offset of more than 9 m. High destruction was made which include, 2333 lives, 10002 injured people, and the damaged buildings were more than 8000. The principal direction analysis was performed, and it was found that the major principle direction of the ground motions recorded near to the Chelungpu fault is perpendicular to the fault which consists large PGA value in the east-west direction. The characteristics of the attenuation relations of peak ground acceleration and peak ground velocity corresponding to the shortest distance from the fault were also studied. It was found that the ground motions at both ends of Chelungpu fault have a large amplitude of acceleration at low-frequency band < 0.4 Hz.

Sasani and Bertero (2000) presented a review on the severity of the pulse-type ground motions, generally encountered in the near field earthquakes, with reference to the performance-based seismic design. The past studies were reviewed, and it was concluded that the pulse type ground motions could bring the structural performance into a critical level imparting high inelastic and ductility demands. The normalized displacement response spectra and the normalized yield coefficient response spectra were constructed for the idealized pulses and real pulse records. These spectra's could be used in the selection of the pulse type record to find out the critical base shear and displacement demands. By observing the trends in the yield response spectra, it was concluded that the large lateral forces could be attracted by the short to medium period structures.

Mavroeidis and Papageorgiou (2002) presented a comprehensive review on the characteristics of near-field ground motions and factors affecting their nature, especially for directivity effect. To study the nature and characteristics of near-field motions, the authors

compiled a large number of near-field ground motions occurred across the world with different tectonic environments, earthquake magnitude, and fault type. The forward directivity effect was emphasized in the study as it is the most common effect which occurs in the near-fault areas. Forward directivity effect happens when the propagation of the fault rupture is towards the site, and the rupture velocity closely approaches to the value of shear wave velocity. It leads to the generation of a long period pulse which contains the cumulative effect of the seismic radiation developed at the fault rupture. The shear dislocation radiation pattern orients the directivity pulse in the fault-normal direction. The authors explained this effect by taking the example of San Fernando, 1971, and Landers, 1992 earthquakes. The fling-step effect is seen in the fault-parallel directions, resulting in large permanent tectonic displacements. The important characteristics of pulse motion like pulse amplitude, pulse period, and number of pulses were briefly discussed. The authors developed a mathematical expression to represent the near-fault ground motions, which can help the engineers to generate the near-fault time histories to be used for seismic analysis and design of structures.

Somerville (2002) provided the state-of-the-art study on the near-field ground motions briefing the different aspects and characteristics related to these types of motions. Different models for predicting dynamic components of near-field ground motions were reviewed. The author investigated the characteristics of different near-field earthquakes namely, Loma Prieta 1989, Kobe 1995, Landers 1992, Northridge 1994, and Kocaeli 1999. It was concluded that the near-field ground motions need special consideration as they contain long period pulses which could cause permanent ground displacement. The near-field pulses have a broadband nature which could cause high peaks in their elastic response spectrum. The dynamic motions which occur in the perpendicular direction to the fault were highly influenced by the long period of pulses which exists in the near-field earthquakes. It was also observed from the considered earthquakes that the pulse period increases with the increase in magnitude. The static ground displacements caused by the near-field earthquakes could impose large displacement demands on the structures.

Mavroeidis and Papageorgiou (2003) proposed an analytical model to describe the impulsive nature of near-field ground motions. The authors had calibrated the proposed model with the real near-fault ground motion records, which were collected from different earthquake events. The model was capable of simulating the time histories and response spectra of near-fault motions. The scaling laws for the different parameters of the model were derived from the regression analysis. It was found that the proposed model can be reliably used by the

earthquake engineers to predict the elastic and inelastic response of conventional and non-conventional structures.

Bray and Rodriguez-Marek (2004) studied the distinct characteristics of the near-field records and proposed a simplified parameterization in order to characterize the near-field earthquakes with directivity effect. The near-field records of total 13 earthquakes were considered which were represented by the pulse period, number of pulses in velocity time history, and the pulse amplitude. The parameterization of the near-field records was carried out to develop empirical attenuation relationships for pulse period and pulse amplitude. It was concluded that the near-field earthquakes with directivity effect could be represented by few sine pulses. The number of velocity pulses is related to the slip distribution of the fault. For the moment magnitude less than 7, soil sites attract near-field earthquakes having longer periods of velocity time histories as compared to the rock sites. The pulse period increases with the increase in the moment magnitude.

Xie *et al.* (2005) investigated the characteristics of near-field pulses by representing the directivity and the fling step effects by eight equivalent pulses. The pulses were classified into four shapes, namely rectangular, quadratic, triangular, and half-sinusoidal for representing the two aforementioned effects. The relationship between the period of the velocity pulse (T_v), peak velocity (V), pulse peak acceleration amplitude (A), and peak displacement (D) were discussed in the dimensionless ratio of AT_v/V and VT_v/D. It was found that there is an increase in the AT_v/V ratio with the increase in the sharpness of the pulse shape. The VT_v/D ratio is same for the fling step effect and changes for the forward directivity effect. The response spectra of different pulses for fixed peak acceleration and peak velocity was compared. It was found that for the fixed value of acceleration response spectra, the spectral acceleration ordinates were higher for the directivity pulses in comparison to those of fling pulses at periods $> 0.5\ T_v$ and $< 2T_v$. The shape and the duration of the pulses highly influence the characteristics of the response spectra.

Wei *et al.* (2006) studied the characteristics of near-fault ground motions containing velocity pulses by comparing their response spectra with that of Chinese aseismic code and non-pulse records. The study was made by considering the earthquake records, with and without pulses, of Northridge 1999 and Chi-Chi 1999 earthquakes. It was observed that the average response spectra for the records with pulses was bigger than that of without pulses after 0.5 sec for Northridge records and 1 sec for Chi-Chi records. The Chi-Chi records possess high spectral acceleration values after 1 sec which could produce high damage in long period structures. Interesting, it was found that there is a crossing point at a particular period (T_j)

between the response spectra of with and without pulse records. The spectral acceleration values were higher for pulse records for periods greater than T_j and lower for periods lesser than T_j. The flat region of the response spectra of records with pulses was longest with largest spectral acceleration values as compared to that of without pulse records and design aseismic code. The authors had also compared the characteristic periods of the response spectra for different cases, and they had found that the characteristic periods for the records with pulses were longer than those of without pules by 0.2 sec and were twice bigger as specified in the Chinese aseismic design code.

Li and Xie (2007) provided the state of the art review on the characteristics of the near-field ground motions elucidating the directivity effect and the fling step effect. The authors pointed out the problems which were created in the past by the influence of near-field effects on the structures. The characteristics of two distinct effects of near-field earthquakes, which are directivity effect and fling step were discussed. The characteristics of near-field earthquakes are influenced mainly by three parameters, namely a source mechanism, slip direction of the rupture fault, and rupture direction with respect to the site. The hanging wall influences the characteristics of the near-field earthquakes; there is a large amplitude and slow attenuation in the ground motion parameters near to the hanging wall. The author highlights few areas which were needed to pay attention regarding the damaging effect and characteristics of near-field earthquakes including: (i) apart from the investigation on horizontal and vertical components of near-field earthquake, the studies should also made with respect to the rotational component of near-field motions; (ii) the efficiency of energy dissipations should be assessed against near-field earthquakes; (iii) performance evaluation methods and strengthening methods of structures should be checked under near-field earthquakes; and studies to include the design provisions in the near-field zones in the design codes should be carried out.

Burks and Baker (2016) reviewed the characteristics of the fling-step effect and proposed a model to predict the important parameters of fling pulse like fling amplitude and period. The model was derived by using the fling pulse parameters like fling displacement and fling pulse period, which were extracted from the records of previous near-field earthquakes. The fling pulse period from the extracted data set was plotted against magnitude for 100 stations, and after that the regression analysis was performed to derive the relation between the moment magnitude and fling period. They had derived the relationship between the fling amplitude, moment magnitude, and closest distance to the fault. The average fault displacements predicted by the proposed model matched well with the predictions of the previous studies.

Yadav and Gupta (2017) reviewed the characteristics of fling-step motions and proposed a mathematical model to simulate the waveform of acceleration and velocity pulses of near-field earthquakes with fling-step effect. A set of 20 ground motion records with fling-step effect was considered. The fling pulses were identified with the help of pulse time window and after that smoothened by five-point moving average method. The mathematical model was based on the pulses extracted after smoothening of original fling pulses and characterized three parameters which were related to the location of the pulse, pulse duration, and pulse period. The parameters related to the pulse amplitude and period were estimated in terms of closest distance from the fault and fault mechanism. It was found that the proposed model was able to simulate the fling pulses and had good agreement with the features of recorded fling pulses with acceptable errors. The authors suggest that the amplitude parameter highly influence the accuracy of the proposed model.

2.3 Effect of Near-Field Earthquakes on the Behavior of Fixed Base Buildings

There are many important studies which were carried out to predict and analyze the behavior of the fixed base buildings under the effect of near-filed earthquakes. The responses due to near-field and far-field earthquakes were also compared.

Iwan (1997) developed a drift spectrum as a measurement technique to calculate the response of the structure subjected to near-field ground motions. Drift spectrum was based on a continuous linear shear beam structural model which was capable of capturing internal deformations of the structure represented in terms of maximum inter-storey drift ratio. Drift spectrum responses were compared to numerical results for two prototype steel buildings having 6 and 20 stories each. The results showed that there was a good agreement in the responses given by drift spectrum as compared to numerical results. Also, the drift spectrum indicates that there was a mode-type and wave-type response of short period and long period structures. The author recommended the use of drift spectrum for structural design purposes and to estimate the drift demands especially for near-field earthquakes.

Elnashai (2000) evaluated the extent of damage inflicted by the Kocaeli (turkey) earthquake occurred on 17th August 1999 by considering a simple structural model. The inelastic dynamic analysis was performed to compute the displacement demands by employing earthquake records of Kocaeli earthquake recorded at four stations, namely, Izmit, Sakarya, Duzce, and Yarimca. The artificial time history record of a European earthquake with a return period of 975 years was also used for comparison purposes. The results were compared with those analyzed for Innovative Concept for Seismic Design of New and Existing Structures

(ICONS) bare frame structure. It was observed that the large inter-storey drift demand of 5% was produced by the Duzce record, which was very large as compared to the demand produced by the European earthquake of the order of less than two percent only. The effect of the considered earthquakes shows that there could occur significant displacement demands even for the structures which were designed according to the modern design codes. The study suggests that detailed investigations should be performed by considering both capacity and demand of different types of earthquakes.

Chopra and Chintanapakdee (2001) compared the various aspects of response spectra for the far-field and near-field ground motions (fault normal component). They have also computed the response of elastic and inelastic single degree of freedom (SDF) systems for both types of ground motions and compared their strength reduction factor, R_y, and the ratio of peak inelastic to elastic deformation (u_m/u_o). Furthermore, they have verified the design equations of R_y and ductility for the inelastic design spectrum for near-field motions. They concluded that the high deformation and strength demands were generated by the fault-normal component of the near-field motions due to the high peak acceleration, velocity, and displacement. Moreover, the fault-normal component has wide acceleration and displacement sensitive regions as compared to that of far-fault motions. For the inelastic SDF systems in the acceleration sensitive region, the R_y is smaller for the fault-normal component as compared to far-fault motions. Also, it was found that the design equations for the inelastic spectrum were also applicable for the near-fault ground motions.

Alavi and Krawinkler (2004) investigated the response of 20-storey, multi-degree freedom system with different base shear strength values and elastic fundamental period, subjected to a set of real near-field earthquakes with directivity effect and different pulse models. Three basic pulses were considered in the study namely, half pulse, multiple pulses, and full pulse to represent the near-fault ground motions. The study concludes that for long period structures, there were high ductility demands in the upper portion of the structure for the strong structure having high base shear strength coefficient $\gamma = 0.4$, and for weaker structure, $\gamma = 0.15$, demand migrates to lower storey levels. The considered pulse models were capable of producing the desired responses close to those obtained by the real near-field records. Moreover, equations using regression analysis were developed relating pulse intensity parameters which could be used with the strength demand spectra for estimating the base shear strength for different storey ductility ratios.

Akkar *et al.* (2005) developed theoretical expressions for estimating the ground storey drift ratio (GSDR) and maximum inter-storey drift ratio (MIDR) for a given set of values of

the beam to column stiffness ratios and spectral displacement in frame buildings subjected to set of near-fault ground motions. The expressions were proposed for the moment resisting frames, which behave in the elastic range and exhibit shear beam behavior. An ensemble of near-field earthquakes, with and without pulse signals were used to obtain the responses. The responses calculated from the derived expressions were also compared with the response history analysis and with the similar procedures developed by other researchers. It was concluded that for the pulse-type motions, the GSDR and MIDR increases as the fundamental period of the structure come nearer to pulse period. The GSDR was highly affected by the variation in the beam to column stiffness ratio. The proposed expressions were able to predict the GSDR, and MIDR demands with good accuracy for pulse-type motions when the ratio of the fundamental period to a pulse period was less than 1.5.

Kalkan and Kunnath (2006b) studied the effect of near-field ground motions on the steel moment frames and evaluated the inelastic responses under an ensemble of real near-field earthquakes with directivity and fling-step effect, far-field earthquakes, and synthetically generated pulse models representing fling-step and forward directivity effect. The nonlinear time history analysis was conducted for three existing steel buildings of 4, 6, and 13 stories with special moment resisting frames. The authors also provided a brief about the characteristics of near-field earthquakes. Finally, the responses of the aforementioned building frames were compared with those of far-field earthquakes. The study revealed that the median maximum demands of inter-storey drift ratio were higher for the near-field earthquakes. Moreover, the fling step effect induces higher inter-storey drift demands in the lower levels of all buildings as compared to directivity effect which predominantly affects the higher modes of the building frame. The amplification of the seismic demands was observed as the pulse period comes nearer to the fundamental period of the structure.

Hatzigeorgiou (2010) derived empirical expressions for the structural behavior factors in order to control ductility demands in bilinear single degree freedom system (SDOF). The vibration period and viscous damping ratio were varied, and the structural response was obtained under actual near-field ground motion records. The nonlinear time history analysis was performed to evaluate the ductility demands of the system. The nonlinear regression analysis was carried out on the response data set to develop unique expressions for the behavior factors. It was found that the derived expressions met the fundamental dynamic conditions and gave reliable behavior factors and hold good agreement with the results of nonlinear time history analysis.

Mazza and Vulcano (2010) investigated the response of three, six, and twelve-storey reinforced concrete frames for rock and soft soil conditions subjected to artificially generated and real near-field earthquakes. The effectiveness of the EC8 code design provisions was assessed by performing nonlinear time history analysis considering near-field earthquakes. It was found that the ductility demands for rock soil conditions is comparable, but it varies widely for the soft soil. The ductility demands were found to be greater under near-field earthquakes as compared to EC8 compatible artificial time histories. The work suggested that the peak ground acceleration (PGA) is an inappropriate parameter to represent the damage potential of the structure under near-fault ground motions as the response highly depends on the ratio of the pulse period to the fundamental period of the structure. The EC8 code provisions were inadequate to account the demands induced by the near-field earthquakes, especially in the soft soils at lower stories of the structure.

Yang *et al.* (2010) performed the inter-storey drift spectral analysis of buildings to evaluate the inter-storey drift demands under near-fault ground motions. The building systems were modeled as a continuous beam model with the shear-flexure cantilever beams with different lateral stiffness ratios. The inter-storey drift ratios (IDR) of building systems were examined under three types of idealized simple pulses, and three types of real near-field earthquakes with forward directivity effect, fling-step effect and the ones which contain no pulses. The inter-storey drift response spectrum was compared for the above-said earthquake excitations by varying lateral stiffness ratios (α). It was concluded that the pulses representing the directivity effect impart larger drift demands because of the multiple cycles of the pulses, which led to the cumulative effects that trigger the responses due to higher modes. Simple pulses which represent the fling-step effect excites the building system with moment resisting frames ($\alpha = 20$) primarily in the fundamental mode and imparts higher deformation demands in the bottom storey levels. The increase in the lateral stiffness ratio shifts the maximum IDR from upper to lower half of the buildings. There was a significant effect of the pulses in the real ground motions as the average IDR due to the presence of pulses was large as compared to that of without pulses.

Ventura *et al.* (2011) investigated the effect of the fling-step effect on the seismic response of reinforced concrete tall building under near-field ground motions. The nonlinear time history analysis was performed on a single degree of freedom system (SDOF) with different values of the period (0.5, 1, 2, 4,8, and 10 seconds) and yield strength considering four near-field earthquakes. The nonlinearity was accounted by adopting an elastic-plastic modified Clough model along with the stiffness degradation and a damping value of 5%. The

variations in the displacements and shear responses were studied under different parameters like the ratio of the structural period to fling rise time, the strength reduction factor, and P-delta effect. It was confirmed from the results that structural displacements were highly influenced by the ratio of the period to fling time ratio. The P-delta effect tends to increase the displacement demand, and these demands were higher for longer periods, greater than four seconds. The responses of a 44-storey building were also investigated under fling displacements. The inter-storey drift demands were found higher in the lower stories as compared to upper one. The fling in the Chi-Chi earthquake produced the highest inter-storey drift demands.

Zamora and Riddell (2011) studied the response of a structure subjected to near-fault earthquakes, with or without pulses and far-fault earthquakes with the aid of elastic and inelastic response spectra. The criteria for the identification of the pulse type motions and the influence of the orientation was also studied. The smoothened spectral shapes of the response spectrum were constructed with the help of Veletsos-Newmark-Hall provisions by considering the response amplification factors in case of elastic systems and response reduction factors in case of inelastic systems. The observations from the study indicate that the orientation of pulse type motions was unpredictable at the site and it is mandatory to perform the analysis in 360 degrees for the detection of pulse type motions. It was recommended to choose the pulse type motions from more than one orientation for predicting the structural responses. The spectra were larger for the pulse type motions as compared to other cases. The ratio of inelastic to elastic spectral ordinates, i.e., response de-amplification factors have larger values for the near-field pulse type motions in the principal direction of the motion. The equal displacement rule was found to be on the conservative side of the displacement sensitive region and having ductility > 3 in velocity sensitive region.

Jamnani *et al.* (2013) investigated the seismic response of reinforced concrete structures with long periods under the fling-step effect produced in the case of Christchurch earthquake, 2011. The displacement ductility demands were evaluated for the single degree of freedom systems (SDOF) with different fundamental periods (1.5, 2, 2.5, 3, 3.5, and 4 seconds) in which the structural behavior was modeled with the help of Takeda model. The nonlinear dynamic analysis was performed considering the Christchurch earthquake record at Heathcote Valley Primary School (HVSC) station, which contains the fling pulse. The displacement ductility demands were compared for the two analysis cases, with and without fling pulse. The results showed that the ductility demand was highly influenced by the ratio of the fundamental period of the structure to the fling pulse period. For the low response reduction factors, 5 or 6, without

fling pulse, and smaller structural periods, less than 2.5 sec, the higher ductility demands were observed in some cases which shows a mixed trend in results for Christchurch earthquake.

Foti (2014) evaluated the seismic performance of a 5-storey building with steel moment resisting frames fitted with two diagonal braces and friction damper under the far-field and near-field earthquakes. The responses were compared for different cases, one in which frames were installed with the friction damper, known as a protected frame and another one in which frame was fitted with the diagonal braces, known as an unprotected frame. Moreover, total ten cases were considered for which the location of the bracings in the frame was varied, and the responses were compared with those of protected frames with the friction dampers installed in substitution of the braces. It was concluded that the friction dampers increase the performance of the frame at lower periods under far-field earthquakes and higher periods under near-field earthquakes. For both near and far field earthquakes, the inter-storey drift and the absolute acceleration was higher in the protected frames at lower levels while the maximum base shear was reduced in all cases of protected frames.

Mazza (2015b) evaluated the nonlinear response of six and twelve storied reinforced concrete frame buildings designed for vertical and horizontal seismic loads subjected to real near-field earthquakes. The nonlinear dynamic analysis was performed to compute the ductility demands considering the horizontal component alone or in combination with the vertical component of ground motion. The effect of earthquakes was monitored at the three different sections of the girders namely, quarter span section, midspan section, and end sections. The results indicate that the ductility demands in the quarter sections and end sections in the girder of the upper stories were highly affected by the action of a vertical component of near-field earthquakes. Moreover, there was a large variation of the axial force in the columns of the lower stories due to the vertical motion. The horizontal component of ground motion highly influences the ductility demands of the end sections. The study suggested that the damaging effects of the vertical components of the near-field earthquakes should be considered in the code provisions.

Alonso-Rodríguez and Miranda (2015) investigated the building response subjected to near-field ground motions by considering simplified continuous building model formed by a cantilever flexure beam which was laterally coupled to the shear beam and governed by seven parameters. The peak responses like inter-storey drifts and floor accelerations were obtained from the closed form expressions by employing pulses proposed by Mavroeidis Papageorgiou (MP). The near-field pulses constitute the summation of three harmonic terms. The responses were compared to the response produced by real near-field ground motions. It was found that

the pulse duration critically affects the acceleration and drift response of the structure. The maximum drift and acceleration demands were directly proportional to the ratio of pulse duration to the fundamental period of the structure if this ratio lies between 0.75 and 1. The closed-form expressions were capable of producing the inter-storey drift demands along the height with good accuracy with a slight underestimation of acceleration demands.

Liossatou and Fardis (2016) conducted the nonlinear response history analysis of the single degree of freedom (SDOF) oscillators to compute the residual displacement demands due to near-fault effects. The reinforced concrete structures considered were represented by four hysteretic models namely, stiffness degrading with cycling, bilinear elasto-plastic, and stiffness cum strength degrading, with or without pinching. The analysis was carried out by employing real near-field earthquake records both with and without fling-step effect. To represent the fling motions, simple wavelets having two or four parameters were also generated to capture the same response as that of near-field ground motions. It was found from the study that two parameter wavelets representing the fling motion overestimate the peak inelastic displacements. The complex wavelets having four parameters, which could represent both fling motion and pulse nature gives reliable estimates of residual and inelastic displacements.

2.4 Effect of Near-Field Earthquakes on the Behavior of Base-Isolated Buildings

The behavior of base-isolated buildings was investigated under the near-fault excitation in many research studies assuming both elastic and inelastic behavior of the isolated building. The characteristics of the isolators were investigated by assuming their bilinear behavior.

Heaton *et al.* (1995) provided a brief on the characteristic of near-field earthquakes and discussed the potential capabilities of large earthquakes in some urban areas of California. The authors investigated the response of two flexible buildings, one is 20-storey steel frame building, and another one is 3-storey base-isolated building installed with rubber pads with bilinear characteristics, subjected to synthesized near-field ground motions. It was found that for the 20-storey building, the first storey drift is more than 6 %, which shows the heavy destruction of near-field ground motions. For base-isolated structure, the maximum striking velocity is found to be 165 cm/s which can cause considerable damage to the structure. The effectiveness of base isolation depends on the type of isolation system used, required performance of the building, size of earthquake employed for building design, and the probability of occurrence of near-field earthquakes.

Jangid and Kelly (2001) compared the real and pseudo-velocity spectra of near-field ground motions oriented in the fault-parallel and fault-normal directions. It was concluded that

near-fault motions contain high energy content at higher frequencies. Moreover, there was a significant difference between the shape of real and pseudo-velocity spectra. The effect of the isolation damping on the flexible structure, modeled as the two-mass model and subjected to near-fault ground motions was also studied. It was concluded that there is an optimum value of isolation damping for which the superstructure accelerations were minimum. The performance of the different type of base isolation systems was also investigated under the normal component of near-fault motions. The Electricite-de-France (EDF) isolation system was found to be the best suitable for the near-field ground motions as it decreases the base displacement more than other systems by transmitting superstructure accelerations which were comparable to high damping rubber bearing (HDR) and lead rubber bearing (LRB).

Matsagar and Jangid (2004) investigated the influence of the isolator characteristics on the base-isolated building. The isolation system was modeled by two different mathematical models, one with equivalent linear viscous damping behavior and the other one is the bilinear hysteretic behavior. The force-deformation loops of the two models were studied for different system parameters like isolator yield displacement, isolation period, and system flexibility considering top floor absolute acceleration and bearing displacement as response parameters. It was observed that the top floor acceleration was underestimated and bearing displacement was overestimated by the equivalent linear model. For the bilinear model, with an increase in yield displacement, there is a significant decrease in top floor acceleration and a marginal increase in bearing displacement. There is a significant difference in the prediction of superstructure acceleration predicted by the two isolation models and hence should be cautiously used to capture the behavior of the isolator.

Ryan and Chopra (2004) conducted the nonlinear response history analysis of the bi-linear base isolation system by formulating the equation of motion of isolation system for which median normalized deformation depends on the normalized strength and isolation period. A single isolator supporting a rigid mass system was subjected to a set of 20 ground motions. A different set of equations was derived with the help of regression analysis to calculate the deformation demand with the given parameters for allowable isolator force and deformation. Numerical examples were solved with derived equations for different system parameters. The results were compared to the equivalent linear procedures which lead to the underestimation of the isolator deformation by 20% - 50% as compared to the responses of nonlinear response history analysis. The authors suggest that for modeling the bilinear isolation system, the yield deformation should be the fixing criteria instead of fixing the ratio of initial to post-yield stiffness ratio.

Jangid (2007) studied the response of base-isolated multi-storey building, which was assumed as the N-storey flexible shear type structure, with lead rubber bearings (LRB) under near-fault ground motions. The bearing displacement and top floor absolute accelerations were considered to measure the response of base-isolated structure and plotted for different system parameters like isolation period, the yield strength of LRB, and superstructure flexibility. It was observed from the study that low values of yield strength will produce significant bearing displacements. The author derived an optimum value of bearing yield strength by minimizing the bearing displacement and top floor absolute acceleration. The optimal value of the yield strength was found to be in the range of 10 % -15 % of the total weight of the structure which was obtained for different values of the isolation period (2, 2.5, and 3 sec) and yield displacement (2.5 and 5 cm). The optimum value of yield strength decreases with an increase in the isolation period. Moreover, the higher yield displacement increases the performance of LRB under near-fault excitations.

Providakis (2008a) investigated the effect of lead rubber bearing (LRB) isolator and viscous damper under the near-field (NF) and far-field (FF) motions. The LRB isolators were designed for three sets of characteristic strength to weight of isolation system ratio, Q/W, and range of isolation periods. The nonlinear time history analysis was performed on two reinforced concrete 3-D buildings having 5 and 6 stories each. The response of the buildings was obtained in terms of base drift, and superstructure drifts for different cases. It was concluded that the addition of supplemental damping in the isolation system would reduce the base drift under NF motions, but increase the superstructure drift under FF motions. The study suggests that the supplemental damping should be cautiously used especially in case of far-field motions as it may make building more rigid resulting in higher responses of the superstructure.

Sharma and Jangid (2009) investigated the effect of initial stiffness of the bilinear isolation system of the 5-storey building. The building model was idealized as a shear-type flexible structure with N-stories. The response is evaluated under three pulse type real earthquake records considering various response parameters namely, top floor acceleration, inter-storey drift, base shear, and base displacement. It was concluded that high initial isolator stiffness and the characteristic strength excites the structure into the higher modes which further leads to increase in inter-storey drift and floor accelerations. For the low ratio of initial stiffness to post-yield stiffness (stiffness ratio), the top floor acceleration was highly influenced by the isolation frequency and for the high value of stiffness ratio, the contribution from the higher frequencies increases which further excites higher modes of the structure and finally leads in large floors accelerations. The bearing displacement and base shear decrease with the increase

in initial stiffness of isolator. The responses even increase for the flexible system and low post-yield stiffness ratios.

Mazza and Vulcano (2012) investigated the effectiveness of the high damping rubber bearing (HDRB) as a base isolation system installed in a 5-storey reinforced concrete building under near-field earthquakes. The combined effect of the horizontal and vertical components of the near-field earthquakes was studied. The stiffness ratio, defined as the ratio of vertical stiffness and analogous value of horizontal stiffness, is varied for the isolator. The HDRB was modeled with the help of two springs and two dashpots (TSTD) model in which a nonlinear spring is placed parallel to a dashpot in both vertical and horizontal directions. The nonlinear seismic analysis was conducted on a 5-storey 2-D frame using step by step procedure which was defined by two parameter integration scheme and consists of an initial stress iterative procedure. The results show that the behavior of the base-isolated structure is similar to the fixed base structure when higher values of stiffness ratio were considered. Moreover, with the increase in stiffness ratio, there is an increase in the ductility demand for columns and girders. There is a significant effect of the vertical ground motion as it induces more variations in the axial load on the columns, especially for the higher values of stiffness ratio. The study suggests that the superstructure should also be designed taking the effect of vertical motions as they can exert tensile loads on the isolators. The horizontal components of the near-field motions can impart high ductility demands in both girders and columns and can cause severe damages to the base-isolated buildings.

Ozdemir and Akyuz (2012) compared the predictions of the maximum isolator displacement of the 3-storey reinforced concrete base-isolated structure with lead rubber bearing (LRB) by equivalent lateral force (ELF) procedure and nonlinear response history analysis (NLRHA) under near-field earthquakes. The NLRHA was performed unidirectionally and bi-directionally employing the near-field records with directivity effect. The effect of soil profile is also investigated by using two sets of records and by varying the shear wave velocity of upper 30 m soil profile, $V_{S,30}$; one set of records have $V_{S,30}$ = (360 m/sec < $V_{S,30}$ < 760 m/sec), regarded as stiffer soil and another one have $V_{S,30}$ = (180 m/sec < $V_{S,30}$ < 360 m/sec), regarded as softer soil. The study was conducted for the wide range of characteristic strength ratios (Q/W). It was concluded that the soil profile significantly affects the maximum isolator displacements when the contribution of the orthogonal component of ground motion record was considered. The maximum isolator displacement is higher in case of stiffer soil. The results of ELF and NRHA holds good agreement with each other.

Cardone *et al.* (2013) performed a parametric study to evaluate the inelastic response of four reinforced concrete base-isolated buildings, each having 2, 4, 6 and 8 stories. Three different isolator bearings were considered namely, lead rubber bearing (LRB), friction pendulum bearing (FPS), and high damping rubber bearing (HDRB). The nonlinear time history analysis was conducted by employing 3 artificial and 4 real Italian seismic records, compatible (on average) to EC8 response spectrum and scaled to two intensity levels, equal to 0.35g and 0.5g. The results of the analyses were compared with those of fixed base counterparts. It was found that with the fewer inelastic cycles experienced by the isolated structure, the peak response of the isolation system is marginally affected by the inelastic behavior of the superstructure. The ductility demand of the superstructure increases with increase in equivalent viscous damping of LRB and FPS. The work suggested that for allowing limited plastic deformations in the base-isolated structure, its collapse limit should be based upon the lateral capacity of the superstructure.

Mavronicola and Komodromos (2014) compared the responses of base-isolated buildings considering sharp bi-linear and smooth plasticity Bouc-Wen nonlinear models for base isolation systems. These two models were used to represent the lead rubber bearing isolators. The two buildings, a 3-storey, and a 5-storey were considered and modeled in two dimensions as a shear-type structure resting on LRB isolators with masses lumped at floor levels. The dynamic time history analyses were performed by employing an ensemble of near-field earthquake records. It was concluded from the study that the sharp bi-linear model slightly underestimates the base displacements at the isolation level. Conversely, the peak floor accelerations and the inter-storey drifts were slightly overestimated with the sharp bi-linear model.

Tavakoli *et al.* (2014) compared the seismic response of fixed base and base-isolated buildings under near and far field earthquakes. The lead rubber isolator was used as a base isolation system. The responses were obtained by performing the nonlinear time history analysis of 2-D frames of 4, 8, and 12 stories each. The results obtained showed that the reduction in the base shear with implementing the base isolation is more in far-field earthquakes. The reduction of the absolute acceleration of the base is not much in base-isolated conditions for near-field earthquakes. Moreover, the maximum reduction is found in the middle floor levels for all buildings and is maximum for far-field earthquakes. The trend in the results also showed that by increasing the number of the floors in the building the effectiveness of the base isolation decreases especially in the case of near-field earthquakes. High inter-storey drift

demands were imposed by the near-field earthquakes on the fixed base structures, especially in the middle storey levels.

Fathi *et al.* (2015) investigated the response of supplemental damping on the base-isolated building frames subjected to the near and far field earthquakes. The supplemental damping was provided with the help of viscous dampers installed along the lead rubber bearing isolator. The nonlinear time history analysis was performed on six 2-D steel building frames with different storey levels, and variation in the supplemental damping was considered in the range from 5% to 40%. The study showed that with the increase in the supplemental damping, the storey drift decreases under far-field earthquakes and increases about 1.5 to 2 times for the near-field earthquakes. Moreover, the base displacements could be reduced by providing extra damping, but it could lead to the large floor accelerations, especially under near-field earthquakes.

Alhan and Öncü-Davas (2016) evaluated the performance of 5-storey base-isolated structure installed with lead rubber bearings having bi-linear behavior and different isolation parameters. The nonlinear time history analysis was conducted for synthetically generated near-field earthquakes for different fault distances, pulse periods, and damping values. It was concluded that the larger pulse periods led to the large base displacements and floor accelerations. The increase in the characteristic force to weight ratio decreases the base displacements. There was a significant effect of the ratio of the isolation period to the pulse period on the response of the structure which could lead to the amplification of floor acceleration demands. This effect was more pronounced for the smaller characteristic force ratios and shorter fault distances. For the long period pulses, period > 5 sec, isolation systems having isolation period < 3 sec and characteristic strength ratio > 10% could only accommodate the high base displacement demands produced by near-field pulses.

Alhan *et al.* (2016) investigated the influence of stiffening of high damping rubber bearing (HDRB) installed in the 6-storey frame under real and synthetically generated near-field earthquakes. Two different models were considered to represent the behavior of HDRB, one is smooth bi-linear hysteretic model ignoring the strain hardening of HDRB, and another one is hysteretic model including stiffening effect taking into account the strain hardening property of HDRB. The nonlinear time history analysis was carried out for the two cases to evaluate the response of base-isolated building in terms base displacements, floor accelerations, and storey drifts. There was a significant effect of the stiffening model on the storey drift and the floor accelerations; the responses increase. It was suggested that the hysteretic model

should be cautiously selected for the accurate representation of HDRB especially in the case of earthquakes having a moment magnitude > 6.5 and near-field earthquakes.

Tsiavos *et al.* (2017) proposed a relationship between the strength reduction factor R_y, the vibration period T_n, and the displacement ductility μ, considering the inelastic behavior of superstructure and isolation system. The base-isolated structure was idealized as a 2-degree of freedom model with the inelastic hysteretic model. The nonlinear time history analysis was performed to evaluate the response of the base-isolated structure considering a suite of 160 earthquakes, which contained both far-field and near-field earthquakes. The statistical analysis was performed to find out the median values of strength reduction factor and displacement ductility from the response data. The main finding of the study was that the displacement ductility demands of the inelastic base-isolated structures were more than the fixed base structure with same strength reduction factor and vibration period. The equal displacement rule was applicable for isolated structures, which have their vibrations periods longer than the periods of their isolation systems.

2.5 Performance Evaluation of Base-Isolated Buildings by Pushover Analysis (POA)

The literature on the application of pushover analysis (POA) for the case of base-isolated buildings is limited. There are only few studies available which had investigated the applicability of pushover methods to estimate the seismic demand imposed on the base-isolated structures in comparison to the accurate predictions provided by the nonlinear time history analysis (NTHA).

Lee *et al.* (2001) proposed a formula to predict the distribution of lateral forces on the base-isolated structure for the seismic load. The isolated structure was idealized as a two-degree freedom system with linear isolation system. The proposed distribution pattern was derived by combining the fundamental mode shape of base-isolated and fixed base structure. The results of the proposed lateral force distribution by proposed formula were compared with that of dynamic analysis, and force distribution given by UBC-91 and UBC-97 for a five-storey reinforced concrete structure with and without a shear wall, and a 15-storey framed structure. The results of 5-storey frame and shear wall structure indicate that the proposed formula was able to predict the distribution of the storey forces as compared to those predicted by UBC-91 and UBC-97. Whereas, the UBC-97 formula highly overestimated the storey forces. For the 15-storey frame structure, the storey forces were underestimated by the proposed formula and hence it is not applicable to medium and high-rise structures, which account the effects due to higher modes.

Doudoumis *et al.* (2006) evaluated the performance of four-storey base isolated reinforced concrete building installed with lead rubber bearings (LRB) with pushover analysis (POA) and nonlinear time history analysis (NTHA). The comparison between the two analyses was made in the terms of maximum base shear, maximum roof displacement, and total number of plastic hinges. The comparison was made on a basis that the value of one response parameter was fixed and the other parameter was compared by both analyses. The NTHA was performed by considering three real earthquake records. The records were scaled to match the long period range of the design response spectrum given in the Greek seismic design code. To make sure that the superstructure would get into the inelastic range, the target design spectrum was scaled to two times than the elastic design spectrum. The pushover analysis was performed by considering the uniform distribution of force as a lateral load pattern. The response values were obtained by NTHA at distinct time intervals and compared with the capacity curve produced by the POA. It was concluded that the maximum base shear corresponding to the top displacement and number of plastic hinges holds a good agreement when compared with the two analyses.

Kilar and Koren (2008) evaluated the performance of four-storey fixed base and based-isolated buildings by the N2 method. Two types of bearing were used to isolate the structure: rubber bearing and lead rubber bearing. Furthermore, three different types of each bearing were used, namely, soft, normal, and hard which were based on their effective stiffness's. The N2 method was carried out by considering the uniform distribution of lateral forces. The target value of the base displacement was obtained by the intersection of the capacity curve with the demand curve for different damping values. The capacity curves of the rubber bearing were linear and nonlinear in case of lead-rubber bearings. The results were presented in terms of base displacements, and relative top displacements for different cases of isolators. It was concluded that N2 method could serve as a valuable tool in predicting the target base displacements for different damping ratios, isolators and performance levels.

Providakis (2008b) investigated the performance of two steel-concrete composite 3-D buildings. The nonlinear pushover analysis was carried out for two five-storey 3D buildings provided with steel-concrete composite slab and steel columns and isolated with the lead rubber bearings (LRB). The LRB isolators were designed for different characteristic strength to weight (Q/W) ratios and different bearing diameters. To investigate the effect of the bracing system on the performance of the base-isolated building, one of the two buildings was provided with the v-bracing systems at the end bays for the full height of the building. The performance of the buildings was evaluated by considering the fact that they were located in the near-fault

region according to the UBC 1997 code. It was observed that the isolation system had led to the reduction of base shear under near-fault excitation but increases the storey drift of the first-floor beam members. The v-bracing provided in the building gave better performance by eliminating the formation of plastic hinges and reducing the storey drift by a factor greater than 1.5.

York and Ryan (2008) derived improved equations to estimate the distribution of lateral forces in the base-isolated structures by performing a nonlinear regression analysis of the response data set generated by conducting nonlinear response history analysis (NLRHA). The multi-storey frame superstructure of single bay having three, six, and nine stories supported on bi-linear isolation system was considered for the analysis. The isolation system was modeled with the bi-linear force-displacement relation. The peak storey shears were evaluated by conducting NLRHA of the considered frame models by employing 20 earthquake records unidirectionally. The effect of a bi-linear isolation system on the distribution of the seismic forces on the superstructure was also studied. Simplified equations from nonlinear regression analysis were developed which relates the k (a function of system parameters) with T_s (superstructure period) and ξ (effective damping). It was observed that the shear coefficient varies linearly with mass ratio with a small variation in building heights. The derived equations reasonably predict the lateral force distribution along the height of the superstructure and base level when compared with the results of other distributions like NLRHA, ASCE 7, and given by Protective system committee (PSC).

Cardone *et al.* (2009) presented a mathematical formulation to predict the distribution of lateral forces in the base-isolated building for linear static analysis considering the nonlinear behavior of different isolation systems. In the proposed formulation, the distributions of the storey shear forces were proportional to the linear combination of the displacement profiles of the first three modes with isolation system modeled by the effective stiffness. The proposed distribution was hence named as 3-MM (3-Mode Method). The combination of coefficients with which the three modes were combined were derived by performing a regression analysis of the results obtained by nonlinear time history analysis (NLTHA). The NTHA was conducted by considering 7 artificial time histories which were compatible with the response spectrum provided by Eurocode 8. Three shear frame buildings having 3, 5 and 8 stories were considered as a lumped mass model installed with different isolation system, namely: Lead Rubber Bearings (LRB) and High Damping Rubber Bearings (HDRB), (ii) Friction Pendulum Bearings (FPB) combined with flat Sliding Bearings (SB) with Low-Damping Rubber Bearings (LDRB)

and (iii) Combinations of flat SB and Shape Memory Alloys (SMA)-based re-centering devices were considered. The proposed method was applied to the aforementioned building models, and the results of the storey shears were compared to that of NTHA, inverted triangular and uniform distributions. They concluded that the 3-MM gives an excellent prediction of the storey shear profiles along the height of the structure with a maximum error of only 10% for all isolation systems. Moreover, the uniform pattern slightly underestimates the storey shears whereas, the inverted triangular pattern largely overestimates the shear forces.

Kilar and Koren (2010) evaluated the seismic performance of the four-storey base-isolated building by using the N2 method and compared the results with those obtained by the NTHA. In the first part of the study, they idealized the capacity curve of the structure into a tri-linear curve on which the initial stiffness was identified corresponding to the first yielding point. They performed a parametric study by conducting the nonlinear dynamics analysis of a single degree of freedom system with different damping ratios and hardening slopes by employing seven artificial accelerograms compatible to EC8 spectrum. The inelastic spectra was derived for a constant reduction factor, and the corresponding ductility was found for different ground motions. It was concluded that there is a good agreement between the calculated ductility and ductility obtained by equal displacement rule. In the second part of the study, the N2 method was applied to the four-storey base isolated building. Three types of lead rubber bearing isolators namely, hard, normal, and soft were used to isolate the building, which confirms to three protection levels of the superstructure. Three different lateral load patterns, namely triangular, 1st mode and, the distribution given by protective system committee (PSC) were used to push the structure. Results were compared with the average values of nonlinear dynamic analysis (NLDA) performed by considering seven artificial records scaled to 0.35g, 0.525g, and 0.70g. It was observed that N2 method provides good agreement with the results of NLDA by using a lateral load pattern given by PSC for which storey drift and damage patterns fit best with NLDA estimates. The storey drifts and damage patterns in the severely damaged structure were reasonably predicted by lateral load pattern corresponding to the 1st mode.

Kilar *et al.* (2011) evaluated the performance of a 3-D fixed base (FB) and a base-isolated (BI) high-rack steel structure which is made to store goods with the extended N2 method. The structure was installed with the elastomeric isolators. Four asymmetric and five symmetric variants of the structure were considered by varying the mass eccentricity and payload occupancy levels. The pushover analysis was performed considering an inverted lateral load pattern for the fixed base structure and for the base-isolated structure an additional

force at the isolation level was applied as prescribed by the protective system committee (SEAONC, 1986). The NTHA was performed considering three ground motion records which match the EC8 spectrum at longer periods. The results of the N2 method were compared to the predictions of individual record and average nonlinear time history analysis (NTHA). Results for the top, relative and base displacements and inter-storey drift were predicted fairly well for FB and BI by the N2 method. The effect of varying mass eccentricity was also studied for FB and BI structures. It was observed that for the relative displacements and maximum storey drifts, the most critical occupancy levels lie between 55% - 85%, giving rise to maximum eccentricities of about 5% - 15%. The base isolation was highly effective in increasing the seismic performance even for high asymmetrical conditions.

Koren and Kilar (2011) investigated the applicability of the N2 method for a 3-D four-storey asymmetric base-isolated reinforced concrete building to estimate its torsional effects. The lead rubber bearing isolators were used with various elastic stiffness's which was categorized as soft, normal, and hard according to their relative elastic stiffness. The stiffness of three isolators was confirmed to provide three protection levels, which will result in the elastic to moderately damaged to severely damaged performance of the superstructure. Different variants of the aforementioned structure were considered in which the asymmetry is created by shifting the center of mass (CM) by 10%, 20%, 30%. Moreover, three different positions of the center of isolation (CI) were considered, namely CI=CM, CI=CS (center of stiffness), and CI = -CM. The N2 method was performed with three different lateral load patterns, including (i) triangular; (ii) proportional to the first model; and (3) as given by the Protective Systems Committee (PSC). For the comparison purpose, the nonlinear dynamic analysis (NLDA) was also performed for an ensemble of 7 EC8 spectrum compatible artificial time histories scaled to 0.35g and 0.525g. The results of the N2 method and average NTHA were compared for base displacements, relative displacements, and ductility factors for plastic hinges. It was concluded that the predictions of the N2 method holds good agreement with the average NTHA results up to small eccentricity of 10% and beyond this range of eccentricity, the displacements were highly overestimated by the N2 method. The lateral load pattern corresponding to 1st mode shape and the PSC load pattern provided the best estimates.

Petrovcic and Kilar (2015) evaluated the performance of three-storey unreinforced masonry (URM) heritage structure isolated with the elastomeric bearings by the non-linear static method and N2 method. The authors have proposed a new modeling technique to model URM structures, which consider the different failure modes of structural elements. The modeling technique was based on the equivalent frame approach, which incorporates the linear

beam elements and the concept of plastic hinges, and accounts only a single failure mode interaction surface to express the seismic failure. The seismic displacement demands of the fixed base and base-isolated structures were calculated by the N2 method, and the performance of the structure was evaluated by considering three discrete limit states as per Eurocode 8-3. It was observed from the comparative results that the fixed base structure undergoes to the severe damage levels as compared to the base-isolated structure, which undergoes only minor damage levels. The base isolation increases the performance of heritage structures by reducing the seismic displacement demands and increasing the displacement capacity of the structure.

Faal and Poursha (2017) compared the applicability of different pushover methods like modal pushover analysis (MPA), the extended N2 method and the N2 method to estimate the seismic demands of 3-storey and 12-storey steel moment base-isolated frames. The lead rubber bearing isolators were used to isolate the buildings. Three types of LRB isolator were designed, namely, hard, normal, and soft, which were having different stiffness's confirming to the three performance levels. The N2 method was carried out by considering three lateral load patterns, namely, the inverted triangular, PSC load distribution, and load pattern corresponding to the 1st mode shape. The nonlinear response history analysis (NLRHA) was also performed by employing twelve artificially generated accelerograms records which were compatible with the ASCE7-05 design spectrum. The NLRHA was performed at three seismic intensities for which records were scaled to 0.4g, 0.6g, and 0.8g. The results obtained by different pushover methods were compared to the mean, and minus one standard deviation of NLRHA results in terms of floor displacements, storey drifts, and plastic hinge rotations. It was observed that the N2 method provides better estimates of the seismic demands and the inelastic effects for the 3-storey base-isolated frame. The increase in the damping ratio and stiffness of isolators deteriorates the efficacy of the pushover methods. It was found that the triangular force distribution highly underestimates the floor displacements. Both load distributions, i.e. 1st mode and PSC distribution gave reliable estimates at 0.4g and 0.6g, for storey displacements and storey drifts. The extended N2 methods gave better predictions of the plastic hinge rotations in the damaged superstructure.

2.6 Performance Evaluation of Base-Isolated Buildings by Incremental Dynamic Analysis and Fragility Analysis.

A very few attempts have been made in looking at the performance of base-isolated buildings and isolation system in the probabilistic terms, especially under near-field

earthquakes. Although, some studies have been made for the base-isolated bridges. The literature on this topic is scanty.

Zhang and Huo (2009) derived the fragility functions to investigate the optimum design parameters and effectiveness of the isolation devices to reduce the potential of damaging earthquakes on base-isolated bridges. Three types of bearing were considered in the study, namely elastomeric bearings, lead rubber bearings, and friction pendulum bearings. Fragility curves were derived from incremental dynamics analysis and probabilistic seismic hazard method by employing 250 ground motion records. Different damage measures were chosen to record the seismic demand on the bridge superstructure and isolation system and monitored for 25 levels of the PGA as intensity measure. The three bearings were modeled with the bi-linear characteristics. Both 2-D and 3-D models of the bridge were considered in the analysis. It was concluded that there was practically no difference between the fragility curves generated by using the raw data, normal regression, and log-normal regression. The fragility curves for the 2-D and 3-D models were comparable for higher damage states. The optimum values of different parameters of the isolation system were obtained by plotting the median values of earthquake intensity against the isolator parameters in the form of contours.

Alam *et al.* (2012) analytically derived the fragility curves for a three-span continuous highway bridge isolated with laminated rubber bearings and lead rubber bearings along with a shape memory alloy retainer (SMA). The bridge was modeled as a 2-D continuous finite element frame. The incremental dynamics analysis was performed under a suite of 20 near-field ground motions and taking the PGA as an intensity measure to measure the demand imposed on the bridge piers and isolation system. The fragility curves for different cases, with and without SMA restrainer, were compared. The study revealed that the failure probability of bridge pier and isolation system in all damage states increases by using SMA restrainer along with the bearing. The median values of PGA for different damage states were lower when SMA restrainer was used which shows that SMA restrained could impose high seismic vulnerability to the bridge components.

Mollaioli *et al.* (2013) evaluated the capability of different intensity measures (IMs) used in incremental dynamics analysis and to derive fragility curves, to predict the inelastic response of the base-isolated buildings under the action of near-field and far-field ground motions. Two reinforced frames of four and six stories each were considered. The isolation system was modeled by a bi-linear hysteretic characteristics. Different isolation periods of both frames were considered: isolation period equal to 2.5, 3, 3.5, and 4 seconds for the 4-storey frame, and 3, 3.5, 4, and 4.5 seconds for the 6-storey frame. The nonlinear dynamic analysis

was performed under a set of 80 ordinary records and 59 pulse-like near-fault records. A wide variety of intensity measures were considered in the study, which was broadly divided into two groups: (i) non-structure specific IMs, which could be directly calculated from ground motion time histories; and (ii) structure specific IMs, which could be calculated from the response spectrum of the time histories corresponding to the period of the structure. It was found from the study that the peak ground acceleration (PGA) is a reliable and efficient intensity measure to predict the maximum inter-storey displacement, maximum roof drift ratio, and maximum base displacement.

Han *et al.* (2014) investigated the performance of an old 7-storey reinforced concrete building designed with non-ductile consideration and retrofitted by the lead rubber bearing isolators. A 2-D frame was extracted from the building for the analysis for which both geometric and material nonlinearities were taken into account. A set of 32 recorded far-field mainshock-aftershock sequences were employed for the analysis of the building. The fragility curves were constructed for deformation sensitive nonstructural components and acceleration sensitive nonstructural components for different damage states. It was concluded that the fragilities of the structural components were only slightly higher when the aftershocks were considered in the case of the un-retrofitted building. In the case of base-isolated building, the fragilities of structural components were same in all damage states.

Bakhshi and Mostafavi (2014) assessed the probabilistic seismic performance of a 3,7, and 12 storied reinforced concrete moment resisting frames isolated with the lead-rubber bearings. Fragility curves were constructed by conducting the nonlinear time history analysis. The seismic uncertainty was considered by using a suite of far-field records and the near-field earthquake records which were in the perpendicular direction to the fault and selected from FEMA(P-695) (2009) code. The cumulative absolute velocity (CAV) was considered as an intensity measure. The structural uncertainties were considered by modeling different material properties like the compressive strength of concrete, the yield strength of reinforcement, Young's modulus of concrete, and viscous damping coefficient as random variables by using the Monte Carlo simulation method. The fragility curves of base-isolated and fixed base structures were compared at different limit states. The fragility curves indicated a better performance of the isolation system in far-field earthquakes and showed a high damage probability in the near-field earthquakes.

Konstantinidis and Nikfar (2015) investigated the response of sliding equipments and contents (EC) that were prone to sliding in the base-isolated building under the action of broadband earthquakes. The various characteristics of the isolation system were studied by

considering two widely used isolation models: the damped linear elastic model and the bio-linear model. The conventional 2-degree of freedom system model was used to model the base-isolated building on which a sliding EC with appropriate friction coefficient was mounted. The incremental dynamic curves were generated by considering 20 broadband ground motions and for different values of coefficient of friction. It was observed that there was an amplification in the sliding displacement with lower friction coefficient values and maximum sliding displacement varied linearly with intensity scale factor. The isolation damping < 20% was effective in reducing the EC displacements and by providing larger value than 20%; there was no addition response reduction. The linear isolation system with large damping was able to effectively reduce the accelerations of the sliding EC, while large hysteretic damping in the bi-linear isolation system could increase the accelerations. The fragility curves were constructed considering a dimensionless intensity measure and its associated engineering demand parameter for different thresholds of capacity, which could be easily used by the structural engineers.

Mazza (2015a) evaluated the seismic performance of a five-storey reinforced concrete base-isolated building installed with fire protected high damping rubber bearings under the effect of near-fault ground motions. The nonlinear response of the base-isolated building with no fire condition was compared with that of with event of fire condition for 45 and 60 minutes of fire resistance. The building was considered to the fire event in five different scenarios for which each scenario corresponds to the fire at each storey level at one time. The EC1 parametric fire curve was used to model the fire action and to distribute the temperature load on the frame members. An incremental dynamic was performed under a suite of seven near-field earthquake records, and seismic damage was calculated in terms of ductility demand of columns and girders. It was concluded that there was a significant decrease in the undamaged strength and ductility of the structure exposed to the fire. Highly unexpected ductility demand was induced in the lower levels of the structure due to the combined effect of fire and near-field motions. The fire event scenarios in the first and second storey levels produced the maximum damage to the structure.

Gong and Xiong (2016) investigated the effect of different control strategies in the probabilistic terms on a 3-D base-isolated building. An eight-storey 3-D benchmark base-isolated building was taken for the investigation to study the effect of proposed modified pseudo negative stiffness (PNS) control in comparison to PNS control and passive damping provided by bi-linear elastomeric isolation system. The incremental dynamic analysis was performed by employing a set of 20 far-fault earthquake records occurred in the California

region to monitor the three damage measures, namely, maximum peak floor acceleration (a_{max}), peak inter-storey drift ratio (θ_{max}), and peak isolator displacement (U_{max}). The response of damage measures was obtained corresponding to the increasing values of intensity measure which was taken as spectral acceleration and optimized for the three damage measures. The probabilistic performance of three control strategies was evaluated by comparing the fragility curves for different damage measures and predefined limit states. It was concluded from the fragility curves that the smallest damage probability was provided by the Modified PNS control and passive control also accompany it will small values at every limit state for the a_{max} and θ_{max}, which depicts the state of structural functionality. The PNS control gave the smallest damage probability followed by the Passive control for U_{max}, which governs the isolation functionality.

Banazadeh *et al.* (2017) compared the fragility curves for the collapse assessment of a 4-storey steel building, a building isolated with lead rubber bearings (LRB), and a building isolated with natural rubber bearings (NRB) fitted along with a viscous damper (VD) under near and far-fault earthquakes. The incremental dynamic analysis was performed for a set of near and far field earthquakes, and the median collapse capacity of the structure was defined by limiting the value of inter-storey drift ratio to 10% or until numerical instability was reached. They concluded that the minimum collapse probability corresponding to the maximum considered spectral acceleration was achieved with the LRB isolated building for far-fault earthquakes and for the near-field earthquakes, the NRB combined with VD gave the minimum collapse probability. The results also indicated that there was a decrease in the performance of the base isolation in near-field earthquakes from the collapse assessment point of view. Furthermore, the supplemental damping provided by the VD improved the performance of the base isolation in near-field earthquakes.

Castaldo *et al.* (2017a) conducted the seismic reliability analysis and developed the fragility curves for two degrees of freedom system (2-DOFS) equipped by the friction pendulum system (FPS). The friction coefficient of the FPS and earthquake characteristics were taken as random variables. The 2-DOFS was defined by the perfectly elastoplastic model, and the behavior of FPS was defined by the velocity dependent model. The fragility curves were derived for yielding superstructure and isolation system for different values of spectral displacement corresponding to different isolation periods and strength reduction factors. It was found that the seismic fragility of isolation decreases and superstructure increases with an increase in the strength reduction factor. The seismic reliability curves of the superstructure and isolation system were also constructed for different cases considering seismic hazard

curves of the L'Aquila site (Italy), as per NTC08 provisions. Finally, seismic reliability regressions were developed between displacement ductility and strength reduction factors.

Hedayati Dezfuli and Alam (2017) investigated the effect of different types of conventional rubber bearings like natural rubber bearing (NRB), high damping bearing (HDRB), and lead rubber bearing (LRB) on the seismic fragility of the highway bridge. The fragility curves concerning to different bearings were constructed for bridge pier and isolation system. The displacement ductility and shear strain were chosen to depict the seismic damage in the bridge superstructure and isolation respectively. It was concluded that the isolation system was a more fragile component of the bridge because it had a higher damage probability. The HDRB showed good performance among other bearings as the bridge was least fragile at all damage states when fitted with HDRB.

Mansouri *et al.* (2017) evaluated the seismic performance of 3-storey and 9-storey base-isolated steel buildings installed with lead rubber bearings (LRB) by performing an incremental dynamic analysis (IDA) and developing the fragility curves. The two benchmark steel buildings of steel project of phase-2 were used along with their fixed base version. To study the influence of isolator characteristics, the LRB isolators were designed separately for each building for different design isolation periods of 2.5, 4, and 5.5 seconds, and characteristic strength to weight ratios (Q/W) of 0.03, 0.06, and 0.09. The IDA was performed using a suite of 22 far-fault records as given in FEMA P695 and the responses of the maximum inter-storey drift ratio were monitored for different cases of the designed isolators. The fragility curves were developed for a number of design time periods and damping ratios of the isolator considering immediate occupancy (IO) and life safety (LS) as two performance levels. They concluded that the base-isolated structures have a high primary slope of IDA curves as compared to the fixed base structure which indicates the reduction in drift response. The performance of the structure was enhanced by the base isolation as it decreases the damage probability for a specific performance level in comparison to the fixed base structure. Interestingly, it was found that high isolator damping could increase the damage probability at lower acceleration levels corresponding to IO but could decrease the damage probability at high acceleration levels corresponding to LS and hence is more effective in the higher performance levels. The probability of failure decreased with the increase in the design period of the isolator in both IO and LS levels.

2.7 Concluding Remarks

Although there have been a number of studies on the behavior and performance evaluation of the base-isolated buildings subjected to both far-field and near-field earthquakes, there is a need for the further research in certain areas as evident from the literature review. They include:

1. For near-field earthquakes, the behavior of the BI buildings and the isolators for extreme earthquake (for a higher level of the PGA) is not exhaustively investigated. Therefore, more elaborated investigations are required to investigate the behavior of the superstructure in the inelastic range and also to investigate if different types of isolators are required under the near-field earthquakes.
2. In most of the literature, the comparison of pushover analysis (POA) with nonlinear time history analysis (NTHA) was made at a single performance point, only near the ultimate state (collapse). A very limited number of responses namely, inter-storey drift and top floor displacement were considered for the comparison. How the results of both analyses compare at different stages of inelasticity and at different performance levels are not widely reported. More exhaustive studies are required in this direction which can reveal the difference between the two analyses at different states of the structure, especially in the inelastic state.
3. Target displacement (peak top storey displacement) specific comparison of responses between the NTHA and the POA for assessing the effectiveness of the lateral load patterns used for carrying out the POA in predicting the nonlinear behavior of the BI building frames is much less compared to the fixed base building frames. Not many types of lateral load distribution patterns for the BI buildings have been developed in this regard. Therefore, more studies are required in this direction.
4. Extensive studies on the fragility analysis of the base-isolated building frames by considering the uncertainty of earthquakes are lacking, especially under the influence of near-field earthquakes with directivity and fling-step effects. The consideration of these two effects of near-field earthquakes is extremely important as they can input different type of demands into the structures. Therefore, exhaustive investigations into the performance of BI building frames in the probabilistic terms under the effect of near-field earthquakes are required.

Chapter 3

The Numerical Study of Base-Isolated Building Frame Under Near and Far Field Earthquakes

3.1 Introductory Remarks

The base isolation is a passive control technology, which is well implemented from last four decades and have an excellent ability to cope up with the high seismic demands induced by the far-field earthquakes. On the contrary, the performance of the base isolation under the near-field earthquakes is still questionable due to the presence of large velocity pulses produced by the directivity effect and large static displacements produced by the fling-step effect, which makes near-field earthquakes highly destructive in nature. They can severely damage the base-isolated buildings and can even cause the failure of the isolation system by demanding large displacements at the isolation level. Several earthquakes confirmed the destructive power of near-field earthquakes, which had occurred in the past like Loma Prieta 1989, Landers 1992, Northridge 1994, Kobe 1995, Chi-Chi 1999 and Kocaeli 1999.

Base-isolated buildings have been analyzed and designed mostly for far-field earthquakes with design level earthquakes in which the superstructure remains linear, but the isolator goes into the nonlinear state. The primary concern of the designed base-isolated structure remains to be the isolator displacement and acceleration of the building. Since the seismic design codes all over the world specify the concept of two-level earthquakes, one extreme earthquake (maximum credible earthquake) and another is design level earthquake, base-isolated buildings designed for the design level earthquakes should be checked for their performances in the extreme level earthquakes. While under design level earthquake the structure is found to remain in the elastic range; sufficient inelastic excursion may take place in the isolated structure in the extreme level earthquake.

In order to extend the design of base-isolated building for near-field earthquakes, the behavior of the base-isolated building in the near-field earthquake has recently become a topic of considerable interest. The behavior of base isolator and base-isolated buildings under such earthquakes could be significantly different as compared to far-field earthquakes. Because of the impulsive type of excitation inputting large amount of energy, the base-isolated buildings can get into significant inelastic state enabling fewer cycles of high inelastic deformations of building to dissipate the energy. As a consequence, significant damage in the isolated structure may be caused.

With this background in view, the study in present chapter deals with the investigation of the effectiveness of base isolation system for the seismic hazard mitigation of buildings, especially under near-field effects. For the study, the nonlinear time history analysis (NTHA) is carried out for a ten-storey building frame, both for the fixed base and base-isolated condition, subjected to near-field ground motions, and the same structure is also subjected to a set of far-field ground motions. Two levels of earthquakes are assumed in the present study, i.e., design level (scaled to have PGA = 0.2g) and extreme level (scaled to have PGA = 0.4g). The selected response parameters for the comparative study are peak values of top floor displacement, acceleration, maximum inter-storey drift, number of plastic hinges, isolator displacement and base shear. The effect of the ratio of post-yield stiffness to initial stiffness of the isolator on the response of base-isolated building is also studied.

3.2 Characteristics of Near-Field Earthquakes

In order to typify the near-field earthquakes in comparison to the far-field earthquakes, a brief account of the characteristics of the near-field earthquakes is presented first.

The near-field earthquakes are recorded within 15-20 km near to the fault and characterized by the presence of critical high-velocity pulses created by forward directivity effect and fling-step effect which makes them more devastating as compared to far-field earthquakes (Bray and Rodriguez-Marek, 2004; Somerville *et al.*, 1997). The near-field earthquakes are influenced by the slip direction of the fault, rupture direction relative to the site, and source mechanism.

The forward directivity effect occurs when the rupture propagates towards the site with a large velocity, which is close to the shear wave velocity as shown in **Figure 3.1**, and the released seismic energy arrives to the site in the form of high energy pulse with a longer period and short duration. Moreover, due to the radiation pattern of shear dislocation of the fault, the directivity pulses are oriented in the fault-normal direction. The directivity pulses are two-sided having a large amplitude, short duration, and the long period, which occurs in the velocity time history of the near-field earthquake records (Hall *et al.*, 1995; Kalkan and Kunnath, 2006b).

On the other hand, the fling-step effect is a result of permanent or static ground displacement produced by the tectonic deformation of the ground. The fling-step effect is associated with the fault rupture mechanism and is observed in the fault parallel direction or along the slip direction. Moreover, the fling-step effect is characterized by the presence of half-cycle high amplitude velocity pulse and has a large static offset in the displacement time history. **Figure 3.2** shows the orientation of the directivity and fling-step effects in strike-slip

and dip-slip faults. In the case of strike-slip faults, as shown in **Figure 3.2(a),** the fault direction is defined by the strike, and the orientation of the rupture directivity pulse is in the strike-normal direction. The fling-step effect producing the static ground displacement is oriented in the strike-parallel direction of the fault. **Figure 3.2(b)** shows the dip-slip fault in which the orientation of rupture directivity pulse is in the direction normal to the fault dip. The fling displacement is parallel to the dip-slip direction.

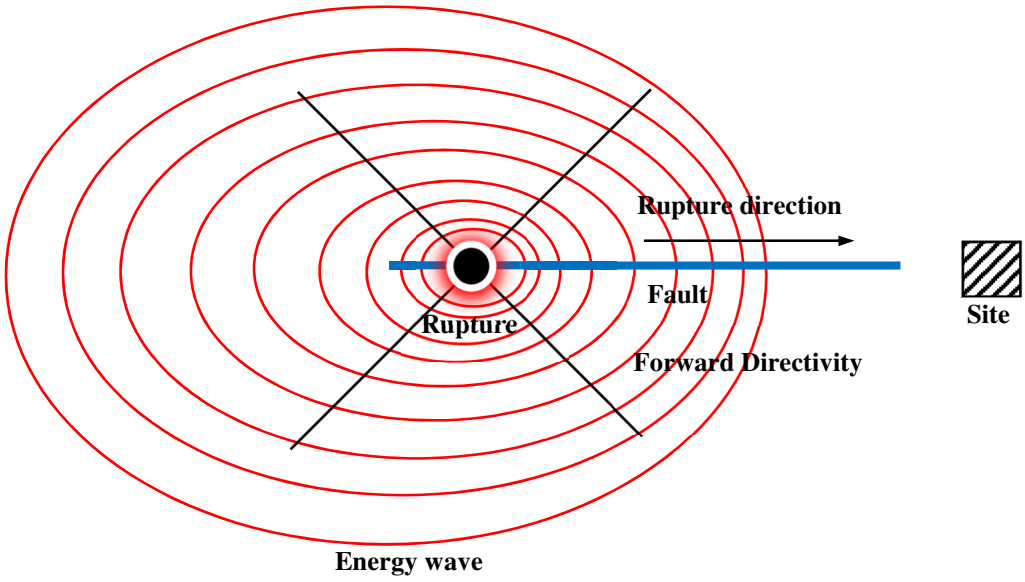

Figure 3.1 Illustration of a Directivity effect

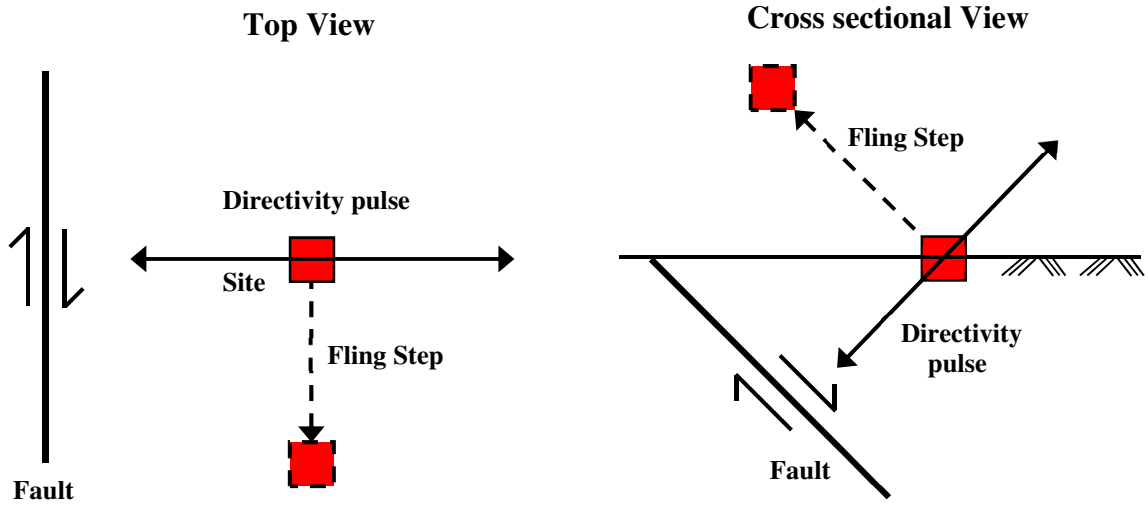

Figure 3.2 Orientation of the Directivity and Fling-step effects

Figure 3.3 compares the velocity and displacement time histories of typical far-field (Loma Prieta-Sunol forest fire station, 1995), near-field with directivity effect (Imperial valley-el centro array#4, 1979), and near-field with fling-step effect (Kocaeli-Sakarya, 1999).

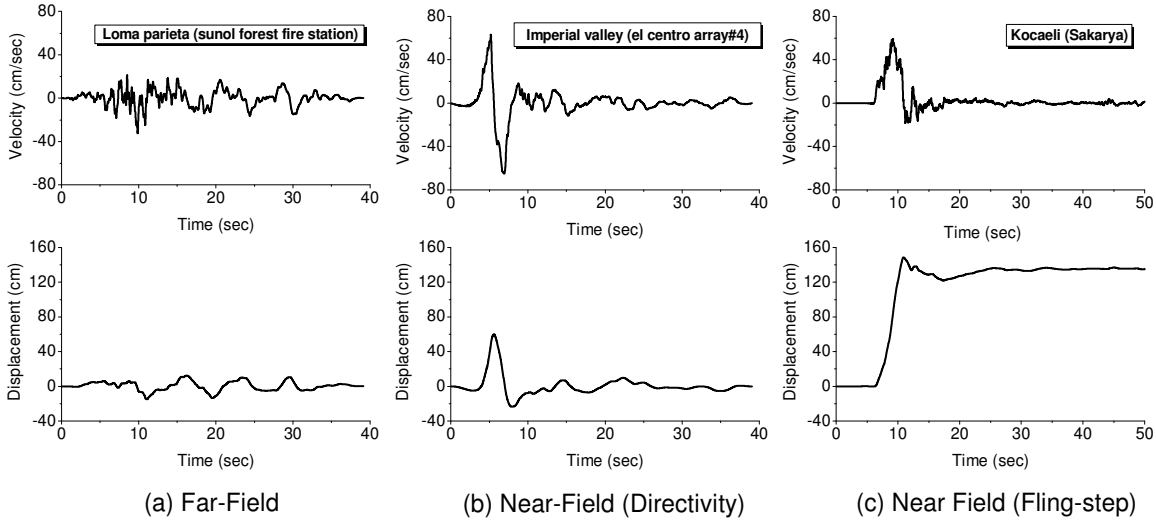

Figure 3.3 Velocity and displacement time history plots of typical near and far field earthquakes

3.3 Analysis of Base-Isolated Building Frame

The superstructure is modeled as a 2-D frame mounted on the isolators placed between he columns and foundation. The frame consists of framing along the column line of the building as discussed in further **section 3.4.1.** The nonlinear time history analysis (NTHA) is performed in SAP (2000) software to evaluate the seismic demands imposed by the earthquakes. The Hibler Hughes Taylor integration scheme is used for NTHA using the value of Beta = 0.25 and Gamma = 0.5. The second order effect, i.e., P-Delta is also considered in the analysis. The Rayleigh damping is defined in the software by providing the damping ratio of 5%, corresponding to the first and second modes of structural vibration as contributions of the higher modes are generally insignificant for the base-isolated structures.

3.4 Numerical Study

The numerical study is conducted with a 10-storey building frame isolated by lead rubber bearing (LRB) isolators. For the comparison purpose, the fixed base version is also considered in the analysis. For the analysis, a set of four far-field and near-field earthquake records have been taken from the Pacific Earthquake Engineering Research Center (PEER) Strong Motion Database, Berkeley (*http://ngawest2002.berkeley.edu/*). Out of the four near-field earthquakes, two are selected with directivity effect and the other two with fling-step effect. All the records have been normalized and then scaled to PGA levels of 0.2g and 0.4g to obtain

the two-level earthquake design concept. All the relevant properties of records like PGA (peak ground acceleration), PGV (Peak ground velocity), and PGD (peak ground displacement) are given in **Table 3.1**. For the reference, the acceleration time histories of the far and near field records scaled to 0.2g are shown in **Figures 3.4 and 3.5.** To estimate the predominant frequencies of the earthquakes, their FFT plots are also shown in **Figures 3.6 and 3.7**. **Figure 3.8** shows the comparison of acceleration, velocity, and displacement response spectra of different far-field and near-field earthquake records considered in the study. In the same figure the first fundamental period of fixed base (FB) and base-isolated (BI) frame is marked. It is seen from the figure that the near-field earthquakes have higher spectral values even for longer time periods for all three types of response spectra, especially earthquakes with fling-step effect, as compared to that of far-field earthquakes. The details regarding modeling and design of the superstructure and base isolators are described in the following subsections:

Table 3.1 Ground Motion Records

S.No.	Year	Earthquake	M_w	Station	Component	PGA (g)	PGV (cm/s)	PGD (cm)
(a) Far Field Records								
1	1994	Northridge	6.7	Beverly hills	MULH, 009	0.42	58.91	13.18
2	1992	Landers	7.3	Cool water	SCE STATION 23	0.42	42.35	13.84
3	1978	Tabas	7.4	Ferdows	L	0.093	5.4	2.24
4	1987	Superstition hill	6.5	Poe road	POE 270	0.45	35.72	8.81
(b) Near Field Records (Forward Directivity effect)								
1	1992	Erzincan	6.69	Erzincan	EW	0.5	64.32	21.91
2	2003	Bam	6.6	Bam	L	0.8	124.1	33.94
(c) Near Field Records (Fling step effect)								
1	1999	Chi Chi	7.6	TCU 052	E	0.36	151.2	210.43
2	1999	Chi Chi	7.6	TCU 068	N	0.46	263.25	430.2

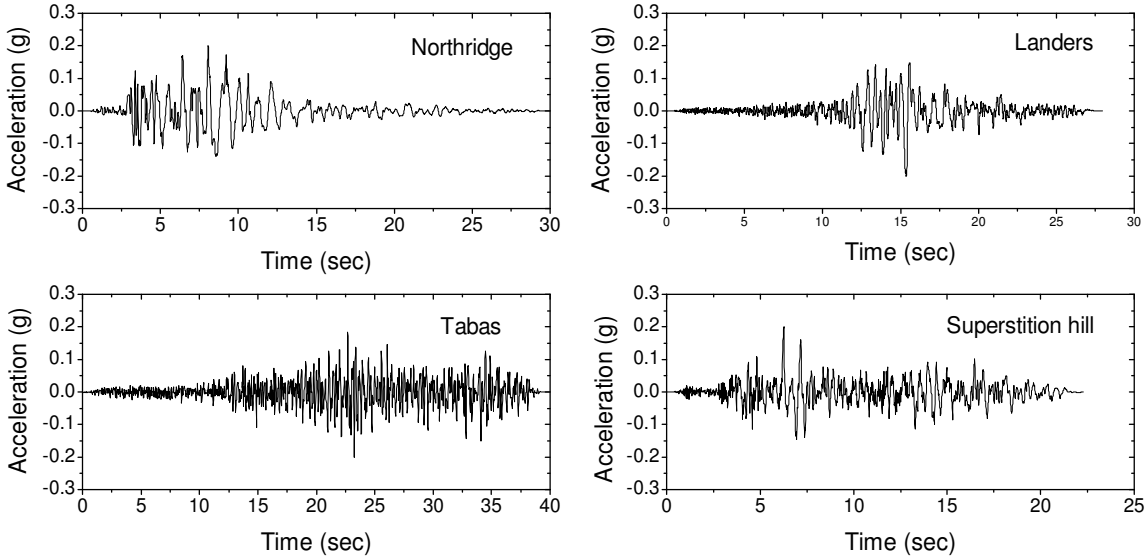

Figure 3.4 Acceleration time histories of far-field earthquakes scaled to PGA = 0.2g

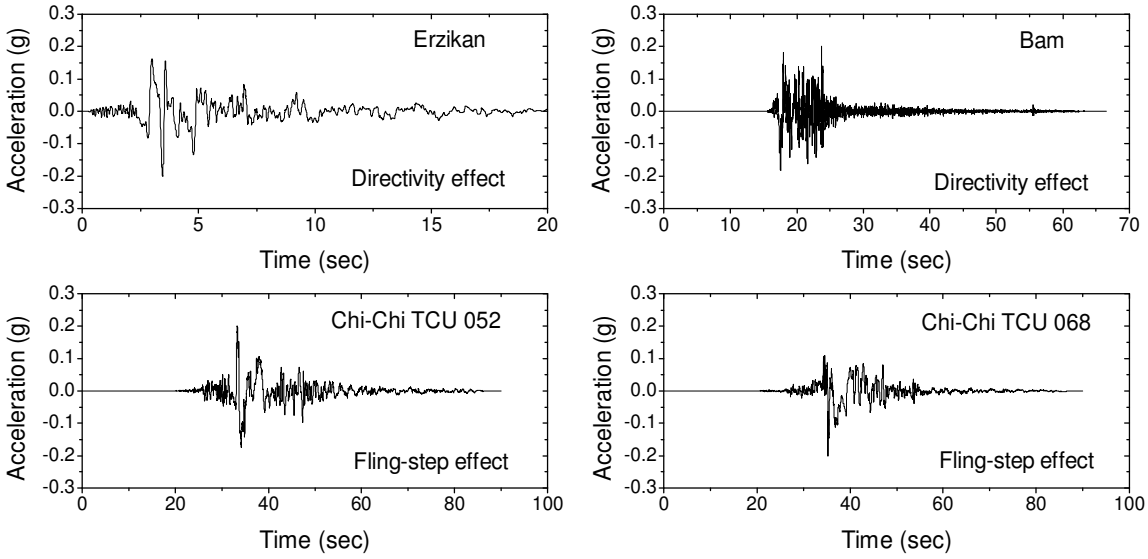

Figure 3.5 Acceleration time histories of near-field earthquakes scaled to PGA = 0.2g

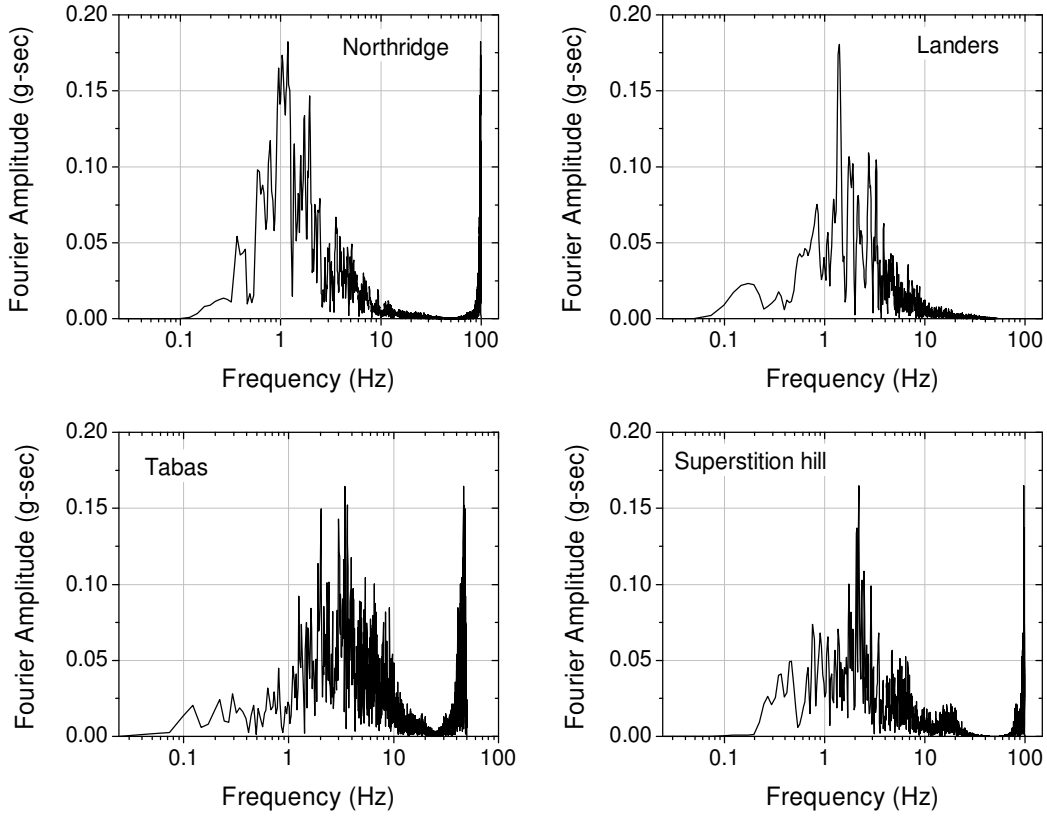

Figure 3.6 The FFT plots of far-field earthquakes

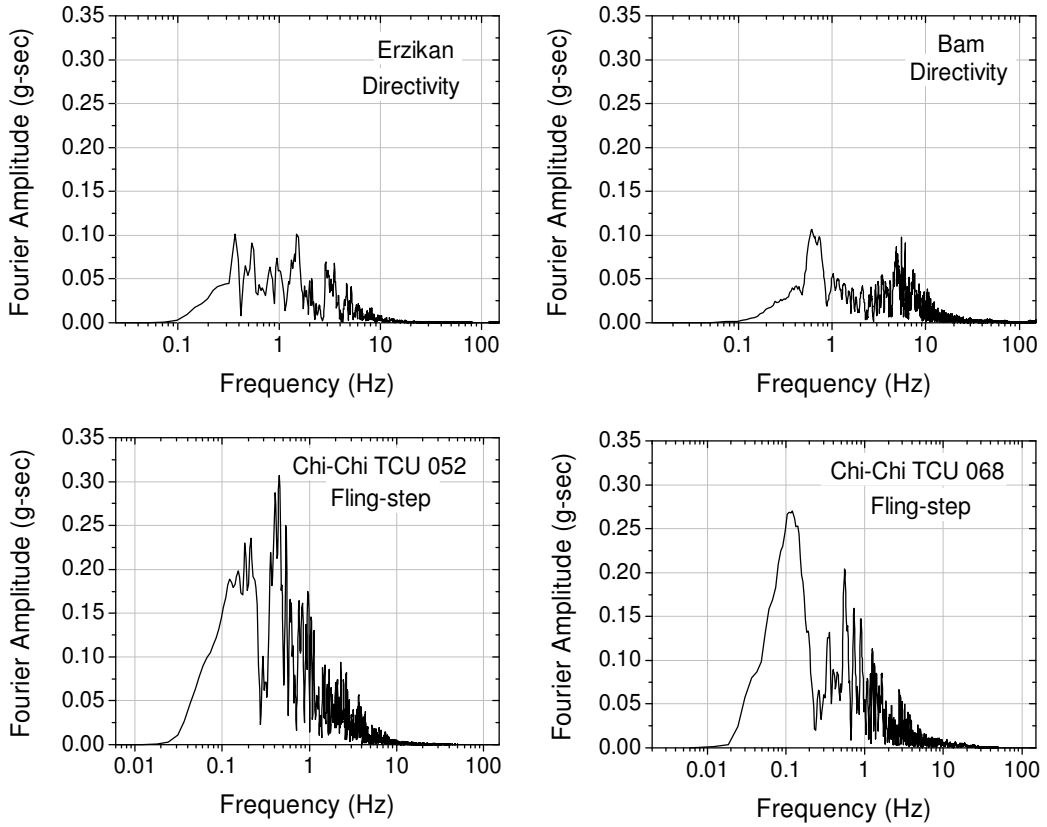

Figure 3.7 The FFT plots of near-field earthquakes

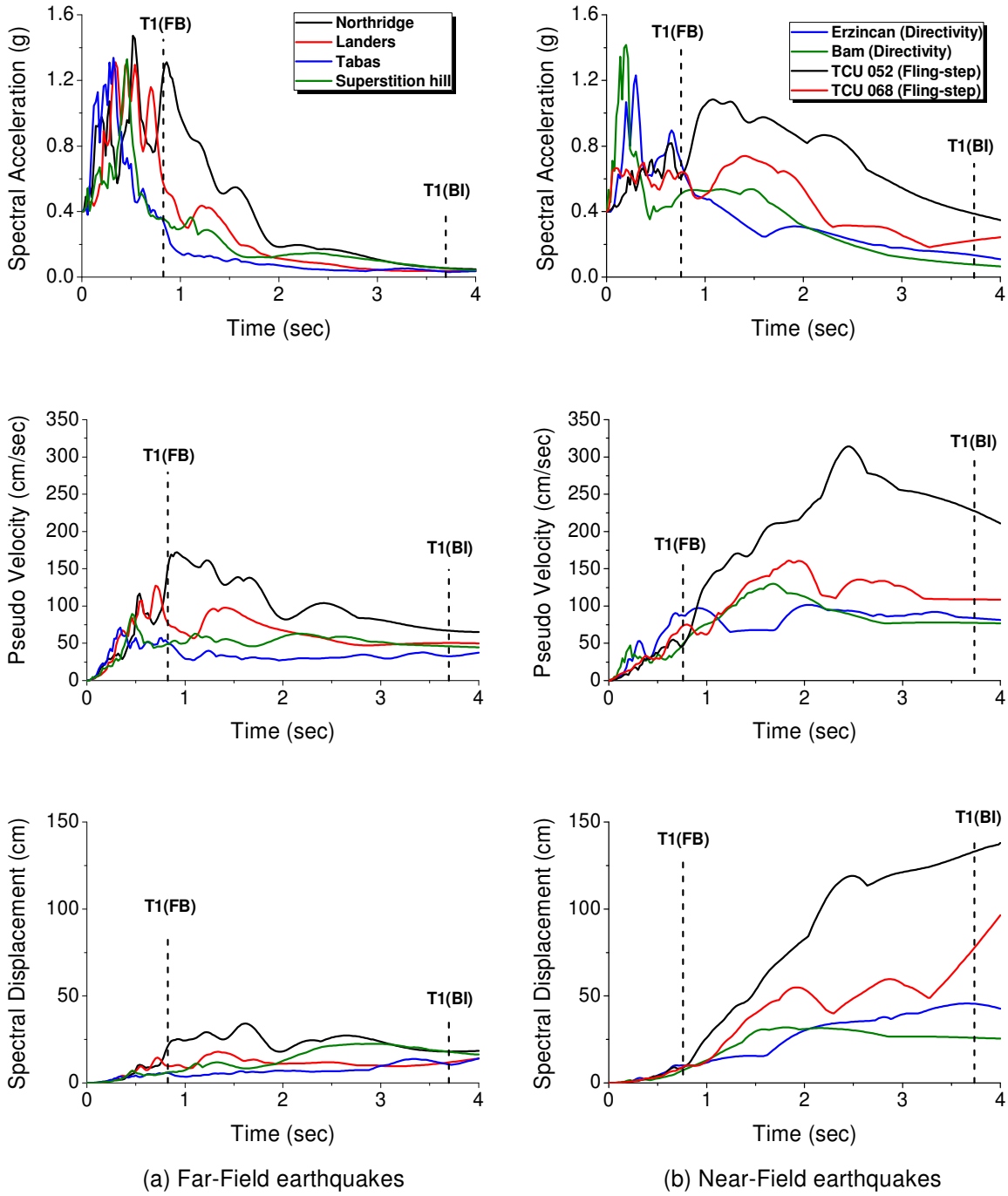

Figure 3.8 Acceleration, velocity, and displacement response spectra (5% damping) of far and near-field records scaled to PGA level of 0.4g along with first fundamental period (T1) of fixed base (FB) and base isolated (BI) frame marked with dotted lines

3.4.1 Modeling and Design of Superstructure

A ten-storey reinforced concrete building with a special moment resisting frames, base-isolated with lead rubber bearings, is considered as a test example. The building is symmetric in its plan having six spans in the longitudinal direction and three spans in the transverse direction of the equal length of 5 m as shown in **Figure 3.9(a)**. The height of each storey is 3.2

m giving a total height of 32 m to the building. The size of all columns is 650 mm x 650 mm, all beams have the same size of 450 mm x 650 mm, and the thickness of slab for all floors is 150 mm.

A typical internal frame in the transverse direction, indicated with red dotted lines in **Figure 3.9(a)**, is considered in the analysis whose elevation view is shown in **Figure 3.9(b).** A two-dimensional model of the frame is created in SAP (2000) software, which is widely used for nonlinear dynamics analysis. The nonlinear behavior of the 2-D frame is modeled by defining the default plastic hinges at the ends of beams and columns at a relative length of 0.1L and 0.9L of element. Default hinge properties of SAP2000 as per FEMA-356 provide moment (M3) hinges to beams considering bending moment and provide coupled bending moment and axial force (P-M3) hinges to columns taking into account the interaction of axial force and bending moment. The moment-rotation characteristics of plastic hinges is defined by five points (A, B, C, D, and E) as shown in **Figure 3.9(c)**.

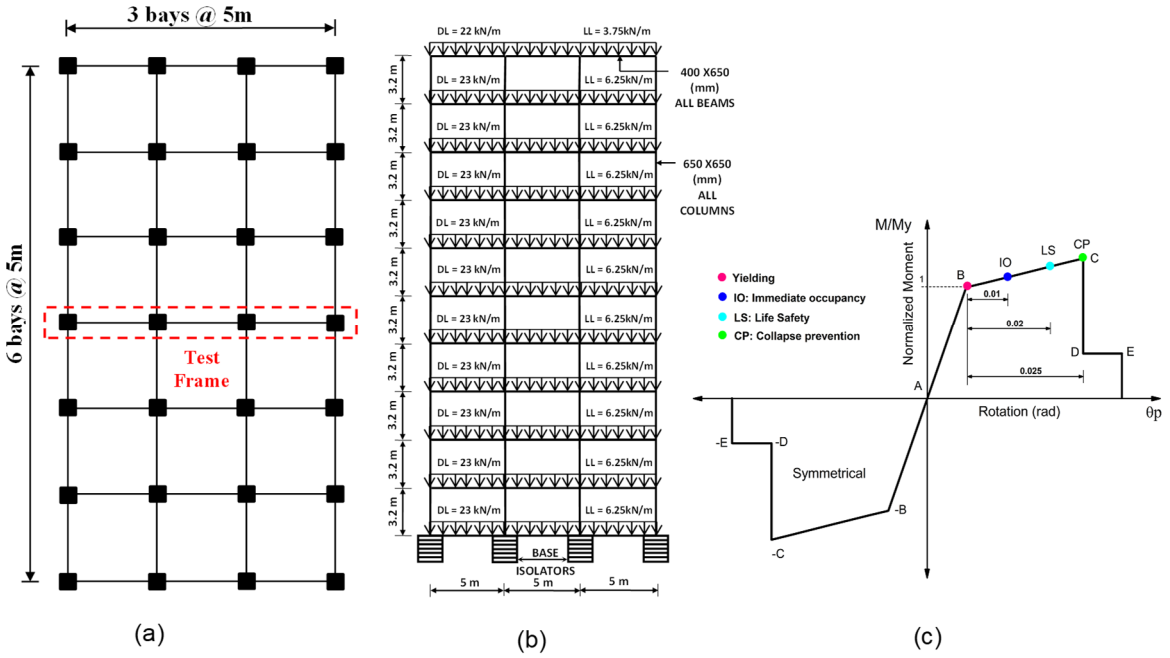

Figure 3.9 Details of building: (a) plan view; (b) elevation view of test frame; (c) typical moment-rotation curve of plastic hinge and acceptance criteria (IO, LS, and CP) as per FEMA-356

The typical rotation values corresponding to the different points on the curve is also shown in the same figure. The default modeling parameters and acceptance criteria for reinforced concrete beams and columns are given in Tables 6-7 and 6-8 of FEMA-356, which are incorporated for default hinges in SAP2000.

The members of the frame are designed according to the Indian standard reinforced concrete code, IS-456 (2000). The gravity loads considered on the frame are represented by dead load of 22 kN/m, on the top floor, and 23 kN/m, on the other floors and a live load having a value of 3.75 kN/m is considered the on the top floor, and 6.25 kN/m, on the other floors.

The seismic design of the building frame is done as per the requirements of the Indian seismic code, IS-1893 (2016), assuming that the building is located in a high seismic zone, classified as the zone (V), Z = 0.36, importance factor (I) = 1, and for medium type (M) soil conditions. Full dead load and 25% of live load are considered in the seismic design. The reinforcement provided in the beams and columns are as per the design carried out by the SAP2000. The plastic moment capacities at the hinge sections are automatically calculated by the SAP2000.

The material properties used in the design include: (i) Cylindrical compressive strength of concrete as 40 MPa; (ii) Modulus of elasticity of concrete, E as 31620 MPa; (iii) Poisson's ratio of concrete, $\nu = 0.2$ and; (iv) Yield Strength and ultimate strength of steel rebar as 415 MPa and 534 MPa respectively. The fundamental vibration periods in the horizontal direction of the base-isolated frame and its fixed base variant are 3.7 seconds and 0.82 seconds respectively.

3.4.2 Modeling and Design of Isolation System

The lead rubber bearings (LRB) are used as an isolation system in the frame. The lead rubber bearing is similar to the laminated rubber bearing which consists of alternate layers of natural or synthetic rubber vulcanized between steel shims along with two thick end plates with the additional central lead core, as shown in **Figure 3.10(a).** The steel plates are strong enough to sustain vertical load, while rubber layers impart horizontal flexibility. The horizontal flexibility of system limits the transmission of ground motions into buildings, whereas isolation damping dissipates seismic energy thereby reduces the base displacement. These bearings are widely studied and implemented in the New Zealand and therefore, sometimes referred as NZ system. This system typically behaves as hysteretic type due to the presence of lead core having a diameter ranging from 15% to 33% of the bonded diameter of the bearing. This type of bearing provides an elastic restoring force and an appropriate size of lead plug, which produces the required amount of damping. The energy-absorbing capacity of the lead core increases the damping of a system that results in limiting the bearing displacement (Kelly *et al.*, 2010). This system also has good properties of fatigue during cyclic loading at the plastic strains.

The force-deformation behavior of bearing has nonlinear characteristics, and its hysteretic behavior is described by Wen's model (Wen, 1976) as shown in **Figure 3.10(b)**. The schematic diagram of the bearing is shown in **Figure 3.10(c),** and the bearing force generated by this system is expressed as:

$$f_b = c_b \dot{u}_b + \alpha_b k_b u_b + f_z \tag{3.1}$$

where f_z is the restoring force due to the presence of lead core and expressed by:

$$f_z = (1 - \alpha_b) F_y \, q \, z_b \tag{3.2}$$

$$\alpha_b = \omega_b^2 M_t q / F_y \tag{3.3}$$

Where u_b is bearing displacement, F_y is the yield strength, stiffness (k_b), damping (c_b) of the isolator are so selected to provide a desired value of the isolation period, T_b (Eq. 3.4), damping ratio, ξ_b (Eq. 3.5) and yield strength coefficient, F_0 (Eq. 3.6)

$$T_b = 2\pi \sqrt{\frac{M_t}{\alpha_b k_b}} \tag{3.4}$$

$$\xi_b = \frac{c_b}{2 M_t \omega_b} \tag{3.5}$$

The value of the yield strength coefficient (F_0) is estimated by the following expression as:

$$F_0 = \frac{F_y}{W_t} \tag{3.6}$$

Where M_t and W_t are the total mass and weight of the building, including isolation floor, respectively, k_b, c_b, and ω_b are respectively the stiffness, damping and natural frequency of bearing, and α_b is the ratio of post to the pre-yielding stiffness of the bearing and its value for LRB system is equal to 0.1. The z_b is the non-dimensional hysteretic displacement component, and it is solved by using hysteretic model, satisfying the nonlinear first-order differential equation as:

$$q\dot{z}_b = -\beta |v_b| z_b |z_b|^{n-1} - \tau v_b |z_b|^n + A v_b \tag{3.7}$$

Where q is the yield displacement of the bearing, β and τ are the strengthening coefficient of the lead plug that controls the shape and size of the hysteresis loop, n and A are the integer constant that controls the smoothness of transition from elastic to a plastic state. The parameters, τ, n and A are so selected to provide a rigid-plastic shape (typical Coulomb-friction behavior).

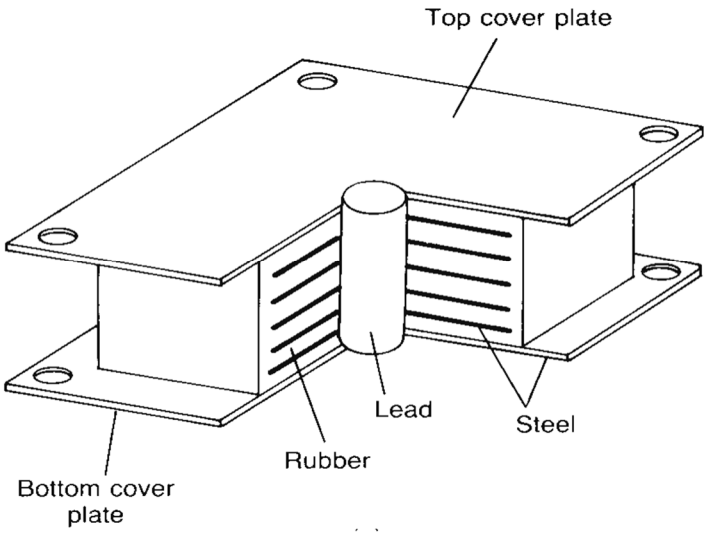

(a) Cross-sectional view

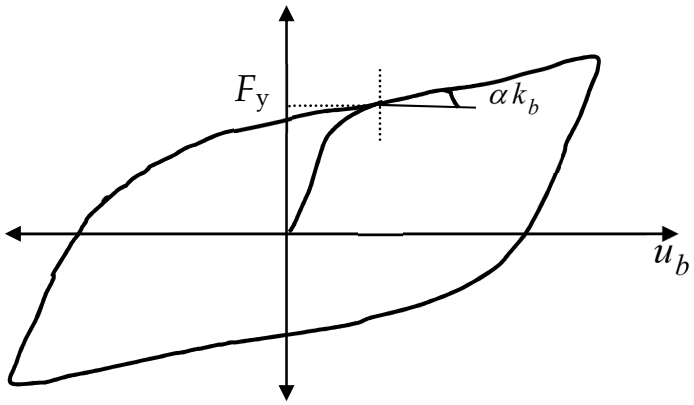

(b) Force-deformation behavior

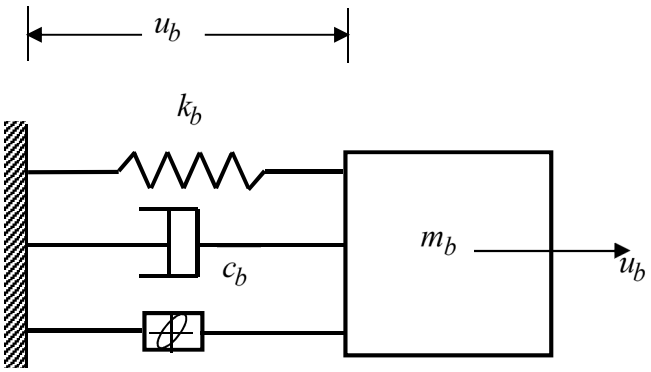

(c) Schematic diagram

Figure 3.10 Lead rubber bearing (NZ system)

The idealized bilinear force-deformation behavior of LRB is based on Bouc-Wen (Park *et al.*, 1986; Wen, 1976) hysteretic model and is shown in **Figure 3.11**. The characteristics of the bilinear force-deformation model are defined by important design parameters including: (i) elastic stiffness, k_1; (ii) post-yield stiffness, k_2; (iii) yield strength, F_y; and (iv) characteristic strength, Q. The aforementioned parameters are calculated as described by Kelly and Naeim (Naeim and Kelly, 1999) and are given below:

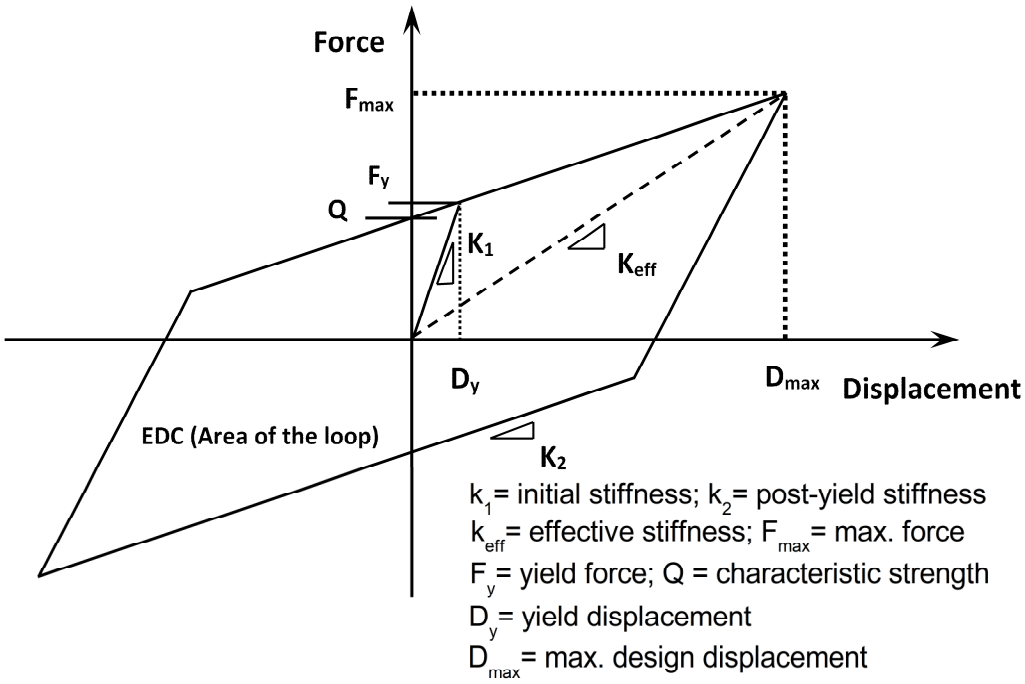

Figure 3.11 The idealized bi-linear curve of LRB isolator

The post-yield stiffness, k_2 is given by the formula:

$$k_2 = \frac{GA_r}{H} \tag{3.8}$$

where A_r is the cross-sectional area of rubber layer, G is the shear modulus of rubber, and H is the total thickness of all rubber layers composing LRB.

The elastic stiffness, k_1 is expressed as the ratio of the yield strength to the yield displacement, $k_1 = F_y/D_y$ and the yield strength of LRB is given by:

$$F_y = Q + k_2 \times D_y \tag{3.9}$$

where D_y is the yield displacement and Q is the characteristic strength of LRB provided by the lead core, which is given by

$$Q = f_{py} \times A_p \tag{3.10}$$

where f_{py} represents the yield strength of the lead core in shear and A_p is the cross-sectional area of the lead core.

The characteristic strength, Q, is also related to k_1, k_2, and D_y as per the following equation:

$$Q=(k_1 - k_2)D_y \tag{3.11}$$

The effective stiffness of LRB, K_{eff}, for a given design maximum displacement, D_{max} can be obtained by:

$$K_{eff} = k_2 + \frac{Q}{D_{max}} \tag{3.12}$$

The effective damping ratio, β_{eff} per cycle, is given by:

$$\beta_{eff} = \frac{4(D_{max} - D_y)Q}{2\pi K_{eff} D^2} \tag{3.13}$$

The energy dissipation (EDC) is the area covered by the hysteretic curve in each cycle as shown in **Figure 3.11** is given by:

$$EDC = 4Q(D_{max} - D_y) \tag{3.14}$$

Isolators are modeled in SAP2000 as non-linear link elements which are used to connect one joint of the frame to the ground. A link element act as one joint grounded spring and is composed of six springs, each for six-deformational degrees of freedom namely, axial, shear, torsion, and pure bending (CSI, 2010). The characteristics of the force-deformation curve are fed manually into the rubber isolator link property data sheet in SAP2000. Base isolator properties which have been used for the analysis of base-isolated building are taken as effective stiffness, K_{eff} = 713 kN/m, initial stiffness, k_1 = 5419 kN/m, effective damping, β_{eff} = 0.1, Post-yield stiffness ratio, γ = is varied as 0.05, 0.10, 0.15, yield force, F_y = 59.61 kN, Vertical stiffness, K_v = 200687 kN/m. For the numerical study, the post to pre-yield stiffness ratio defined by γ is considered as 0.10. The effect of γ on the response behavior of the isolated structure is separately studied at the end. The fundamental period of the 10-storey base-isolated frame is 3.7 seconds, and its fixed base version have 0.82 seconds.

3.5 Discussion of the Results

In order to investigate the behavior of the base-isolated building frame, taken as an illustrative example, responses are critically examined under the two assumed levels of earthquakes (PGA = 0.2g and 0.4g) considered in the present study. At the lower PGA level,

the base-isolated structure is expected to behave elastically or to get into the inelastic state marginally by showing the formation of plastic hinges. At the higher PGA level, the plastic hinges are formed in the base-isolated frame. **Table 3.2** shows some typical values of the response parameters for PGA level of 0.4g. It is clearly seen from the table that the base-isolated frame gets into the inelastic state at the considered PGA level. However, hinges depicting B state as per **Figure 3.9(c)** are only formed.

The behavior of a specific base-isolated frame taken as a numerical example in this study under different earthquakes is discussed response wise in the following subsections.

Table 3.2 Response quantities for typical far-field and near-field earthquakes at PGA = 0.4g

Earthquake	Frame type	Base shear (kN)	Top storey abs. acc. (m/sec2)	Max. storey drift (mm)	Peak top floor disp. (mm)	Peak 1st floor disp. (mm)	Isolator disp. (mm)	Nonlinear hinges					
								B	IO	LS	CP	D	E
Northridge (FF)	FB	2108	5.23	29.93	166.66	16.26		113	3	0	0	0	0
	BI	604	2.28	4.09	196.8	183.36	180	45	0	0	0	0	0
Reduction		71%	56%	86%	-18%								
Landers (FF)	FB	1422	5	20.88	132.9	8.8		94	0	0	0	0	0
	BI	421	1.93	3.41	119	99	95.58	21	0	0	0	0	0
Reduction		70%	62%	84%	11%								
Bam (NF-D)	FB	1828	4.77	29.58	160.6	15.6		103	0	0	0	0	0
	BI	744	1.53	7.42	288.96	252.12	790	38	0	0	0	0	0
Reduction		70%	62%	84%	11%								
Chi-Chi TCU 052 (NF-FS)	FB	2780	4.64	61	360	41		91	33	5	0	1	2
	BI	2278	2.8	44	1238	1006	962	92	23	2	0	0	0
Reduction		18%	40%	28%	-244%								

FF = Far-field; NF= Near-field; D = Directivity effect; FS= Fling-step effect

3.5.1 Maximum Top Floor Displacement

Figures 3.12(a-d) show the typical time histories of top floor displacements for both far-field and near-field earthquakes with PGA level of 0.2 g and 0.4 g. For the near-field earthquakes, responses for two types namely, with directivity and fling step effects are shown. It is seen from the figures that the response time history of the fling-step earthquake is distinctly different than other earthquakes. Further, the maximum top floor displacement is significantly

large. This is due to the fact that the fling-step effect suddenly induces a large displacement in the isolator.

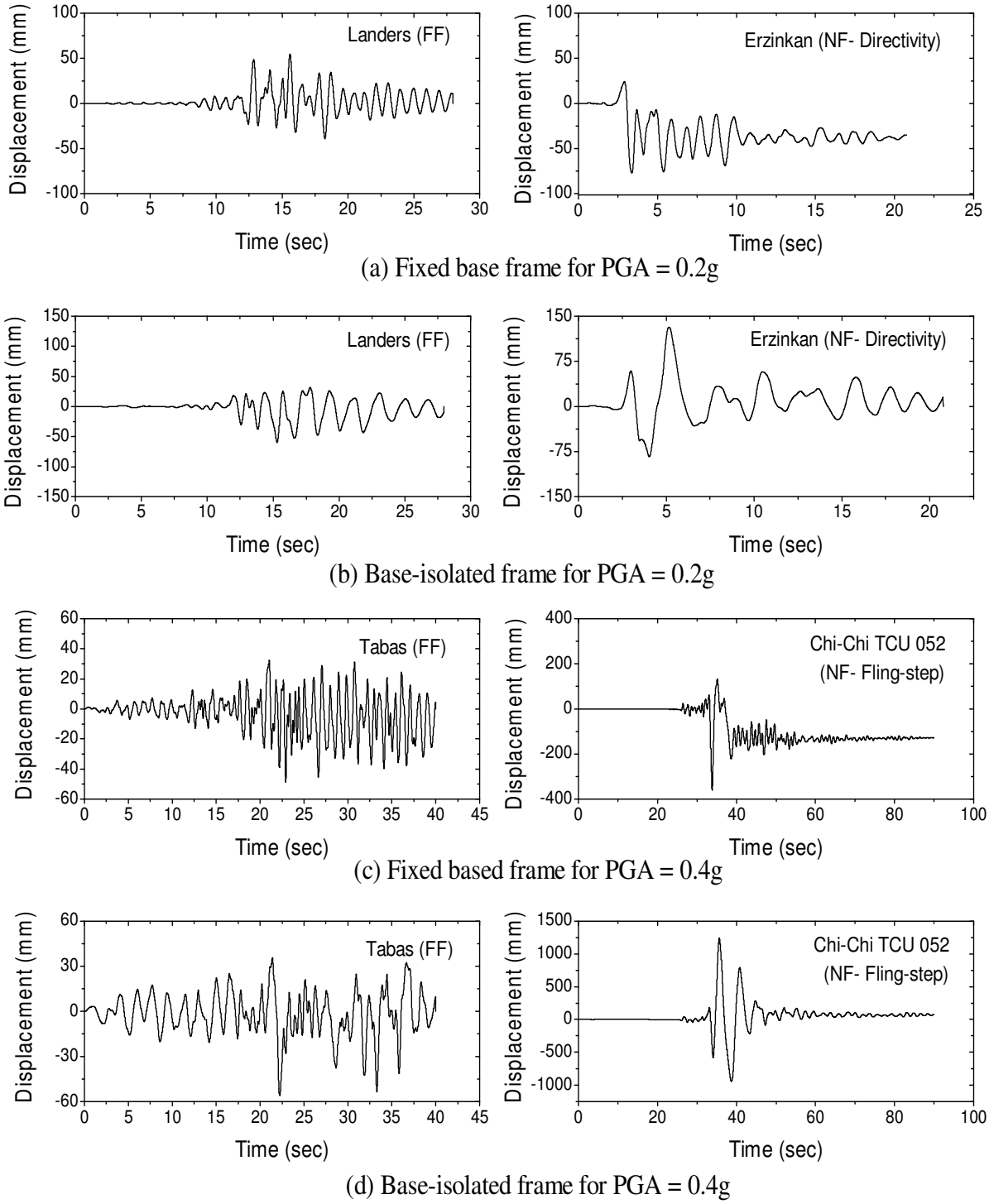

Figure 3.12 Time histories plots of top floor displacement for the fixed base and base-isolated frames for typical far-field (FF) and near-field (NF) earthquakes at two PGA levels

The height-wise maximum storey displacement profiles for both building frames under the action of different type of earthquakes are represented in terms of the storey drift ratio (SDR), which is defined as the maximum storey displacement normalized by the building height and is shown in **Figures 3.13 and 3.14** for two considered PGA levels.

It is observed from the figures that at both PGA levels, there is a significant difference between the SDR demands of far-field and near-field earthquakes for both fixed base and base-isolated frames. For the fixed base frame, as expected, the SDR demands significantly increases with increase in the storey level. Moreover, the difference in the SDR demands between the near and far field earthquakes is very less at PGA = 0.2g as shown in **Figure 3.13(a)**. On the contrary, this difference is significant at the PGA = 0.4g. The difference between the SDR demands for near-field earthquakes with directivity and fling-step effect is more pronounced at PGA = 0.4g as shown in **Figure 3.14(a)**.

For the base-isolated frame, the variation in the SDR demands along the storey level is very less, as expected. The SDR demands are higher for the near-field earthquakes even at lower PGA level of 0.2g in the near-field earthquakes as the structure is significantly pushed due to the presence of pulse type excitation. This effect is more pronounced at the PGA level of 0.4g. Note that the SDR for the near-field (Chi-Chi) earthquakes are largest for both frames.

3.5.2 Force-Displacement Behavior of Isolator

Figures 3.15(a-c) show the typical plots of the force-displacement behavior of the isolators under different types of earthquakes. It is seen from the figures that force-displacement characteristics of the isolators are different for different types of the earthquake and PGA levels. For far-field earthquakes, many cycles of isolator displacement take place, which are closely spaced in the central zone. The area of the hysteresis loop widens at the higher value of the PGA. The hysteretic energy dissipation (HED) by isolator is 8 kN-m at PGA = 0.2g and 45 kN-m at PGA = 0.4g.

For the near-field earthquakes (directivity and fling-step effect), the hysteresis curves elongate and provides large value of isolator displacement at the higher value of the PGA of 0.4g. The numbers of hysteresis cycles within the loop are fewer as compared to that of the far field earthquake. The HED for the nearfield earthquake with directivity effect is 94 kN-m at PGA= 0.2g level and 333 kN-m at PGA = 0.4g. The HED for the nearfield earthquake with fling-step effect is 713 kN-m at PGA = 0.2g level and 2132 kN-m at PGA = 0.4g level. It is observed that for the same level of PGA, the value of HED is very high in case of near field earthquakes as compared to far field earthquake.

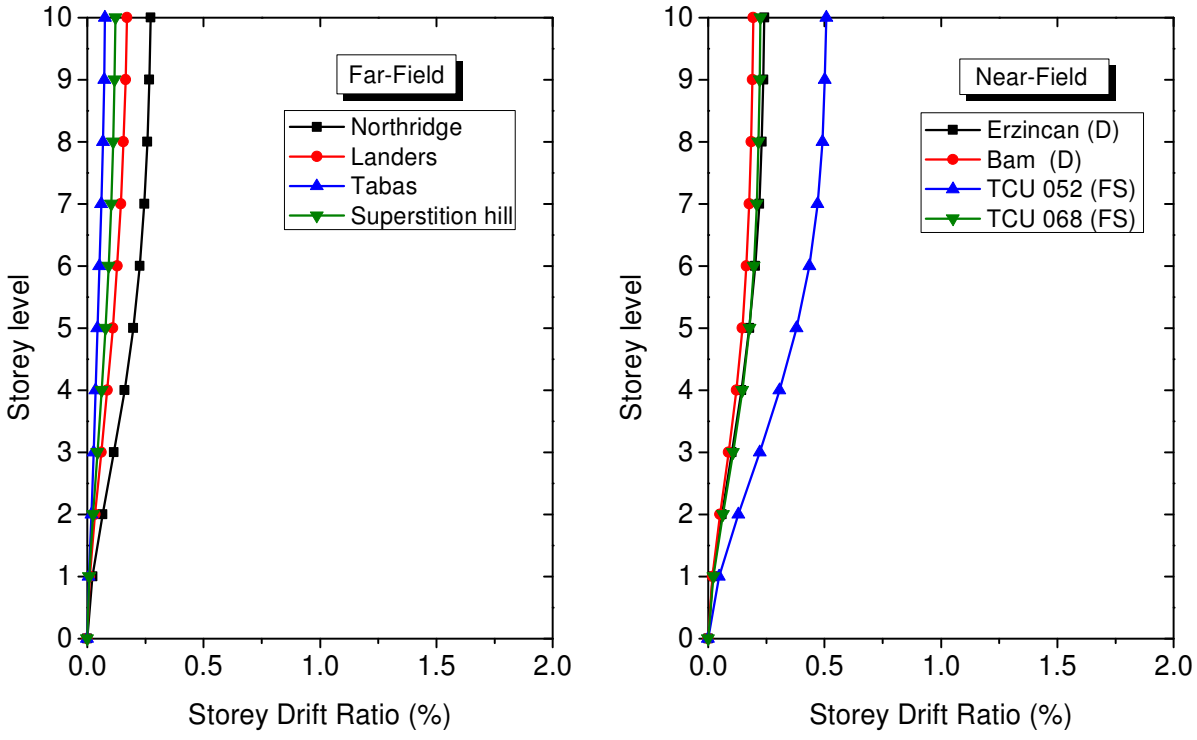

(a) Storey drift ratio for fixed base frame

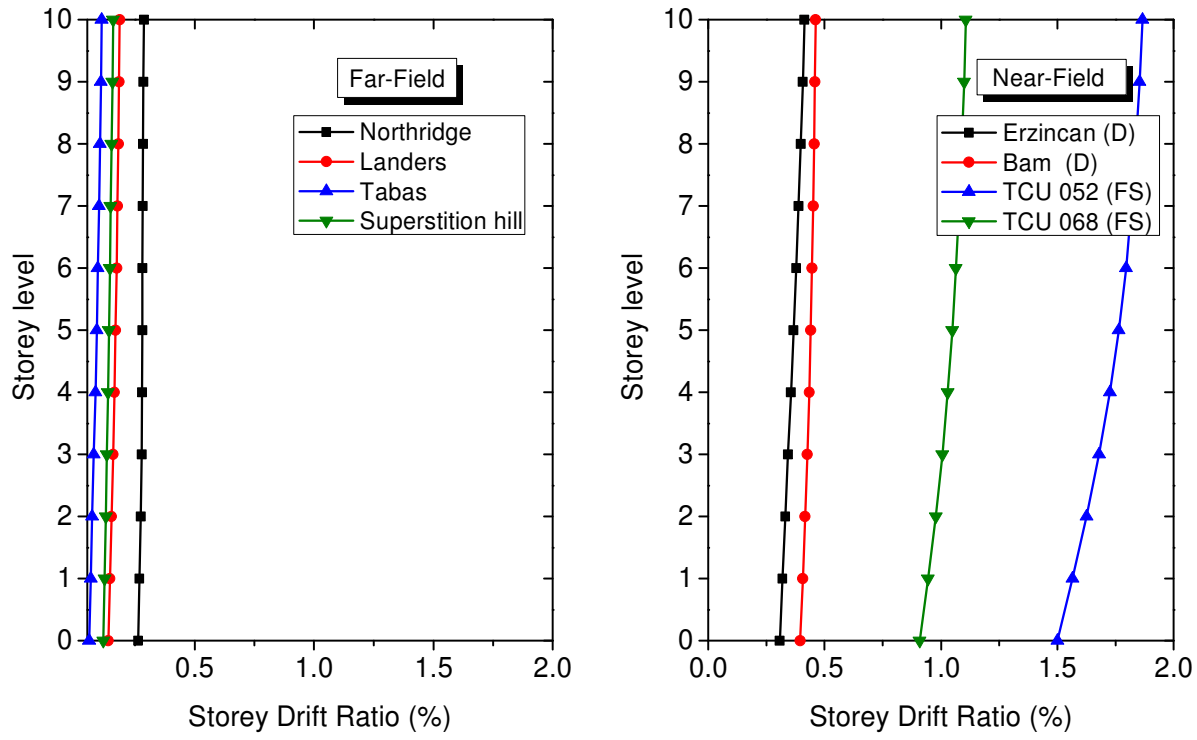

(b) Storey drift ratio for base-isolated frame

Figure 3.13 Height-wise variation in the storey drift ratio under far-field (FF) and near-field earthquake (NF) with directivity (D) and fling-step (FS) effect at PGA = 0.2g

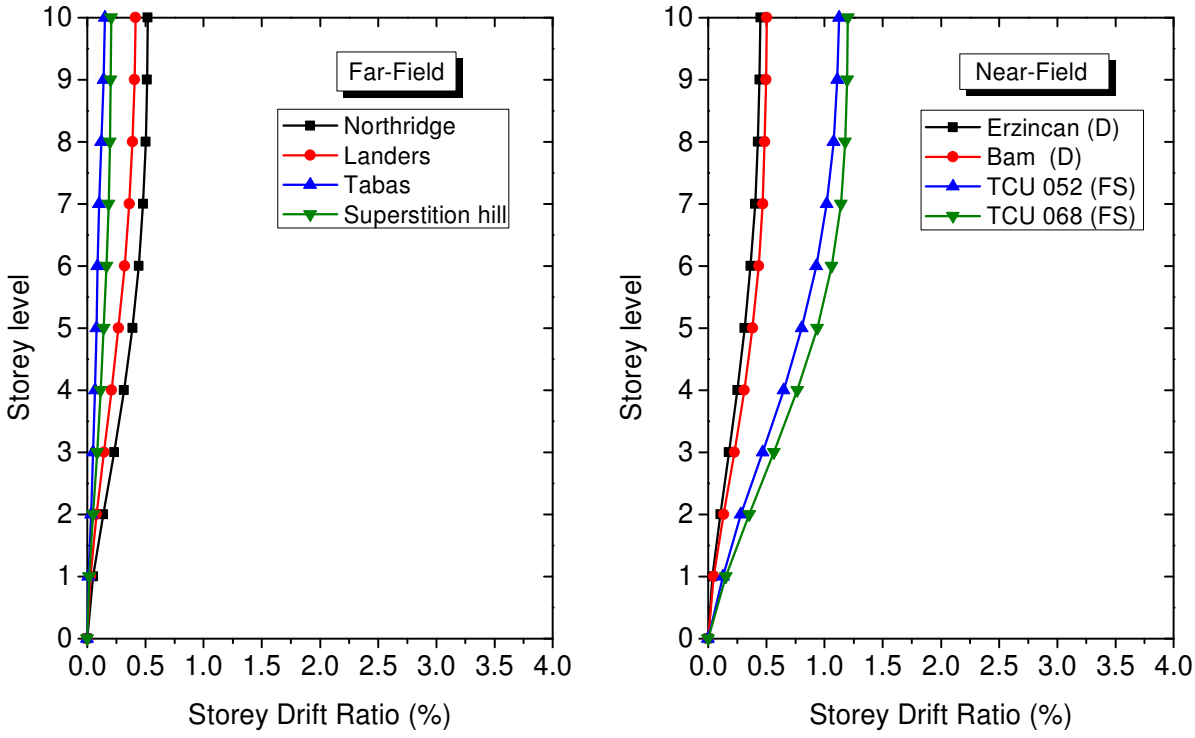

(a) Storey drift ratio for fixed base frame

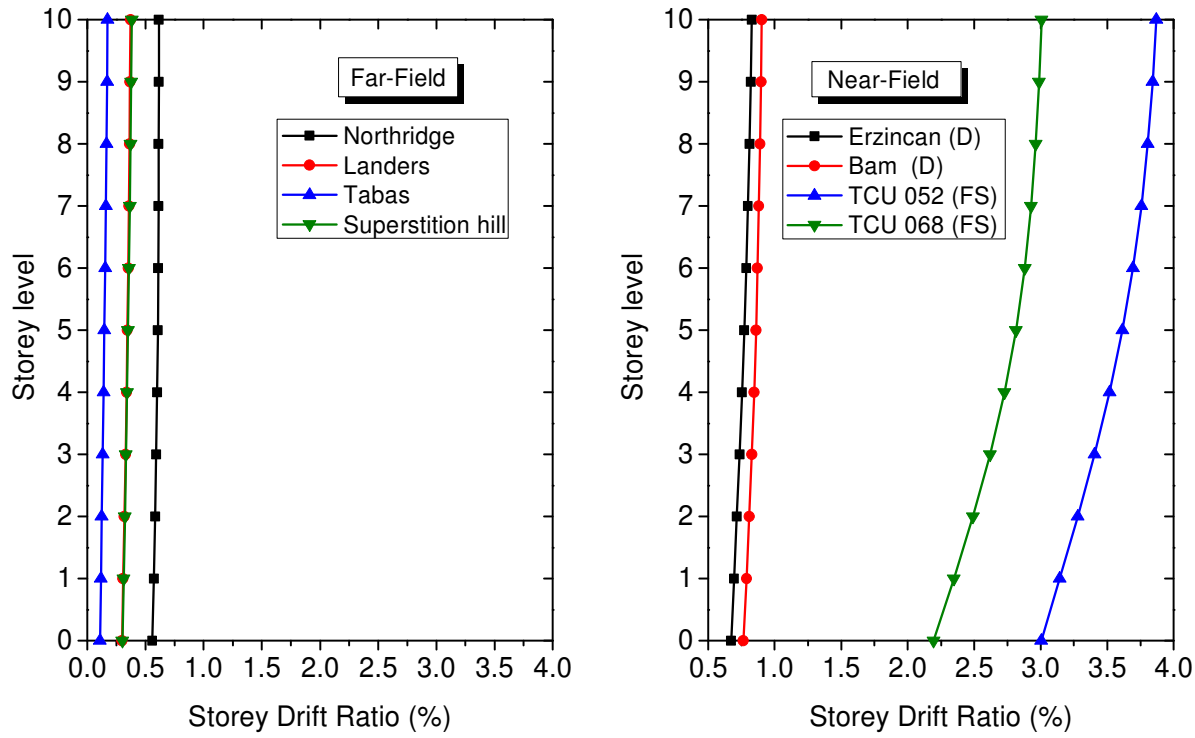

(b) Storey drift ratio for base-isolated frame

Figure 3.14 Height-wise variation in the storey drift ratio under far-field (FF) and near-field earthquake (NF) with directivity (D) and fling-step (FS) effect at PGA = 0.4g

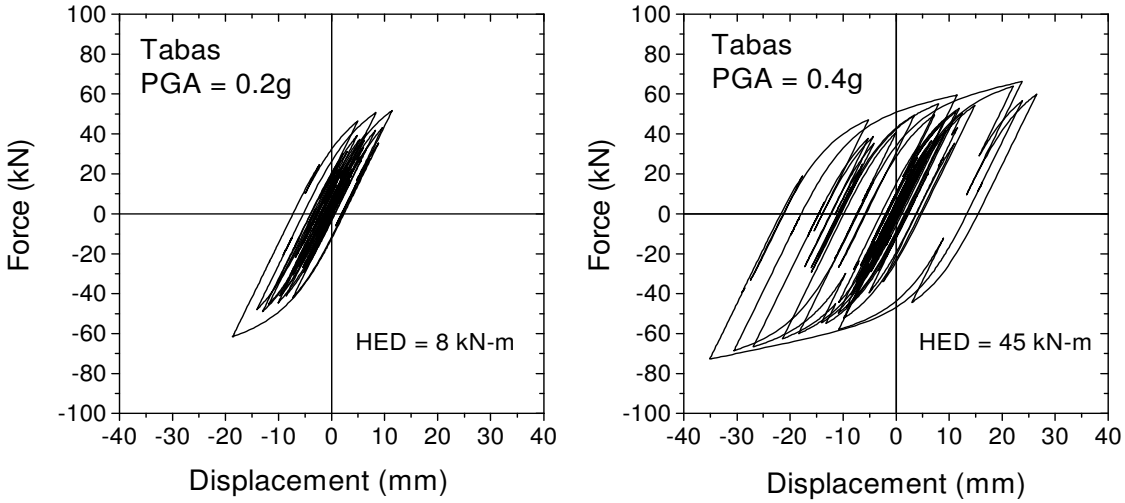

(a) Far field earthquake

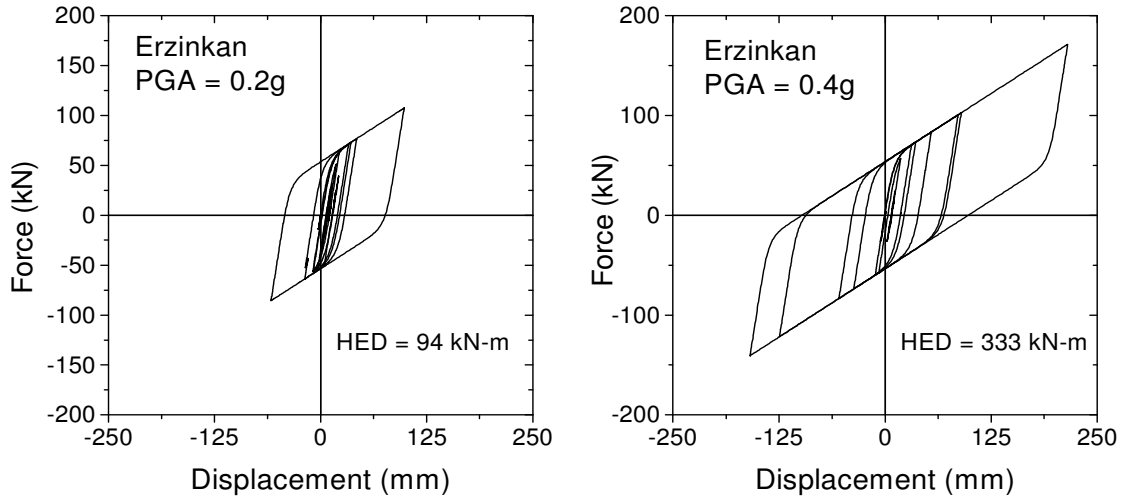

(b) Near field earthquake with directivity effect

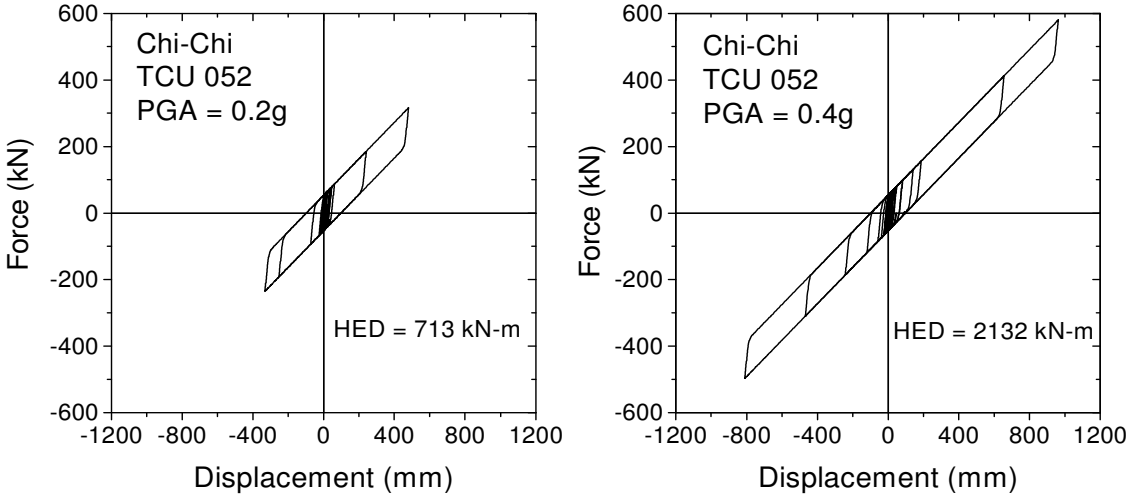

(c) Near field earthquake with fling-step effect

Figure 3.15 Force-displacement curves for isolator for typical earthquakes

3.5.3 Maximum Isolator Displacement

Figure 3.16(a and b) shows the maximum isolator displacement under near and far field earthquakes at the two PGA levels. The maximum isolator displacement depends on the PGA level. For the earthquakes with 0.4g, the maximum isolator displacement is nearly about two times that for PGA level of 0.2g. The maximum isolator displacement considerably increases for near-field earthquakes as compared to far-field earthquakes. Out of the two types of near-field earthquakes, the fling-step earthquake provides very large maximum isolator displacement, especially for the upper level of the PGA.

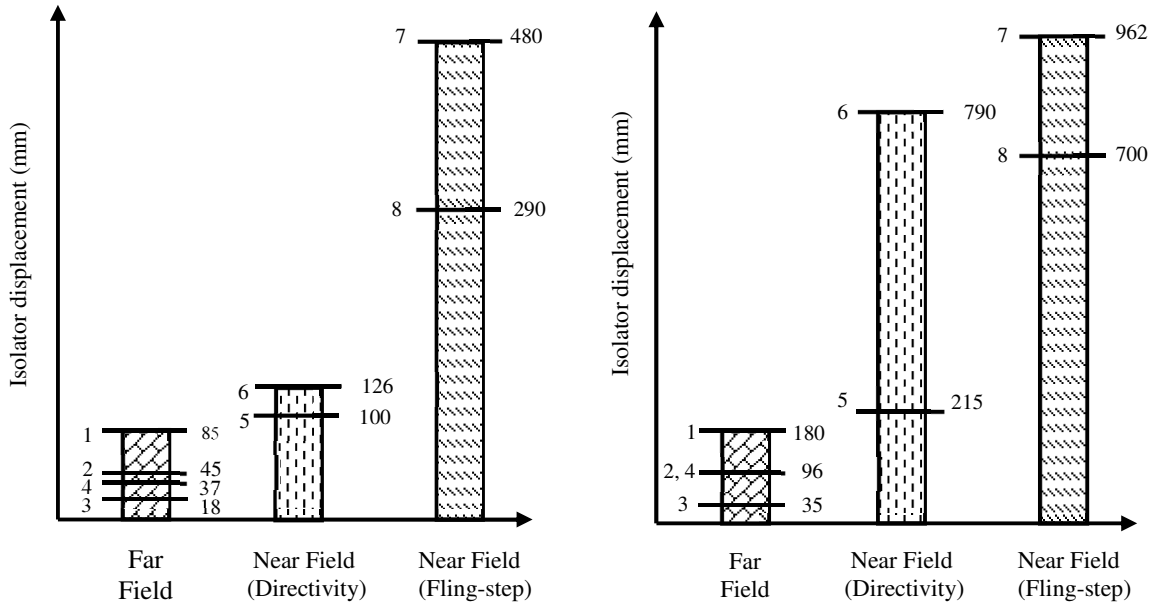

1. Northridge; 2. Landers; 3. Tabas; 4. Superstition hill; 5. Erzincan; 6. Bam; 7. Chi-Chi TCU 052; 8. Chi-Chi TCU 068

(a) PGA = 0.2g (b) PGA = 0.4g

Figure 3.16 Maximum isolator displacement under near-field and far-field field earthquakes at two PGA levels

3.5.4 Base Shear

Figures 3-17(a and b) show the percentage reduction in base shear for the base-isolated frame as compared to the fixed-base condition. It is seen from figures that for both PGA levels, i.e., 0.4 g and lower level, i.e., 0.2 g acceleration, the reductions in the base shear for far-field earthquake vary between 65% and 75%.

For near-field earthquake with directivity effect, the reduction in base shear response is also considerable, of the order of 60 %, for the two levels of the PGA. However, for the near-

field earthquake with fling-step effect, the reduction in base shear is drastically reduced to a value of 18 % for the PGA of 0.4g and 27 % for the PGA of 0.2g. This shows that base isolation for the near-field earthquake with the fling-step effect may prove to be ineffective so far as the reduction of base shear is concerned.

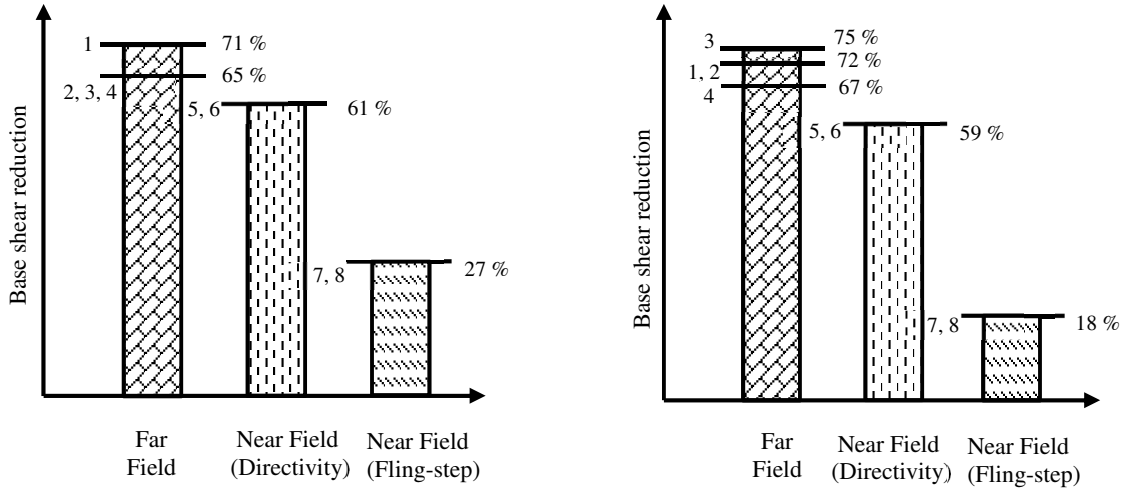

1. Northridge; 2. Landers; 3. Tabas; 4. Superstition hill; 5. Erzincan; 6. Bam; 7. Chi-Chi TCU 052; 8. Chi-Chi TCU 068

(a) PGA = 0.2g (b) PGA = 0.4g

Figure 3.17 Percentage reduction in base shear

3.5.5 Top Storey Absolute Acceleration

Figures 3.18(a and b) show the reduction of top storey absolute acceleration for the base-isolated structure for far-field and near-field earthquakes. The reduction in the top storey absolute acceleration widely varies with different earthquakes, far field earthquakes in the range of 50 % - 78 % for both PGA levels. For the near-field earthquake with directivity effect, the response reduction of top storey absolute acceleration is found to be considerable, which varies between 62 % and 74 % for both levels of PGA. For near-field earthquake with fling-step effect, the effectiveness of base isolation for the reduction of top storey absolute acceleration is reduced but not as much as the case of base shear. The reduction typically varies between 40 % to 60 %.

3.5.6 Maximum Inter-Storey Drift

Figures 3.19(a and b) show the percentage reduction in maximum inter- storey drift. There is a wide variation in percentage reduction in the maximum inter-storey drift depending upon the type of earthquake. For far-field earthquakes, the maximum reduction could be of the order of 87 % for both levels of the PGA. The minimum reduction could be as low as 40 % observed for the PGA level of 0.2 g. For near-field earthquake with directivity effect, the

reduction in maximum inter-storey drift is quite significant, i.e. of the order of 71 % - 75%. Base isolation is found to be quite ineffective for the reduction of storey drift for the near-field earthquake with fling-step effect as the reduction in maximum inter-storey drift is found to be of the order of 20 % - 30 %.

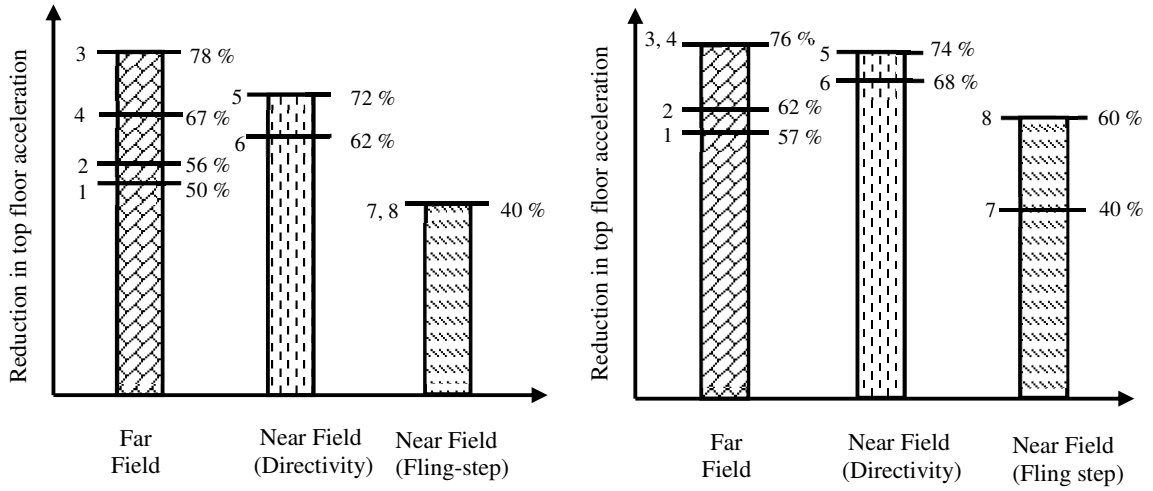

1. Northridge; 2. Landers; 3. Tabas; 4. Superstition hill; 5. Erzincan; 6. Bam; 7. Chi-Chi TCU 052; 8. Chi-Chi TCU 068

(a) PGA = 0.2g (b) PGA = 0.4g

Figure 3.18 Percentage reduction in top floor absolute acceleration

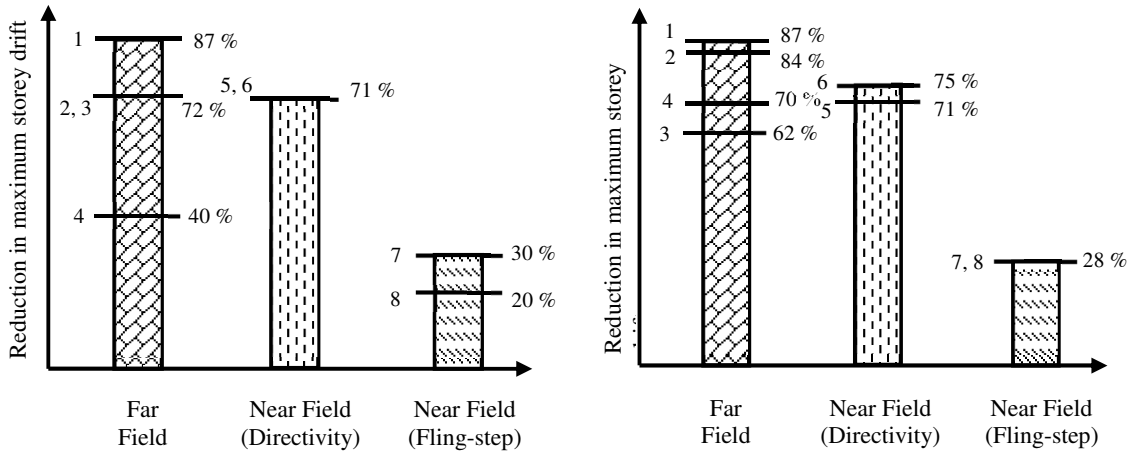

1. Northridge; 2. Landers; 3. Tabas; 4. Superstition hill; 5. Erzincan; 6. Bam; 7. Chi-Chi TCU 052; 8. Chi-Chi TCU 068

(a) PGA = 0.2g (b) PGA = 0.4g

Figure 3.19 Percentage reduction in maximum inter-storey drift

The height-wise variation of the inter-storey drift ratio is shown in the **Figures 3.20 and 3.21** for the fixed base and base-isolated frames at PGA levels of 0.2g and 0.4g. It is observed from the figures that the maximum inter-storey drift occurs between 2^{nd} – 6^{th} storey levels. The Chi-Chi earthquake induces maximum drift demands both in the fixed base and the base-isolated frames at both PGA levels. For the same earthquake, the drift demands are comparable in both fixed base and base-isolated building frames, which shows the ineffectiveness of base isolation system towards the response (inter-storey drift) induced by the high energy pulses present in the near-field Chi-Chi earthquake records. The inter-storey drift demands produced by near-field directivity earthquake are lower than that of fling-step effect. There is a large reduction in the inter-storey drift demands in the base-isolated frame under far-field earthquakes, which shows the effectiveness of the isolation system for this type of earthquake.

There is a large variation of the maximum inter-storey drift (MIDR) demands imposed by the different far-field and near-field earthquakes. At PGA = 0.2g **(Figure 3.20(a)),** for the fixed base frame, the highest MIDR demand imposed by the far-field earthquakes ranges between 0.1% to 0.5%, which is comparable to those for the near-field earthquakes with directivity effect. For the base-isolated frame, the MIDR demands are drastically reduced for different far-field earthquakes, which ranges from 0.08% to 0.1%. The reduction in the MIDR demand for base-isolated frame is not drastic under near-field earthquakes, which ranges from 0.1% to 0.2% for near-field earthquakes with directivity effect. Near-field earthquakes (Chi-Chi) with fling-step effect imposes high MIDR demands of the order of 0.7%

For the PGA level of 0.4g **(Figure 3.21)** the MIDR demands are increased as expected for both building frames. More interestingly, the demands for the near-field earthquakes are highly amplified. For far-field earthquakes, the MIDR ranges between 0.1% to 1% for the fixed base frame and 0.1% to 0.12% for the base-isolated frame. For near-field directivity earthquakes, the demand ranges between 0.3% to 0.8% for the fixed base frame and 0.2% to 0.4% for the base-isolated frame. For near-field earthquakes with fling-step, the demand ranges between 0.4% to 2.2% for the fixed base frame and 0.4% to 1.6% for the base-isolated frame.

Thus, the MIDR demands induced by the near-field earthquakes are highly amplified as compared to the those for far-field earthquakes with an increase in the PGA level. At the upper PGA level, the MIDR demands for the base-isolated frame is comparable to those for the fixed-base frame under the effect of near-field earthquakes for both directivity and fling-step effect. Therefore, at the higher level of PGA, the base-isolation system is not effective in terms of reducing MIDR demands.

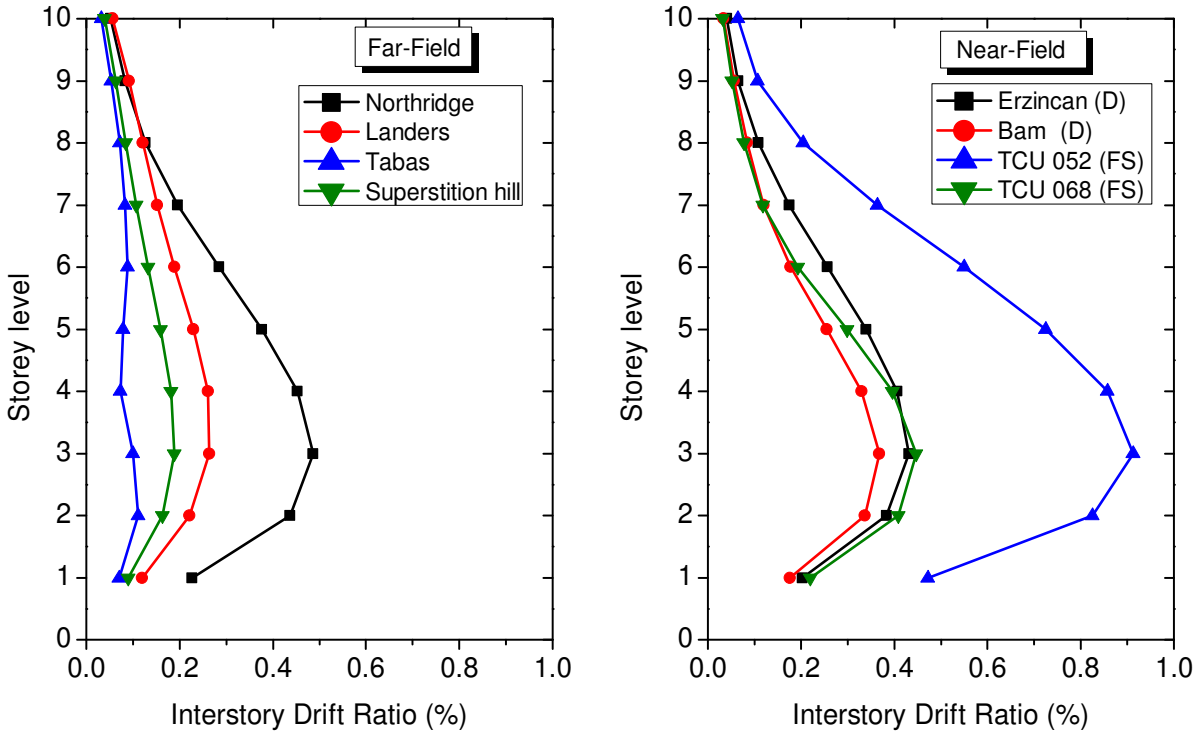

(a) Inter-story drift ratio for fixed base frame

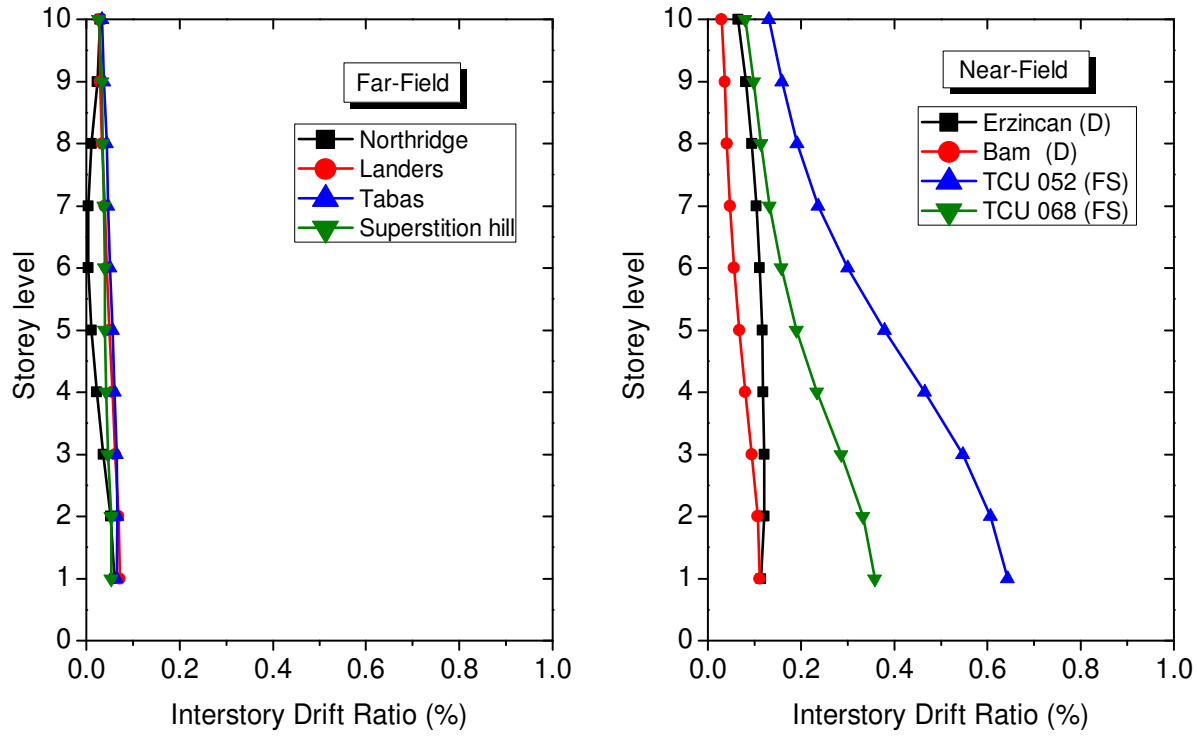

(b) Inter-story drift ratio for base-isolated frame

Figure 3.20 Height-wise variation in the inter-storey drift ratio under far-field (FF) and near-field earthquake (NF) with directivity (D) and fling-step (FS) effect at a PGA = 0.2g

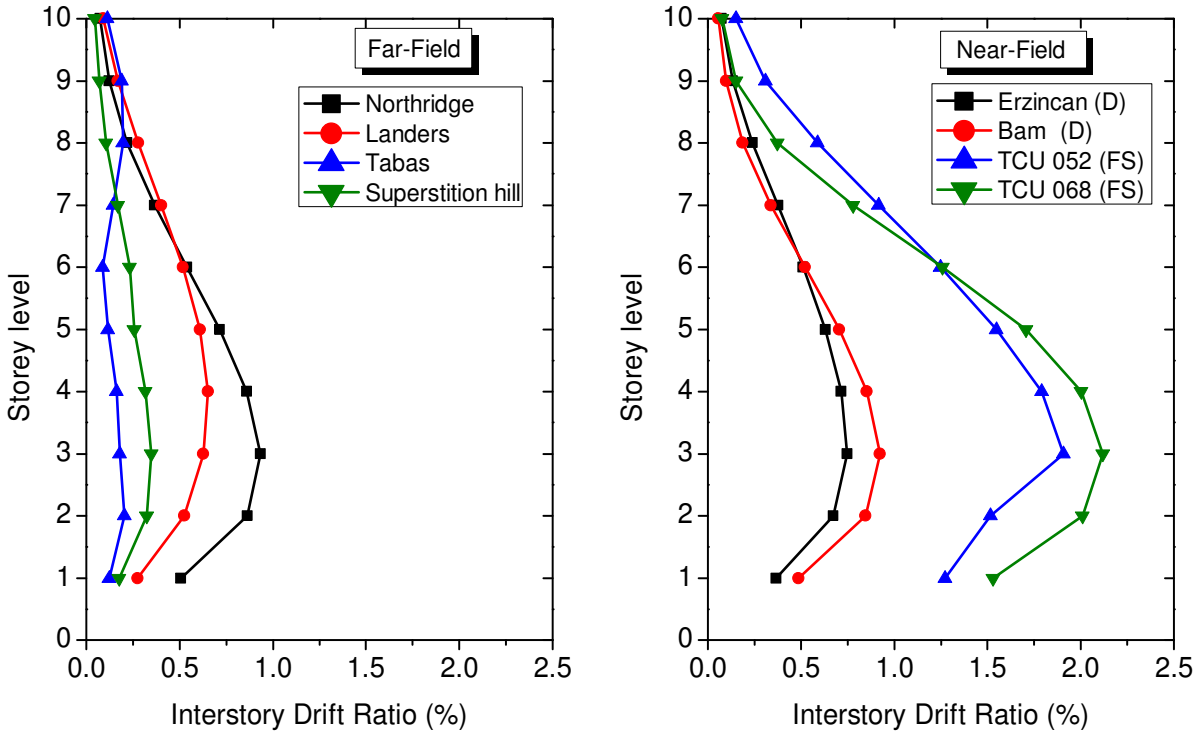

(a) Inter-story drift ratio for fixed base frame

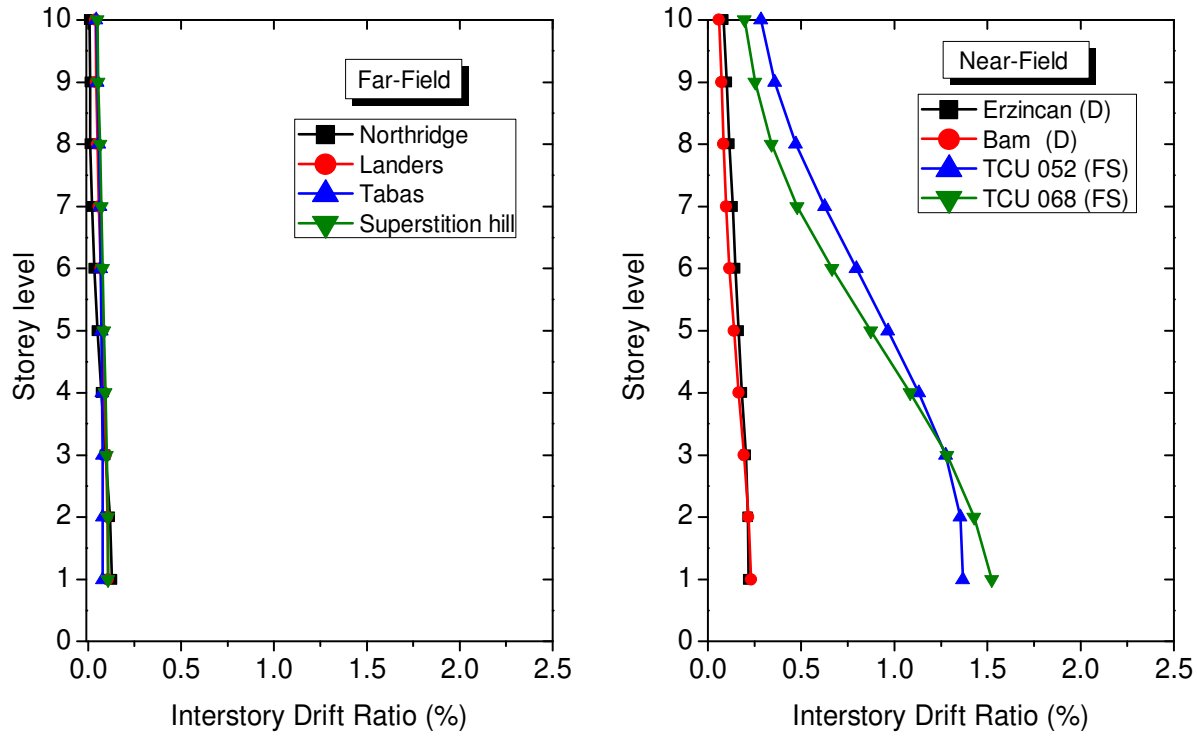

(b) Inter-story drift ratio for base-isolated frame

Figure 3.21 Height-wise variation in the inter-storey drift ratio under far-field (FF) and near-field (NF) earthquakes with directivity (D) and fling-step (FS) effect at a PGA = 0.4g

3.5.7 Number of Plastic Hinges and Hinge Pattern

For most of the base-isolated structures, it is expected that the structure will remain in the elastic range for the lower level of the PGA, whereas for an extreme level earthquake, i.e. for the higher level of PGA, the structure may undergo into inelastic excursions.

Figure 3.22(a and b) compare between the plastic hinges formed for the fixed base and base-isolated frames. It is seen from the figure that for the far-field earthquakes, the number of plastic hinges formed at PGA = 0.4g is considerably greater compared to the PGA = 0.2g for fixed base structure, as it would be expected. At PGA = 0.4g, the number of hinges formed in the fixed base structure varies between the 68 and 116. For the base-isolated structure, it is reduced to 12 – 45 showing that at higher level of PGA the base-isolated structure gets into inelastic range, but the extent of the inelastic excursion is considerably reduced.

For the near-field earthquakes, the same observation holds good for earthquakes with directivity effect. For earthquake with fling-step effect, the number of plastic hinges formed in the base-isolated structure is quite large. The inelastic excursion is nearly the same as that for the fixed base case.

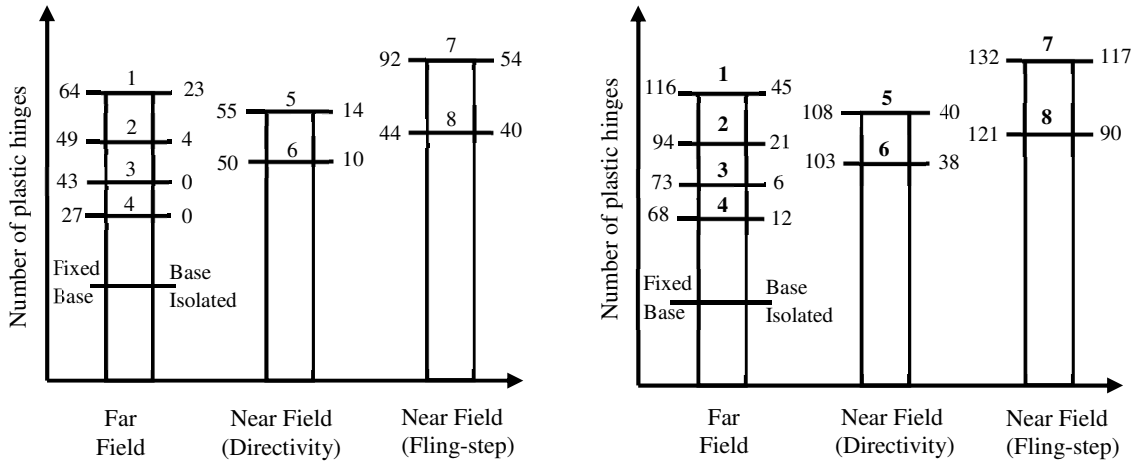

1. Northridge; 2. Landers; 3. Tabas; 4. Superstition hill; 5. Erzincan; 6. Bam; 7. Chi-Chi TCU 052; 8. Chi-Chi TCU 068

(b) PGA = 0.2g (b) PGA = 0.4g

Figure 3.22 Number of plastic hinges for different earthquakes at two PGA levels

The variation in the hinge pattern formed in the fixed base and base-isolated frames for typical far and near-field earthquakes at two PGA levels is shown in the **Figures 3.23 and 3.24**.

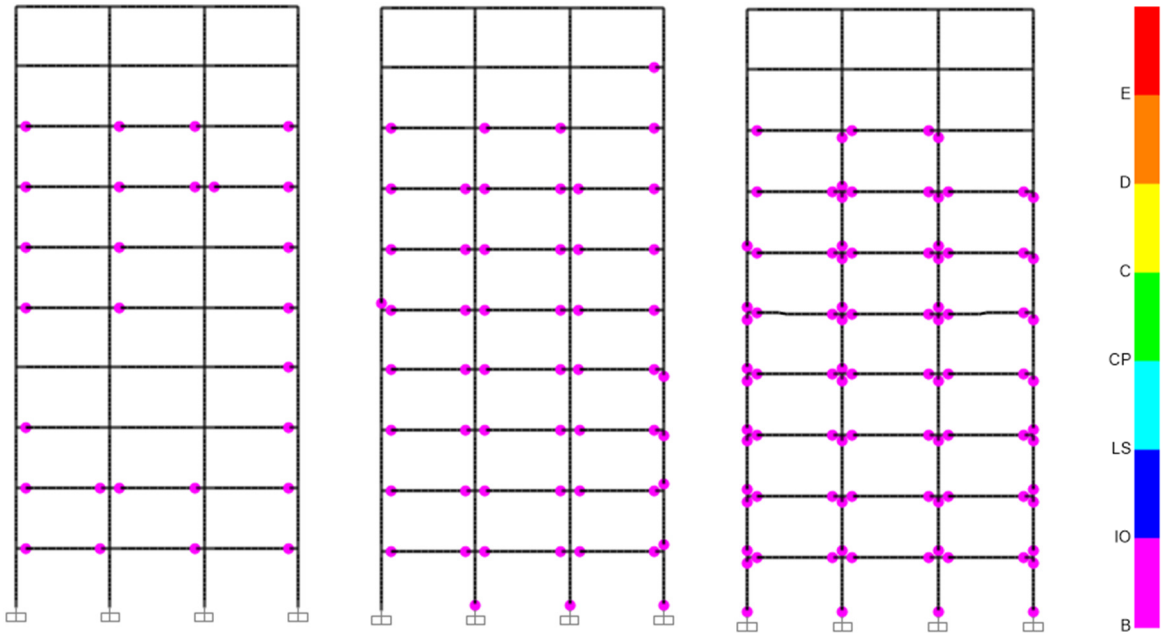

Tabas (27 hinges) (Far-field) | Erzincan (55 hinges) (Near-field, directivity) | Chi-Chi TCU 052 (92 hinges) (Near-field, fling-step)

(a) Plastic hinge pattern in fixed base frames

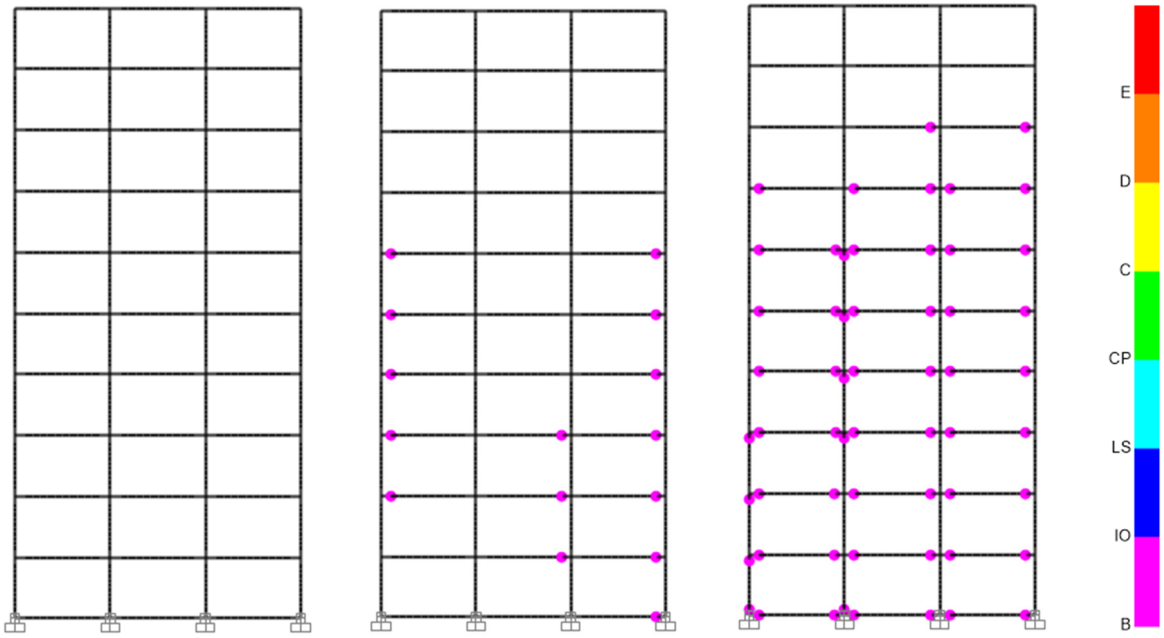

Tabas (0 hinges) (Far-field) | Erzincan (15 hinges) (Near-field, directivity) | Chi-Chi TCU 052 (58 hinges) (Near-field, fling-step)

(b) Plastic hinge pattern in base-isolated frames

Figure 3.23 Plastic hinge pattern formed in fixed base and base-isolated frames under different earthquakes at PGA = 0.2g

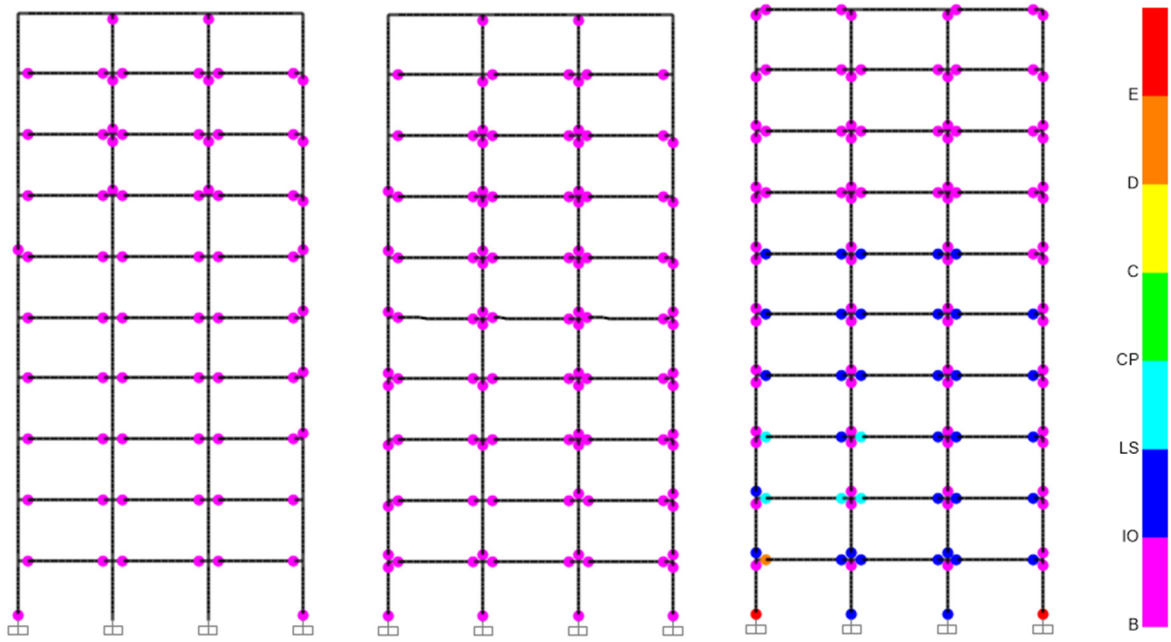

Tabas (73 hinges) (Far-field) | Erzincan (108 hinges) (Near-field, directivity) | Chi-Chi TCU 052 (132 hinges) (Near-field, fling-step)

(a) Plastic hinge pattern in fixed base frames

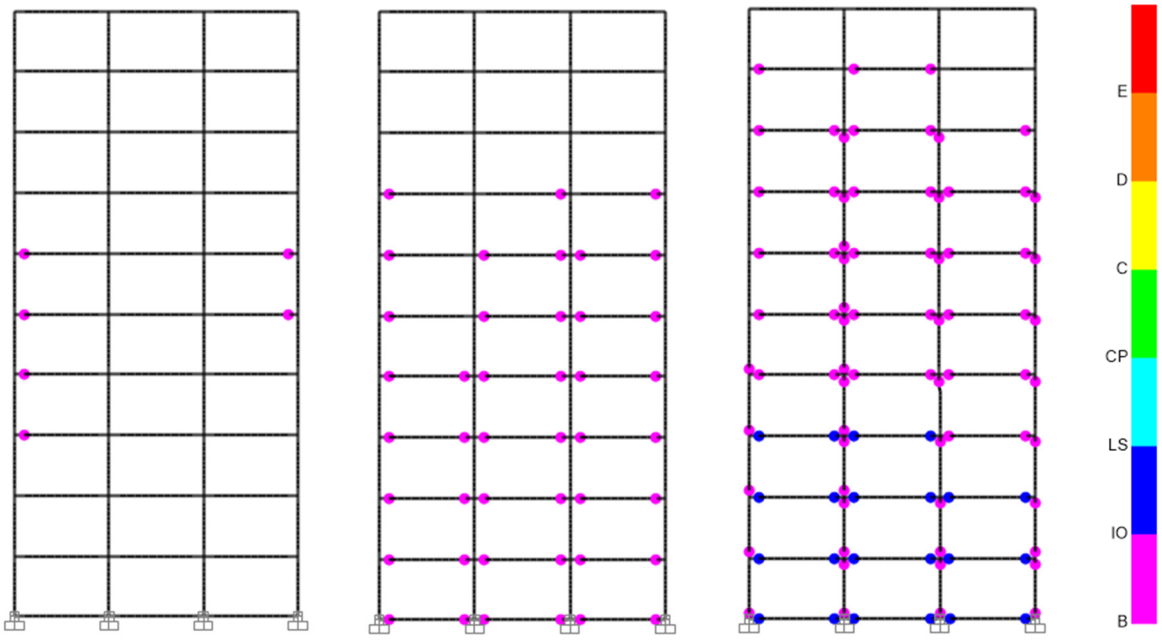

Tabas (6 hinges) (Far-field) | Erzincan (40 hinges) (Near-field, directivity) | Chi-Chi TCU 052 (117 hinges) (Near-field, fling-step)

(b) Plastic hinge pattern in base-isolated frames

Figure 3.24 Plastic hinge pattern formed in fixed base and base-isolated frames under different earthquakes at PGA = 0.4g

The inelastic performance of the building frame is investigated by prediction of plastic hinge formation in the fixed base (FB) and base-isolated (BI) subjected to near and far-field earthquakes. The plastic hinges are formed against different performance levels (B, IO, LS, CP) as per FEMA 356 given in **Figure 3.9(c).** It is observed from the **Figures 3.23 and 3.24** that there is no hinge formation in the base-isolated frame for far-field earthquake (Tabas) at 0.2g and only 6 B level hinges are formed at 0.4g as compared to the fixed base frame, which shows the high effectiveness of a base isolation system.

The same trend in the pattern of plastic hinges is observed in the near-field earthquake (Erzincan) with directivity effect, but the formation of plastic hinges is more in the base-isolated frame as compared to that for the far-field earthquakes. On the contrary, there is a large number of plastic hinges formed in the base-isolated frame in case of a near-field earthquake (Chi-Chi TCU 052) with fling-step effect even at the lower level of PGA = 0.2g. The maximum number of hinges are formed under the same earthquake for both building frames having severe damage up to E level for the fixed base, and there is a reduction of inelasticity in base-isolated condition, but still, the structure goes into the high inelastic state.

For a lower level of the PGA, it is observed that the base-isolated structure either remains in elastic range or marginally gets into the inelastic range for far-field earthquakes. However, for the near-field earthquakes, the base-isolated structure significantly gets into the inelastic range.

3.6 Effect of Post to Pre-Yield Stiffness Ratio

The effect of the post to pre-yield stiffness ratio of the isolator on the behavior of base-isolated building for different earthquakes in terms of different response quantities is shown in **Figure 3.25(a and b)**. From the figures, it is seen that the effect of the post to pre-yield stiffness ratio on the percentage reduction of responses for the considered far-field earthquakes is not significant. For the near-field earthquake with directivity effect, the effect is quite pronounced for base shear and storey drift. For $\gamma = 0.05$, i.e., nearly elastoplastic behavior of isolator is observed, the percentage reduction in storey drift increases significantly. The same thing is observed for a near-field earthquake with fling-step effect. However, the percentage reduction in storey drifts is significantly reduced in the case of a near-field earthquake with fling-step effect.

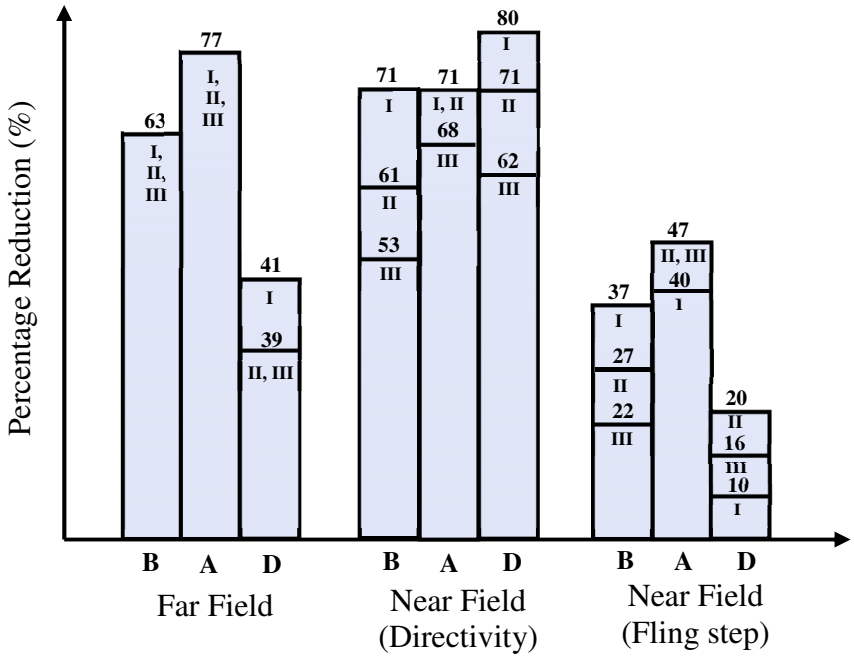

B = Base shear; A = Absolute acceleration; D = Maximum storey drift,
I → γ = 0.05, II → γ = 0.10, III → γ = 0.15

(a) PGA = 0.2g

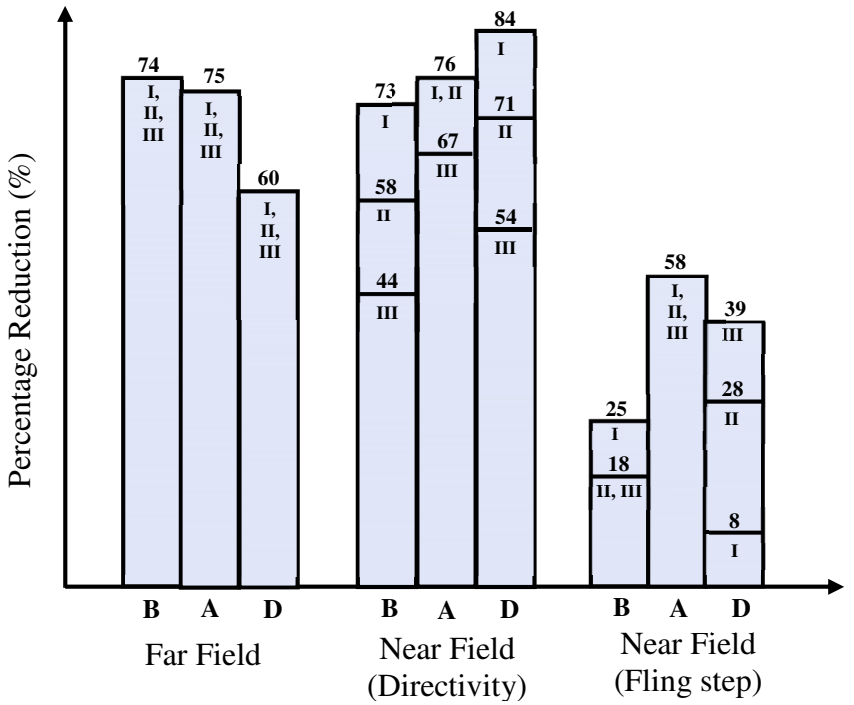

B = Base shear; A = Absolute acceleration; D = Maximum storey drift,
I → γ = 0.05, II → γ = 0.10, III → γ = 0.15

(b) PGA = 0.4g

Figure 3.25 Percentage reduction in response for different value of γ for different type of earthquakes (far-field = Tabas; near-field (directivity) = Erzincan; near-field (fling-step) = Chi-Chi TCU 068

Figure 3.26 (a and b) show the number of plastic hinges formed for different values of γ and for both PGA levels of earthquakes. It is seen from the figure that for a lower PGA level of 0.2g; no plastic hinges are formed for the far-field earthquake for all values of γ, i.e., the isolated structure remains in the elastic range. For the near-field earthquake with directivity and fling-step effects, the isolated structure gets into the inelastic range even for a value of PGA = 0.2g. However, the number of plastic hinges formed is less, especially for the earthquake with directivity effect. The number of hinges formed is not very sensitive to the variation of γ for the near-field earthquake with fling-step effect. For the upper-level of earthquake, i.e., PGA = 0.4g, the isolated structure marginally gets into the inelastic range with very few numbers of plastic hinges formed for a far-field earthquake. For the near-field earthquake with directivity effect, the number of plastic hinges formed for γ = 0.05 is considered very less as compared to the other two values of γ. For the near-field earthquake with the fling-step effect, the isolated structure undergoes large inelastic excursion with the number of plastic hinges formed nearly equal to 103. The number of plastic hinges formed is not sensitive to the variation of γ.

3.7 Design Implementations

From the above discussion of results, it is apparent that the isolators which are designed for the base-isolated building subjected to far-field earthquakes are not suitable for use in the case of near-field earthquakes. The seismic demands on the isolator for the near-field earthquakes are considerably higher, e.g., for the case of 0.2g level of earthquake, the maximum isolator displacements are 480 mm and 290 mm for Chi-Chi TCU 052 E (0.66 km from rupture plane) and Chi-Chi TCU 068 N (0.32 km from rupture plane) earthquakes respectively. For the 0.4g level of earthquake, these displacements increase considerably to about 960 mm and 790 mm for Bam l (1.7 km from rupture plane) and Chi-Chi TCU 052 E (0.66 km from rupture plane) earthquakes respectively. Other special types of isolators are to be designed for accommodating such large isolator displacements without causing instability in the system, or maximum isolator displacement is to be limited to a lower value requiring a hybrid control strategy (base isolator along with an active control device). Further, the maximum ductility demand in the base-isolated structure for the near-field earthquake with fling-step effect (0.2g level) is of the order of 9.66 (**Table 3.3**), and maximum rotation in the plastic hinge is of the order of 0.0076 radians (**Table 4.4**). The corresponding values for the 0.4g level of the earthquake are 14.37 and 0.0236 radians respectively. Therefore, the design

of the superstructure should be able to accommodate such high ductility demand, specifically the rotational demands in the plastic hinges for the 0.4g level of earthquake.

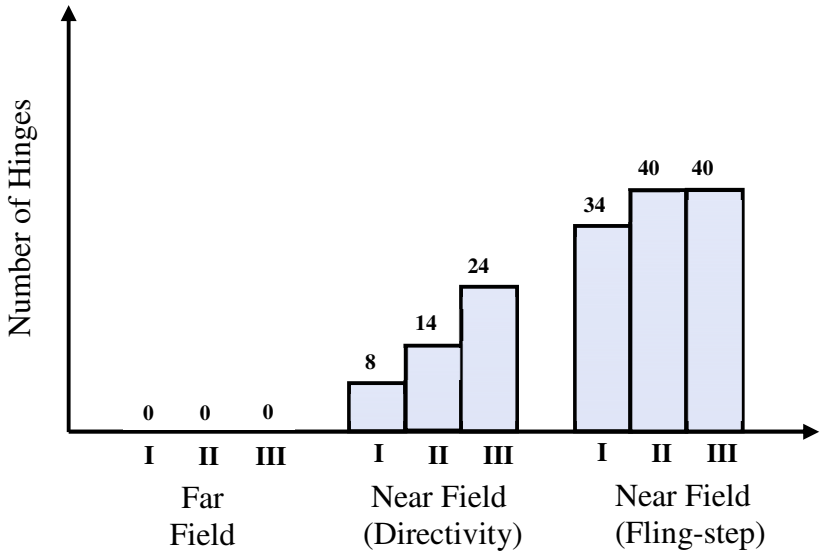

I → γ = 0.05, II → γ = 0.10, III → γ = 0.15

(a) PGA = 0.2g

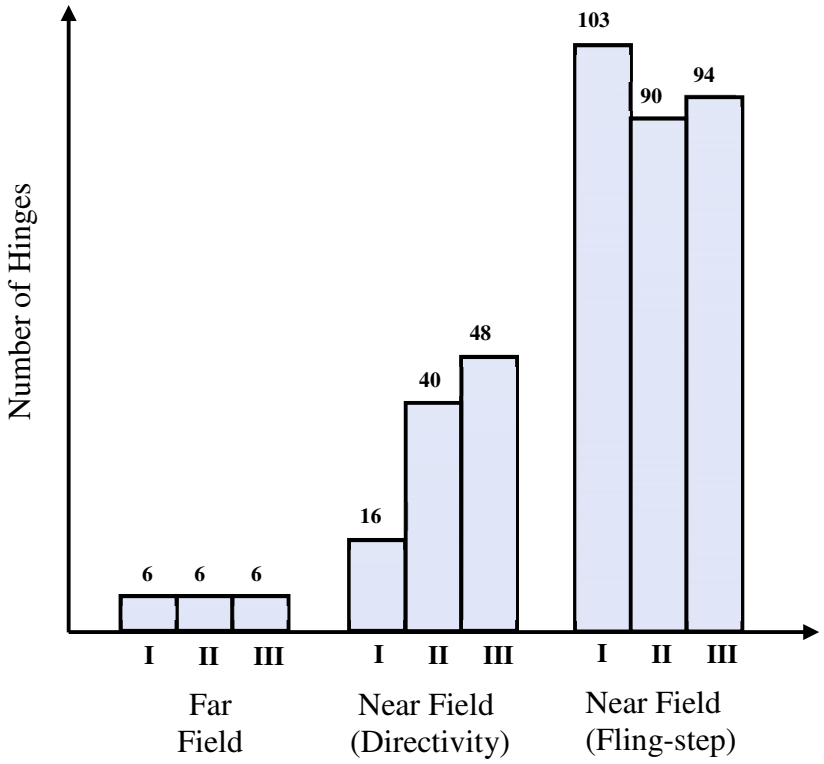

I → γ = 0.05, II → γ = 0.10, III → γ = 0.15

(b) PGA = 0.4g

Figure 3.26 Number of hinges for different values of γ for earthquakes with two PGA levels, far-field = Tabas; near-filed (directivity)= Erzincan; near-field (fling-step) = Chi-Chi TCU 068

Thus, the seismic design of base-isolated structure requires suitable specifications on the limits of the ductility and the plastic rotation in the hinges for the near-field earthquakes. More numerical studies are required in order to obtain such suitable specifications. For special structures like nuclear power plants, some experimental studies have been carried out for high damping rubber bearing isolators to explore maximum and minimum values of isolator displacements for different PGA levels which are possible to achieve (Perotti *et al.*, 2013). The work mentioned above amply demonstrates the need for clear specifications (in probabilistic terms) of maximum base isolator displacement and ductility demands of the isolated structure for the use of base isolation of special structures like the nuclear power plants. No such guidelines are available at present for near-field earthquakes.

Table 3.3 Ductility demand for floor displacement under far-field and near-field earthquakes

Earthquakes	1st-floor ductility				2nd-floor ductility			
	0.2g		0.4g		0.2g		0.4g	
	FB	BI	FB	BI	FB	BI	FB	BI
Landers (FF)	1.94	1	4.80	4.12	5	1	8	2.42
Erzincan (NF, D)	3.70	2.65	6.28	5	3.98	2.25	8.80	3.90
Chi-Chi TCU052 (NF, FS)	10.8	9.6	23.44	14.37	9.66	9	23.27	13.96

FB = fixed base; BI = base-isolated; FF = far-field; NF = near-field; D = directivity; FS = Fling-step

Table 3.4 Maximum rotation in the plastic hinge

Earthquakes	Maximum Plastic hinge rotation (radians)			
	0.2g		0.4g	
	FB	BI	FB	BI
Landers (FF)	0.00208	0.00005	0.00656	0.00002
Erzincan (NF, D)	0.00401	0.000264	0.00775	0.00126
Chi-Chi TCU052 (NF, FS)	0.00985	0.00758	0.03458	0.02358

FB = fixed base; BI = base-isolated

The need for a different design specification and a different design criterion for an isolated structure is highlighted in a recent study by (Alhan and Öncü-Davas, 2016). They investigated the performance limits of seismically isolated 5-storey benchmark building under near-field earthquakes using a nonlinear time history analysis for a large number of simulated

pulse type ground motions. Although the structure and the fault distance considered in the present study are different from those of the above investigation, some comparison of the maximum base displacement and the peak floor acceleration can be made between the two in order to show that the results of the present study are quite reasonable. In the present study, the pulse period, T_p is = 2.225 sec, the ratio of the pulse period to isolation period is T_p/T_i=0.6, PGA=0.4g, and the fault distance = 0.66 km. The maximum base displacement and maximum peak floor acceleration are found to be 96 cm and 2.8 m/sec^2 respectively. Alhan and Öncü-Davas (2016) reported the responses for a similar pulse period (T_p = 2 sec) as 70 cm for maximum base displacement and 4 m/sec^2 for maximum floor acceleration (with T_p/T_i = 1 and fault distance as 3 km). Further, they reported that large base displacement, of the order of 2.5 m and floor acceleration, of the order of 12 m/sec^2 are observed for a long pulse, T_p=5 sec, and PGA=0.65g (T_p/T_i=1). Thus, not only the base isolation design for a near-field earthquake is to be very much different from that for far-field one, but also the specifications for the performance limits for the two should be much different.

3.8 Conclusions

The behavior of base-isolated building frame is investigated for both near-field and far-field earthquakes in order to show the difference between the response characteristics of the system for the two types of the earthquake. Two types of near-field earthquake namely, with directivity effect and fling-step effect, are considered. Two levels of the PGA are also asumed consistent with the present earthquake design philosophy. The difference in the behavior is shown with the help of percentage reduction in (i) base shear; (ii) top storey absolute acceleration; and (iii) maximum inter-storey drift. Apart from these, the nonlinear excursion of the base isolator and inelastic deformation of the base-isolated structure under different types of earthquakes are highlighted. Finally, the effect of the post to pre-yield stiffness on the response behavior of the base-isolated structure is investigated. The numerical results arising from the investigation of a specific 10-storey base isolated building frame considered in the present study lead to following conclusions:

1. For the two levels of the PGA of earthquake considered in the study, the reductions in base shear, top floor absolute acceleration and maximum inter-storey drift are significant for far-field earthquake and near-field earthquake with directivity effect.
2. For the near-field earthquake with fling-step effect, the percentage reductions in the above response quantities are considerably reduced, indicating that the base isolation proves to be ineffective for this type of near-field earthquake.

3. The time history of the top storey displacement for the near-field earthquake with fling-step effect is distinctively different than those for the other earthquakes.
4. Force-deformation loop of the isolator differs widely with the type of earthquakes; for the near-field earthquakes, the numbers of loops are fewer and hysteresis loops are elongated yielding large isolator displacement, especially for the higher level of PGA. For far field earthquakes, isolator has undergone large numbers of hysteresis cycles concentrated in the central zone; isolator displacement is less.
5. The hysteretic energy dissipated by the isolation system under the effect of near-field earthquakes is large as compared to that of far field earthquakes.
6. For the higher level of PGA of 0.4g, the base-isolated building undergoes inelastic excursion; however, the inelastic effect is considerably reduced as compared to that for a fixed base building for far-field earthquakes and near-field earthquakes with directivity effect.
7. For the near-field earthquake with fling-step effect, the base-isolated building frame gets into the inelastic range even for the lower value of the PGA; for the higher level of the PGA, the extent of the inelastic excursion is not reduced by providing the base isolation. Thus, ductility demand is not reduced.
8. The effect of post to pre yield stiffness ratio of the isolator on the response behavior of the isolated structure differs widely with the nature of earthquake; for far-field earthquake, the effect is not very significant for both levels of PGA; the effect is very pronounced for near-field earthquakes so far as the percentage reduction in responses is concerned; for near-field earthquake with fling-step effect, the formation of plastic hinges is not very sensitive to the variation of γ for upper the level of PGA.

Chapter 4

Applicability of Capacity Spectrum Method for Base-isolated Frames at Different Performance Points

4.1 Introductory Remarks

The Nonlinear time history analysis (NTHA) is recognized as the most rigorous performance evaluation procedure which is able to predict the inelastic behavior in every member of a superstructure for a given seismic demand with adequate reliability. However, still, it is not a preferred performance evaluation tool for the structural designers due to some of its limitations like, it requires greater computational efforts, requires a suite of ground motion time histories for which response of the structure is very sensitive, and also needs proper modeling of members and material behavior (Elnashai and Di Sarno, 2008). These limitations of NTHA demanded the need to develop simpler methods, which could be easily applied to reasonably predict the strength capacity and inelastic demand of the structure. This resulted in the development of nonlinear static analysis, also called pushover analysis (POA) in 1970s to evaluate the seismic performance of the structure whose foundation was laid by the work of Takeda *et al.* (1970), Freeman *et al.* (1975), Freeman (1978), and Saiidi and Sozen (1981) .

At present, the performance evaluation is done by various methodologies, most popular ones are capacity spectrum method (CSM) as per ATC-40 (1996), Coefficient method (CM) as per FEMA-356 (2000), modified CM and CSM as per FEMA-440 (2005), N2 method adopted in EC8 (Fajfar and Gaspersic, 1996). With the development in the field of pushover analysis, many other methods are proposed by the various researchers as listed in the Chapter-1 (Introduction).

The capacity spectrum method (CSM) is widely used to obtain the performance point of the structure against the seismic demand imposed on the structure. Ample of research studies have been carried out for the application of the CSM and other nonlinear static procedures in the case of fixed base buildings.

Whereas, the studies about the performance evaluation of the base-isolated buildings by the pushover analysis methods are scanty. A very few studies which are available related to this topic are briefed in the chapter-2 (literature review). The past studies on base-isolated building frames either perform target displacement comparison or comparison is made at a single performance point only near at the ultimate state (collapse) of the building for a limited

number of responses, which do not show how results of both analyses (CSM and NTHA) compare at different stages of inelasticity and different performance levels. Therefore, more exhaustive studies are required in this direction.

The validity of the evaluated performances of the structure is investigated by comparing the results of CSM or other nonlinear static procedure with those of NTHA. The comparison is made in several ways. One of the major components of research on the pushover analysis was to develop suitable lateral load distribution pattern, which can provide the least differences between the results of CSM and NTHA.

Keeping the above background in view, the study in the present chapter attempts to make a contribution on the applicability of the capacity spectrum method (CSM) at various performance points for two base-isolated (BI) reinforced concrete frames (5-storey and 10-storey) and their corresponding version of fixed base frames. In particular, the present study aims to investigate the efficacy of the (CSM) in the prediction of seismic demands as compared to (NTHA) for base-isolated building frames at different performance points, ranging from elastic to plastic state of the structure. In order to make the study comprehensive one, the comparison is done for a large number of response quantities. Five-storey and ten-storey base-isolated building frames with stiff, medium, and flexible lead rubber bearing (LRB) isolators, which are defined by their effective stiffness, are considered for analysis.

4.2 Theoretical Background

Two types of analyses are performed in this chapter namely, the pushover analysis and the nonlinear time history analysis (NTHA). The pushover analysis extended to obtain the performance point of the structure is popularly known as capacity spectrum method (CSM). Hence, the CSM method is described briefly in the following subsection. Both CSM and NTHA is coded in various professional softwares.

4.2.1 Capacity Spectrum Method

The capacity spectrum method was first introduced by the joint work of Freeman *et al.* (1975) in the pilot study of evaluating the seismic risk of existing buildings at the Puget Naval Shipyard, Washington. The CSM is a graphical procedure in which the capacity curve of the structure is intersected with the demand spectrum in order to get the performance point. The performance point indicates the likely displacement demand of the structure which is imposed by a specified level of seismic intensity. The procedure is well doccumented in ATC-40.

The capacity curve is a plot of base shear vs. top displacement obtained by performing the pushover analysis of the structure. The structure is pushed by predefined invariant lateral load pattern up to a specified target displacement or until the structure reaches to the collapsed state. The base shear and top lateral displacement are noted at every increment of the load, and finally, the relation between the base shear vs top displacement is plotted as depicted in **Figure 4.1**

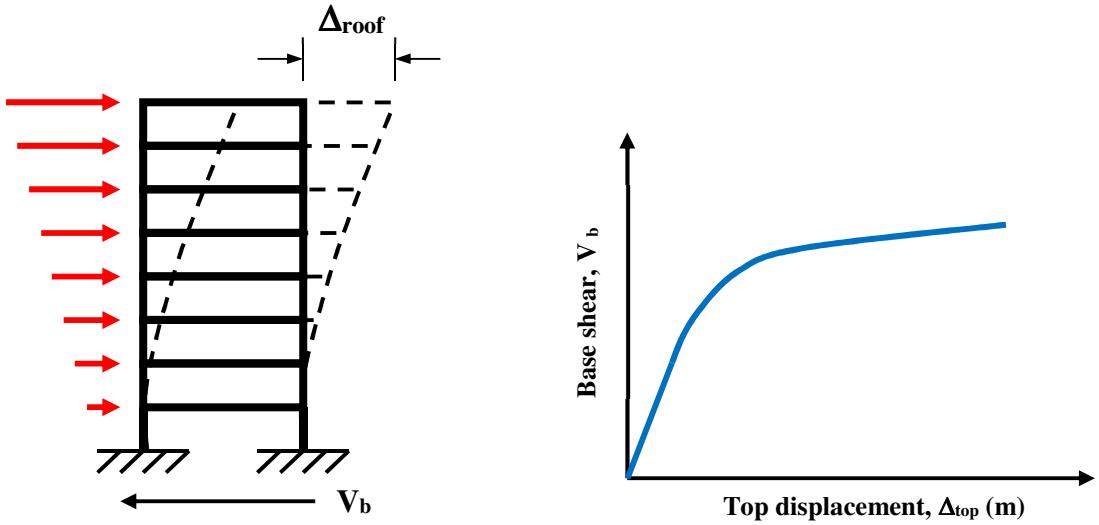

(a) Lateral push (b) Capacity curve

Figure 4.1 The pushover Analysis

The Capacity curve obtained by the pushover analysis of multi degree of freedom (MDOF) model is transformed into the capacity spectrum of single degree freedom model (SDOF) in the ADRS (acceleration demand response spectra) format as depicted in **Figure 4.2** by the following equations:

$$S_a = \frac{V/W}{\alpha_1} \tag{4.1}$$

$$S_d = \frac{\Delta_{top}}{PF_1 \varphi_{top,1}} \tag{4.2}$$

$$PF_1 = \left[\frac{\sum_{i=1}^{N} (w_i \phi_{i1})/g}{\sum_{i=1}^{N} (w_i \phi_{i1}^2)/g} \right] \tag{4.3}$$

$$\alpha_1 = \frac{\left[\sum_{i=1}^{N}\left(w_i\phi_{i1}\right)/g\right]^2}{\left[\sum_{i=1}^{N} w_i/g\right]\left[\sum_{i=1}^{N}\left(w_i\phi_{i1}^2\right)/g\right]} \qquad (4.4)$$

Where, PF_1 is the modal participation factor for 1st mode, α_1 is the modal mass co-efficient for the 1st mode, w_i/g is the mass of level i, ϕ_{i1} is amplitude of 1st mode at level i, N is the total number of floor levels, V is the base shear, W is the total dead load plus appropriate live load, Δ_{roof} is roof displacement, S_a is spectral acceleration, S_d is spectral displacement.

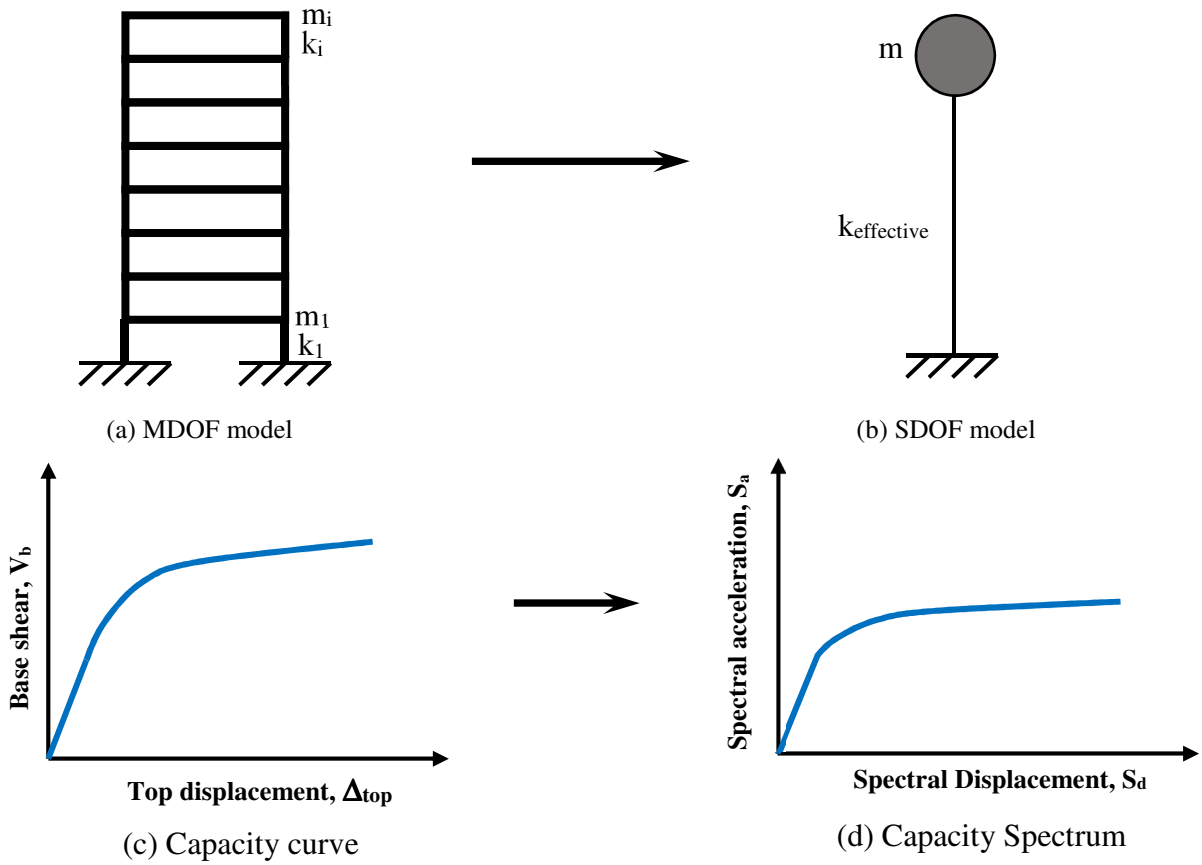

Figure 4.2 Transformation of capacity curve to capacity spectrum

The elastic 5% (damping) demand spectrum, which is in the Sa (spectral acceleration) and T (time) format is converted to the ADRS format as shown in **Figure 4.3** by **Equations 4.5** and **4.6**. The **Figure 4.4** shows the capacity spectrum superimposed on the demand spectrum in the traditional and ADRS format.

$$S_d = \frac{1}{4\pi^2} T^2 S_a \tag{4.5}$$

$$T = 2\pi \sqrt{\frac{S_d}{S_a}} \tag{4.6}$$

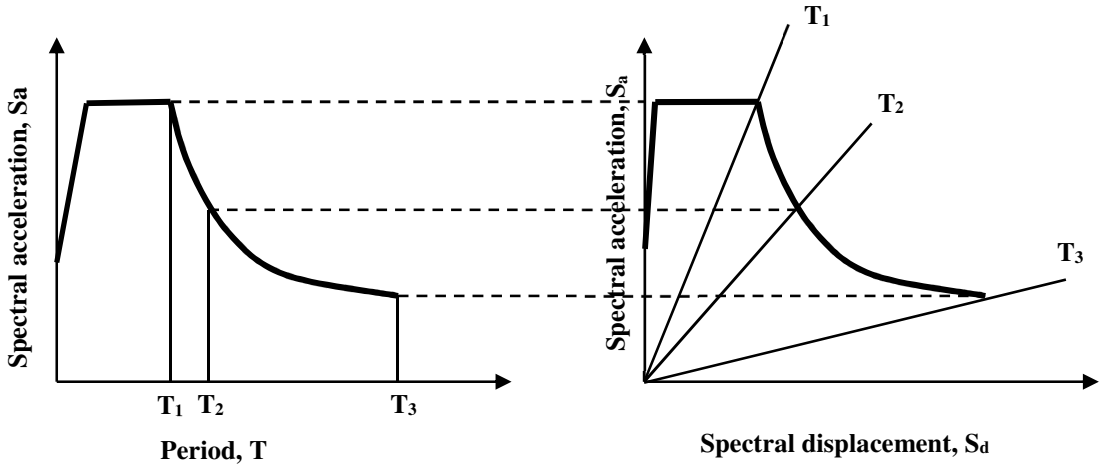

(a) Traditional format (S_a vs T)

(b) ADRS format (S_a vs S_d)

Figure 4.3 Representation of demand spectra in two different formats

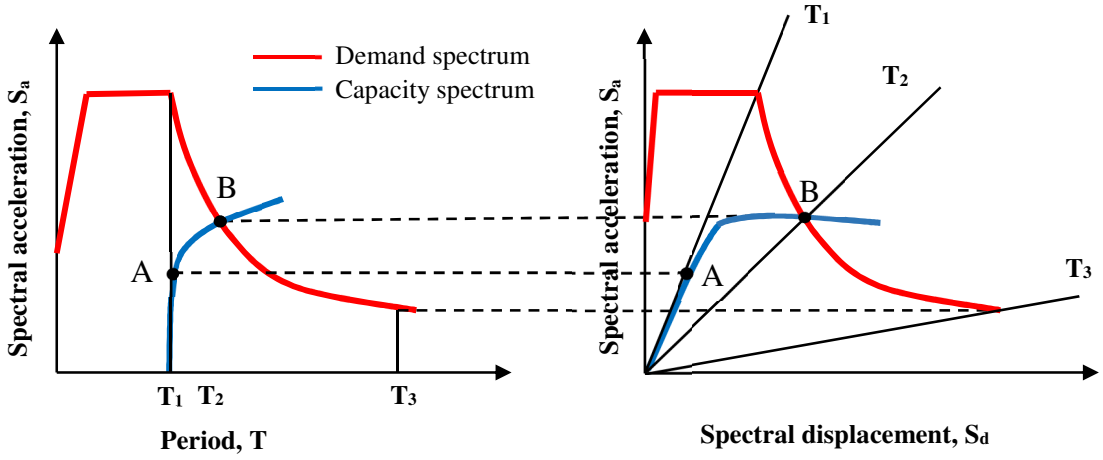

(a) Traditional format (S_a vs T)

(b) ADRS format (S_a vs S_d)

Figure 4.4 Representation of superimposed capacity spectrum on the demand spectrum

After plotting the capacity curve and demand curve in the ADRS format, ATC-40 provides three graphical procedures namely, procedure A, procedure B, and procedure C to obtain the performance point. In the present study, the procedure B is used to obtain the performance points, which is well incorporated in SAP2000 software.

According to the procedure B, after plotting the capacity curve and demand curve on the same graph in ADRS format, the bilinear curve of the capacity spectrum is developed. The initial stiffness of the building will provide the initial slope of the bilinear curve. The post-yield slope is found by extending the second segment of the bilinear curve through the capacity spectrum at a point P, having spectral displacement S_{di}, given by equal displacement rule as shown in **Figure 4.5**. The second segment should be rotated about the point P (a*, d*) to balance the two areas to become equal as shown in **Figure 4.6.** Further, the effective damping β_{eff}, is calculated for different points (a_{pi}, d_{pi}), which are taken nearby to the point P (a*, d*) on the post-yield segment of the bilinear curve. For each considered d_{pi}, the related value of β_{eff}, a_{pi} point is plotted on the same graph as shown in **Figure 4.7** and all the points are joined with a line called locus of performance points (LOPP). The performance point is obtained where the LOPP cuts the capacity spectrum. The actual damping with respect to the performance point is calculated and reduced demand spectrum is plotted corresponding to the calculated damping by applying appropriate reduction factors given in the ATC-40.

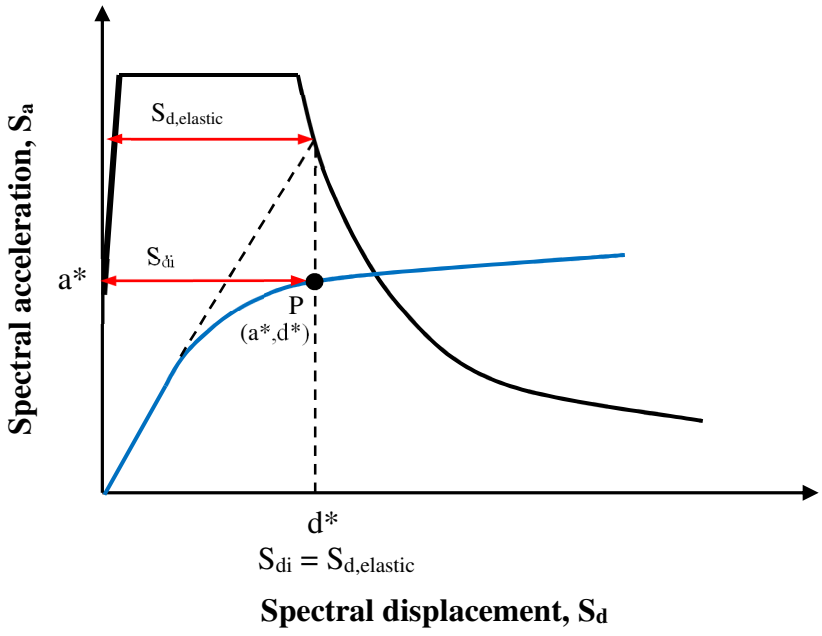

Figure 4.5 The equal displacement rule

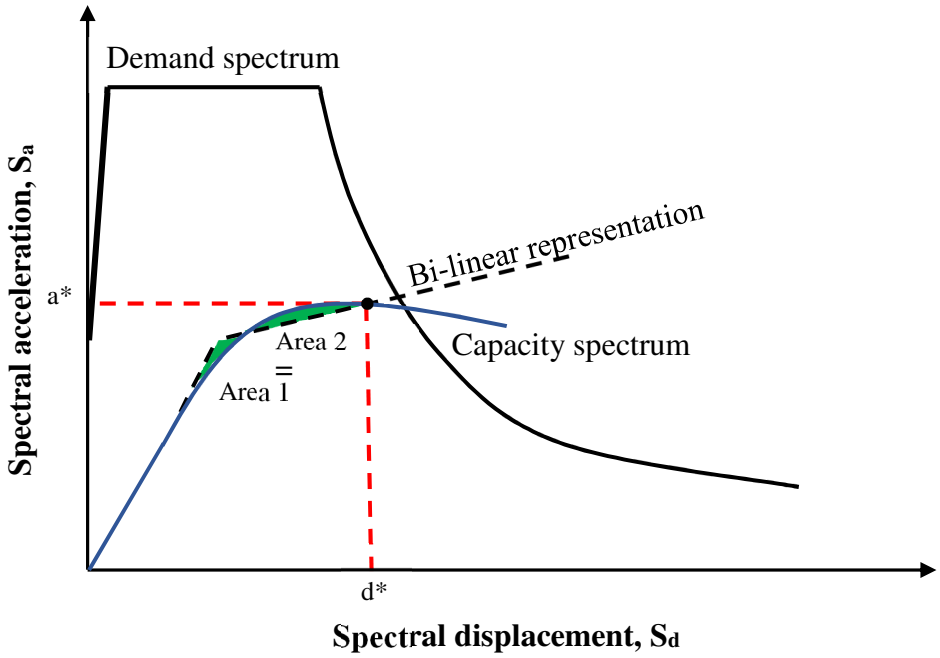

Figure 4.6 The bi-linear representation of the capacity spectrum

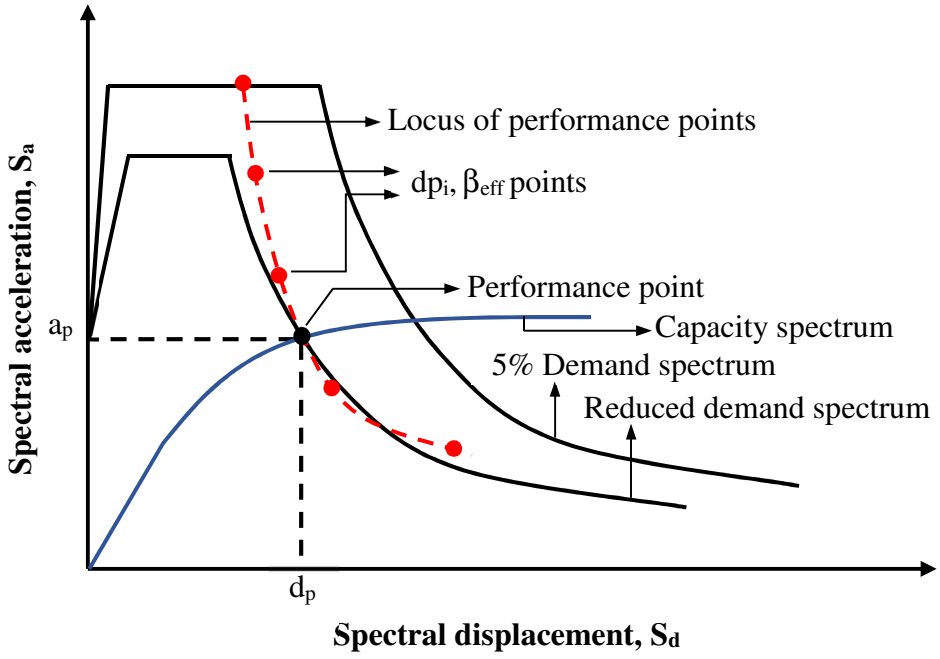

Figure 4.7 Performance point as per ATC-40 (procedure B)

4.2.2 Nonlinear Time History Analysis (NTHA)

The NTHA is performed by solving the incremental dynamic equation of motion of multi degree of freedom system. Crucial to the analysis is the specifications of the backbone curves at the sections of the superstructure and isolator. While, the plastification hysteric damping in the yield sections and the isolator are included through the inelastic stiffnesses

(stiffness nonlinearity associated with material nonlinearity), structures linear damping is included by the way of Rayleigh damping corresponding to first two fundamental modes of the structure. There are many numerical integration schemes to integrate the incremental equation of motion. Different softwares use different integration algorithms. One of the most popular integration schemes used in earthquake engineering is Newmark's Beta method.

4.2.3 Implementation in Software

The capacity spectrum method (CSM) and the nonlinear direct integration time history analysis (NTHA) are performed in SAP2000. The direct integration approach using the Hibler Hughes Taylor integration scheme is used for the analysis using the value of Beta = 0.25 and Gamma = 0.5. The second order effect, i.e., P-Delta is also considered. The Rayleigh damping is defined in the software by providing the damping ratio of 5%, corresponding to the first and second modes of structural vibration as the contributions of the higher modes are generally insignificant for the base-isolated structures.

Only one lateral load pattern is considered in the generation of capacity curves for CSM, which is proportional to the shape of the first mode both for the fixed base and base-isolated frames. The purpose of considering only one lateral load pattern is due to following reasons:

- The first mode primarily governs the response of base-isolated buildings as 99% of the mass is excited in the first mode for both building frames.
- It is found in the literature related to the application of NSP to base-isolated buildings that the response parameters are better predicted by the lateral load pattern corresponding to 1st mode shape even if there is severe damage to the structure (Doudoumis *et al.*, 2006; Kilar and Koren, 2010).

For the fixed base and base-isolated buildings, the effective (β_{eff}) damping of the system is calculated as the combination of viscous damping (β_0), that is inherent in the structure and the equivalent hysteretic damping (β_{eq}) as given by **Equation 4.7**. The β_0 is typically assumed to be 5% for reinforced concrete structures.

$$\beta_{eff} = \beta_0 + k\beta_{eq} \tag{4.7}$$

The β_{eq} is calculated as (Chopra, 2001)

$$\beta_{eq} = \frac{W_d}{4\pi W_s} \tag{4.8}$$

where W_d is the energy dissipated by damping in a single cycle, and W_s is associated with the maximum strain energy.

The k factor in the **Equation 4.7** is the measure of actual hysteretic effect in the building, which depends on the quality of the seismic resisting system and the duration of the ground motion. The ATC-40 simulates three categories of structural behavior types A, B, C with good, average and poor hysteretic behavior, with strong pinching effects. The k value is assigned 1, 2/3 and 1/3 corresponding to the type A, B and C structure behavior respectively. In the present study, the type B structure behavior is assumed for which the k factor corresponds to 2/3.

The effective damping as described above is obtained at every performance point. The damping reduction factors are used to decrease the elastic response spectrum (5% damped) with damping greater than 5% of critical damping. The damping reduction factor is calculated by the SAP2000 as per Table 8-3 of ATC-40 for different building behavior types.

The target displacement is set at a displacement stage more than the anticipated failure displacement. The SAP2000 automatically fixes this value at 4% of the total building height. However, the analysis is automatically terminated at the point of collapse of the structure. For the present study, the maximum pushover displacement at collapse is of the order of 0.6 m which is much less than the target displacement set. Further, the maximum lateral displacement is not the order of magnitude different than the design displacement of the isolator. These points will be discussed further in the numerical section. performance points are obtained by the capacity spectrum method as given in ATC-40 (procedure B) which is well incorporated in SAP2000.

4.3 Numerical Study

The numerical study is conducted with a 10-storey and a 5-storey building frame isolated by lead rubber bearing (LRB) isolators. The two building frames are selected to represent a high-rise and a low-rise building respectively. Three types of LRB bearing are designed for different design isolation periods. The details regarding the modeling and design of building frames and isolators are provided in the following subsections:

4..3.1 Modeling and Design of the Superstructure

The same 10-storey frame used in the Chapter-3 is used in the study conducted in the present chapter. In addition, a 5-storey frame is also used which have the same geometrical configuration and loading conditions as of 10-storey frame. For the 5-storey building frame,

the size of all columns and beams have the same size throughout the building height and is 500 mm x 500 mm, for columns; 300 mm x 550 mm, for beams. The details regarding the modeling of the frame is same as a 10-storey frame, which is given in Chapter 3 (section 3.4.1). For the sake of convenience, the two building frames considered in the study are shown in **Figure. 4.8**

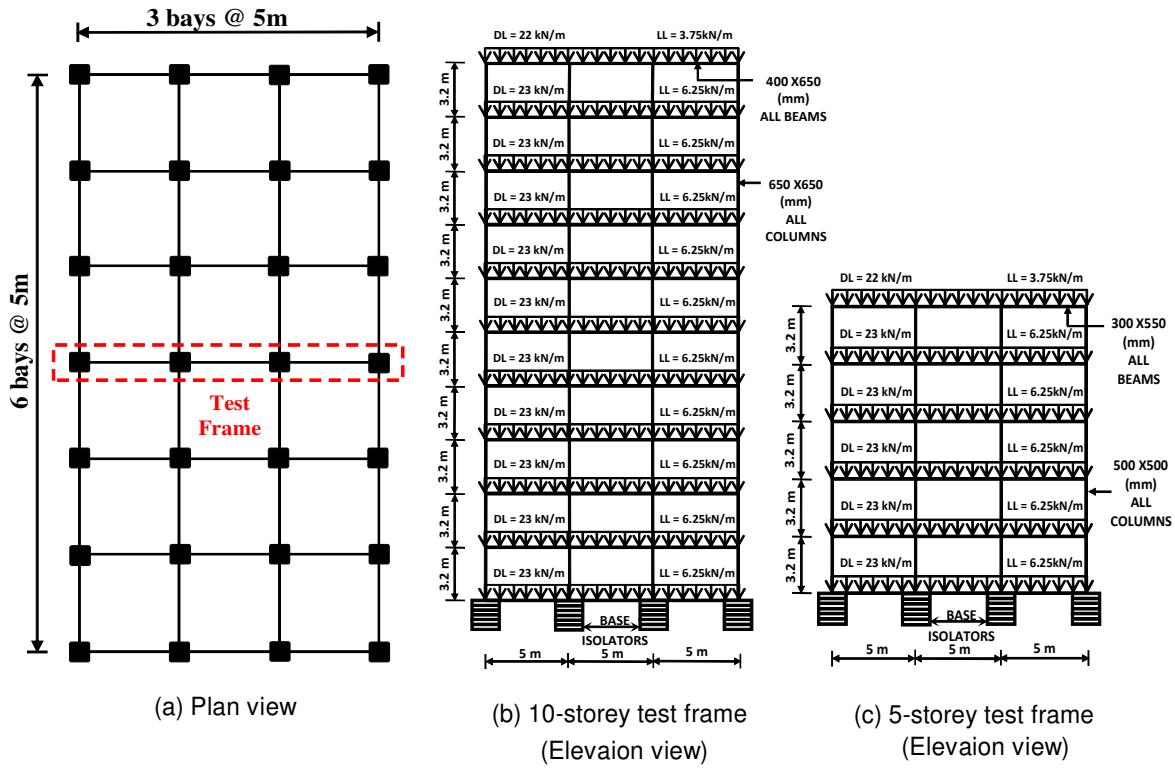

Figure 4.8 Details of building frames

4.3.2 Modeling and Design of Isolators

The New Zealand system lead core rubber bearings (LRB) are used for the isolation system. To investigate the characteristics of the base isolator, three different types of isolators namely, stiff (S), medium (M), and flexible (F) are designed specifically to each building frame. The three isolators are defined by their equivalent stiffness's which gives the desired isolation time period of the two frames. The designed isolators cover a wide range of isolation time period and effective stiffness which correspond to three protection levels:

- Stiff isolators that have a high effective stiffness and leads the superstructure to get into inelastic state.
- Medium isolators which keep the superstructure more into the elastic state as compared to the inelastic state.
- Flexible isolator which keeps the superstructure majorly into the elastic state enabling to produce minimum inelastic effects in the superstructure.

The isolators are designed as per the design guidelines provided by Naeim and Kelly (1999), and Datta (2010) for full dead load and 0.25% of the live load with the ratio of k_2/k_1 taken as 0.1 and by assuming the ad hoc values of separation time period between fixed base and base-isolated frame, which are notionally selected to satisfy the behavior of the superstructure to comply with the three states defined as states 1 to 3. Note that the state1 is stipulated for an isolator designated as stiff; state2 is designated as a medium; State3 is designated as flexible.

The characteristics of the three designed isolators namely, stiff, medium, and flexible are provided in **Table 4.1**.

Table 4.1 Characteristics of isolators designed for two building frames

Isolator	Isolation Period, T_{iso} (sec)	Effective stiffness, K_{eff} (kN/m)	Elastic stiffness, k_1 (kN/m)	Post yield stiffness ratio, $\gamma = k_2/k_1$	Characteristic strength, Q (kN)	Yield strength, F_y (kN)	Design disp. D_{max} (mm)
(a) For 5-storey frame							
Stiff	1.7	1127	8876	0.1	40	44.38	151
Medium	2	774	5757	0.1	31	34.54	170
Flexible	2.3	585	4444	0.1	28	31	203
(b) For 10-storey fame							
Stiff	2.5	1126	8927	0.1	56.47	62.5	213
Medium	3	760	5667	0.1	45.78	51	256
Flexible	3.5	558	4342	0.1	39.15	43.42	298

The effective stiffnesses for the three isolators are calculated from the assumed values of isolator time periods and other design parameters are then determined using the design guidelines as mentioned above. The objective of choosing three types of isolators is to show the difference in the behaviors of the superstructure for different (relatively) flexible isolations. The important characteristics of the force-deformation of the isolators are calculated by the equations provided in chapter-3 (section 3.4.2).

The bilinear force-deformation (hysteresis) curves for different isolators designed for 5-storey and 10-storey building frames are also shown in **Figure 4.9**. Note that the Q values for the three isolators are different (Table 4.1) which might not be clearly visible in the figure because of the scales adopted for drawing the figure. The identification details of various

variants of 5-storey and 10-storey building frames for the fixed base and base-isolated conditions along with the natural periods of the first two modes are given in **Table 4.2**.

Table 4.2 Variants of 5-storey and 10-storey building frames

5-Storey Frame ID	T_1 (sec)	%mass	T_2 (sec)	%mass	10-Storey Frame ID	T_1 (sec)	%mass	T_2 (sec)	%mass
FB5	0.56	81.4	0.177	10.4	FB10	0.82	79	0.268	10.3
BI5-S	1.7	99	0.317	0.287	BI10-S	2.5	99.7	0.445	0.23
BI5-M	2	99.7	0.321	0.141	BI10-M	3	99.8	0.450	0.11
BI5-F	2.3	99.8	0.323	0.082	BI10-F	3.5	99.9	0.453	0.06

FB = Fixed Base; BI = Base Isolated; S, M, F are stiff, medium, and flexible isolators

T_1 and T_2 corresponds to the first two fundamental periods of the frames

4.3.3 Time History Records for Numerical Study

The nonlinear time history analysis (NTHA) of 5-storey and 10-storey building frames for both FB and BI conditions are carried out by employing four synthetically generated artificial time histories compatible with ATC-40 response spectrum. Real scaled earthquake records whose spectrum can be matched at a single or a few periods with ATC-40 spectrum are not used since they cannot be uniformly applied to obtain all performance points; only artificially generated compatible time histories can serve this purpose. The ATC-40 response spectrum compatible time histories referred as artificial1 to artificial4 are generated by SeismoArtif (2016) software for performing NTHA as shown in **Figure 4.10**. The Fourier amplitude spectrum for the four simulated time histories (Artificial 1-4) is shown in **Figure 4.11**, where the energy content of the ground motion against the fundamental period of the two building frames for FB and BI conditions are marked. The comparison between the ATC-40 response spectrum and response spectrum of simulated compatible time histories is shown in **Figure 4.12.**

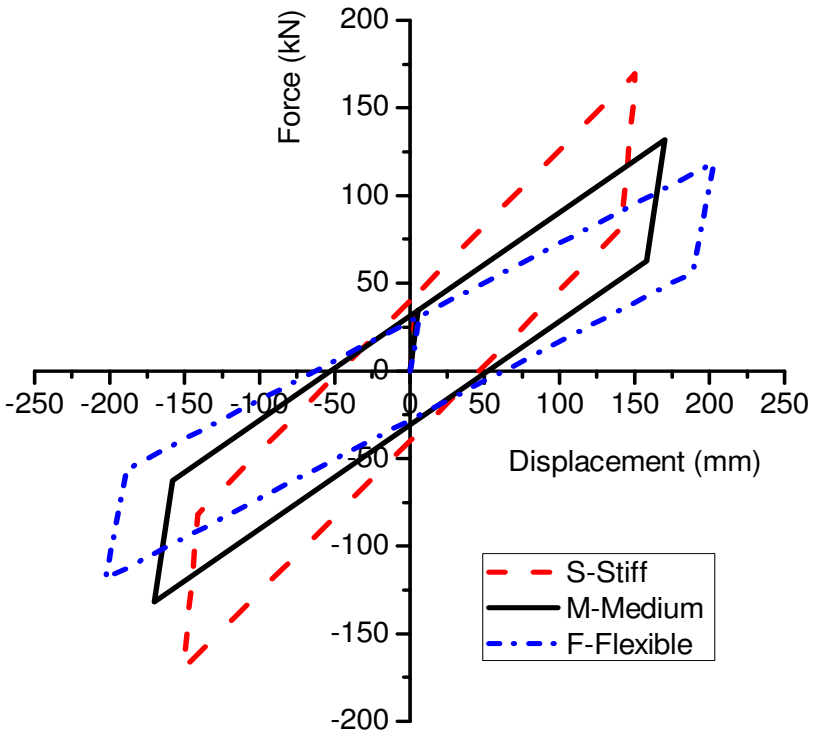

(a) Isolators designed for 5-storey frame

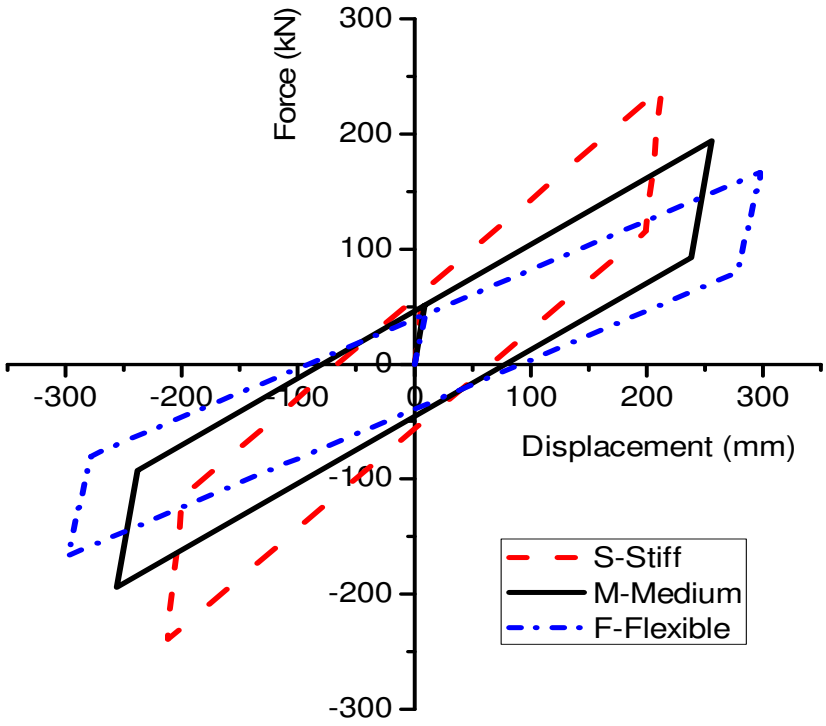

(b) Isolators designed for 10-storey frame

Figure 4.9 Hysteresis curves of stiff (S), medium (M), and flexible (F) LRB isolators designed for two building frames.

The artificial time histories are scaled to PGA level from 0.1g to 0.5g @ 0.05g interval and for a PGA level corresponding to the collapse point on the capacity curve as given in **Table 4.3**. The response quantities are averaged for the ensemble of four artificial time histories to obtain the mean NTHA responses to be compared with the responses obtained by CSM.

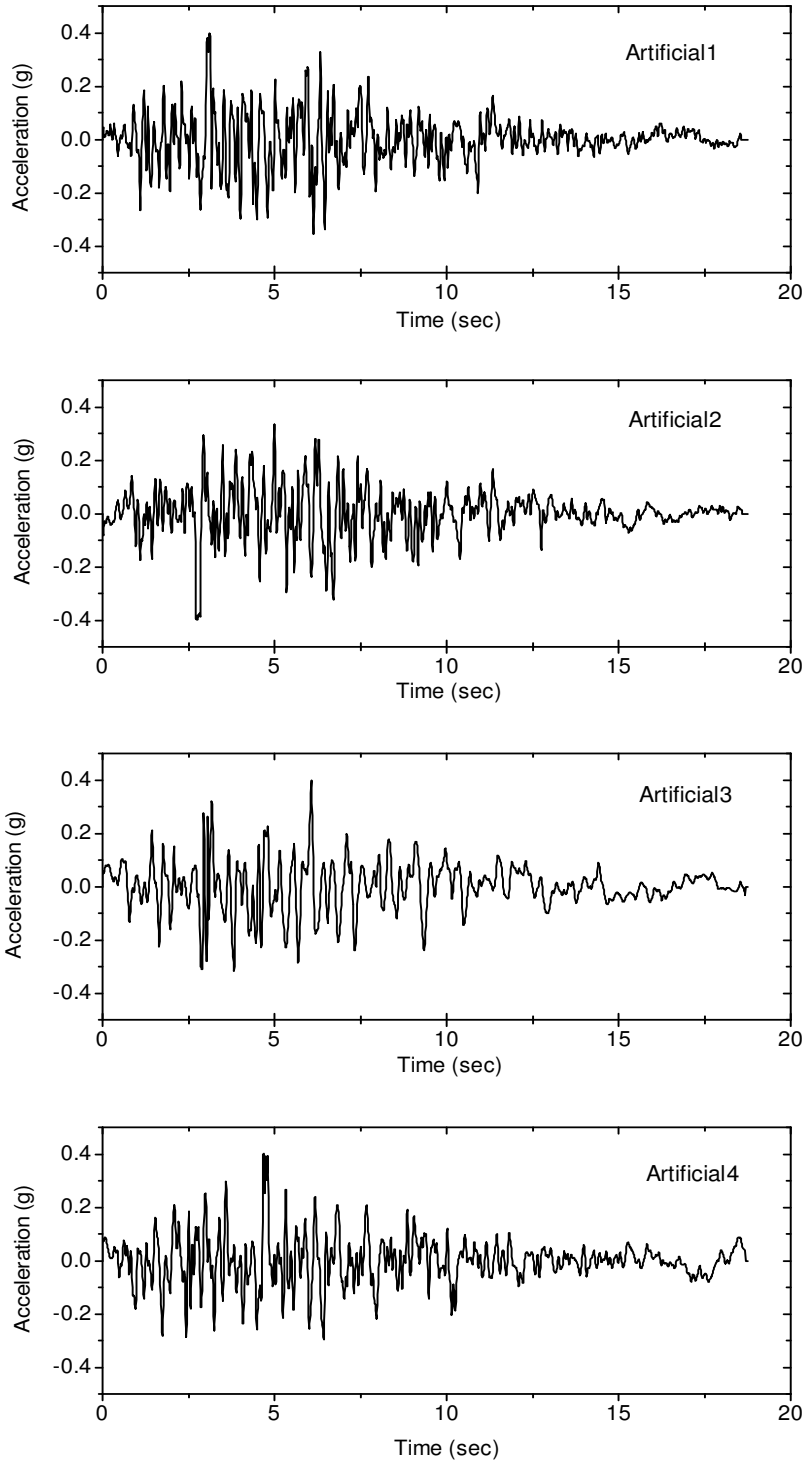

Figure 4.10 ATC-40 response spectrum compatible acceleration time histories, Artificial1 to Artificial4, scaled to a PGA level of 0.4g

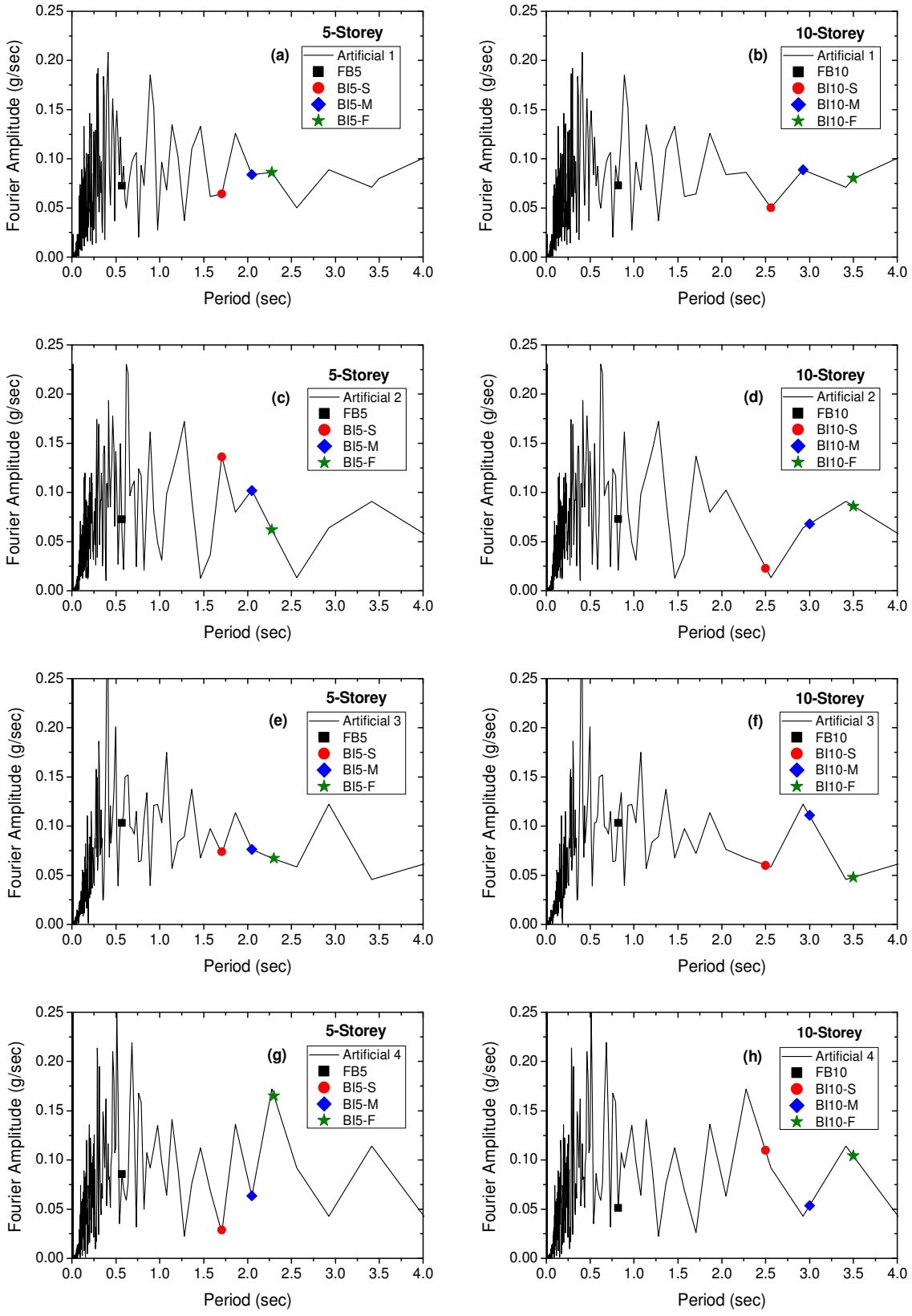

Figure 4.11 Fourier amplitude spectrum of artificial time histories (Artificial1-4) scaled to 0.4g showing its energy content marked corresponding to the fundamental period of building frames

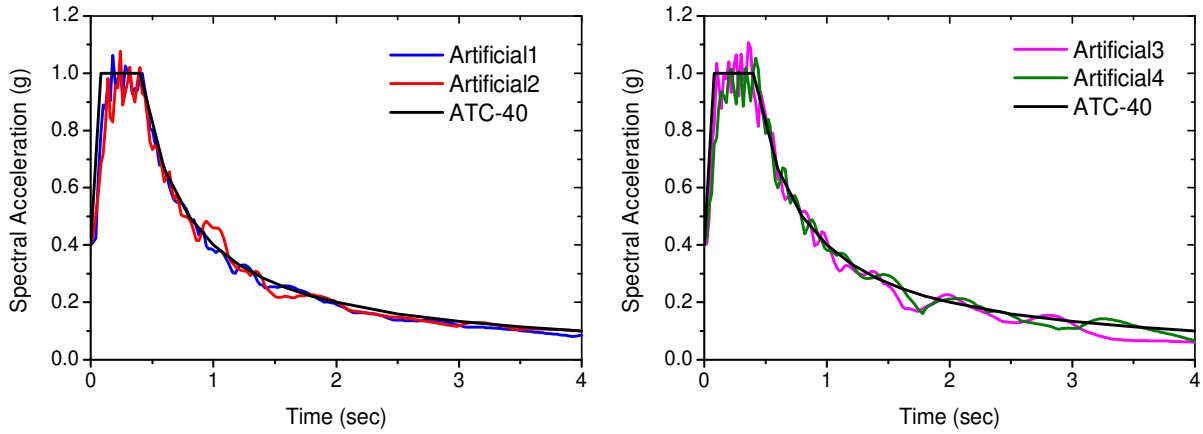

Figure 4.12 Comparison of acceleration response spectrum of artificial time histories with that of ATC-40

Table 4.3 PGA values for performance points coinciding with collapse points

5 Storey frame ID	PGA for PP at CP	10 Storey frame ID	PGA for PP at CP
FB5	0.72g	FB10	0.74g
BI5-S	0.80g	BI10-S	0.76g
BI5-M	0.86g	BI10-M	0.78g
BI5-F	0.91g	BI10-F	0.8g

PP = Performance Point; CP = Collapse Point; FB = Fixed Base; BI = Base Isolated

4.4 Discussion of Results

The capacity curves for the two building frames with FB and BI conditions are shown in **Figure 4.13**. It is seen from the figures that capacity curves significantly differ between the FB and BI frames. Further, the capacity curves for three types of base isolators differ significantly, nature remaining almost the same. For the 5-storey frame, base shear, as well as the target displacement of the collapse point is less as compared to the 10-storey building frame. Note that the collapse point is considered as the last point on the capacity curve after which the base shear suddenly drops to a significant value as indicated with a red dot in **Figure 4.13**. It is seen from the **Figures 4.20 and 4.21** (showing the plastic hinge patterns, which are discussed later in section 4.4.3) that a large number of plastic hinges are formed for both FB (at PP@0.74g) and BI (at PP@0.78g) frames at the collapse point confirming to CP level. Thus, the collapse of the frames occurred due to the rotations of the hinges reaching the specified ultimate values as per the FEMA 356 guidelines.

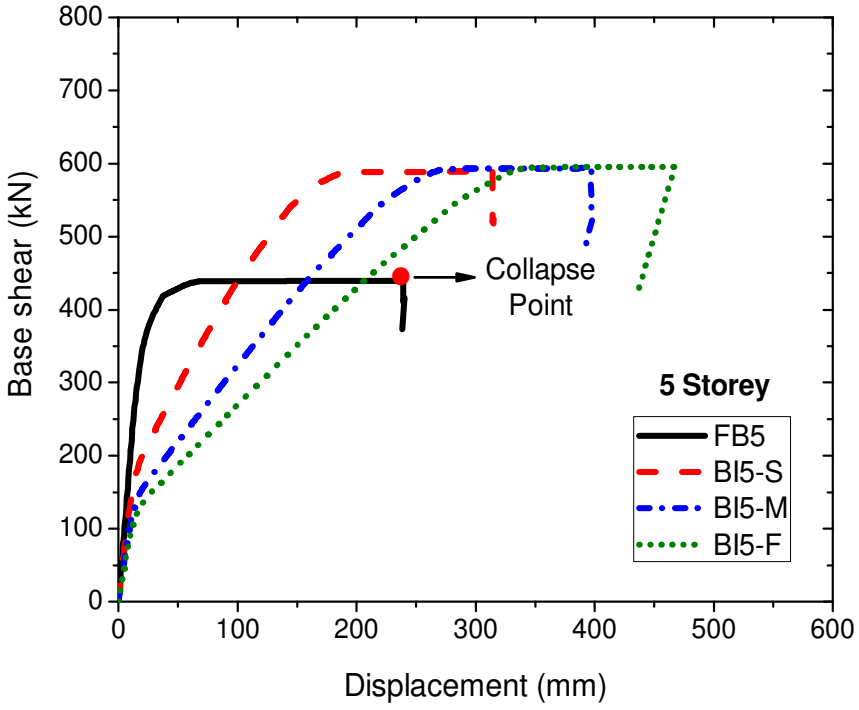

(a)

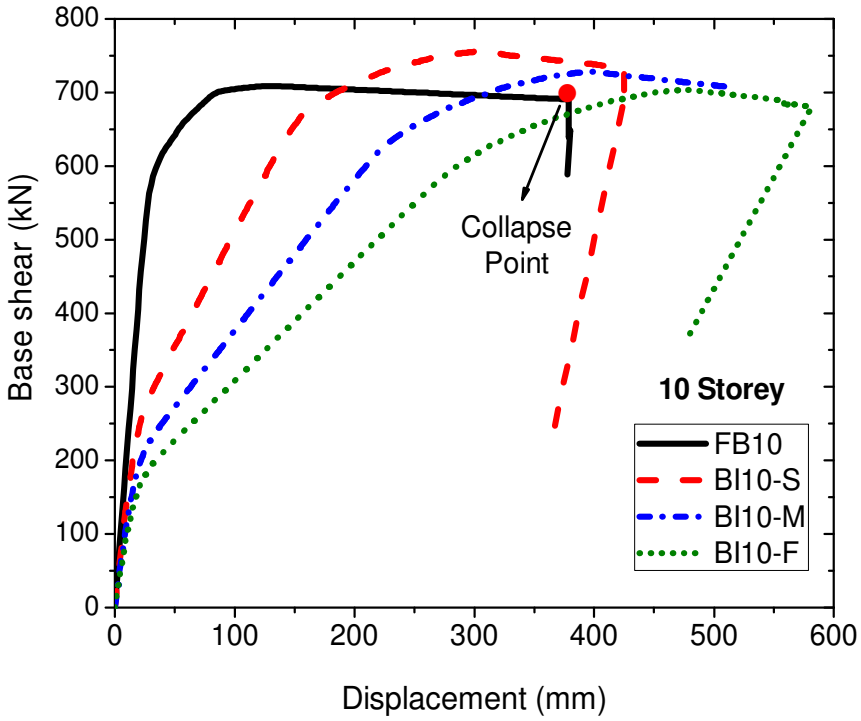

(b)

Figure 4.13 Capacity curves of 5-storey and 10-storey for both fixed base (FB) and base-isolated (BI) frames with stiff (S), medium (M), and flexible (F) isolators.

Further, it is seen that the base shear at the collapse point for the BI-frame is more compared to the FB frame. The difference is more in the case of the 5-storey building frame. This is expected because the 10-storey frame is more flexible as compared to the 5-storey frame and base isolation proves to be less effective for flexible systems. It may be seen from the figure that in the elastic range (a linear portion of the capacity curve), the base shears are significantly less in the BI building frame as compared to FB building frame as it would be expected. However, during the inelastic excursion (curved and flat portion of the capacity curve), the FB frame undergoes more into the plastic state as compared to the BI-frame. As a consequence, the base shear in the FB frame becomes less as compared to the BI-frame at the collapse point. Further, the distribution of the lateral load pattern adds to the enhanced base shear for the BI-frame because the load pattern corresponding to the 1st mode shape in BI-frame is close to uniform distribution which imparts extra force at bottom stories, whereas for the FB frame it is close to the inverted triangular pattern (which have very less force at bottom stories) as the capacity curves are obtained by performing NSP using the load pattern shape corresponding to the 1st mode.

4.4.1 Performance Points (PP)

It has been seen from the previous studies that most of the comparisons between NSPs and NTHA are made concerning the failure point or collapse point of the capacity curve regarding limited response quantities. There exists a limited number of studies on how NSP compares with NTHA at different stages of the nonlinear excursion from elastic to the plastic state of the structure (Mwafy and Elnashai, 2001). To investigate this issue, ATC-40 response spectrum is scaled to different levels of PGA to obtain the demand curves to be superimposed on the capacity curve in (Acceleration Displacement Response Spectrum) ADRS format as prescribed in ATC-40. Performance points are obtained by CSM (procedure B) as per ATC-40 corresponding to different PGA levels, indicating different states of the structure during the inelastic excursion. Furthermore, in the present study, the performance points are obtained at PGA levels ranging from 0.1g to 0.5g at an interval of 0.05g, as shown in **Figs. 4.14 and 4.15**, which covers the entire range of PGAs from the design level earthquake to maximum considered earthquakes, which are ordinarily used for the design purposes. More importantly, the PGA of the ATC-40 response spectrum is also scaled to obtain performance point at the collapse point of the capacity curve as shown in the figures. At this point, a partial collapse mechanism might have formed leading to the singularity of the stiffness matrix.

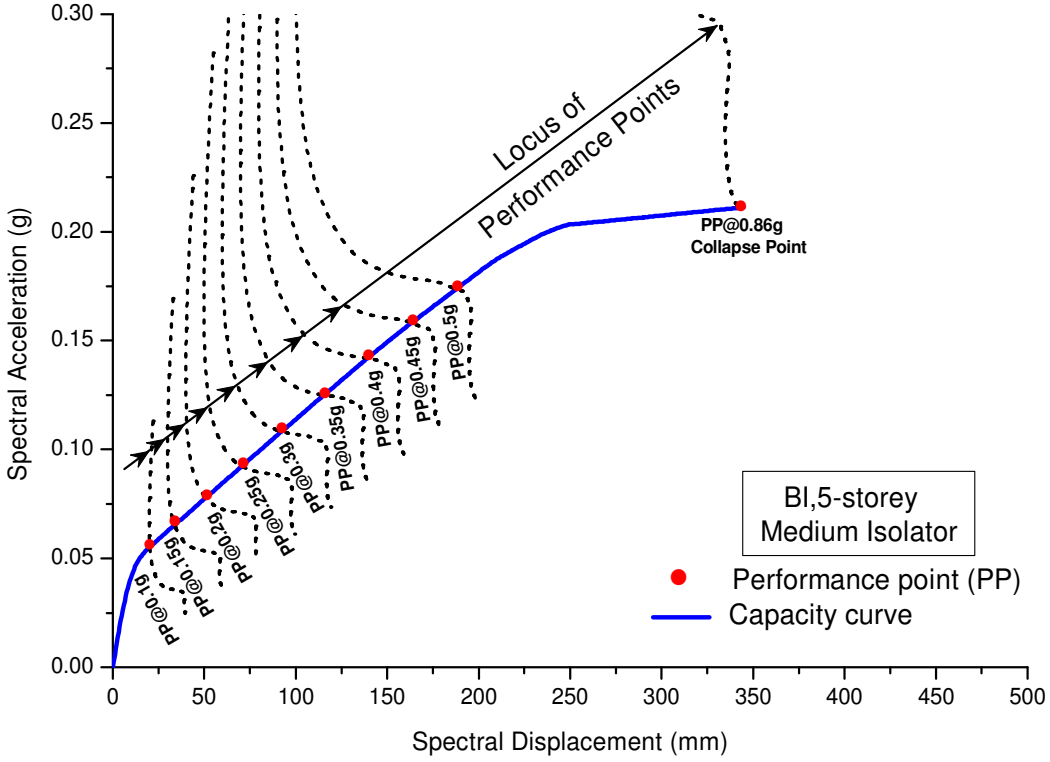

Figure 4.14 Performance points of 5-storey base-isolated building frame obtained by CSM as per ATC-40 (Procedure B) at all considered PGA levels.

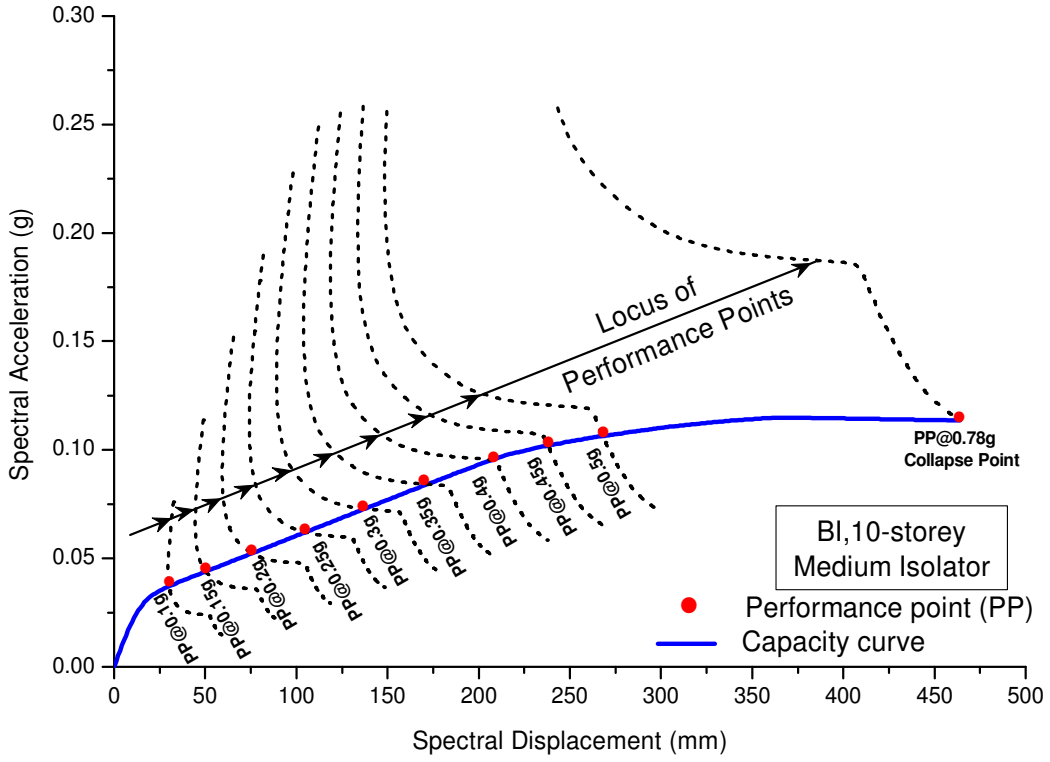

Figure 4.15 Performance points of 10-storey base-isolated building frame obtained by CSM as per ATC-40 (Procedure B) at all considered PGA levels.

Note that the performance points shown in the figure correspond to the characteristic effective damping (β_{eff}). The PGA values for which the performance points are obtained at collapse points of the capacity curves for various cases are shown in **Table 4.3**. Further, it may be noted from the table that difference between the PGA values corresponding to the collapse points of FB and BI with flexible isolator is of the order of 5% only. Thus, for the example problem considered here, it appears from the point of view of capacity under lateral loading that base-isolating a 10-storey building is not as effective as compared to a 5-storey building. Also, **Fig. 4.16** shows the performance points corresponding to typical PGA levels for the two building frames with FB and BI having different base isolators.

4.4.2 Comparison Between the Results of CSM and NTHA

Demand curve, which corresponds to ATC-40 response spectrum for 5% damping for each PGA level provides a performance point, characterized by the effective damping (β_{eff}). This effective damping is obtained by SAP2000 by applying appropriate damping coefficients as per ATC-40 procedure B. The response characteristics of the structure at each performance point obtained from the CSM are compared with those of NTHA, carried out with the scaled ATC-40 compatible time histories to the corresponding PGA level for which performance point is obtained as shown in **Figure 4.17.** Note that PGA level consistent with the performance point obtained at collapse point by CSM is used in the NTHA and is different for different building frames as given in **Table 4.3**.

The comparison of between CSM and NTHA is made by considering various response quantities, including: (i) top storey displacement; (ii) base shear; (iii) maximum inter-storey drift; (iv) number of plastic hinges; (v) extent of plastic rotation represented by square root of the sum of squares (SRSS) of maximum plastic hinge rotations; and (vi) reserve strength at a performance point; (vii) maximum isolator displacement (MID). Note that in CSM, there is only one value of plastic hinge rotation at a plastic hinge, whereas in NTHA there exists a time history of rotation at a plastic hinge.

For discussion purposes, SRSS of plastic hinge rotations for NTHA denotes the SRSS of absolute maximum rotation of all plastic hinges. This comparison is intended to illustrate how the difference in the responses between CSM and NTHA for the BI frames differs from that of FB frames.

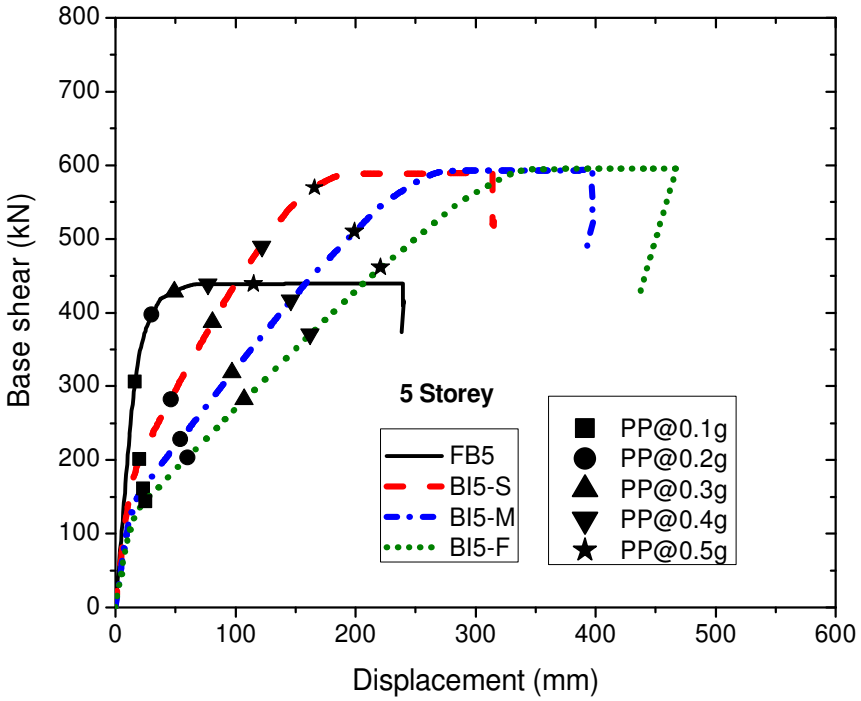

(a)

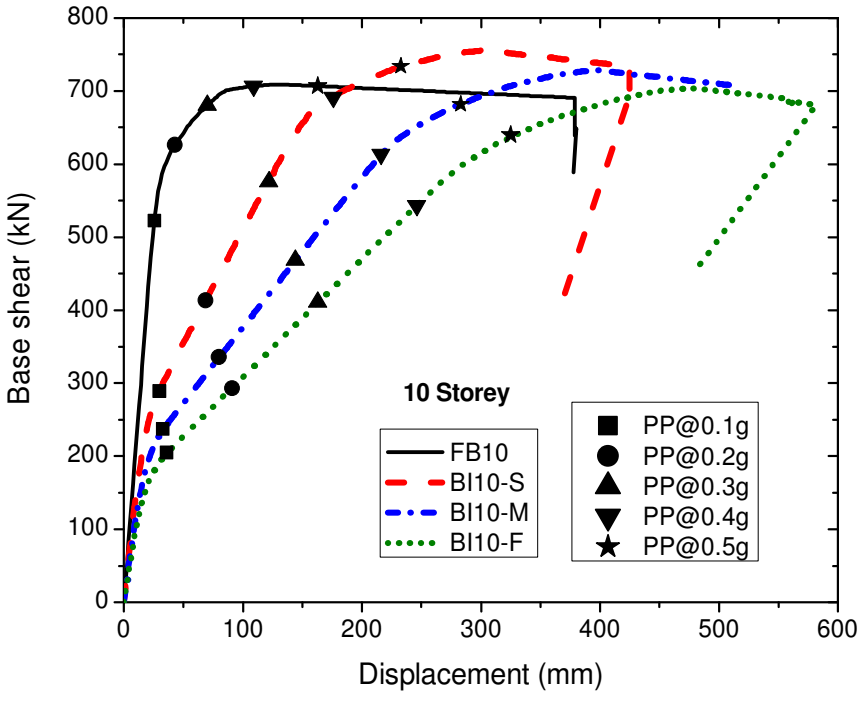

(b)

Figure 4.16 Performance points (PP) corresponding to typical PGA levels of 5-storey and 10-storey for both fixed base and base-isolated frames with stiff (S), medium (M), and flexible (F) isolators.

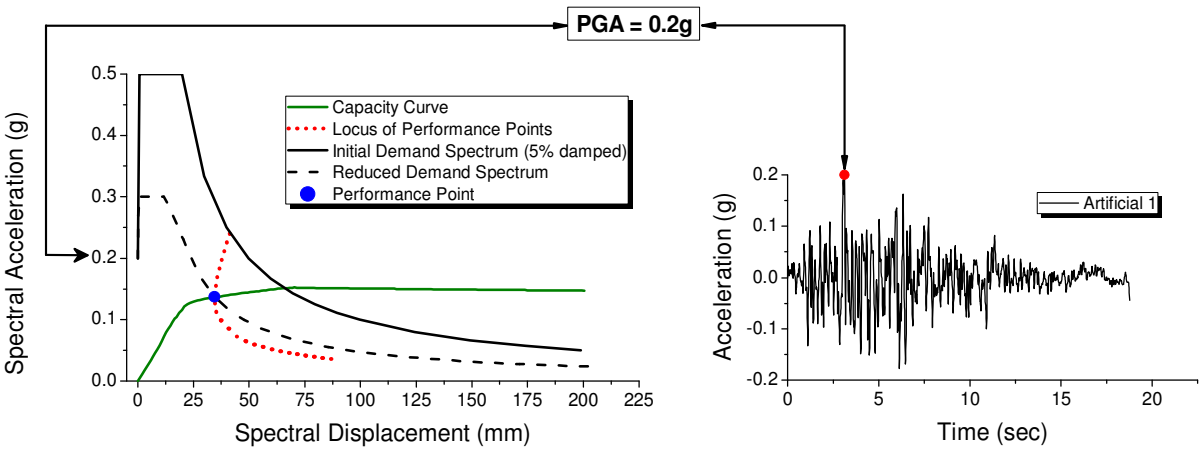

(a) Performance Point by CSM, ATC-40 (Procedure B) at specified PGA level of 0.2g

(b) Time History for NTHA at specified PGA level of 0.2g

Figure 4.17 Comparison method to compare several response quantities at a performance point corresponding to a typical PGA level obtained by CSM and NTHA

4.4.3 Comparison of Number of Plastic Hinges and Hinge rotation

Figure 4.18 shows the number of plastic hinges formed at different performance points (corresponding to different PGA levels) for the 10-storey FB and BI frames. It is seen from the figure that the number of plastic hinges at various performance points for the BI-frame is much less as compared to the FB frame for both CSM and NTHA as it would be expected. Furthermore, the number of plastic hinges in the BI-frame increases from the flexible base isolator to the stiff base isolator.

The number of plastic hinges for the stiff isolator is nearly 1.5 times that of the flexible base isolator at a performance point corresponding to a PGA of 0.5g. The reason for the less number of plastic hinges in the BI-frame may be attributed to the fact that it gets into much less inelastic range because of the effect of base isolation. In the case of NTHA, base isolators absorb much seismic energy because of hysteretic effect, thus relieving the superstructure from the effect of the full seismic energy coming from the ground. In the case of CSM, most of the deformation takes place at the level of isolator limiting the displacement in the superstructure to the minimum.

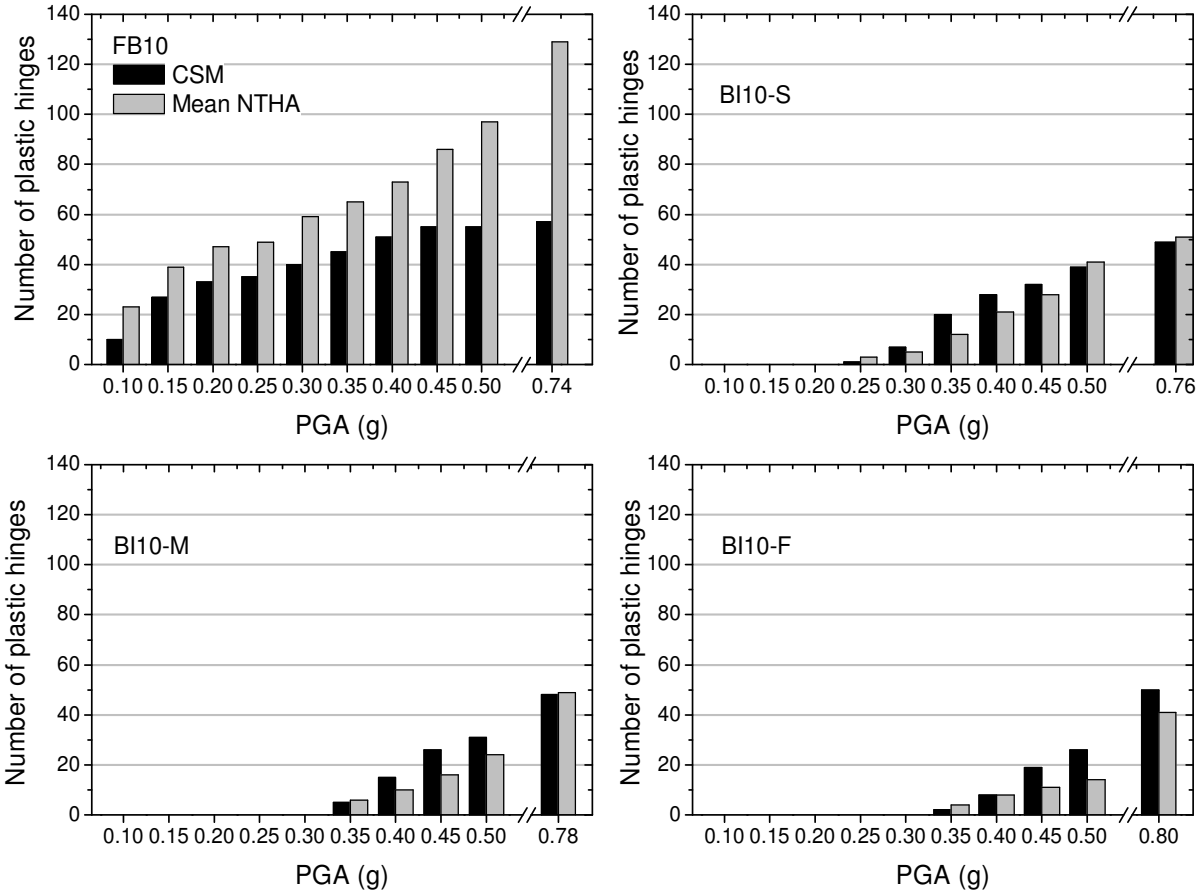

Figure 4.18 Number of plastic hinges for the 10-storey fixed base (FB) and base-isolated (BI) frames with stiff (S), medium (M), and flexible (F) isolators at different PGA levels

When the number of plastic hinges at different performance points is compared between CSM and NTHA, in the fixed base frame, it is observed that the numbers of plastic hinges formed in NTHA are comparatively more than that of the CSM. The difference increases with the increase in PGA value. At a PGA level of 0.5g, the number of plastic hinges in NTHA is about 1.65 times of that in CSM. For the BI-frame in the same figure, an opposite trend is observed, i.e., the number of plastic hinges in NTHA is found to be less than that in CSM. Further, the difference between the numbers of plastic hinges obtained from the two analyses is less than that observed for the FB frame.

Table 4.4 summarizes the performance levels of the plastic hinges of 10-storey building frames designated by the IO, LS, and CP for three performance points at PGA levels of 0.3g, 0.5g and PGA corresponding to the collapse point on the capacity curve. The table shows that a mere comparison between the numbers of plastic hinges formed in CSM and NTHA for different PGA levels does not reflect the difference between the overall inelastic states of the

frame, but rotations of the plastic hinges should also be taken into account in comparing the overall inelastic effect exhibited in the two analyses.

Table 4.4 Comparison in the plastic hinge states between CSM and NTHA in the 10-storey building frames

Building Frame ID	PGA Level	Number of plastic hinges at different Hinge States						SRSS of Plastic Hinge Rotation (Radians)	
		B-IO		IO-LS		LS-CP			
		CSM	Mean NTHA	CSM	Mean NTHA	CSM	Mean NTHA	CSM	Mean NTHA
FB10	0.3g	40	59	0	0	0	0	0.0160	0.0137
BI10-S		7	5	0	0	0	0	0.0005	0.0001
BI10-M		0	0	0	0	0	0	0.0	0.0
BI10-F		0	0	0	0	0	0	0.0	0.0
FB10	0.5g	50	97	5	0	0	0	0.0497	0.0255
BI10-S		39	41	0	0	0	0	0.0289	0.0016
BI10-M		31	24	0	0	0	0	0.0174	0.0008
BI10-F		24	14	0	0	0	0	0.0112	0.0004
FB10	0.74g*	19	125	6	4	32	0	0.1305	0.0425
BI10-S	0.76g*	21	51	10	0	19	0	0.1100	0.0103
BI10-M	0.78g*	21	49	10	0	18	0	0.1082	0.0034
BI10-F	0.8g*	22	41	13	0	15	0	0.1017	0.0037

S= Stiff, M= Medium, and F= Flexible isolators; * indicates PGA level at collapse point

The Square root of the sum of squares (SRSS) of maximum plastic hinge rotations of all hinges formed is taken as an indicator to show the overall inelastic effects in the frame in addition to the number of plastic hinges as shown in **Table 4.4** for the 10-storey frames. It is seen from the table that although NTHA provides a greater number of plastic hinges as compared to CSM for the FB frame, the SRSS of the plastic hinge rotations is nearly the same for both analyses at a PGA level of 0.3g. For a PGA of 0.5g, NTHA provides a greater number of plastic hinges, but SRSS of plastic hinge rotations is more for CSM, nearly two times that of NTHA. This is due to the fact that some of the plastic hinges (5 hinges) are in the higher range of plastic rotation level, i.e., IO-LS range for CSM, whereas for NTHA none of the plastic hinges enters into this range, all hinges remain in B-IO range. At the collapse point, rotations in the plastic hinges in CSM get into much more inelastic range as compared to NTHA as indicated by the values of SRSS of plastic hinge rotations.

For the BI-frame, CSM shows more inelastic effect as compared to NTHA both in terms of the number of plastic hinges and the SRSS of plastic hinge rotations. The SRSS of plastic hinge rotations in NTHA is significantly less indicating less overall inelastic effect. Thus, CSM significantly overestimates the actual extent of the inelastic effect in the base-isolated frames, for the three types isolators considered, in terms of the SRSS of plastic hinge rotations.

The reason for the less overall inelastic effect exhibited in NTHA is attributed to the fact that the actual energy dissipation in hysteresis during inelastic excursion is realistically captured in the NTHA, while in CSM, only equivalent energy dissipation is depicted at the performance points by way of equivalent damping.

For the 5-storey building frame, the comparison between the number of plastic hinges formed in the CSM and NTHA are shown in **Figure 4.19**. It is seen from the figure that the trend of the results is nearly the same as observed in the case of 10-storey building frame except that the total number of plastic hinges formed are less for the 5-storey frames as it would be expected. **Table 4.5** compares the number of plastic hinges for different performance levels at typical PGA levels for 5-storey frame. It is noted that the trend of results remains same as for 10-storey frame.

Table 4.5 Comparison in the plastic hinge states between CSM and NTHA in the 5-storey building frames

Building Frame ID	PGA Level	Number of plastic hinges at different Hinge States						SRSS of Plastic Hinge Rotations (Radians)	
		B-IO		IO-LS		LS-CP			
		CSM	Mean NTHA	CSM	Mean NTHA	CSM	Mean NTHA	CSM	Mean NTHA
FB5	0.3g	25	32	0	0	0	0	0.0152	0.0153
BI5-S		6	15	0	0	0	0	0.0016	0.0005
BI5-M		3	0	0	0	0	0	0.0004	0.0
BI5-F		1	0	0	0	0	0	0.0001	0.0
FB5	0.5g	16	53	16	0	0	0	0.0462	0.0304
BI5-S		23	19	0	0	0	0	0.0161	0.0019
BI5-M		15	12	0	0	0	0	0.0075	0.0006
BI5-F		12	11	0	0	0	0	0.0037	0.0004
FB5	0.72g*	10	49	7	12	19	0	0.1052	0.0445
BI5-S	0.80g*	11	25	5	0	15	0	0.0904	0.0078
BI5-M	0.86g*	11	22	5	0	15	0	0.0899	0.0044
BI5-F	0.91g*	11	19	5	0	15	0	0.0914	0.0037

S= Stiff, M= Medium, and F= Flexible isolators; * indicates PGA level at collapse point

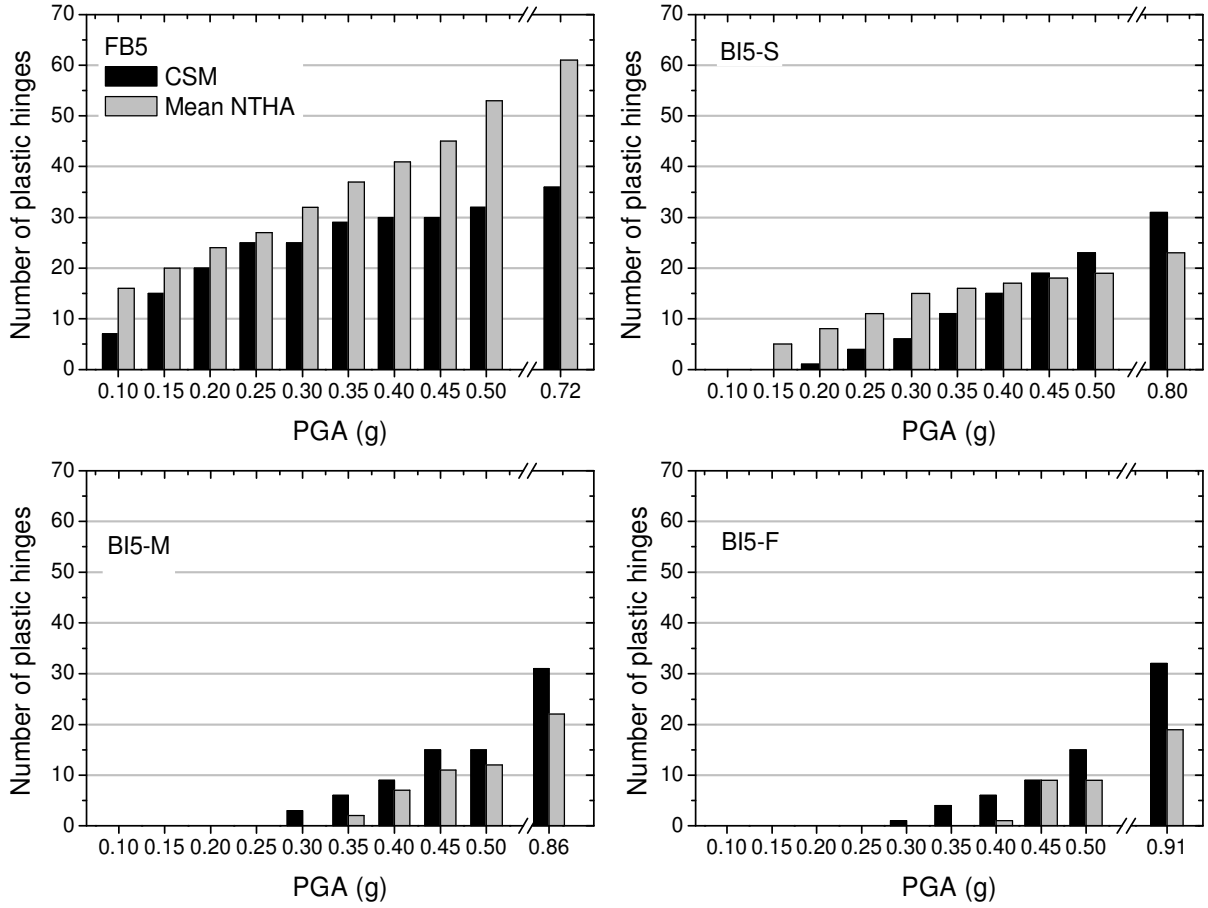

Figure 4.19 Number of plastic hinges for 5-storey fixed base (FB) and base-isolated (BI) frames with stiff (S), medium (M), and flexible (F) isolators at different PGA levels.

For the convenience of understanding the inelastic effect introduced in the frame at different performance points, the pattern of plastic hinges developed in the 10-storey BI (with medium isolator) and FB frames, for both CSM and NTHA, at typical performance points consistent with PGA levels of 0.2g, 0.3g, 0.4g, 0.5g and PGA level corresponding to collapse point is shown in **Figures 4.20** and **4.21** respectively. It is seen from **Figure 4.20** that for the BI-frame, no plastic hinge is formed up to a PGA level of 0.3g. After this PGA level, plastic hinges start forming in the frame, and a maximum of 49 plastic hinges form at the collapse point for both CSM and NTHA. However, the plastic hinge patterns are different in the two analyses. For the CSM, the plastic hinges are formed in all three levels, i.e., B-IO, IO-LS, and LS-CP, while for NTHA they belong to the level of only B-IO. Even when the capacity curve is obtained with a uniform load distribution, the same hinge patterns are observed for CSM. Therefore, even though the number of plastic hinges is the same for the two analyses, the inelastic effect exhibited in the CSM is more.

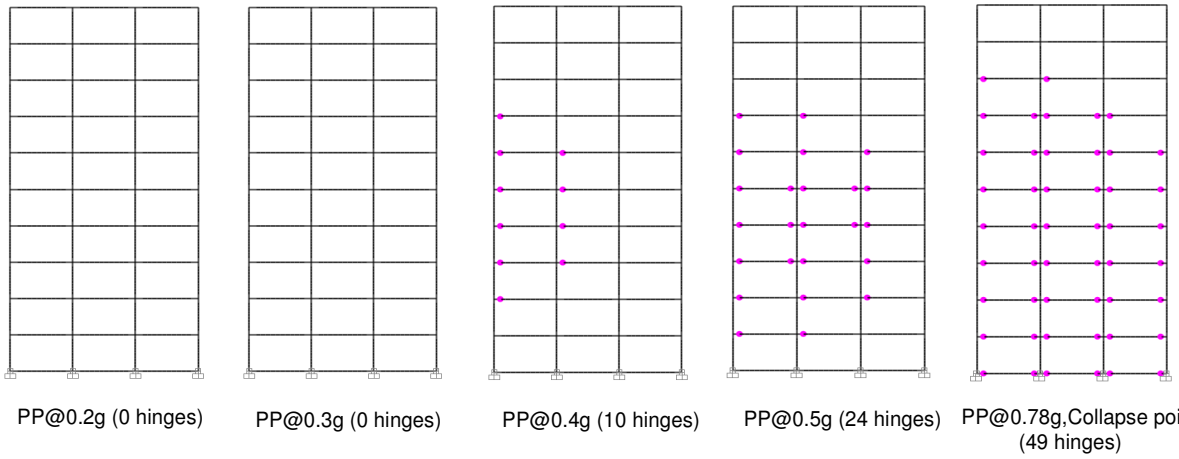

(a) NTHA for Artificial-1 time history (10-storey, Base Isolated frame with medium isolator)

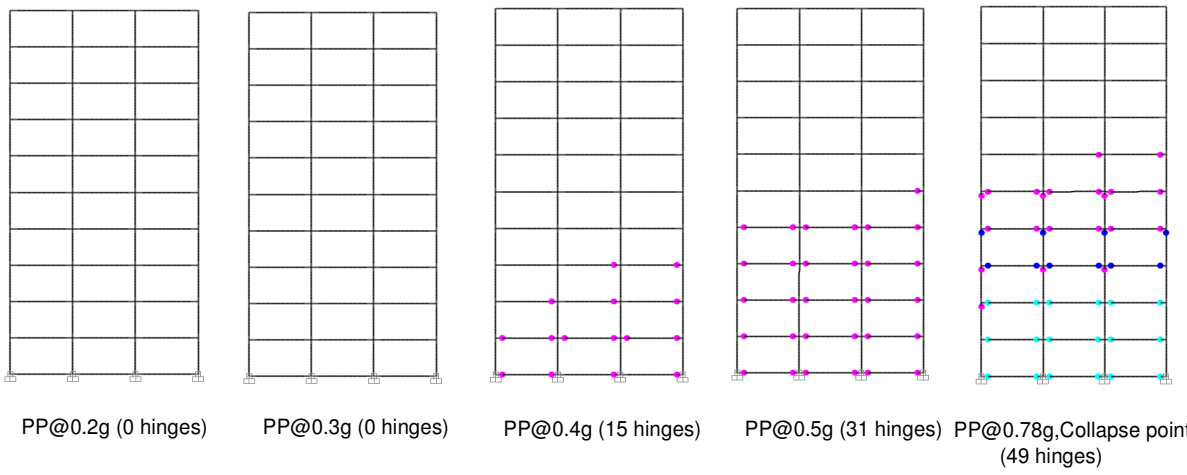

(b) Capacity Spectrum Method (10-storey, Base Isolated frame with medium isolator)

Figure 4.20 Plastic hinge pattern of the 10-storey base-isolated frame showing location and hinge states (B-IO, IO-LS, and LS-CP) determined by CSM and NTHA at typical performance points

For the fixed base frame as depicted in **Figure 4.21**, the numbers of plastic hinges formed for CSM and NTHA are different; they are more for NTHA. Further, it is seen that a significant number of plastic hinges are formed even at a PGA level of 0.2g. This shows that the fixed base frame undergoes more into the inelastic effect as compared to the BI-frame. Moreover, it can be clearly seen from the figure that beyond 0.4g, the pattern of formation of plastic hinges changes significantly. For the NTHA, in spite of the fact that there is formation of more number of plastic hinges beyond 0.4g, still, all the plastic hinges remain in the B – IO level. On the contrary, in the CSM, less number of hinges are formed, but some of them get into the higher level of the plastic state, i.e., IO – LS. This effect is more pronounced and clearly

seen at collapse point where large number of plastic hinges were formed in CSM gets into a higher level of plastic rotation, i.e., LS – CP, which shows the high inelastic effect exhibited in the CSM as compared to NTHA. The same pattern of hinge formation is observed in the 5-storey FB, and BI building frames and hence for brevity is not shown here.

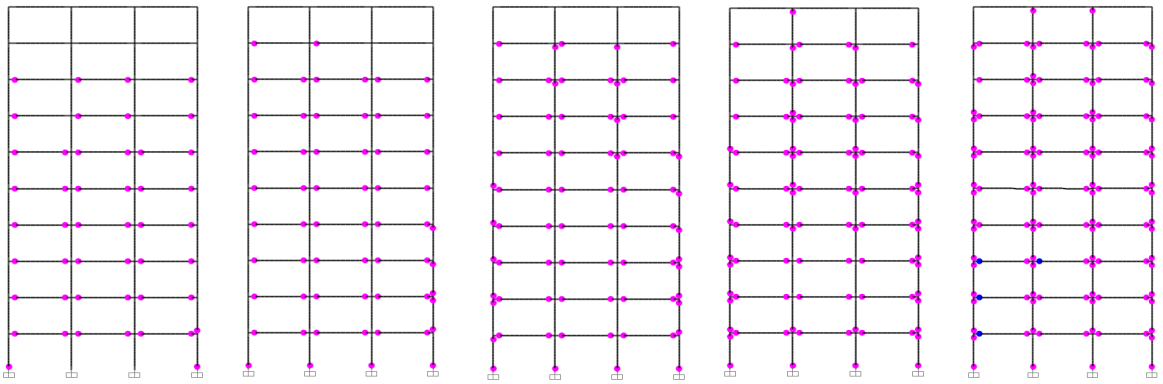

(a) NTHA for Artificial-1 time history (10-storey, Fixed Base frame)

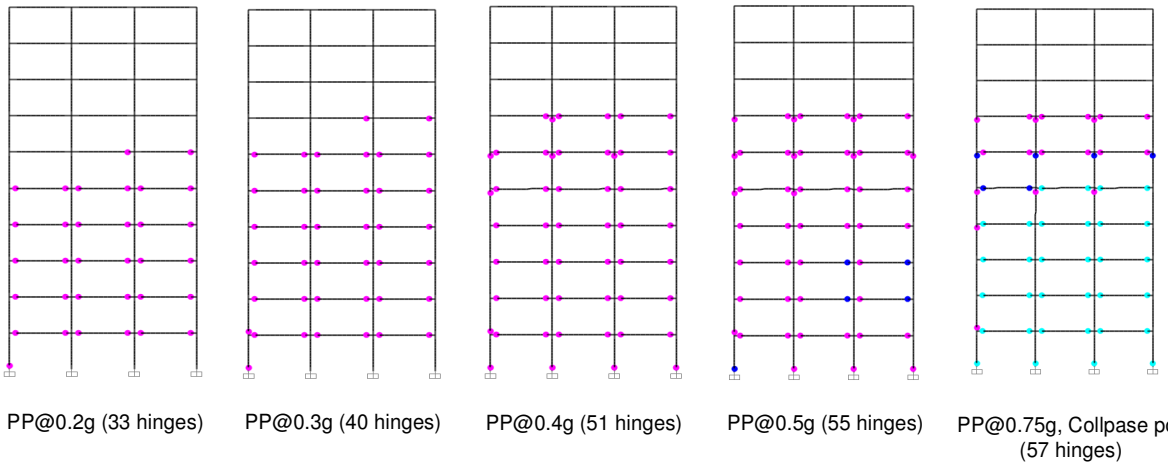

(b) Capacity Spectrum Method (10-storey, Fixed Base frame)

Figure 4.21 Plastic hinge patterns of the10-storey fixed base frame showing location and hinge states (B-IO, IO-LS, and LS-CP) determined by CSM and NTHA at typical performance points

The trend in the overall inelastic effect in the 5-storey frames at two performance points corresponding to PGAs of 0.3g, 0.5g, and PGA corresponding to the collapse point in the capacity curve remains the same as that of the 10-storey frame. Therefore, results for the 5-storey are not shown here. The observations may be summarized as: (i) for the FB frame, the

number of plastic hinges formed is more in NTHA as compared to CSM but the overall inelastic effect exhibited in NTHA is less as depicted by SRSS of plastic hinge rotations; (ii) at the collapse point of the capacity curve, the overall inelastic effect is significantly more in CSM as compared to NTHA; (iii) base isolation keeps the structure in the elastic range nearly up to a PGA level of 0.2g and there is practically no difference between the results of CSM and NTHA; (v) for the BI frame at higher PGA value, CSM provides much more inelastic effect as compared to NTHA indicated by both the number of plastic hinges and the SRSS value of plastic hinge rotations.

The reason for the difference between the numbers of plastic hinges and SRSS of plastic hinge rotations obtained by the two analyses is due to the difference in the total inelastic effects caused in NTHA and the CSM. In NTHA, it is a complex phenomenon arising out of several factors including: (i) possible participation of higher modes in NTHA for the formation of plastic hinges; (ii) opening and closing of the plastic hinges due to alternating loads leading to the change in the instantaneous stiffness of the sections at which hinges are formed; (iii) dissipation of the energy due to the hysteretic effect and (iv) the stiffness degradation due to damages introduced in the structure (change in mechanical properties in structure with damage). In CSM, it is primarily governed by the elements of inelastic analysis under monotonic loading.

In the case of a fixed base frame, the number of plastic hinges formed is more for NTHA as compared to CSM. At the same time, the SRSS of the plastic hinge rotations is less for NTHA as compared to CSM. More number of plastic hinges are formed in NTHA because of the factors (i) and (ii) as mentioned above. On the other hand, less SRSS of plastic hinge rotations takes place in NTHA primarily due to the factor (iii). Net effect is to produce less inelastic effect in NTHA as compared to CSM, manifested as having relatively more number of plastic hinges with less average SRSS plastic hinge rotations.

In the case of a base-isolated frame, the number of plastic hinges formed are nearly the same in NTHA and CSM for higher PGA level. Further, the SRSS of plastic hinge rotations is more in CSM as compared to NTHA. The reason for this may be primarily attributed to the effect of hysteretic energy dissipation, which is not realistically captured by the CSM. Other factors as mentioned above might also contribute to this phenomenon, but to a lesser extent.

The difference between CSM and NTHA in terms of other response quantities of interest are examined keeping in view the difference in the overall inelastic behavior of building frames exhibited in CSM and NTHA.

4.4.4 Comparison Between Maximum Top Storey Displacement

Table 4.6 compares between the maximum top storey displacement as obtained by CSM and NTHA in the 5-storey and 10-storey for both FB and BI building frames at performance points corresponding different PGA levels. Note that the values provided in the abovesaid table are computed with respect to the NTHA values. It is observed from the table that for the 10-storey FB frame, up to a performance point corresponding to 0.35g, the difference between CSM and NTHA is small (of the order of 10%). With further increase in PGA, the difference between the two analyses increases and it is of the order of 50% at a PGA of 0.5g and 145% at the collapse point.

Table 4.6 Percentage difference between maximum top storey displacement obtained by CSM and NTHA for 5-storey and 10-storey building frames

PGA level (g)	Percentage difference (%)							
	5-Storey frames				10-Storey frames			
	FB5	BI5-S	BI5-M	BI5-F	FB10	BI10-S	BI10-M	BI10-F
0.1	0	-9	-4	0	-4	20	18	-3
0.15	-4	0	6	14	-9	42	15	5
0.2	-9	10	23	40	-11	68	19	23
0.25	-7	19	44	61	-9	54	34	47
0.3	-4	31	62	78	-3	49	47	72
0.35	0	40	78	72	7	52	68	91
0.4	10	51	85	71	19	53	86	103
0.45	19	56	87	77	31	56	100	116
0.5	32	69	88	86	50	63	110	114
At collapse point	96	85	91	106	145	97	90	63

For the 10-storey BI-frame, the difference between the two analyses is small (of the order of 10% up to a PGA level of 0.15g (only for flexible isolator) and after that it increases with an increase in the PGA. At higher PGA values, it is considerably higher as compared to the FB frame. The difference ranges between 60% - 115% at a PGA level of 0.5g depending upon the type of isolator (stiff, medium, and flexible). At the collapse point, this difference goes up to 60% - 100%. The reason for the higher difference between CSM and NTHA for the BI-frame is because of the isolator displacement which varies considerably between CSM and NTHA, the reason for which would be explained in section 4.4.7

For both FB and BI-frames, the difference in maximum top storey displacement between CSM and NTHA increases at higher PGA levels. This is due to the reason that at higher PGA levels the frames get into more inelastic state, but the overall inelastic effect is exhibited less in NTHA as compared to CSM (already discussed in the previous section). As a consequence, this difference increases.

For the 5-storey building frame, the trend of results remains the same as that of the 10-storey frame except in the different numerical values of the percentage difference between the two analyses at different PGA levels as shown in **Table 4.6.**

4.4.5 Comparison Between Maximum Inter-Storey Drift

Table 4.7 compares between the maximum inter-storey drift obtained by CSM and NTHA for the 5-storey and 10-storey frames. Note that the values provided in the abovesaid table are computed with respect to the NTHA values. It is seen from the table that for the 10-storey FB frame, the difference between the responses obtained by two analyses is less, of the order of 10% up to a PGA level of 0.3g. Above this PGA level, this difference increases to 70% at 0.5g. This shows that maximum inter-storey drift compares well between NTHA and CSM up to the value of the PGA = 0.3g even when the structure gets sufficiently into the inelastic state. It can be surmised that CSM is faithfully able to predict the inter-storey drift up to the design level earthquake (0.2g-0.3g), considered for this study. However, there might be a significant difference between the maximum inter-storey drifts obtained by CSM and NTHA depending upon the PGA level. Note that NTHA gives lower values of inter-storey drift.

For the 10-storey BI-frame, it is observed that there is a significant difference between the maximum inter-storey drift obtained by CSM and NTHA. This difference increases with the increase in the PGA level; up to a PGA level of 0.2g, the difference is less than 10% (with medium and flexible isolators) and increases to 373% with stiff isolator, 480% with medium isolator, and 459% with flexible isolator at a PGA level of 0.5g. Thus, this increase in the difference with increase in the PGA level also depends upon the type of isolator used (stiff, medium, and flexible). The reason for this difference between CSM and NTHA is due to the fact that for NTHA, the superstructure tends to vibrate more like a rigid body; as a result, the maximum inter-storey drift is significantly reduced. In the case of CSM, the maximum inter-storey drift is like that of a flexible base structure in which both elastic and inelastic actions are significantly present leading to sizable maximum inter-storey drift.

Table 4.7 Percentage difference between maximum inter-storey drift obtained by CSM and NTHA for 5-storey and 10-storey building frames

PGA level (g)	Percentage difference (%)							
	5 Storey frames				10 Storey frames			
	FB5	BI5-S	BI5-M	BI5-F	FB10	BI10-S	BI10-M	BI10-F
0.1	4	-8	4	5	-1	23	-4	1
0.15	-1	21	17	21	2	43	7	2
0.2	-9	27	28	36	-1	42	8	10
0.25	-9	36	38	29	1	25	18	24
0.3	-5	47	53	33	8	30	24	39
0.35	1	69	69	42	18	63	41	53
0.4	6	184	66	53	30	172	79	81
0.45	13	159	100	76	42	278	237	237
0.5	25	234	150	102	70	373	480	459

Further, when the structure gets more into the inelastic state at higher PGA levels, the inter-storey drift substantially increases in CSM because of the formation of more plastic hinges going into higher plastic level leading to a large difference in the maximum inter-storey drift between NTHA and CSM. The difference somewhat decreases for the flexible isolator. For the flexible isolator, the BI structure behaves nearly in the same manner as that for stiff isolator in NTHA, but the inelastic action is less for the flexible isolator as compared to the stiff isolator in CSM. As a consequence, the less difference in inter-storey drift is observed in the two analyses.

As shown in **Table 4.7**, for the 5-storey building frame, it is observed that the trend of results remains almost the same as that of the 10-storey frame. The percentage differences are less observed between the results of the two analyses. CSM is able to reasonably predict the maximum inter-storey drift up to a PGA level of 0.4g for FB frames with percentage difference less than 10%.

In **Figures 4.22 and 4.23**, the height wise distribution of inter-storey drift ratio is shown for a few selected performance points in 5-storey and 10-storey fixed base and base-isolated frames with medium isolator. It is seen from the figures that the difference in maximum storey drifts between CSM and NTHA is not significant in both 5-storey, and 10-storey BI frames up to a PGA level of 0.3g, after that the difference between the two analyses increases significantly with increase in PGA levels consistent with the performance points. Note that for FB frames, these differences are large only after a PGA level of 0.4g.

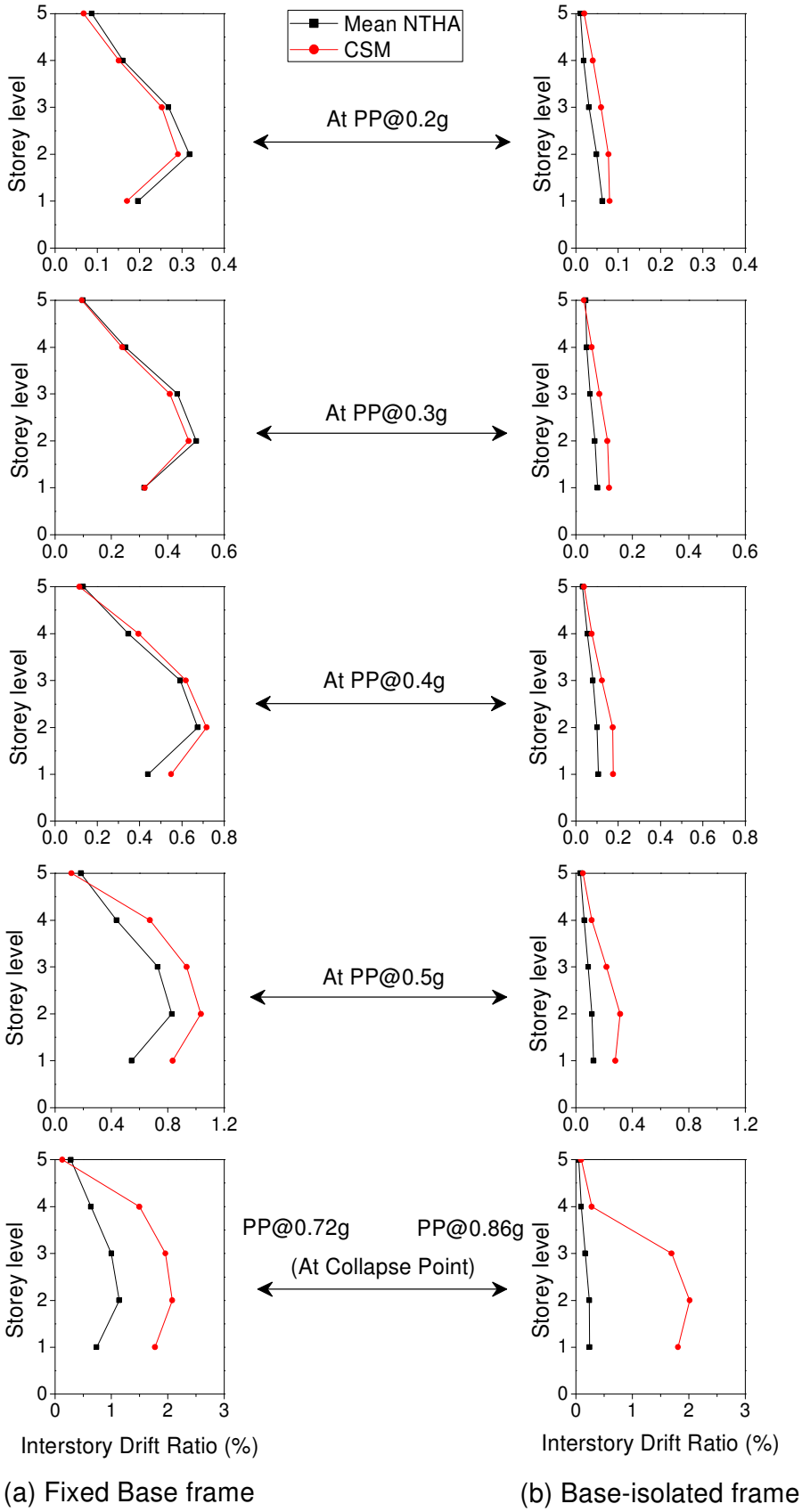

Figure 4.22 Height-wise variation of Inter-storey drift ratio in 5-storey frames determined by CSM and NTHA at different performance points (PP)

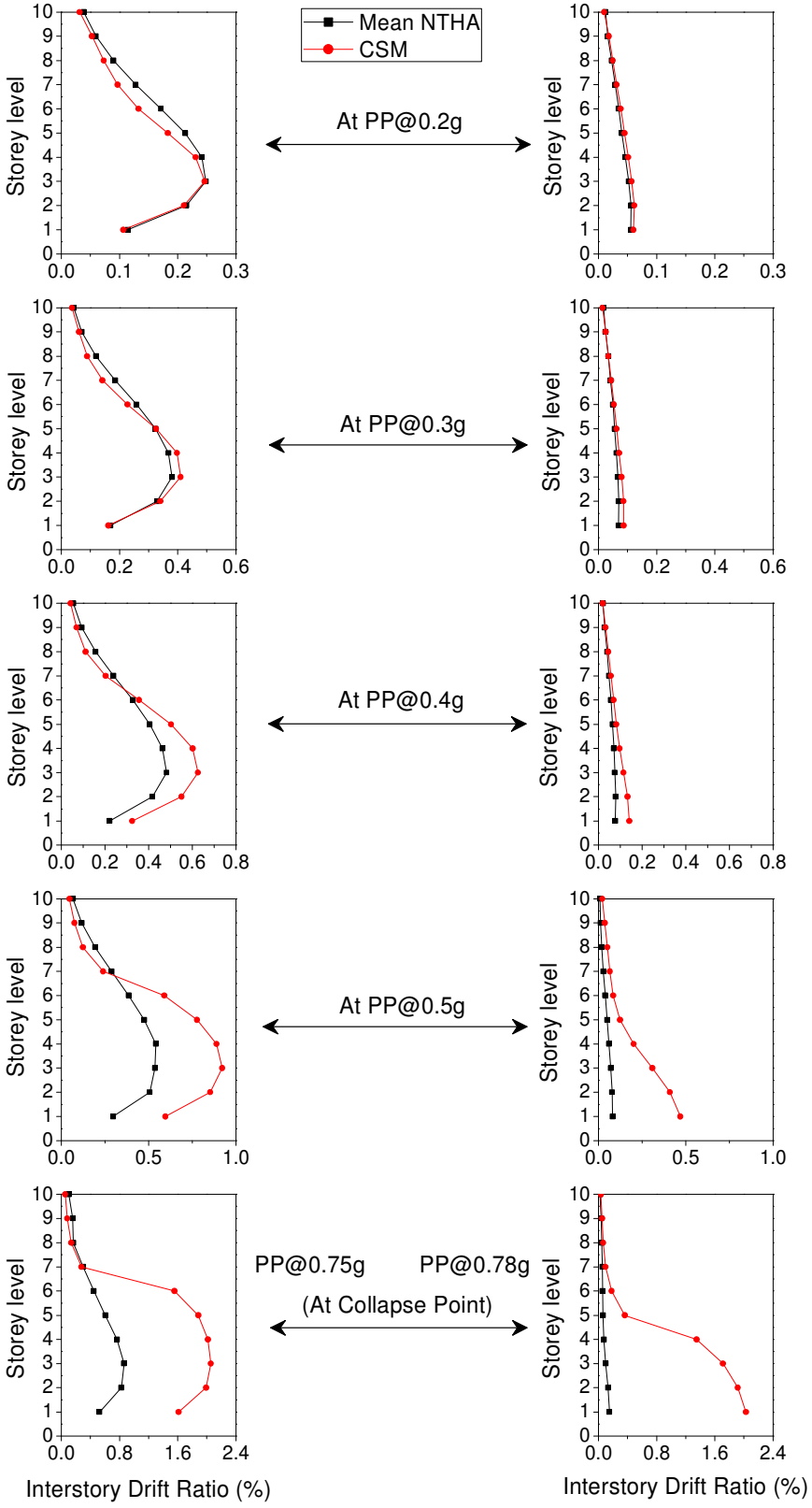

Figure 4.23 Height-wise variation of Inter-storey drift ratio in 10-storey frames determined by CSM and NTHA at different performance points (PP)

4.4.6 Comparison Between Base Shear and Residual Capacity

Figure 4.24 shows the percentage difference between the base shears and residual capacity obtained by CSM and NTHA for the 10-storey FB and BI building frames. Note that the percentage difference is shown with respect to NTHA values. It is seen from the figure that for the FB frame, the difference in base shear increases with increase in PGA, the reason being that the capacity curve becomes almost flat after a performance point corresponding to a PGA of 0.3g as shown in **Figure 4.13** (for 10-storey FB frame) keeping the base shear almost constant. On the contrary, the base shear continues to increase with an increase in PGA level in NTHA and hence, the difference between the two analyses increases. The base shears obtained by NTHA are found to be always greater than those in CSM. At the collapse point, the difference is of the order of 65%. Associated with the base shear is the residual capacity of the frame, which is defined as the difference between base shears at the collapse point and any considered performance point for CSM. For NTHA, the residual capacity is defined as the difference between the base shears obtained from the time history analysis with PGA values corresponding to the collapse point and the considered performance point of the capacity curve. Note that this difference is only taken for the sake of comparison. The actual collapse in NTHA may occur at a higher value of PGA.

The difference between the residual capacities obtained by CSM and NTHA for the 10-storey frame is also shown in **Figure 4.24**. It is seen from the figure that for the FB frame, the percentage difference between the residual capacities obtained by CSM and NTHA for any performance point is found to be large. This the case because there exists a large difference between the base shears obtained by the two analyses.

Further, it is seen from the figure that for the BI frames the percentage difference in base shear also increases with increase in PGA level because of the flatness of the capacity curve after performance point corresponding to a PGA level of 0.5g **(Figure 4.13).** Note that the base shears obtained by the NTHA are less. It is also seen from the same figure that for the BI frames the difference in base shear does not follow a constant trend as that observed for FB frames as it varies with the PGA level and type of isolator. In the range of PGA level of 0.2g to 0.5g, in general, there is an increase in the difference with the increase in the PGA level. It is also seen from the figure that the difference is less than 20% up to a certain PGA level with the different type of isolators, i.e., up to 0.2g with stiff isolator, up to 0.25g with medium and flexible isolators. At the collapse point, this percentage difference is reduced, and the difference depends upon the type of isolator used. Hence, CSM is able to reasonably predict the base shear up to a particular PGA level, which depends upon the type of isolator being used.

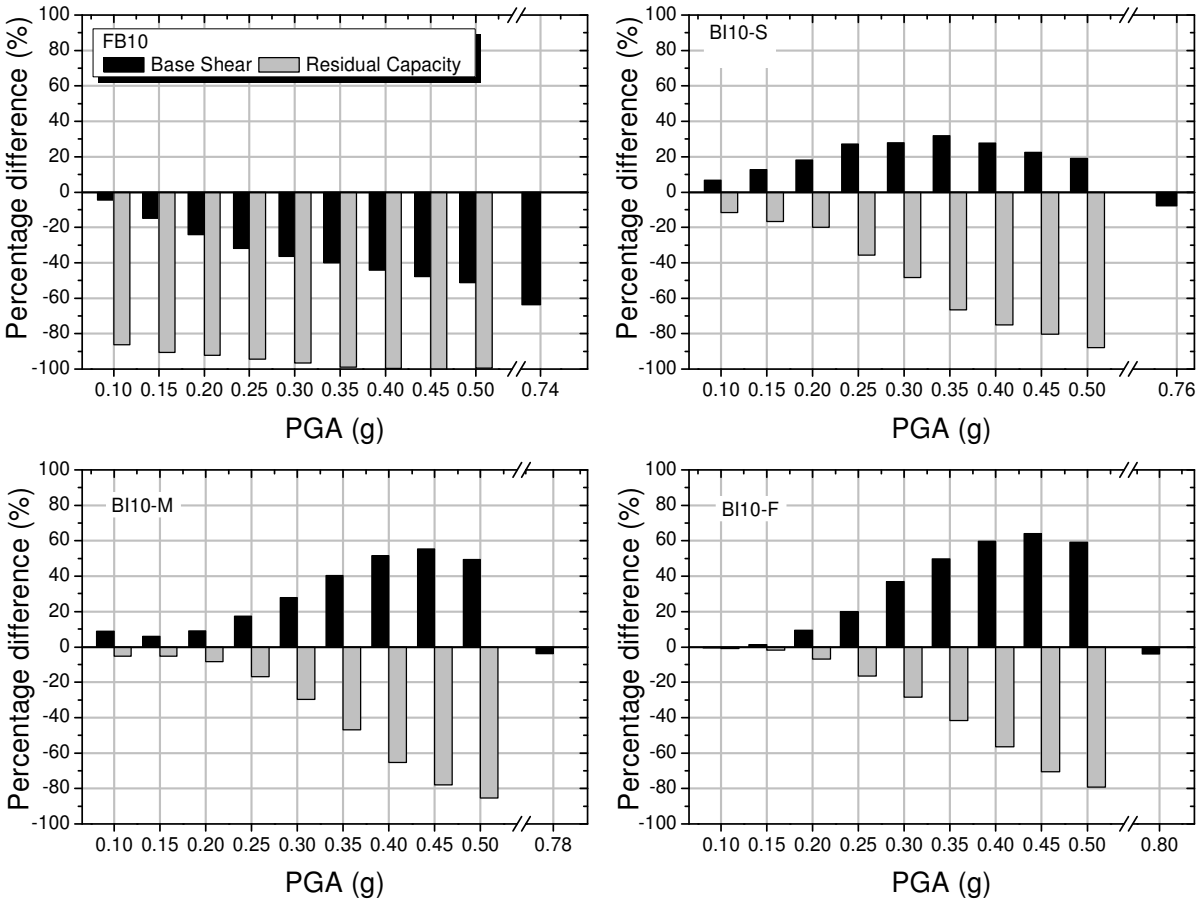

Figure 4.24 Percentage difference between base shear and residual capacity obtained by POA and NTHA for 10-storey FB and BI frames.

Figure 4.24 also depicts the trend in the residual capacity for 10-storey BI frames with a different type of isolators. The residual capacity for all isolators at any performance points is found to be more for NTHA, and its percentage difference between two analyses is less than 25% up to a PGA level of 0.25g, after that this percentage difference increases with increase in PGA level. The variation largely depends upon the value of base shear at the collapse point which varies with the type of isolator.

The trend in the percentage difference between the base shears and residual capacity obtained for CSM and NTHA for the 5-storey building frame remains nearly the same as that of the 10-storey frame except for the numerical values which differ and is shown in **Figure 4.25**. CSM reasonably predicts the residual capacity up to a PGA level of 0.25g with stiff and medium isolator.

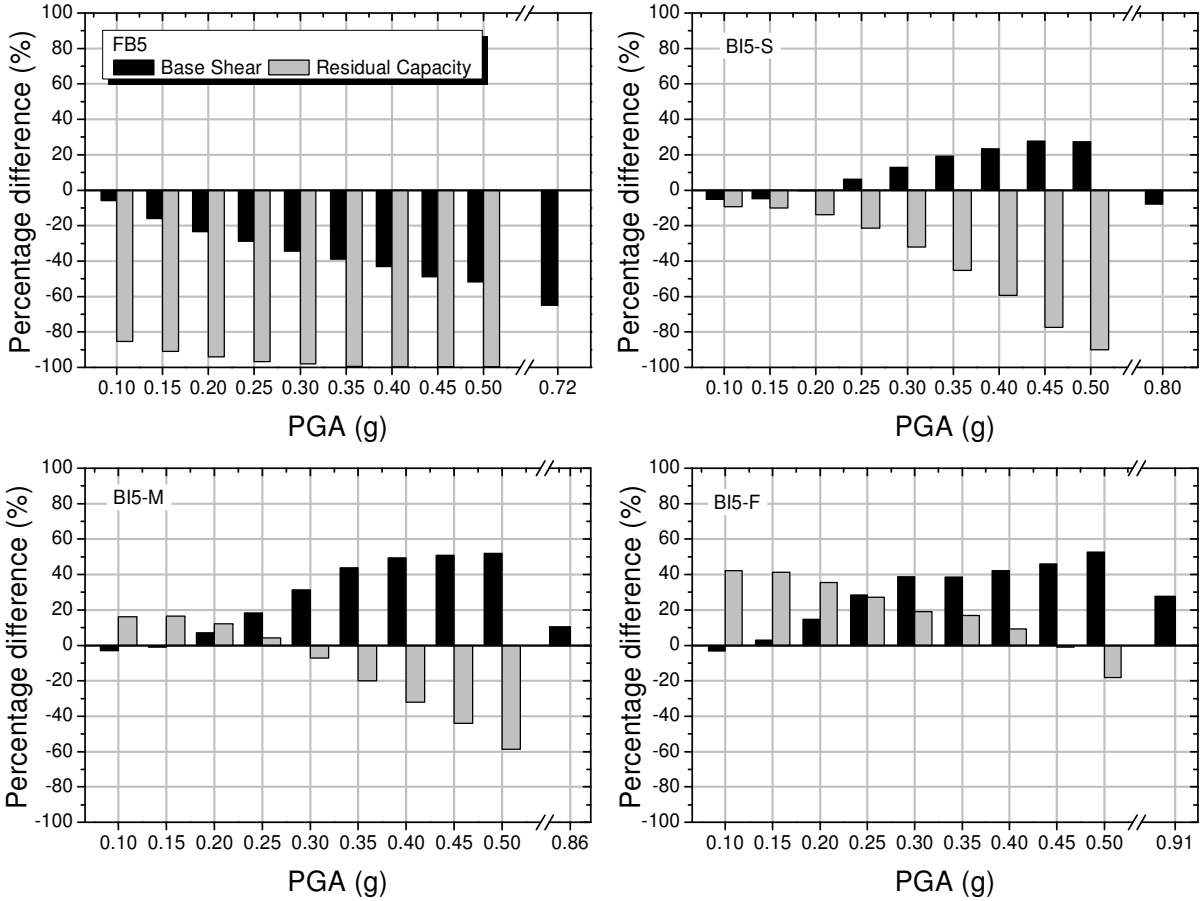

Figure 4.25 Percentage difference between base shear and residual capacity obtained by POA and NTHA for 5-storey FB and BI frames

4.4.7 Comparison Between Maximum Isolator Displacement (MID)

The percentage difference between the isolator displacements obtained from the two analyses for three isolators at different performance points, including the collapse point is shown in **Figure 4.26** for both 5-storey and 10-storey BI frames. The percentage difference changes with different performance points. Unlike the percentage difference in other response quantities, it does not monotonically increase or decrease with PGA values; the difference increases up to a particular PGA value, and then, it decreases. Note that the NTHA provides less values of maximum isolator displacement. Thus, for each type of isolator, there exists a PGA value for which the maximum difference is observed. For the 10-storey frame, at the collapse point, this percentage difference decreases to nearly 1% for stiff isolator and 6% for medium and flexible isolators. The maximum difference is found to be 112% occurring at a PGA of 0.45g. The reason for this is attributed to the difference in the energy dissipation mechanism in CSM and NTHA at different PGA levels. In CSM, the energy dissipation in the

isolation system is considered by way of an equivalent damping at a performance point, whereas NTHA considers the actual energy dissipation due to the hysteresis effect.

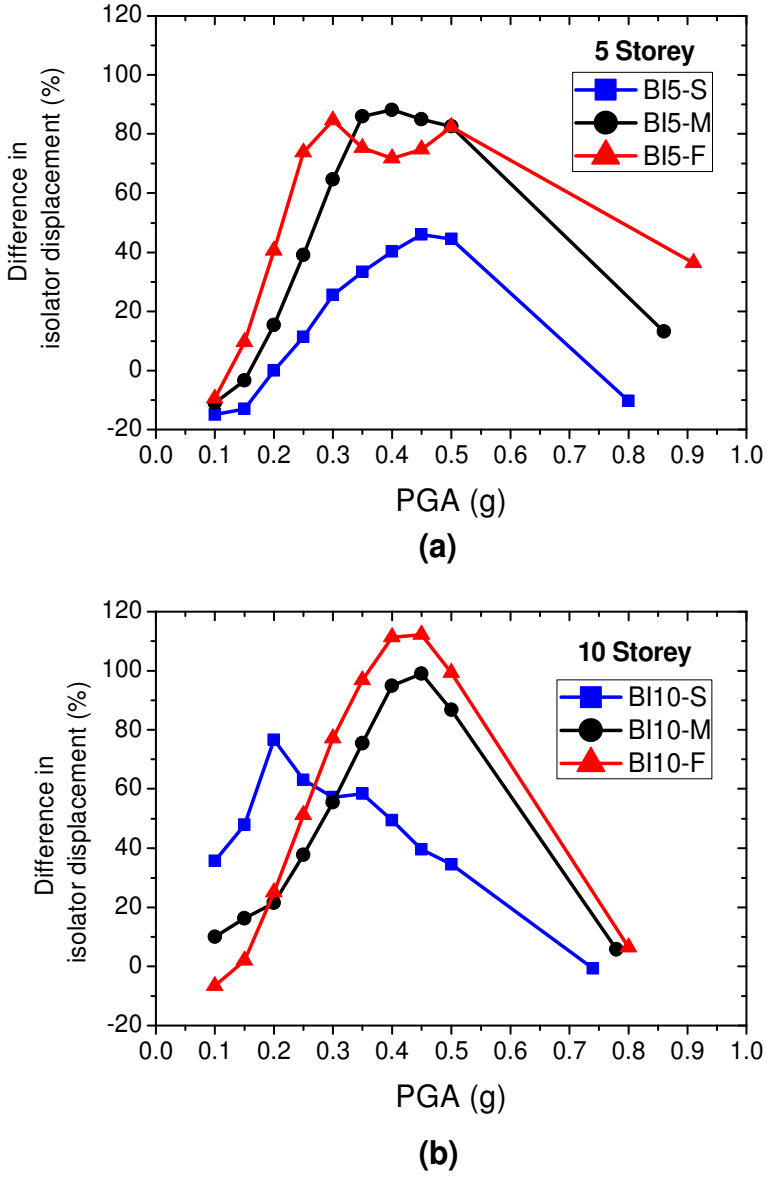

Figure 4.26 Percentage difference between maximum isolator displacement obtained by POA and NTHA for 5-storey and 10-storey BI frames with stiff (S), medium (M), and flexible (F) isolators.

Figure 4.27 shows the maximum isolator displacements obtained by CSM and NTHA at typical performance points for the 10-storey base-isolated frame. The difference in the energy dissipations increases with increase in PGA in a complicated manner up to a certain PGA value, and then it decreases with further increase in PGA. The predictions of CSM are reasonably good up to a PGA of 0.2g with stiff and medium isolators.

For the 5-storey building frame, the trend of results remains the same as that obtained for the 10-storey frame except that the decrease in the percentage difference is more as shown in **Figure 4.26**.

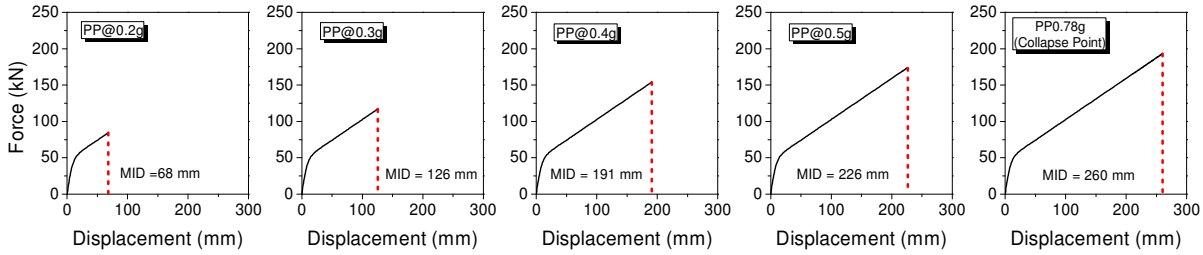

(a) Capacity Spectrum Method (10-storey, Base-Isolated frame with medium isolator)

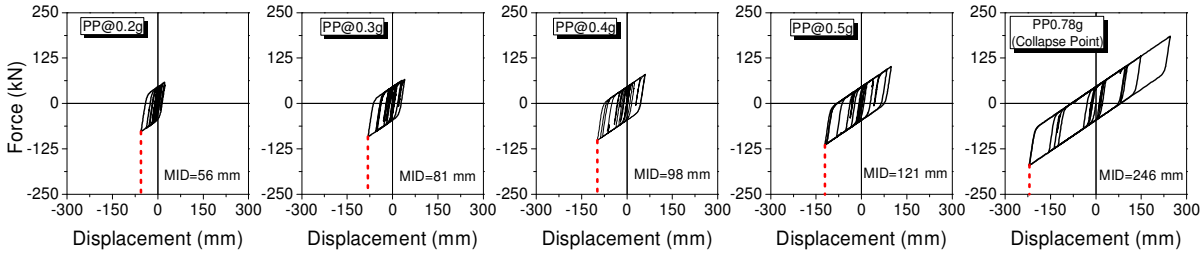

(b) NTHA for Artificial-1 time history (10-storey, Base-Isolated frame with medium isolator)

Figure 4.27 Comparison of maximum isolator displacement (MID) for 10-storey base-isolated (medium isolator) frame at different performance points (PP) obtained by CSM and NTHA (MID values indicated by red dotted lines)

4.5 Conclusions

An extensive study on the difference between the responses predicted by the capacity spectrum method (CSM) and the nonlinear time history analysis (NTHA) is carried out for the base-isolated (BI) building frames at different performance points. For this purpose, two building frames, one 5-storey and the other 10-storey are considered. The effect of base isolator characteristics is included by considering three lead rubber bearing (LRB) isolators namely, stiff, medium, and flexible. In order to typify these differences for BI-frames, the same differences are also cited for the fixed base (FB) building frames as a reference. The ATC-40 response spectrum is used for finding different performance points consistent with PGA values ranging from 0.1g to 0.5g. This leaves the scope for the possibility of formation of plastic hinges from immediate occupancy (IO) level to collapse prevention (CP) level. ATC- 40 response spectrum compatible time histories are used for the NTHA and scaled to aforementioned PGA values for which various performance points are obtained by the CSM, thus enabling the comparison between the two analysis methods for a wide range of

performance points of the structure up to the collapse point. Response quantities which are considered in the analysis include (i) base shear; (ii) top storey displacement; (iii) maximum inter-storey drift; (iv) number of plastic hinges; (v) SRSS of plastic hinge rotations; (vi) residual capacity; and (vii) maximum isolator displacement. To summarize the main findings of the study, the PGA levels corresponding to performance points are divided into three segments, i.e., 0 – 0.2g, 0.25g – 0.4g, and 0.45g – PGA level of the collapse point which varies with the nature and base condition of the frame. The comparison between CSM and NTHA in terms of response quantities of interest are examined in the aforementioned three segments. On the basis of the specific FB and BI frames analyzed in the present study, following conclusions are drawn from the above investigation:

1. At the performance point consistent with a PGA level of 0.2g, which is taken as a measure of design basis earthquake for the present study, none of the plastic hinges are formed in BI-frame in both CSM and NTHA. Therefore, the inelastic effect is not introduced into the BI frames up to the design level PGA. The fixed base frame undergoes moderate damages, showing the formation of plastic hinges, at the performance point consistent with the design level earthquake.

2. No significant difference is observed between the response quantities of interest obtained by the CSM and the NTHA for performance points up to a PGA level of 0.2g for the BI frames. The same is true for the FB frames as well.

3. For all the performance points in the zone of PGA level of 0.25g – 0.4g, different degrees of differences are observed between the response quantities of interest obtained from the two analyses for both BI and FB frames.

4. The degrees of difference depend on the different response quantities of interest, isolator stiffness, and the level of PGA at which performance point is obtained.

5. For the BI frames with medium and flexible isolators, the degrees of difference are less for the residual capacity, the base shear, and the maximum isolator displacement as compared to the peak top storey displacement, the maximum inter-storey drift, and the SRSS of plastic hinge rotations. In general, it is observed that the degree of difference in responses between the two analyses is less in FB frames.

6. Beyond the PGA level of 0.4g, differences between the responses obtained by the CSM and the NTHA significantly increases for BI frames. These differences are relatively less for the FB frames.

7. Considering the above points and specific frames analyzed in this study, it may be inferred that the CSM could be a good replacement for NTHA in predicting the peak values of the responses of the BI frames for the performance points up to the design level earthquake, i.e., 0.2g. Beyond the design level of the earthquake (0.2g), CSM should be cautiously used for predicting the inelastic behavior of BI buildings at different performance points up to a PGA level of 0.4g, which is taken the extreme level earthquake (2 times as design level earthquake) for the present study.

4.6 Research Contributions

The numerical study presented in the present chapter has yielded to the following contributions:

1. Assessment of the efficacy of the Capacity Spectrum Method in contrast with Nonlinear Time History Analysis for base-isolated frames.
2. Comparison of seismic demands for base-isolated frames and fixed base frames at different performance points ranging from the elastic to the plastic state of the structure.
3. Covers comparison of large number of demand measures which are not comprehensively looked at in other studies.
4. Reveals how Capacity Spectrum Method predicts the inelastic behaviour of base isolated frames at various PGA levels.
5. Effect of base isolation characteristics on the response quantities of interest by considering three types of isolators namely, flexible, medium, and stiff defined by the equivalent stiffness of isolators.

Chapter 5

Assessment of Proposed Lateral Load Patterns in Pushover Analysis for Base-Isolated frames

5.1. Introductory Remarks

Pushover analysis is now accepted as a method for assessing the performance and the design verification of building structures (Freeman, 2004; Kilar and Fajfar, 1997). Pushover analysis is also used in the performance-based design to meet the required performance objectives and to estimate the inelastic seismic demands imposed by the earthquakes (Chandler and Lam, 2001; Ghobarah, 2001; Hasan *et al.*, 2002; Krawinkler, 1996a; Krawinkler, 1996b; Krawinkler and Seneviratna, 1998). A lot of research has been carried out for the development of a wide variety of the nonlinear static analysis, considering not only the philosophical concept, but also the lateral load patterns (LLPs) to be used in the analysis.

Pushover analysis uses invariant height-wise lateral load distribution pattern to calculate the inelastic seismic demands of the structure which is likely true if the structure is vibrating in a single mode or the fundamental mode. Conversely, when the inelastic deformation takes place in the structure, the identification of the inertial forces and the seismic demands by single lateral load distribution becomes approximate, although it can give conservative results.

A considerable amount of research has taken place on the application of the pushover analysis to fixed base structures for which estimation of the seismic demand predicted by the POA was compared with that of the nonlinear time history analysis (NTHA) predictions (Bracci *et al.*, 1997; Elnashai, 2001; Kunnath and Kalkan, 2004; Mahdi and Soltan, 2011; Martinelli and Faella, 2015; Mwafy and Elnashai, 2001) by considering different lateral load patterns. On the contrary, there are only a few studies available which deals with the estimation of seismic demands in the base-isolated structure by incorporating different lateral load patterns in pushover analysis. The research on the development of the lateral load patterns for POA which can provide a close estimation of the seismic demands in comparison to the estimates of the NTHA has still a long way to go.

From the comprehensive review of different studies on the application of different lateral load patterns provided in the chapter-2 (literature review). The review shows that the effectiveness of different lateral load patterns was investigated at a single target displacement, which depicts only one state of the structure. Further, the comparison of estimates provided by

the POA and NTHA is made for less response parameters at a single target displacement. The earthquakes considered in NTHA for comparison were only a few far-field ground motion records. This leaves a scope for further studies to be conducted in this area.

With this background in view, the objectives of the present study are set to investigate the effectiveness of different **proposed** (new) lateral load patterns used in the POA for evaluating the seismic demands of BI buildings at different target displacements in comparison to the NTHA. The precise objectives of the study carried out in this chapter are outlined in the chapter-1 (Introduction).

5.2. Theoretical Background

Although the procedures for POA and NTHA are well established and substantial parts have been presented in the previous chapter (in the context of CSM), the pushover analysis carried out in this chapter with special emphasis on the lateral load distribution patterns is presented for the sake of completeness.

In the pushover over analysis, the structure is pushed by the predefined invariant lateral load pattern up to a specified target displacement or until the structure reaches to the ultimate state. The lateral load pattern is the approximation of the lateral forces which are likely to be acted on the structure in the event of an earthquake. There are several lateral load patterns which have been applied in the pushover analysis for the case of the base-isolated structure. The most common LLPs are: (i) uniform force distribution; (ii) triangular profile; (iii) pattern proportional to the shape of 1st mode; (iv) the pattern given by the protective systems committee of structure engineer association of north californio (SEAONC, 1986) in which an inverted triangular distribution over the height of the structure is considered along with an addition concentrated force at the base as per **Equation 5.1**.

The lateral force F_i at i_{th} level of the structure is given by:

$$F_i = \frac{(V_b - F_b)}{R} \frac{w_i h_i}{\sum_{i=0}^{n} w_i h_i} \tag{5.1}$$

$$V_b = K_{eff} D_b \tag{5.2}$$

$$F_b = \frac{V_b}{W} W_b \tag{5.3}$$

where w_i is the weight of i_{th} the storey level, h_i is the height of the i_{th} the storey level, V_b is the base shear at the isolation level, K_{eff} is the effective stiffness of the isolator, D_b is the base displacement, F_b is the concentrated force at base level proportional to the base mass, W_b,

and the total seismic weight of the structure is W. The different lateral load patterns are represented in **Figure 5.1.**

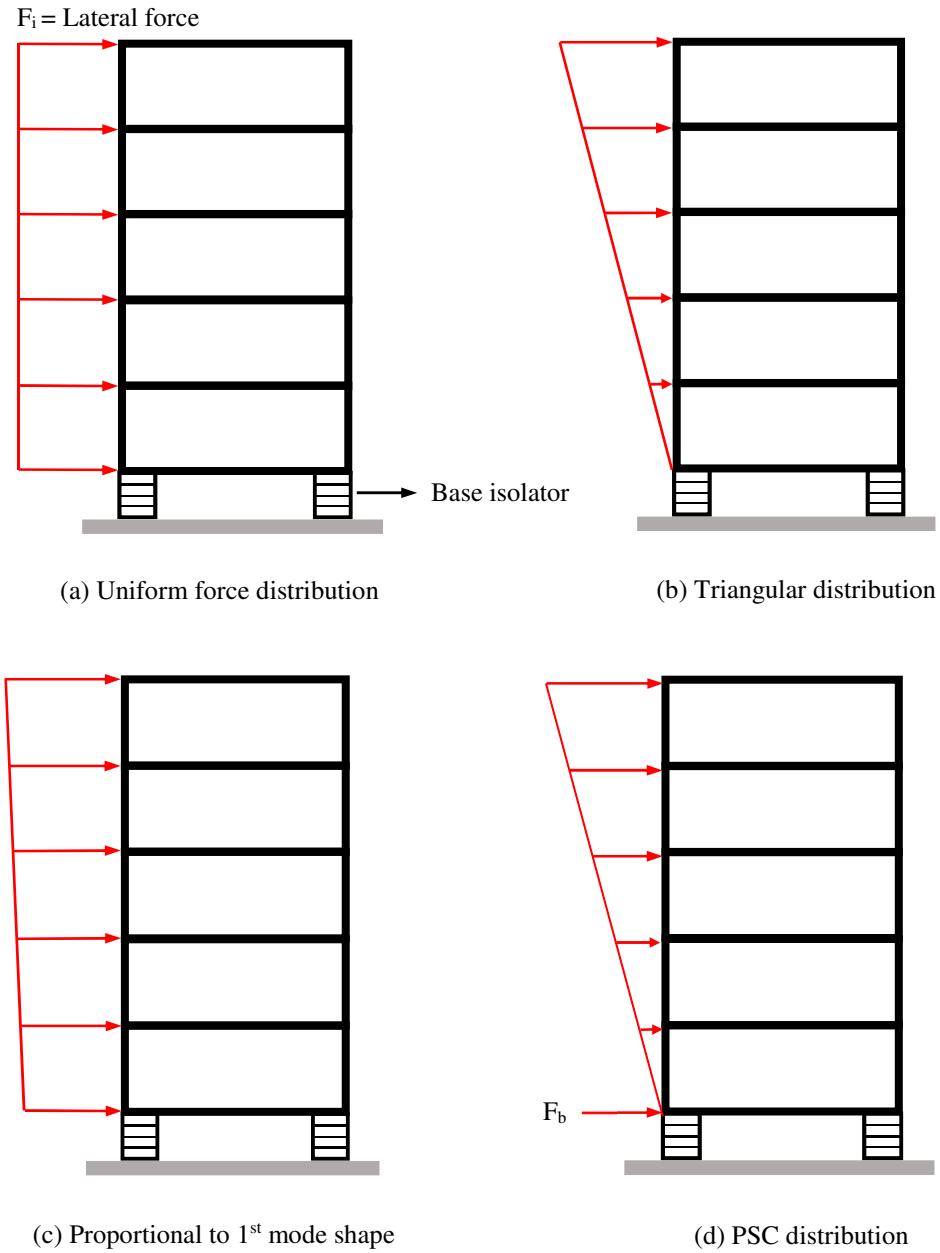

Figure 5.1 Different lateral load patterns for pushover analysis

Pushover analysis has been performed using different types of invariant lateral load patterns (LLPs) proposed by different authors. These load patterns are at best good guesses of the load patterns that conform to the entire range of elastic to inelastic excursion of the structure. It is well-known fact that the load pattern varies at every instant of time and it is difficult, if not impossible to describe a single load pattern remaining valid for the entire range of vibration. Thus, in describing the LLP for performing POA, different invariant LLPs, which

are proposed, cannot be fully justified from the rigor of theoretical point of view. Most of the load patterns are determined from the consideration of load patterns emerging out of the conventional modal response spectrum analysis, which is valid only in the elastic range.

Extending these load patterns in the inelastic range cannot be theoretically justified. Because of this reason, any proposed LLP used in the POA has been verified against the NTHA results. It is found in the literature that different degrees of error are there in the estimates produced by all the LLPs. From the above observations, it may be concluded that the use of classical modal combination rules, to develop LLPs for the POA does not have much sanctity. Any type of modal combinations may be attempted like those proposed by the Kalkan and Kunnath (Kalkan and Kunnath, 2004; Kunnath, 2004) in which weighted summation of modal lateral forces is used to develop the LLPs.

Four lateral load patterns (LLPs), LLP-1 to LLP-4 are used in the present study. The first LLP, LLP-1, which is widely used load pattern, is proportional to the shape of the first mode. Two new lateral load patterns are proposed here, which are: (i) lateral load pattern (LLP-2) derived from the square root of sum of squares (SRSS) of first three mode shapes of the BI structure and (ii) two variants of lateral load patterns (LLP-3 and LLP-4) are derived by modifying the uniform lateral load distribution. The details of the LLPs are given below:

1. **LLP-1:** It is the classical single mode LLP conforming to the shape of 1st mode, which is widely used by other researchers (Doudoumis *et al.*, 2006; Faal and Poursha, 2017; Kilar and Koren, 2010; Koren and Kilar, 2011). Note that when the superstructure of the base-isolated structure undergoes inelastic excursion, this LLP does not remain valid anymore. The degrees of variation depend upon the inelastic excursions undergone by the superstructure.
2. **LLP-2:** A load pattern is evolved by combing the variation of load in each mode in root means square sense, i.e., an SRSS combination of first three mode shapes of the base-isolated building. This LLP contradicts the classical concept of modal response spectrum analysis. However, it is to be noted that modal response spectrum analysis is not valid in the inelastic range and therefore, emphasis on the rigor of maintaining the concept of response spectrum analysis is futile. The attempt is to evolve a load pattern which would predict a good response in the inelastic range subjected to the verification against NTHA. A similar attempt was made by Kalkan and Kunnath (Kalkan and Kunnath, 2004; Kunnath, 2004) in which weighted summation of modal lateral forces

is used to obtain the LLPs as mentioned before. The concept of the development of LLP-2 is based on two premises:

(i). The distribution of load along the height is one-sided, i.e., positive side, which is a rational assumption for the equivalent load pattern throughout the entire range of analysis.

(ii). This proposed load pattern will lead to the single capacity curve as opposed to the modal pushover analysis (MPA) developed by Chopra and Goel (2002), which essentially is a multi-modal pushover analysis and uses the concept of response spectrum analysis to obtain the peak response by combing the modal contributions. The MPA appears to have a major drawback that in the context of performance-based seismic design, different performance points are obtained for different modes which cannot be rationally combined into a single performance point. The proposed LLP-2 gets rid of this problem by providing a unique performance point on the capacity curve.

3. **LLP-3 & LLP-4:** Both LLP-3 and LLP-4 are variations of the uniform load distribution which is quite reasonable so long as the base-isolated structure is in the elastic range. The LLP-3 modifies the uniform load distribution pattern by converting it to a rectangular distribution with upper half to bottom half ratio taken 0.5 for LLP-3 and 0.75 for LLP-4. In this way, the structure is subjected to 100% uniform lateral load at the lower half part and 50% at the upper half part of the structure in LLP-3. In LLP-4, 100% of uniform load is considered at the lower half of the structure and 75 % at the bottom half of the structure. The reason for making the bottom half heavier is due to the fact that in the inelastic range, load from the top is transferred to the bottom part of the superstructure because of the formation of more number of plastic hinges as more inelastic excursion takes place. Note that the two values of load distribution at upper half of the structure considered as 50% and 75% for LLP-3 and LLP-4 are taken as trial values; the intent is to investigate, if uniform load pattern is modified in this fashion it would provide better predictions by POA as compared to the other load patterns.

Note that the proposed load patterns are intuitive and subjected to the verification against NTHA.

To evaluate the performance of the BI building frames, two types of analysis are performed: (i) pushover analysis (POA); and (ii) nonlinear time history analysis (NTHA). The type of NTHA carried out here is explained in the previous chapter. Both the analyses

are performed in SAP2000 software using two-dimensional models of the building frames. Note that the P-Delta effects are considered in both analyses.

The mode shapes of the two base-isolated building frames considered in the previous chapter are shown in **Figure 5.2** The pictorial representation of the different LLPs for the 5-storey, and 10-storey frame is shown in **Figure 5.3** and, their values are depicted in **Figure 5.4**.

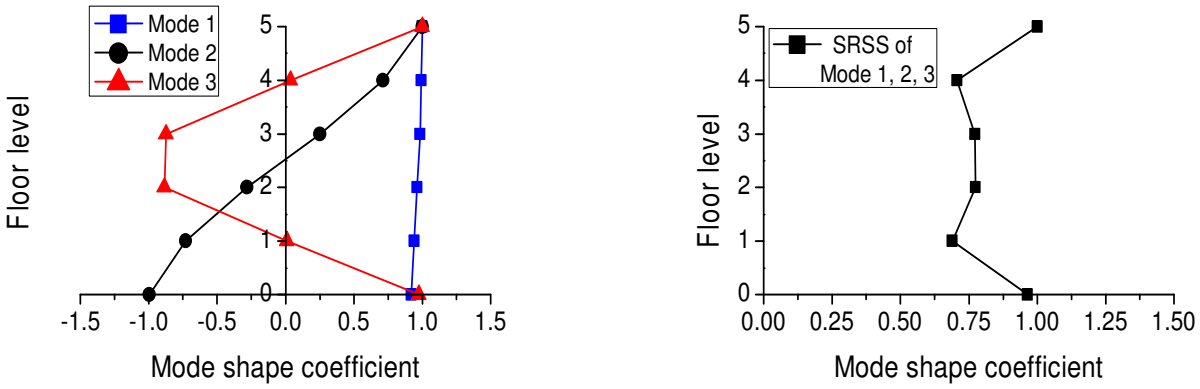

(a) mode shapes of 5-storey base-isolated

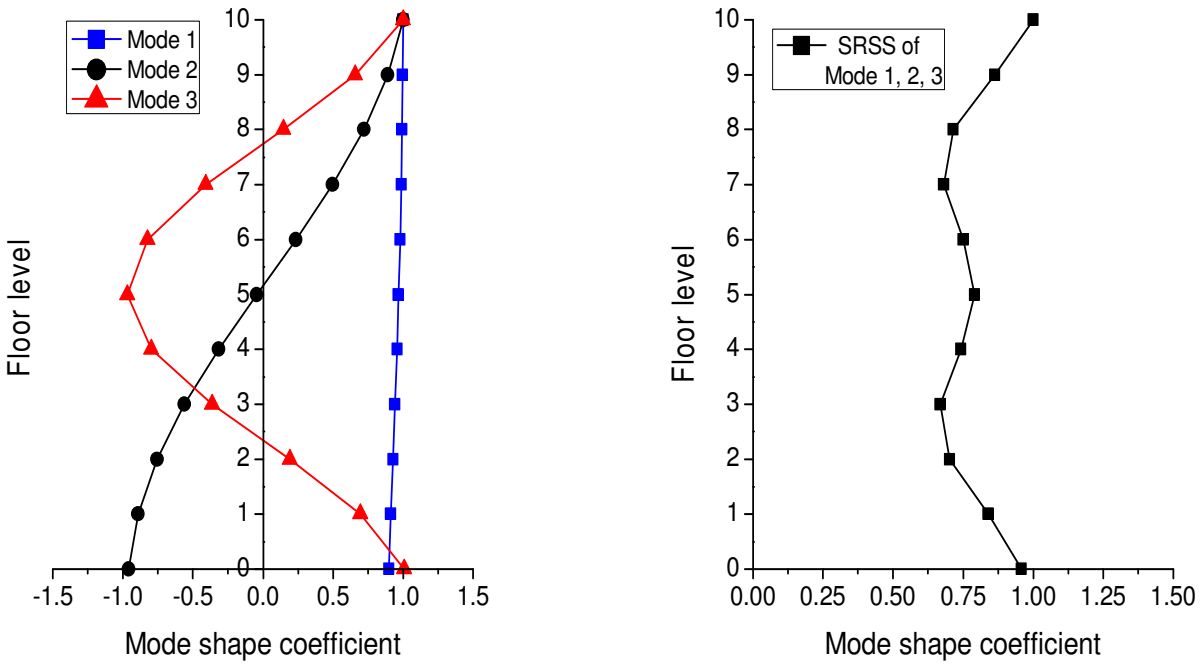

(b) mode shapes of 10-storey base-isolated frame

Figure 5.2 First three natural vibration modes and their SRSS pattern for 10-storey and 5-storey base-isolated frames

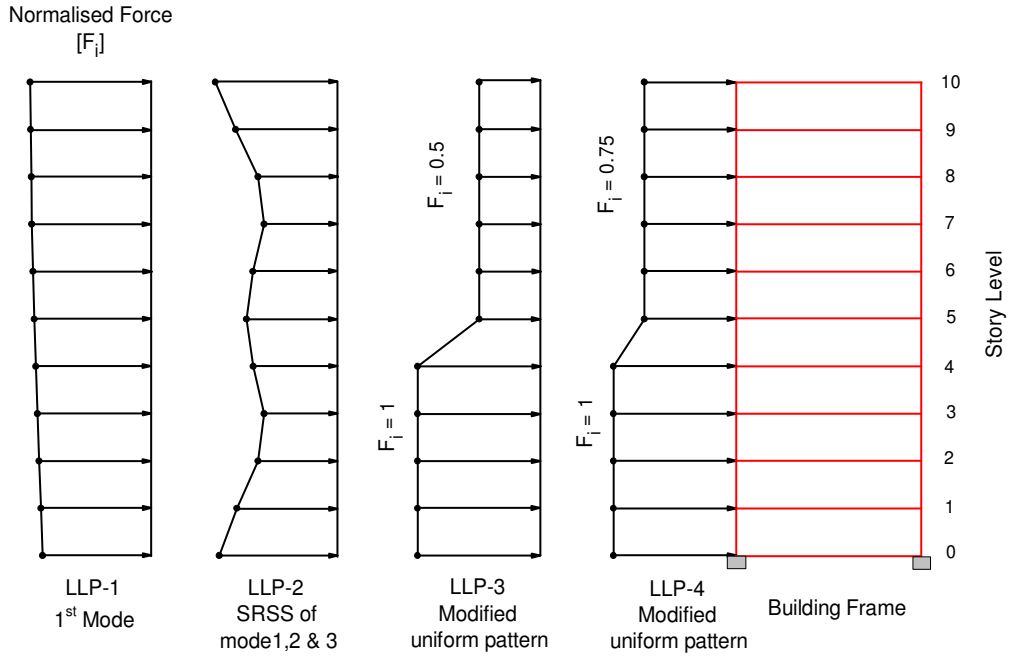

(a) LLPS for 10-story frame

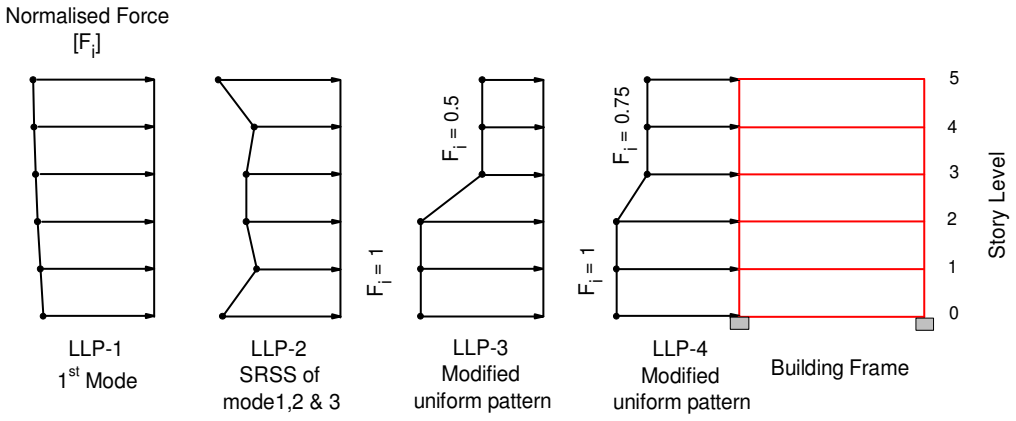

(b) LLPS for 5-story frame

Figure 5.3 Different lateral load patterns (LLPs), LLP-1 to LLP-4 used in pushover analysis of 5-storey and 10-storey frames

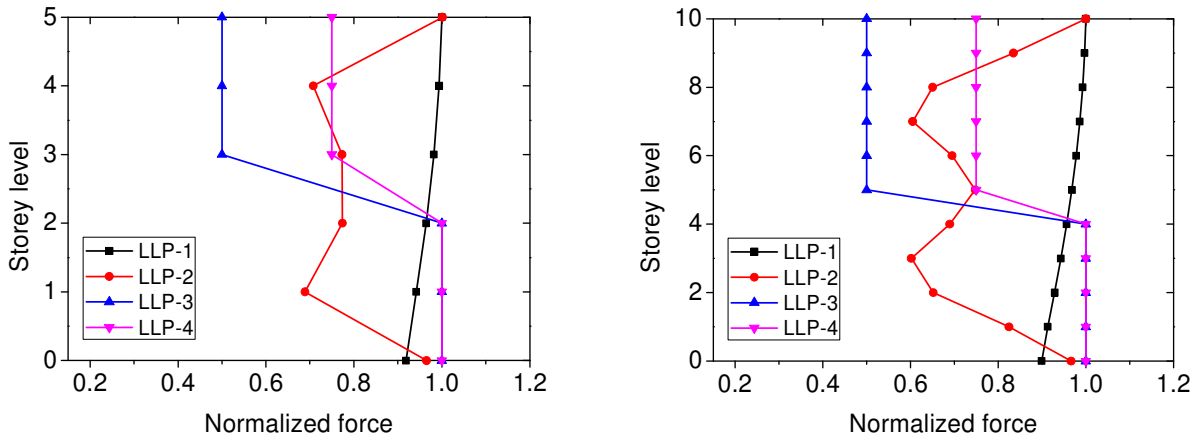

(a) 5-storey frame

(b) 10-storey frame

Figure 5.4 Different lateral load patterns (LLPs), LLP-1 to LLP-4 used in pushover analysis of 5-storey and 10-storey frames

To investigate the effect of earthquakes, three different types of earthquakes are employed in performing NTHA namely, far-field, near-field with directivity effect and near-field with fling-step effect. The far-field records are selected from FEMA(P-695) (2009) report. The near-field records (forward directivity and fling-step) are selected which have Joyner Boore distance, R_{jb}, less than 15 km. An ensemble of five earthquakes is used for each type of earthquakes as shown in **Table 5.1**. Far-field and near-field with directivity records are taken from the Pacific Earthquake Engineering Research Center (PEER) ground motion database of Berkeley. Near-field records are processed ones and are taken from the study of Kalkan and Kunnath (2006b). The mean elastic acceleration spectrums of different types of earthquakes are shown in **Figure 5.5.**

5.3. Numerical Study

The effectiveness of the proposed lateral load patterns is investigated by performing the pushover over analysis on a 10-storey and a 5-storey building frame isolated by lead rubber bearing (LRB) isolators. The two building frames considered in the present study are same as considered in the chapter-4. The medium type base-isolator is used for the base isolation for the two frames. The modeling and designing details of frames and medium isolator remains same as provided in the chapter-4. For the reference, the bilinear characteristics of isolators used for both building frames are provided in **Table 5.2.**

Table 5.1 Characteristics of Earthquake Records

S.No.	Year	Earthquake	M_w	Station	Component	PGA (g)	PGV (cm/s)	PGD (cm)
(a) Far Field Records								
1	1995	Kobe	6.9	Nishi-Akashi	000	0.51	37.28	9.53
2	1992	Landers	7.3	Cool water	TR	0.42	42.35	13.84
3	1978	Tabas	7.4	Ferdows	L	0.093	5.4	2.24
4	1987	Superstition hill	6.5	Poe road	270	0.45	35.72	8.81
5	1971	San Fernando	6.6	LA Hollywood stor	090	0.21	18.87	12.42
(b) Near Field Records (Forward Directivity effect)								
1	1992	Erzincan	6.69	Erzincan	EW	0.5	64.32	21.91
2	1994	Northridge	6.69	Sylmar Converter Sta East	018	0.83	117.5	34.45
3	1979	Imperial Valley	6.53	EL Centro Diff. Array	270	0.35	75.58	57.15
4	1992	Cap Medocino	7	Petrolia	090	0.66	89.68	29
5	1999	Kocaeli	7.4	Duzce	180	.31	58.86	44.06
(c) Near Field Records (Fling step effect)								
1	1999	Chi-Chi	7.6	TCU 052	NS	0.44	216	709.09
2	1999	Chi-Chi	7.6	TCU 068	NS	0.36	294.14	895.72
3	1999	Chi-Chi	7.6	TCU 072	EW	0.46	83.60	209.67
4	1999	Chi-Chi	7.6	TCU 065	EW	0.76	128.32	228.41
5	1999	Kocaeli	7.4	Sakarya	EW	0.41	82.05	205.93

Table 5.2 Bilinear characteristics of isolators

Isolator	Isolation Period, T_{iso} (sec)	Effective stiffness, K_{eff} (kN/m)	Elastic stiffness, k_1 (kN/m)	Post yield stiffness ratio, $\gamma = k_2/k_1$	Characteristic strength, Q (kN)	Yield strength, F_y (kN)	Design disp. D_{max} (mm)
LRB-1 (10-storey)	3	760	5667	0.1	45.78	51	256
LRB-2 (5-storey)	2	774	5757	0.1	31	34.54	170

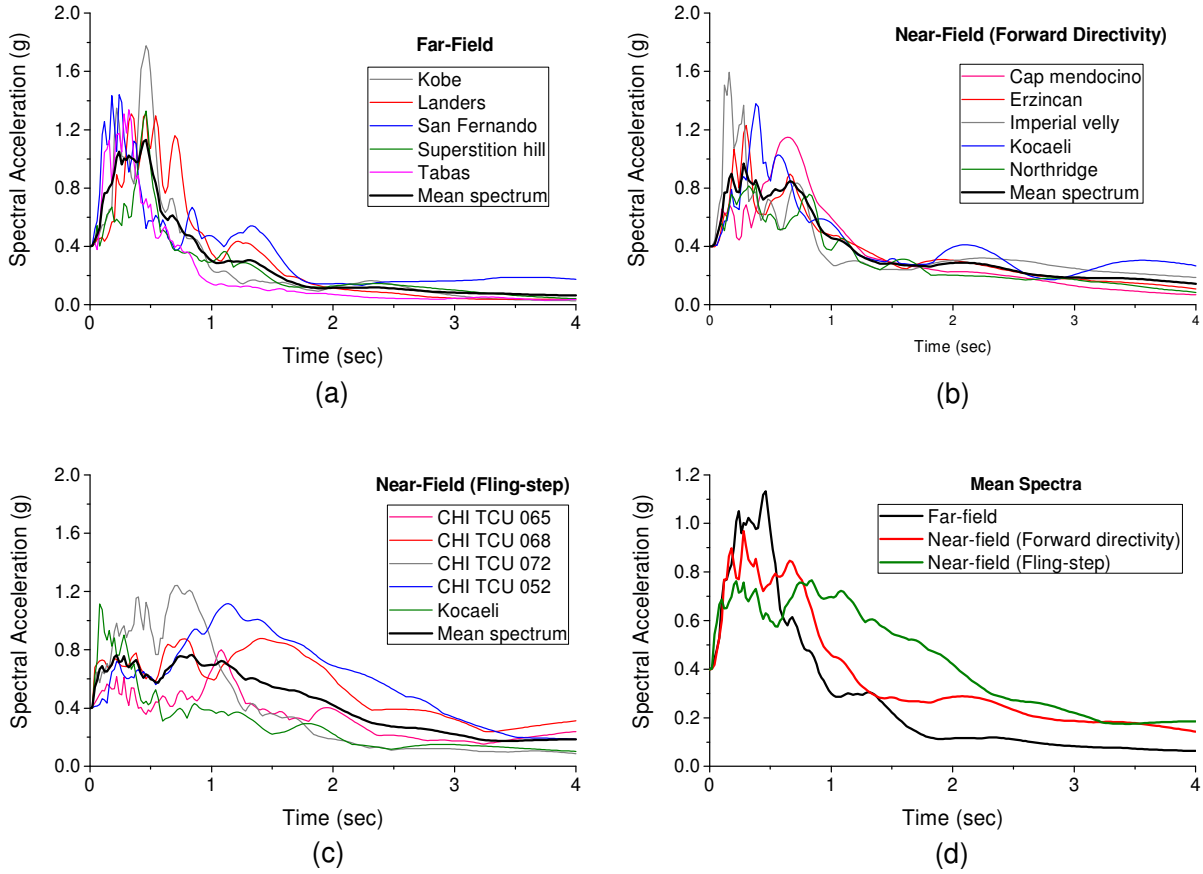

Figure 5.5 Mean acceleration response spectra (5% damping) of five records scaled to PGA of 0.4g of different earthquakes: (a) far-field (FF); (b) near-field, forward directivity; (c) near-field, fling-step; (d) comparison of the mean spectrum of different types of earthquakes.

5.3.1 Evaluation Criteria

Response parameters are evaluated at three different target displacements (TD). The target displacement at which the responses of NTHA and POA are compared, can be fixed from different considerations, for e.g. Kalkan and Kunnath (2007) fixed the target displacement as the 1.5% of the roof drift ratio of the building, which does not have any co-relation with the overall damage state of the building. For the present study, the target displacements are adopted by corelating them with the damage states namely, no damage, which is consistent with TD-1 (structure remains in the elastic range), slight damage, which is consistent with TD-2 (yielding onset of plastic hinges), and extensive damage, which is consistent with TD-3 (onset of strength of strength degradation).

From the numerical study, the TD-1 is fixed such that MIDR lies within range of 0% - 0.15% (no damage). Similarly, TD-2 lies within MIDR range of 0.15% - 0.7% (slight damage), and TD-3 lies within MIDR range of 0.7% - 2% extensive damage) respectively. These ranges

of MIDR corresponds to elastic (TD-1), elastic plastic (TD-2), and plastic (TD-3) states on the capacity curve of both frames as shown in **Figure 5.6** with red lines. Note that these states are visually identified on the capacity curves as (i) Elastic state in the second linear portion; (ii) Elastic- plastic state on the curved portion after the second linear slope; and (iii) Plastic state in the flat portion of the capacity curve. Note that all the three target displacements are the same for different lateral load patterns considered in the study, as there has been not much difference found in the states depicted by load patterns as shown in the figure. In the same figure the discrete points from the NTHA results corresponding to the three target displacements are shown.

In order to find out which LLP works out best, a rational comparison of the results of POA with the benchmark results of NTHA is made at a specified target displacement. For this purpose, the peak ground acceleration (PGA) levels of the time history records of all the considered earthquakes are appropriately scaled to make the peak top floor displacement (resulting from NTHA) equal to the specified target displacement (TD-1, TD-2, and TD-3) used in POA (Kalkan and Kunnath, 2007; Kunnath and Kalkan, 2004). The scaled PGA values of the considered earthquakes required for achieving a specified target displacement for five and ten-storey frames are shown in **Tables 5.3 and 5.4** respectively

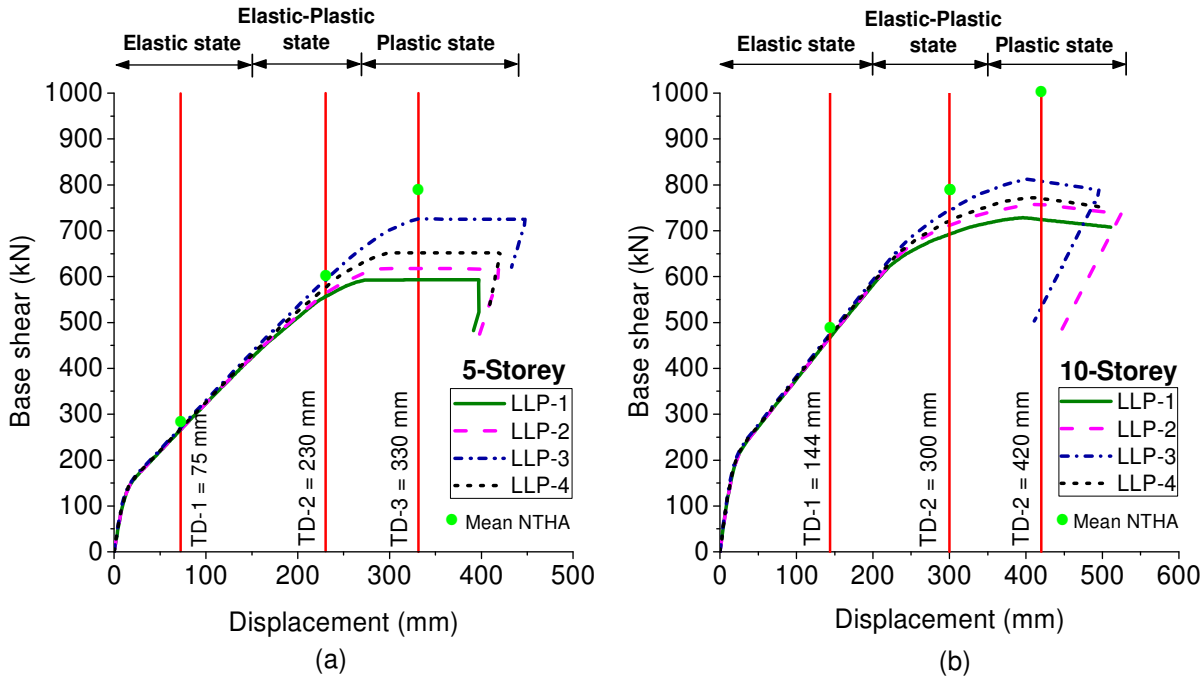

Figure 5.6 Capacity curves of the base isolated building frames obtained by different LLPs indicating different target displacements which lie in three states of structure: (a) 5-storey frame and (b) 10-storey frame

Table 5.3 Scaled PGA values of earthquake records for 5-storey building frame

S.NO	Earthquake	Scaled PGA (g) values at different Target Displacements		
		TD-1 = 75 mm	TD-2 = 230 mm	TD-3 = 330 mm
(a) Far-Field Records				
1	Kobe	0.45	1	1.34
2	Landers	0.28	1.07	1.42
3	Superstition Hills	0.48	1.15	1.5
4	Tabas	0.88	1.97	2.65
5	San Fernando	0.25	0.61	0.87
(b) Near-Field (Forward Directivity) Records				
1	Northridge	0.29	0.69	0.93
2	Imperial valley	0.245	0.5	0.64
3	Kocaeli	0.195	0.5	0.64
4	Erzincan	0.22	0.49	0.64
5	Cap mandocino	0.2	0.5	0.68
(c) Near-Field (Fling-Step) Records				
1	Chi-Chi TCU 052	0.09	0.215	0.3
2	Chi-Chi TCU 068	0.12	0.265	0.355
3	Chi-Chi TCU 065	0.25	0.58	0.76
4	Kocaeli	0.26	0.67	0.95
5	Chi-Chi TCU072	0.26	0.69	0.95

Table 5.4 Scaled PGA values of earthquake records 10-storey building frame

S.NO	Earthquake	Scaled PGA (g) values at different Target Displacements		
		TD-1 = 144 mm	TD-2 = 300 mm	TD-3 = 420mm
(a) Far-Field Records				
1	Kobe	0.62	1.266	1.77
2	Landers	0.55	1.1	1.51
3	Superstition Hills	0.58	0.98	1.29
4	Tabas	1.22	2.19	2.86
5	San Fernando	0.3	0.475	0.6
(b) Near-Field (Forward Directivity) Records				
1	Northridge	0.35	0.66	0.865
2	IV	0.208	0.315	0.395
3	Kocaeli	0.21	0.315	0.395
4	Erzincan	0.245	0.46	0.62
5	Cap mandocino	0.26	0.51	0.72
(c) Near-Field (Fling-Step) Records				
1	Chi-Chi TCU 052	0.14	0.308	0.385
2	Chi-Chi TCU 068	0.103	0.178	0.245
3	Chi-Chi TCU 065	0.25	0.385	0.485
4	Kocaeli	0.3	0.57	0.73
5	Chi-Chi 072 NS	0.3	0.58	0.785

5.3.2 Evaluation of Lateral Load Patterns (LLPs)

Evaluation of the seismic demands predicted by the different lateral load patterns used in the pushover analysis are examined at a particular target displacement by comparing their responses with those of NTHA. The different response parameters include peak storey displacement, maximum inter-storey drift, and the number of plastic hinges, SRSS of plastic hinge rotations, maximum base shear, and maximum isolator displacement. The comparison is made with the help of root mean square (RMS) error defined by **Equations 5.4 and 5.5**.
For a response parameter, RMS is obtained as:

$$RMS_l = \sqrt{\frac{1}{5}\sum_{i=1}^{5}(ERi_{ijlt})^2} \tag{5.4}$$

where i is the earthquake number for each type of earthquake (i = 1 to 5); j is the type of earthquake (far-field, near-field directivity and near-field fling-step); t is the target displacement (TD-1, TD-2 and TD-3); l is the type of lateral load pattern used in POA (LLP 1-4) and the error (ER) is given by:

$$ER_{ijlt} = \frac{(POA)_{lt} - (NTHA)_{ijt}}{(NTHA)_{ijt}} \times 100 \tag{5.5}$$

In which, $(POA)_{lt}$ stands for the absolute maximum value of a response quantity obtained by the POA using load pattern l for the target displacement t and $(NTHA)_{ijt}$ denotes the same obtained by the NTHA for the number of earthquakes i in the type of earthquake j for the target displacement t. Higher the value of RMS more is the difference between the results of the two analyses. The evaluation of seismic demands predicted by POA with different LLPs is discussed in the next section.

5.4 Discussion of Results

The evaluation of the prediction by different lateral load patterns is examined in terms of RMS error and is made response wise in next subsections:

5.4.1 Evaluation of Peak Storey Displacement (PSD)

Figures 5.7 and 5.8 illustrate the variations of the RMS errors of PSDs obtained by different LLPs along the height of the frames at different target displacements for the 5-storey and then 10-storey building frames respectively. It is seen from the **Figures 5.7(a and b) and 5.8(a and b)** that for all types of earthquakes and BI-frames, the RMS errors along the height

of the building are negligible, maximum of the order of 10%, at TD-1. At TD-2, they are small, maximum of the order of 12%; the LLP-3 provides the least error.

The above trend of variation is observed because the isolator displacement predominantly governs the target displacement at TD-1 (elastic state) and TD-2 (elastic to plastic static). Consequently, no significant difference between the displacement profiles obtained by different LLPs is found. Since the differences in the displacements obtained by NTHA and POA are small for all types of earthquakes, the RMS errors are also negligible.

As shown in **Figures 5.7(c) and 5.8(c),** at TD-3, the RMS errors at the upper storey levels are negligible, of the order of 2% for all types of earthquakes and both BI frames. At the bottom storey levels, the RMS errors significantly increase, with the maximum error of the order of 30% produced by LLP-1 at the base; LLP-3 provides the minimum error of the order of 10% in case of 5-storey frame and 20% in the 10-storey frame. The reason for the large errors at the bottom storey levels is due to the more inelastic effect exhibited by the POA with all LLPs at TD-3 (plastic state) compared to that exhibited by NTHA. The reason is well explained later when RMS errors in SRSS of plastic hinge rotations are discussed.

Also, the peak storey displacement profiles of the frames are represented in terms of the storey drift ratio, which is defined as the maximum storey displacement normalized by the building height. **Figures 5.9 and 5.10** compares the storey drift ratio along the height of the five and ten-storey frames estimated by different LLPs with mean NTHA estimates at different target displacements and types of earthquakes considered.

It is observed from the **Figures 5.9(a and b) and 5.10(a and b)** at TD-1 and TD-2, for all building frames and earthquakes, the prediction of PSD by all LLPs does not have large differences in comparison to mean NTHA results. On the contrary, at TD-3, the PSDs are highly underestimated by all LLPs at bottom storey levels in both frames and for all earthquakes. Specifically, LLP-1 provides largest underestimations and LLP-3 gives the nearest estimations of the PSD for all considered target displacements, building frames, and types of earthquakes.

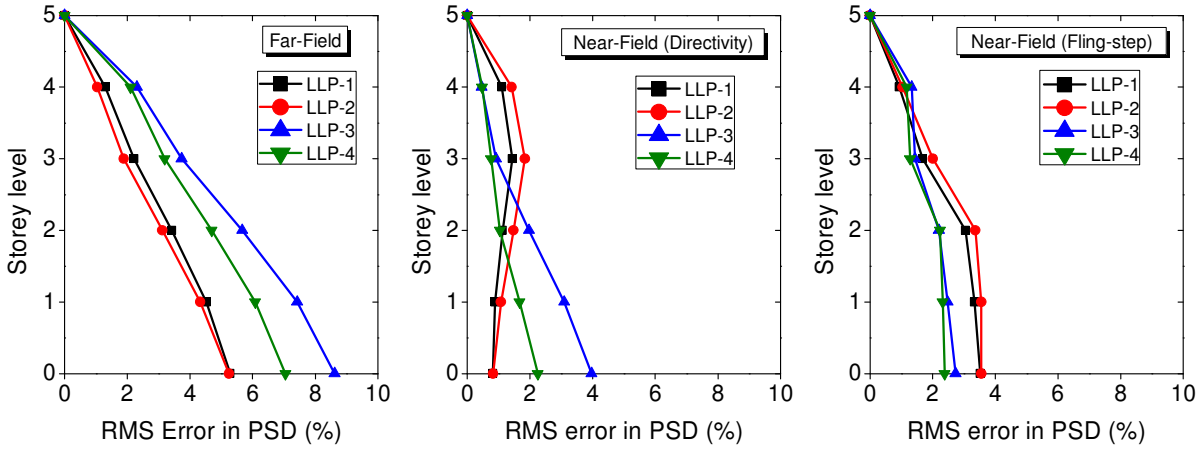

(a) RMS error in 5-storey frame at TD-1 = 75 mm

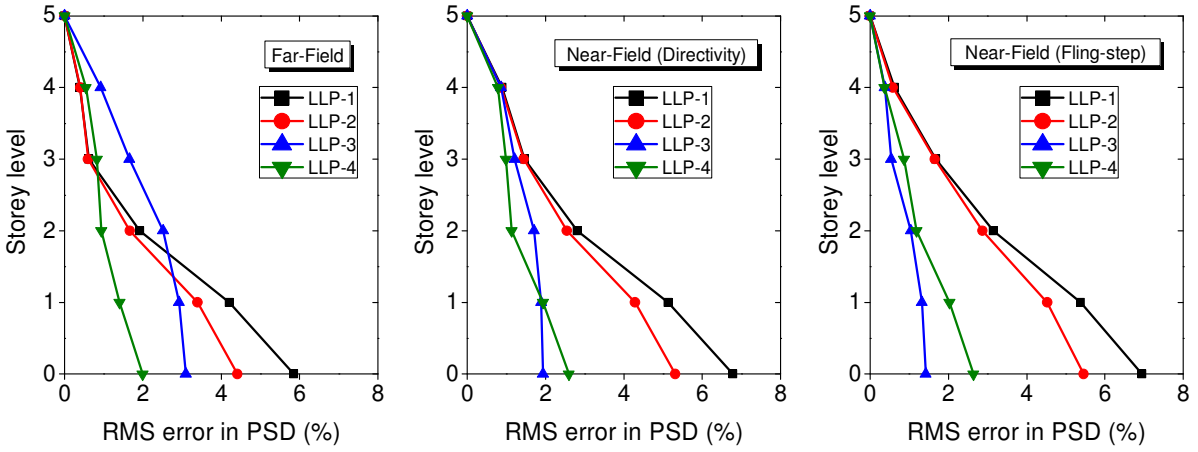

(b) RMS error in 5-storey frame at TD-2 = 230 mm

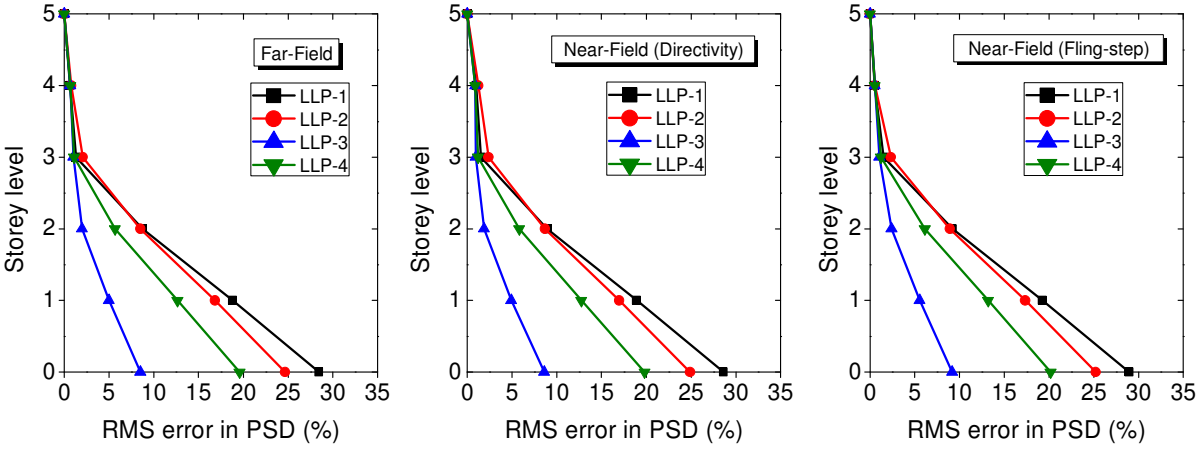

(c) RMS error in 5-storey frame at TD-3 = 330 mm

Figure 5.7 RMS error exhibited by different LLPs in the prediction of peak storey displacement (PSD) of the 5-storey frame for far-field, near-field (directivity), and near-field (fling-step) earthquakes at different target displacements

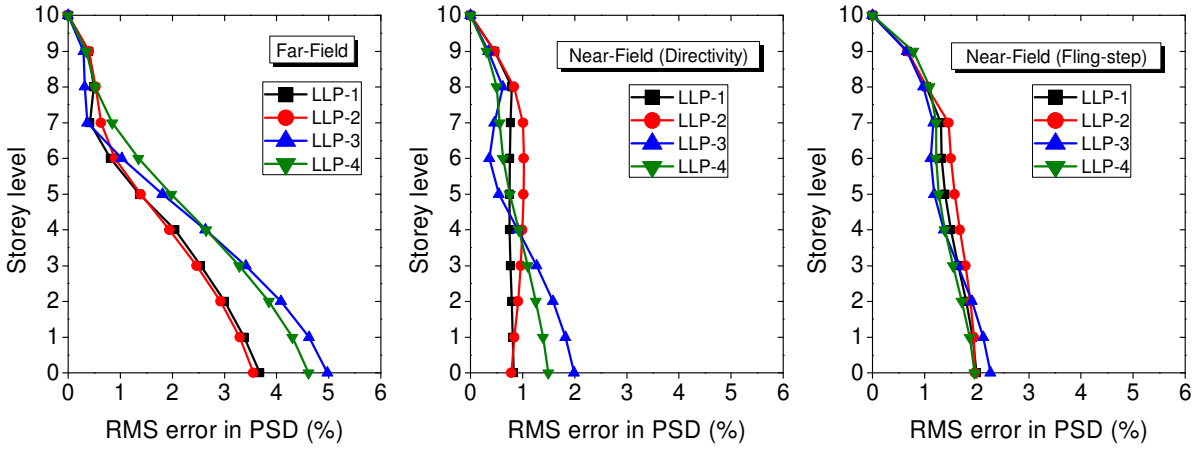

(a) RMS error in 10-storey frame at TD-1 = 144 mm

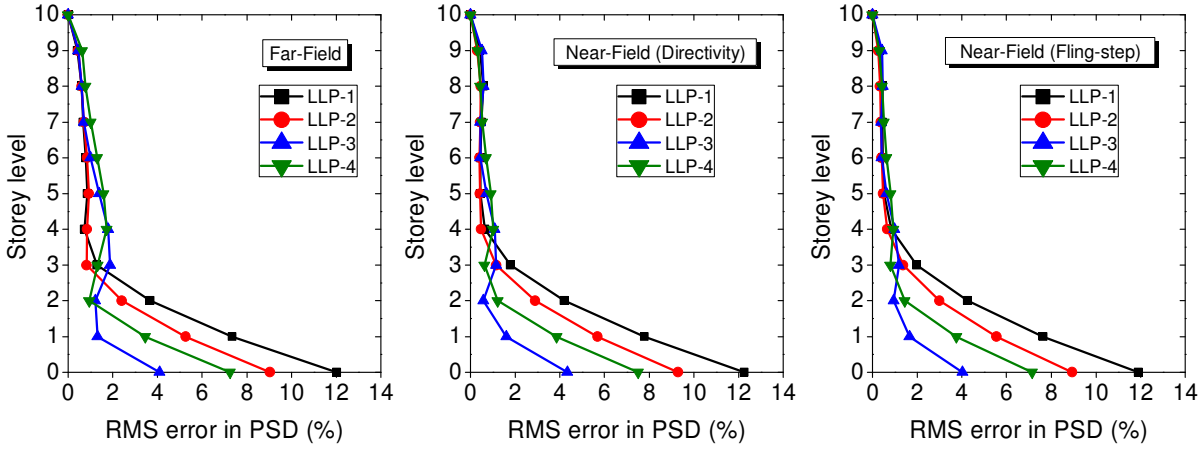

(b) RMS error in 10-storey frame at TD-2 = 300 mm

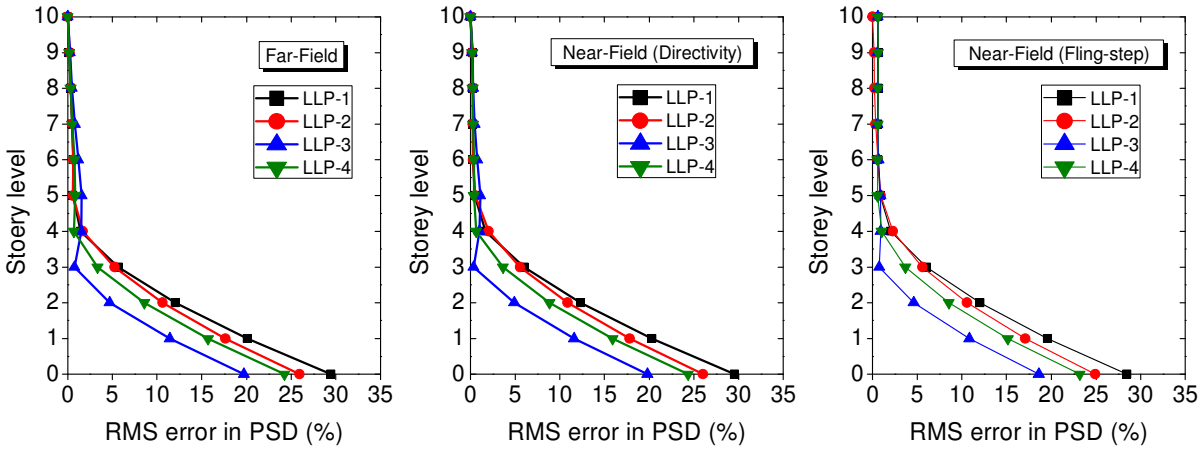

(c) RMS error in 10-storey frame at TD-3 = 420 mm

Figure 5.8 RMS error exhibited by different LLPs in the prediction of peak storey displacement (PSD) of the 10-storey frame for far-field, near-field (directivity), and near-field (fling-step) earthquakes at different target displacements

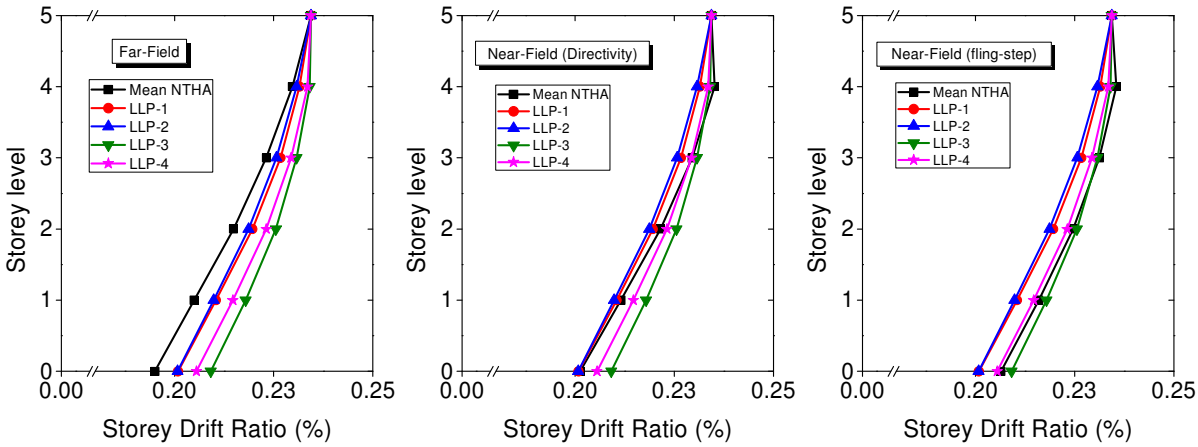

(a) Storey drift ratio of 5-storey frame at TD-1 = 75 mm

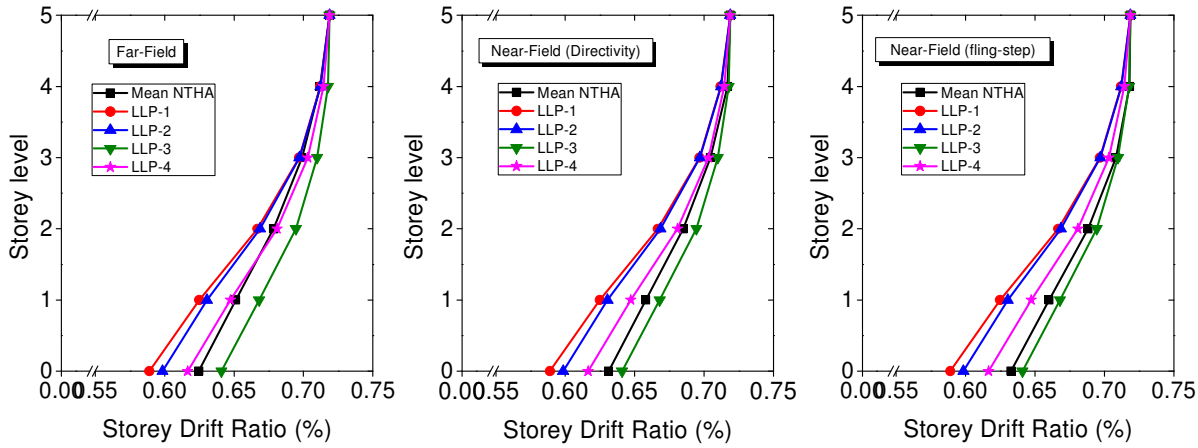

(b) Storey drift ratio of 5-storey frame at TD-2 = 230 mm

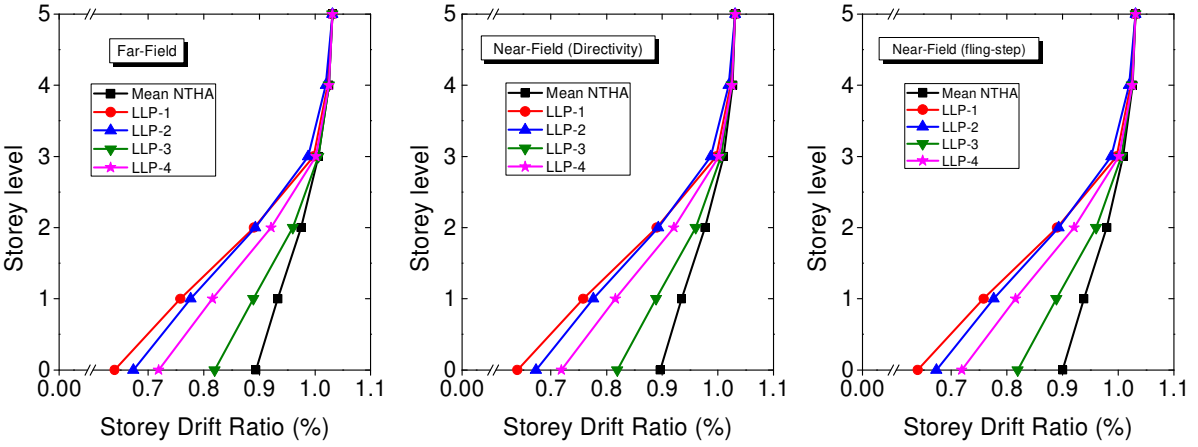

(c) Storey drift ratio of 5-storey frame at TD-3 = 330 mm

Figure 5.9 Height-wise variation of peak storey displacements of the 5-storey frame for far-field, near-field (directivity), near-field (fling-step) earthquakes compared to different LLPs at different target displacements (TD)

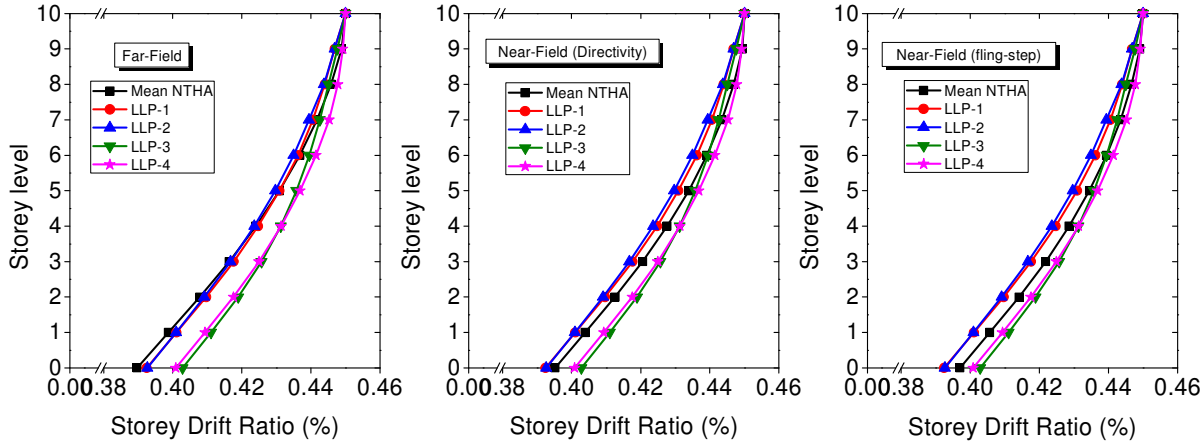

(a) Storey drift ratio of 10-storey frame at TD-1 = 144 mm

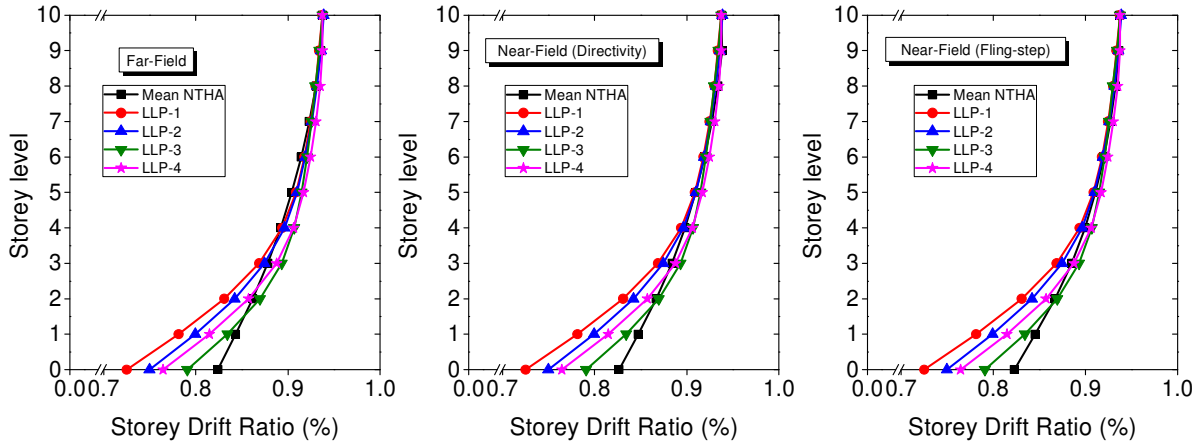

(b) Storey drift ratio of 10-storey frame at TD-2 = 300 mm

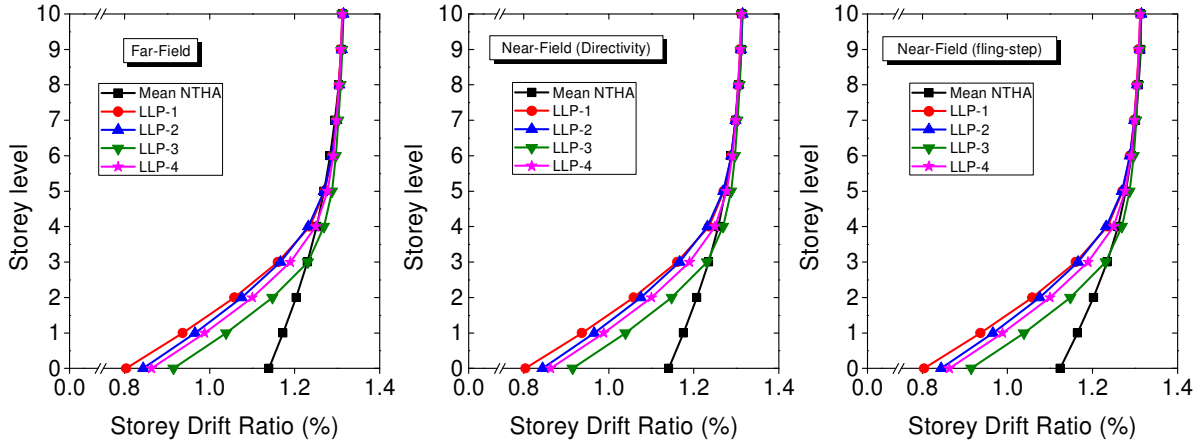

(c) Storey drift ratio of 10-storey frame at TD-3 = 420 mm

Figure 5.10 Height-wise variation of peak storey displacements of the 10-storey frame for far-field, near-field (directivity), near-field (fling-step) earthquakes compared to different LLPs at different target displacements (TD)

5.4.2 Evaluation of Inter-Storey Drift Ratio (IDR)

Figures 5.11 and 5.12 show the heightwise variation of the RMS errors in IDR in the 5-storey and the 10-storey frames for three types of earthquakes and at different target displacements. It is observed from the figures that the RMS errors increase from lower storey levels to upper storey levels. Different LLPs produce different RMS errors. Even at TD-1 **(Figures 5.11(a) and 5.12(a)),** the errors are large for both frames. The RMS errors remain less than 10% at lower storey levels and increase to a maximum of 60% at the top storey level. The LLP-1 and the LLP-4 provide less error.

This large difference in the IDR at the top floor level is caused due to the difference in the natures of the elastic responses of the building frames obtained by NTHA and POA. While in NTHA, the variation of the maximum lateral displacement along the height of the frame is nearly a trapezoidal shape having some curvature towards the top, the displacement pattern along the height of the frame in POA follows the usual shear mode of deformation in the elastic state. The former variation of maximum lateral displacement is caused due to the fact that the displacement in the elastic state in NTHA is largely governed by the fundamental mode shape of BI frames. This difference in the nature of elastic responses along the height of the frames has tended to the large difference in the maximum inter-storey drift at the top storey level between NTHA and POA.

Conversely, an opposite trend in the RMS errors is observed at TD-2 and TD-3. It is observed from **Figures 5.11(b and c), and 5.12(b and c)** that the RMS errors significantly increase from the upper to the bottom storey levels, which is opposite to that found at TD-1. RMS errors for the upper storey levels (above 4^{th} storey in the 5-storey frame and above 5^{th} storey in the 10-storey frame) remain in the range of 10% - 50% at TD-2 and TD-3. On the contrary, significant errors are found at lower storey levels, and they increase as the target displacement moves from TD-2 to TD-3. The LLP-1 produces the maximum error at the bottom storey levels in both frames; 200% and 330%, corresponding to TD-2 and TD-3 in the 10-storey frame; and 60% and 300% corresponding to TD-2 and TD-3 in the 5-storey frame. The least errors are provided by LLP-4 at TD-2 of the order of 30% and by LLP-3 at TD-3 of the order of 85% in the 5-storey frame. In the 10-storey frame, LLP-3 provides least errors of 90% and 200% at TD-2 and TD-3 respectively.

Also, in **Figures 5.13 and 5.14**, the IDR profiles of 5-storey and 10-storey frame estimated by the different LLPs are compared with mean NTHA estimates. The trend of results for the two frames, at all target displacement and considered earthquakes, are same as discussed in terms of RMS errors and hence are not discussed here again.

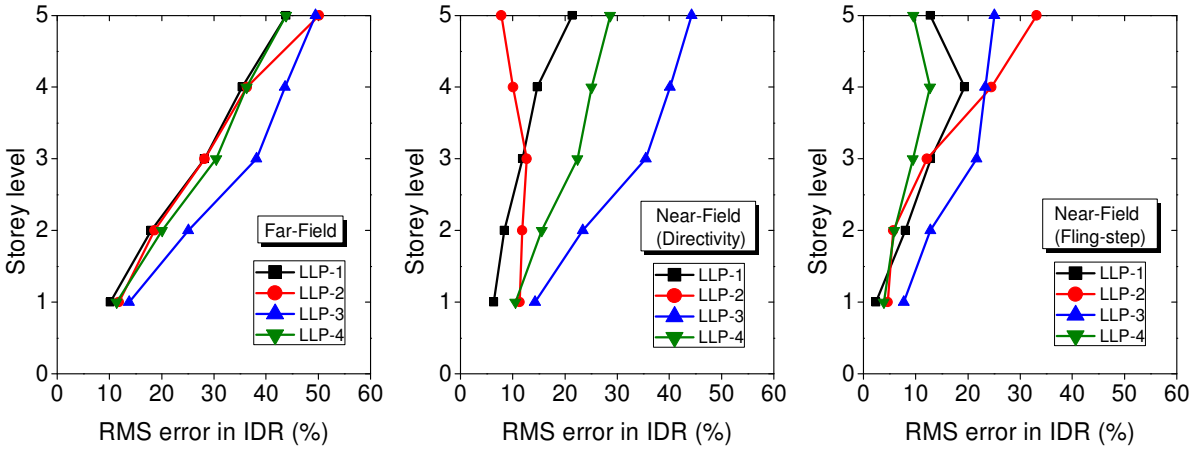

(a) RMS error in 5-storey frame at TD-1 = 75 mm

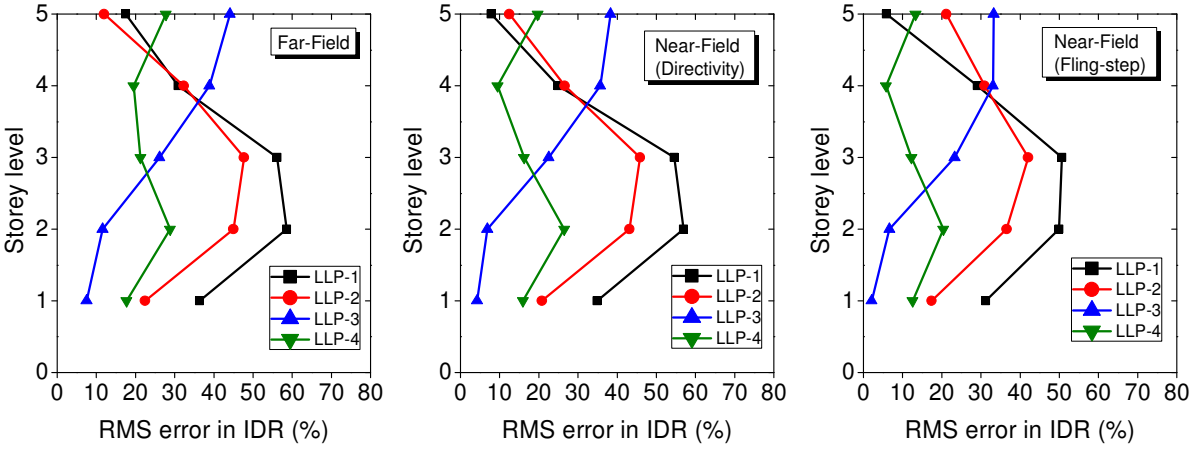

(b) RMS error in 5-storey frame at TD-2 = 230 mm

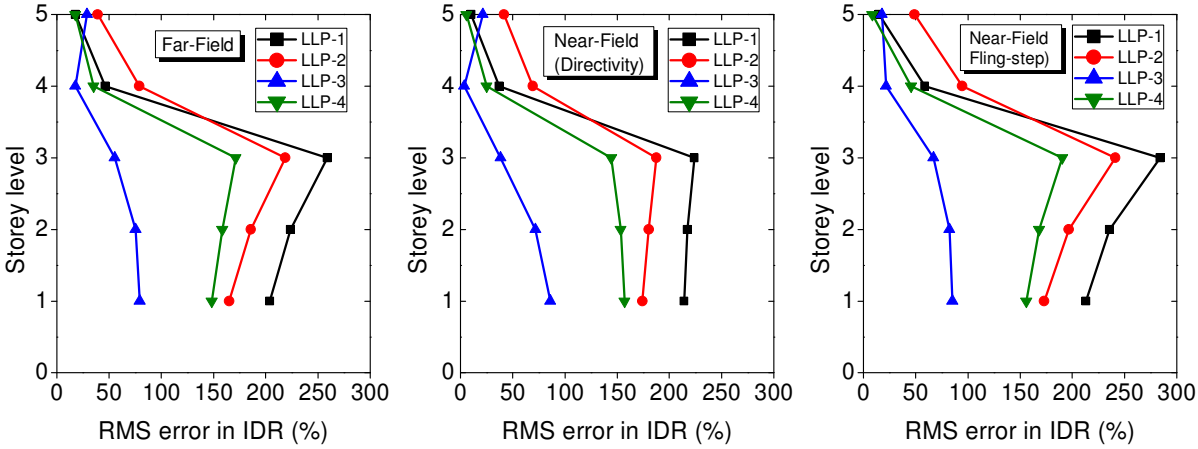

(c) RMS error in 5-storey frame at TD-3 = 330 mm

Figure 5.11 RMS error exhibited by different LLPs in the prediction of inter-storey drift ratio (IDR) of the 5-storey frame for far-field, near-field (directivity), near-field (fling-step) earthquakes at different target displacements

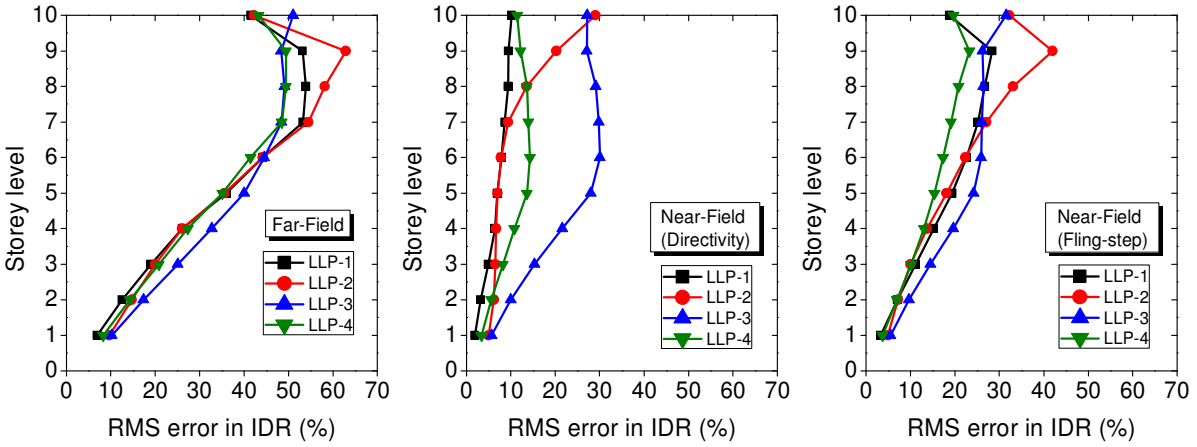

(a) RMS error in 10-storey frame at TD-1 = 144 mm

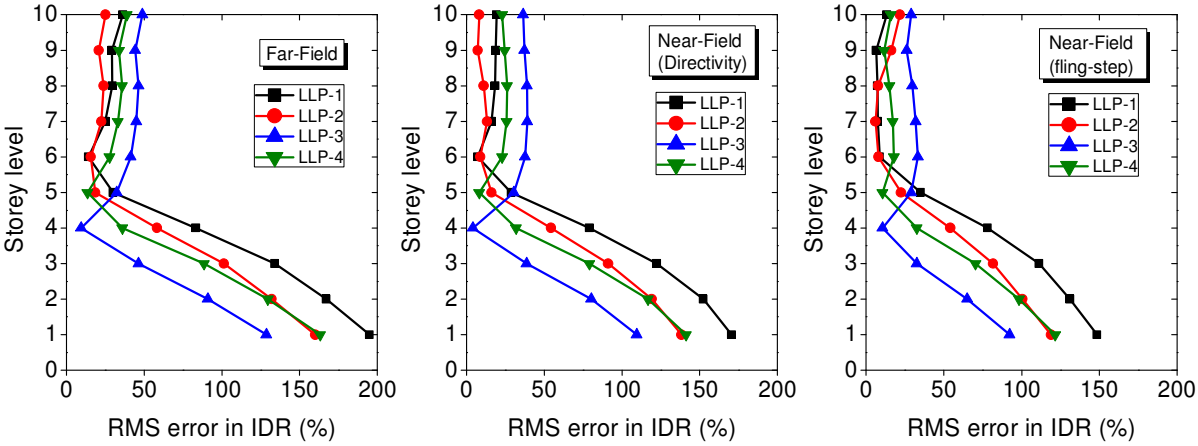

(b) RMS error in 10-storey frame at TD-2 = 300 mm

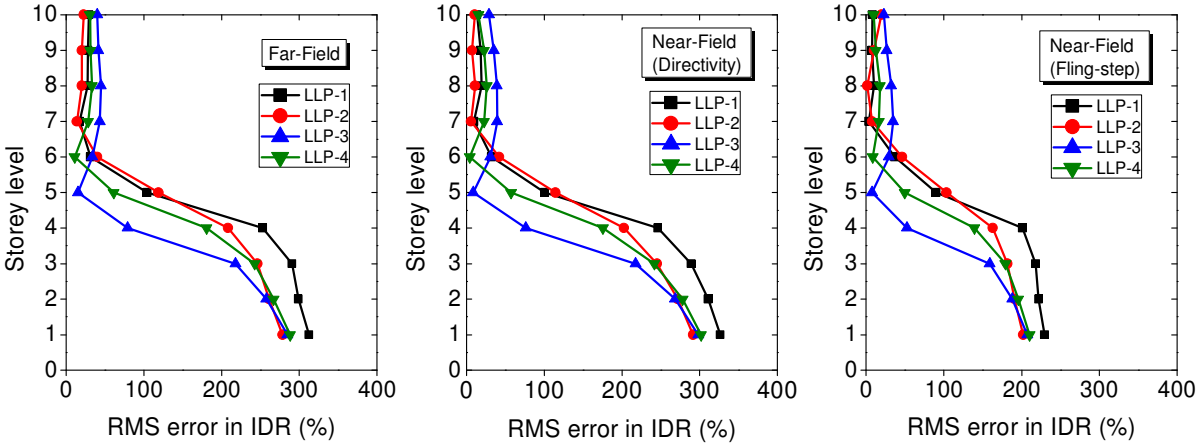

(c) RMS error in 10-storey frame at TD-3 = 420 mm

Figure 5.12 RMS error exhibited by different LLPs in the prediction of inter-storey drift ratio (IDR) of the 10-storey frame for far-field, near-field (directivity), near-field (fling-step) earthquakes at different target displacements

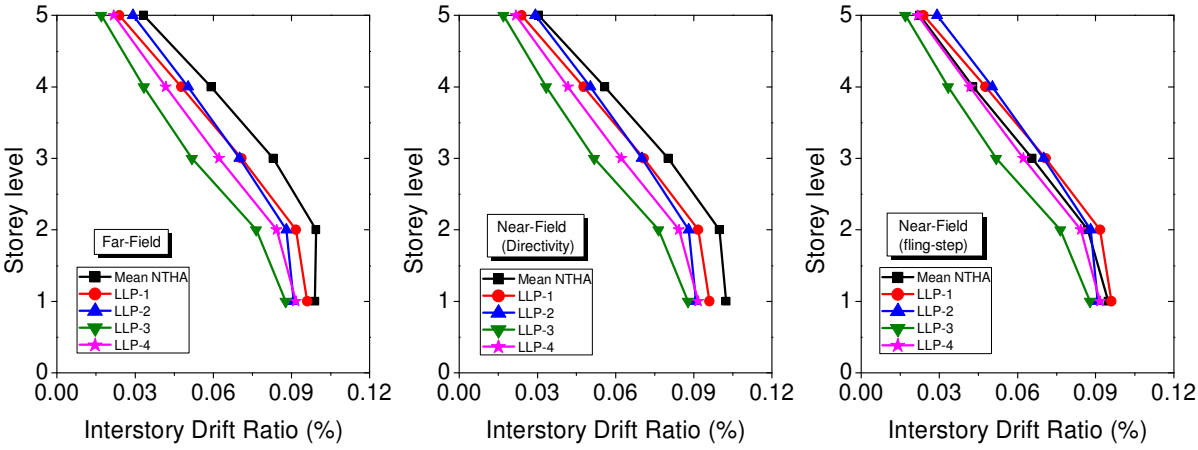

(a) Inter-story drift ratio of 5-storey frame at TD-1 = 75 mm

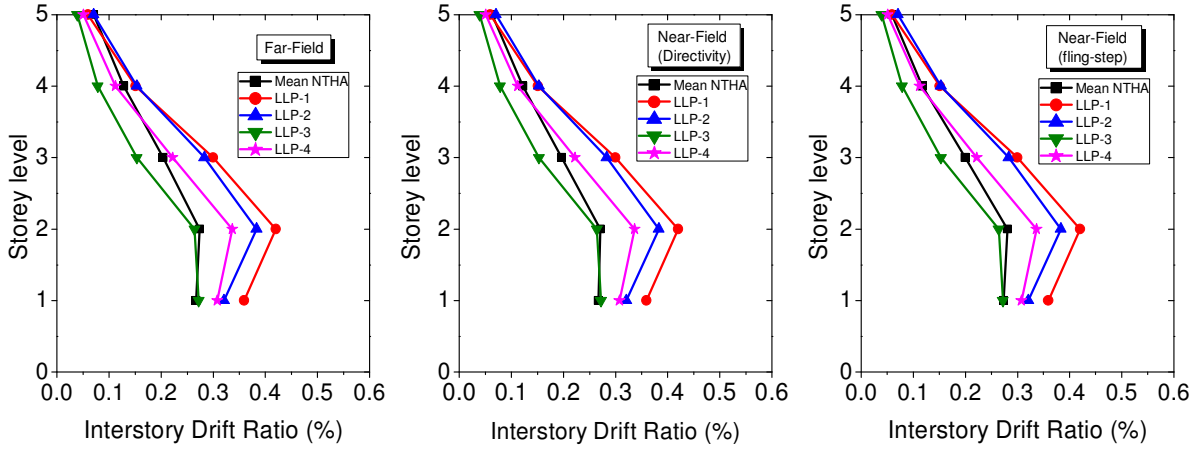

(b) Inter-story drift ratio of 5-storey frame at TD-2 = 230 mm

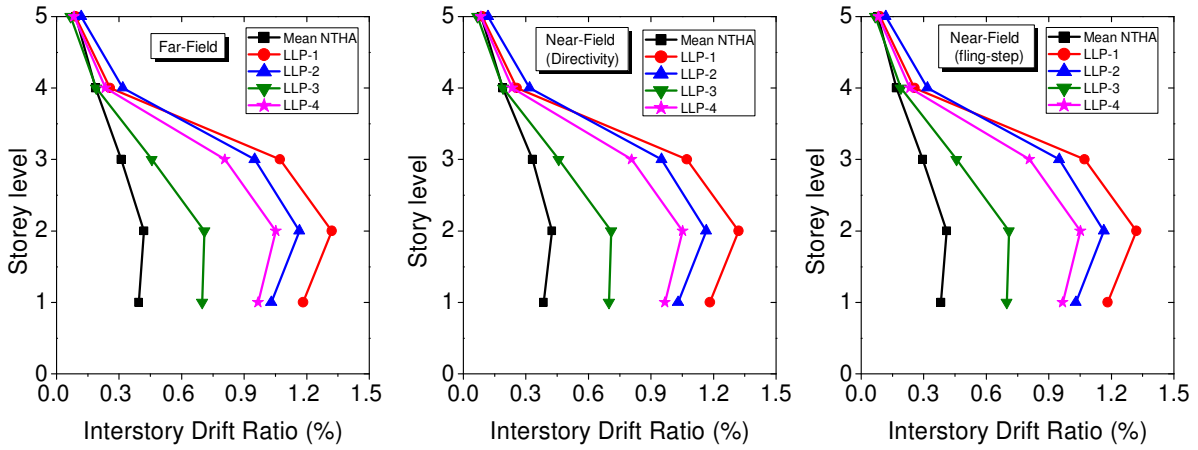

(c) Inter-story drift ratio of 5-storey frame at TD-3 = 330 mm

Figure 5.13 Height-wise variation of inter-storey drift ratio of the 5-storey frame for far-field, near-field (directivity), near-field (fling-step) earthquakes compared to different LLPs at different target displacements (TD)

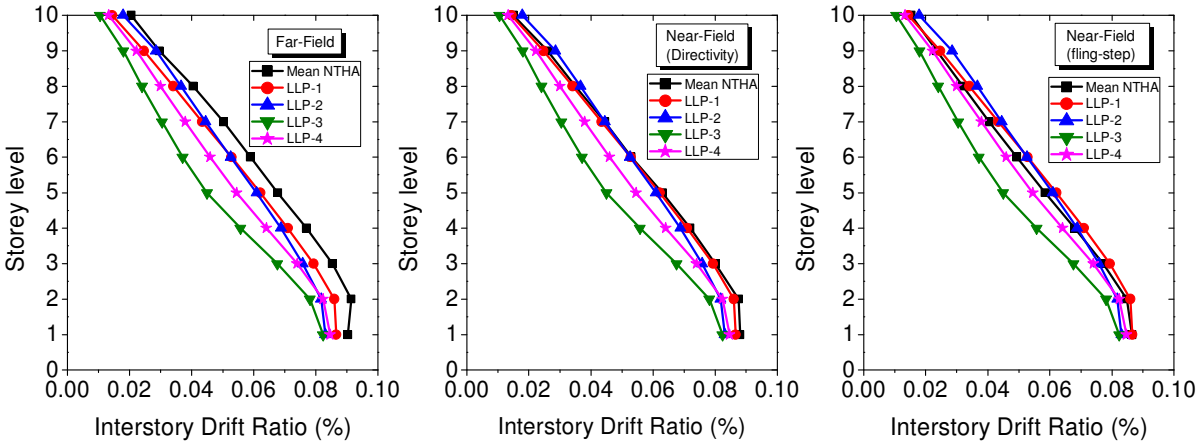

(a) Inter-story drift ratio of 10-storey frame at TD-1 = 144 mm

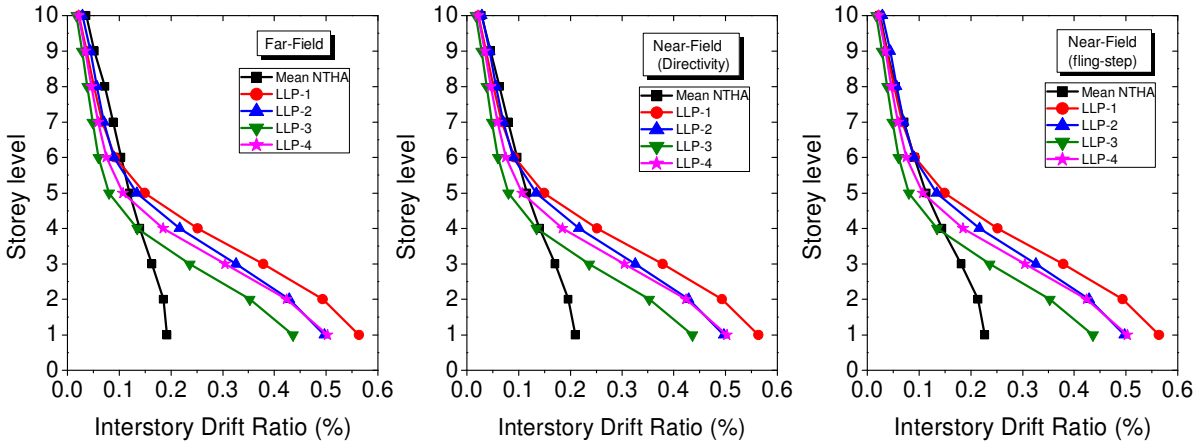

(b) Inter-story drift ratio of 10-storey frame at TD-2 = 300 mm

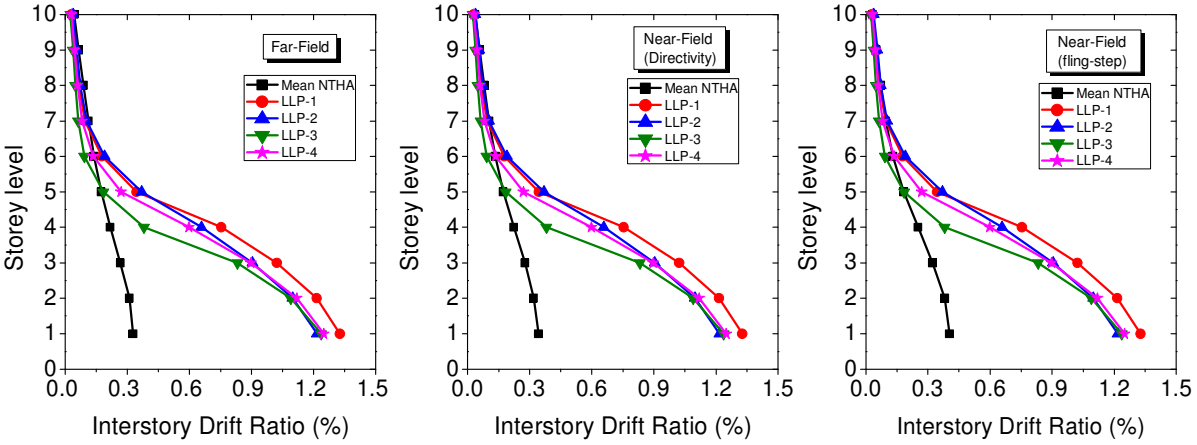

(c) Inter-story drift ratio of 10-storey frame at TD-3 = 420 mm

Figure 5.14 Height-wise variation of inter-storey drift ratio of the 10-storey frame for far-field, near-field (directivity), near-field (fling-step) earthquakes compared to different LLPs at different target displacements (TD)

The reason for the large errors in IDR values is due to the higher inelastic effect produced by POA as compared to NTHA at the bottom storey levels. This fact is depicted in **Figure 5.15** which shows the heightwise variation of the maximum rotation of the plastic hinges formed in the beams at each storey level in POA using different LLPs for both building frames. In the same figure, the same variations are shown for typical earthquakes. It can be seen from the figure that all LLPs produce higher values of maximum plastic rotations as compared to NTHA at bottom storey levels at TD-2 and TD-3. Moreover, it can be observed from the figure that LLP-3 gives the nearest estimations to NTHA for both frames.

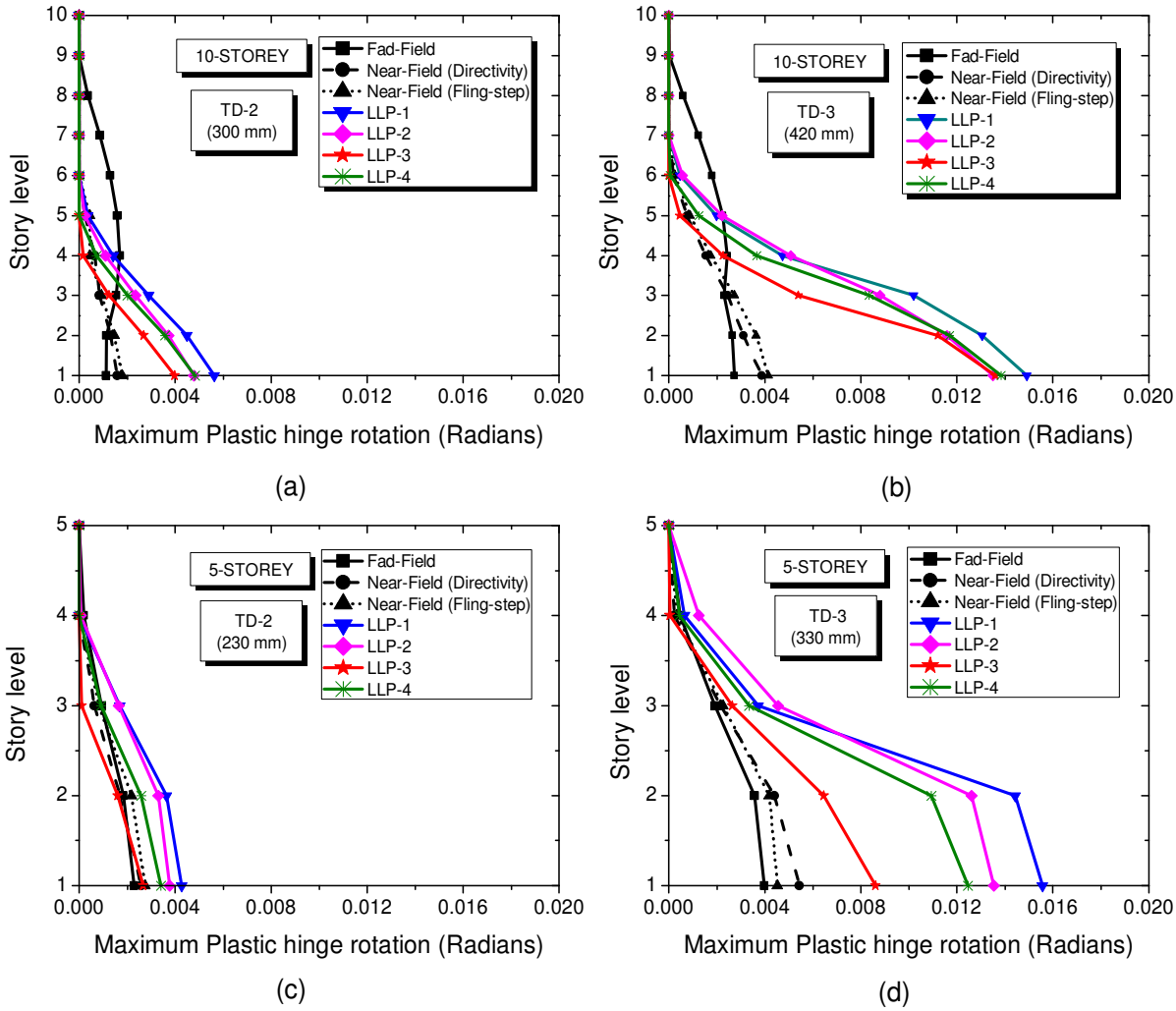

Figure 5.15 Height wise variation of maximum plastic hinge rotations in beams for five and ten-storey frames at two target displacements: (a) 10-storey at TD-2; (b) 10-storey at TD-3; (c) 5-storey at TD-2; and (d) 5-storey at TD-3.

5.4.3 Evaluation of Maximum Base Shear (MBS)

Figure 5.16 shows the RMS errors in base shear at all target displacements for far-field earthquakes in the 5-storey and 10-storey frames respectively. It is seen from the figure that the trend in the errors for both frames remains nearly the same corresponding to a particular target displacement. The different errors produced by all LLPs are small, less than 5% and 12% for 5-storey and 10-storey frames respectively at TD-1 and TD-2. The LLP-3 provides minimum errors. The reason for the less error is because there are no or insignificant inelastic effects produced in the frames at the elastic and the elastic-plastic states. As a consequence, the difference in the effective stiffness's of the frames between POA and NTHA is very less resulting in nearly the same maximum base shears.

On the contrary, the RMS error at TD-3 (plastic state) increases to a higher value, maximum of nearly 28%, which is provided by LLP-1. The LLP-3 provides the minimum error; 7% for the 5-storey frame and 20% for the 10-storey frame. The reasons for the large errors are twofold; (i) at TD-3, the frame gets highly into inelastic state which makes a large difference between the effective stiffness's of the frames during NTHA and POA and (ii) the capacity curves at TD-3 (plastic state, **Figure 5.6**) obtained by POA become flat making the value of base shear nearly insensitive to the variation of target displacement at this state. On the other hand, the base shear increases with increase in PGA, which is required to achieve higher target displacement in the case of NTHA.

The aforementioned trends of the results are also observed same for near-field earthquakes for both building frames, and hence, they are not shown here for brevity.

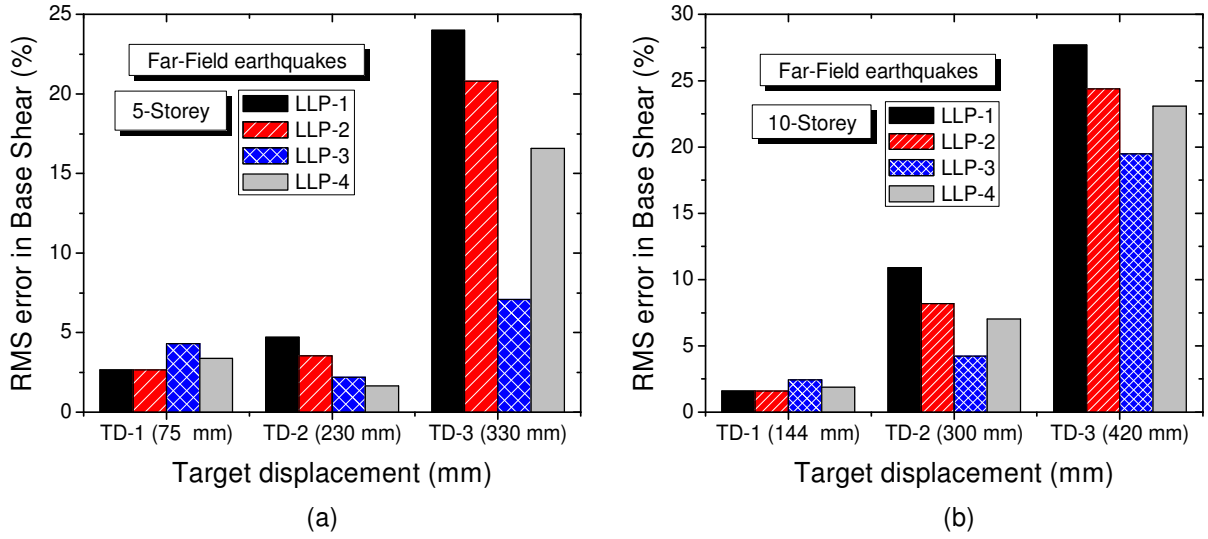

Figure 5.16 RMS error exhibited by different LLPs in the prediction of base shear for the far-field earthquakes in two frames: (a) 5-storey frame and (b) 10-storey frame

5.4.4 Evaluation of Maximum Isolator Displacement (MID)

Figure 5.17 illustrates the RMS errors in maximum isolator displacement produced by different LLPs for the 5-storey and the 10-storey frames, at different target displacements, and for far-field earthquakes. It is seen from the figures that at TD-1 and TD-2, the errors remain below 10% in both frames. At TD-3, errors are significant for all LLPs with maximum error produced by LLP-1, of the order of about 30%, and minimum error is produced by LLP-3, of the order of 10% in 5-storey frame and 20% in 10-storey frame. The errors are of the same order for near-field earthquakes for both building frames, and hence, the results are not presented here.

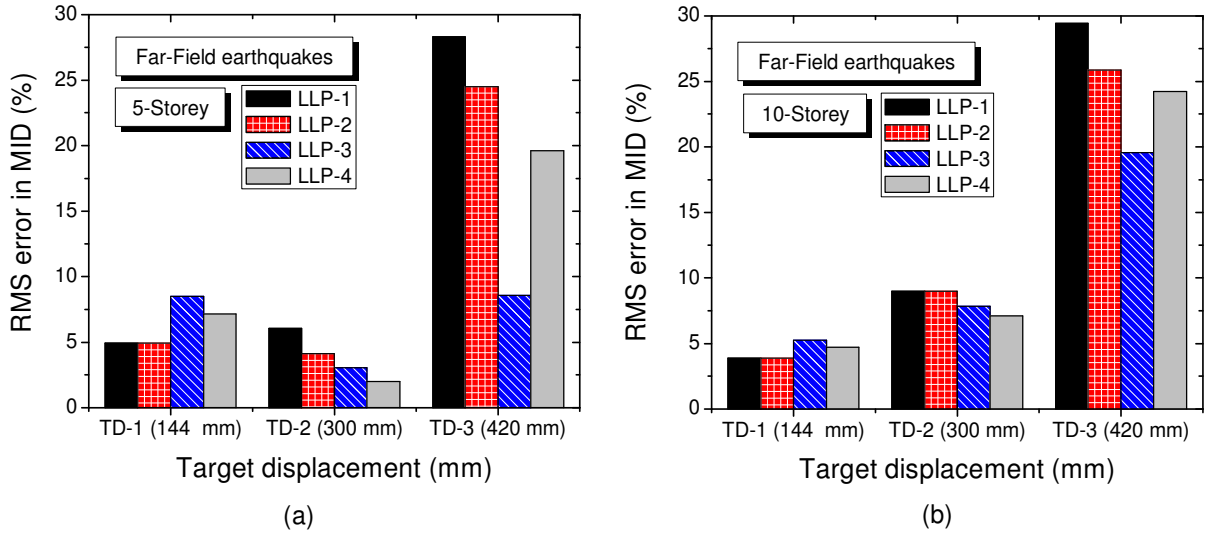

Figure 5.17 RMS error exhibited by different LLPs in the prediction of maximum isolator displacement (MID) for the far-field earthquakes in two frames: (a) 5-storey frame; (b) 10-storey frame

5.4.5 Evaluation of the Number of Plastic Hinges

The number of plastic hinges formed by different LLPs and NTHA in both building frames at all target displacement levels is shown in **Tables 5.5 and 5.6**. It is observed from the tables that, at TD-1, for the far-field earthquakes, a large number of plastic hinges are formed in NTHA in both building frames; no plastic hinge is formed in POA for all LLPs. This is due to the fact that large PGA values are required to achieve TD-1 for far field earthquakes as given in **Tables 5.3 and 5.4** for both building frames. For such higher levels of PGA, plastic hinges are expected to form in NTHA. Since TD-1 falls in the elastic range of the capacity curve, no plastic hinge is formed in POA. At TD-2 and TD-3, plastic hinges are formed in both NTHA and POA; the number of plastic hinges is found to be more in NTHA. At TD-2, LLP-1 provides

the number of plastic hinges closest to that of NTHA and LLP-3 gives the least number of plastic hinges. At TD-3 the same trend is observed.

In the same tables, the number of plastic hinges is shown for near-field earthquakes with directivity effect. Unlike the far field earthquakes, the near-field earthquakes do not introduce plastic hinges in NTHA at TD–1 for 10-storey frame and very less, of the order of 2-3 hinges in the 5-storey frame. This is due to the fact that the PGA levels required by near-field (directivity) earthquakes to achieve TD-1 are smaller as compared to those of far-field earthquakes (see **Tables 5.3 and 5.4**). At these levels of PGA, any of the plastic hinges do not form in NTHA.

At TD-2, the number of plastic hinges formed in NTHA is about 18 for the 10-storey frame and 32 for the 5-storey frame. LLP-1 provides nearly the same number of plastic hinges as that of NTHA. LLP3 provides the minimum number of plastic hinges. At TD-3, a maximum number of 48 and 30 plastic hinges are formed in the 5-storey and 10-storey frame by LLP-1; NTHA provides a less number of plastic hinges. LLP-3 yields the least number of plastic hinges among all LLPs considered in POA. The same trend of results is observed for near-field earthquakes with fling-step effect as shown in the same tables.

Table 5.5 Comparison of the number of plastic hinges formed in the 5-storey frame by different LLPs and Mean NTHA

Analysis Type	Number of Plastic hinges		
	TD-1 = 75 mm	TD-2 = 230 mm	TD-3 = 330 mm
POA (LLP-1)	0	21	30
POA (LLP-2)	0	19	33
POA (LLP-3)	0	13	28
POA (LLP-4)	0	15	29
Mean NTHA (FF)	12	21	30
Mean NTHA (NF-D)	2	18	28
Mean NTHA (NF-FS)	3	18	26

POA = pushover analysis; LLP = lateral load patterns; NTHA = nonlinear time history analysis; FF = far field; NF = near field; D = directivity; FS = fling step

Figure 5.18 depicts the RMS errors in the estimation of the number of plastic hinges for far-field earthquakes in the 5-storey and the 10-storey frames, at different target displacements, and for different earthquakes. Note that errors are only shown at TD-2 (elastic-plastic state) and TD-3 (plastic state) since no plastic hinge is formed at TD-1 as it is in the elastic state. It is seen from the figure that variation in the errors produced by different LLPs, at different target displacements, is small in case of the 10-storey frame as compared to the 5-

storey frame. Furthermore, the errors generated by the far field earthquakes are more as compared to the near-field earthquakes for both building frames.

Table 5.6 Comparison of the number of plastic hinges formed in the 10-storey frame by different LLPs and Mean NTHA

Analysis Type	Number of Plastic hinges		
	TD-1 = 144 mm	TD-2 = 300 mm	TD-3 = 420 mm
POA (LLP-1)	0	32	48
POA (LLP-2)	0	32	49
POA (LLP-3)	0	25	39
POA (LLP-4)	0	28	45
Mean NTHA (FF)	22	49	60
Mean NTHA (NF-D)	0	32	43
Mean NTHA (NF-FS)	0	33	43

POA = pushover analysis; LLP = lateral load patterns; NTHA = nonlinear time history analysis; FF = far field; NF = near field; D = directivity; FS = fling step

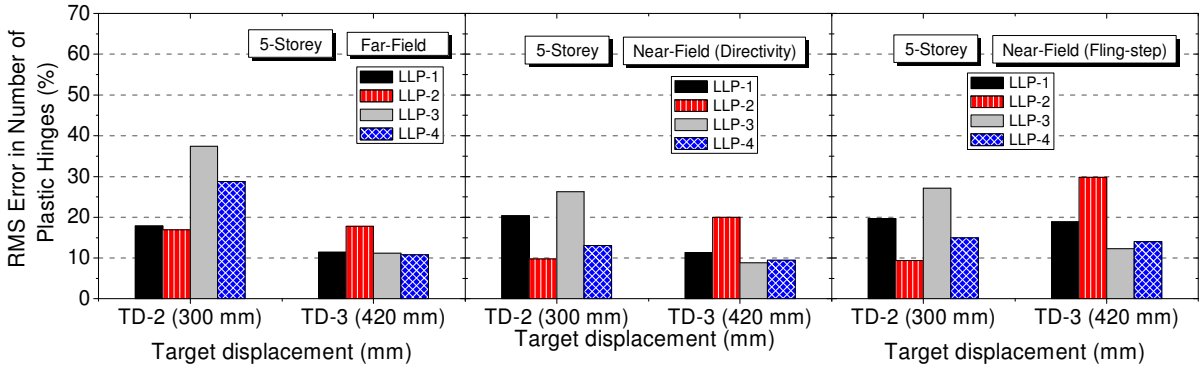

(a) RMS error in number of plastic hinges in 5-storey frame

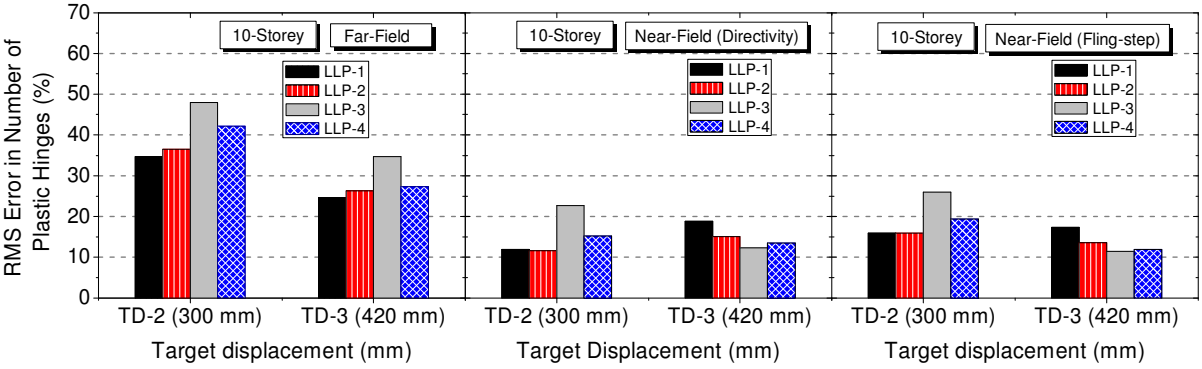

(a) RMS error in number of plastic hinges in 10-storey frame

Figure 5.18 RMS error exhibited by different LLPs in the prediction of the number of plastic hinges for the far-field, near-field (directivity), and near-field (fling-step) earthquakes at TD-2 and TD-3

For the far-field earthquakes, the minimum error is produced by LLP-1; 35% and 25% at TD-2 and TD-3 respectively for the 10-storey frame and less than 15% for the 5-storey frame. The LLP-3 produces the maximum error maximum error; 37% for the 5-storey frame and 48% for the 10-storey frame.

For the near-field earthquakes, the minimum error is produced by LLP-1, ranging between 15% - 20% and maximum error is provided by LLP-3, of the order of 25%, in the 10-storey frame. For the 5-storey frame, there is considerable variation in the errors estimated by different LLPs. LLP-4 provides the minimum error, less than 15%, at TD-2 and TD-3.

5.4.6 Evaluation of SRSS of Plastic Hinges Rotation

Figure 5.19 shows the RMS errors in SRSS of plastic hinge rotations in both building frames at TD-2 and TD-3 for the far-field and the near-field earthquakes. It is observed from the figure that LLP-1 provides the maximum errors and LLP-3 provides the minimum errors for both frames at all target displacements. LLP-1 provides maximum errors in the range of 300% - 450% at TD-2 and TD-3 in the 10-storey frame and 120% in the 5-storey frame. The minimum errors are given by LLP-3, in the range of 170% - 255% at TD-2 and 255% - 400% at TD-3 for the 10-storey frame. For the 5-storey frame, LLP-3 provides a small error, of the order of maximum up to 15% at TD-2 and in the range of 100% - 130% at TD-3.

The reason for large errors in the SRSS of plastic hinge rotations is attributed to the fact that the actual energy dissipation in the system is captured by the NTHA through hysteresis loops, whereas the POA underestimates it because of monotonic equivalent nonlinear static analysis. While the effective stiffness of the system primarily govern the number of plastic hinges formed in both analyses, the SRSS of maximum plastic hinge rotations is more governed by the total energy dissipation of the system, which the POA cannot capture realistically. Thus, SRSS of plastic hinge rotations is a better indicator of the inelastic state of the structure compared to the number of plastic hinges.

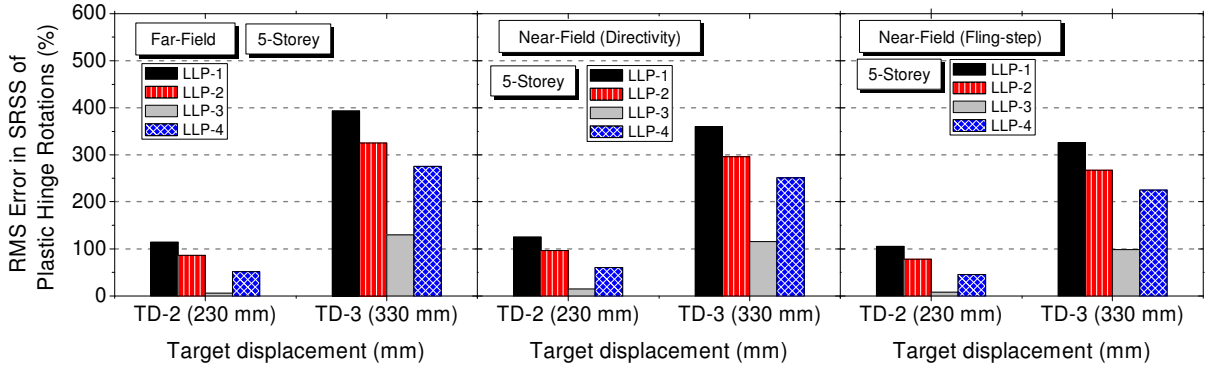

(a) RMS error in SRSS plastic hinges in 5-storey frame

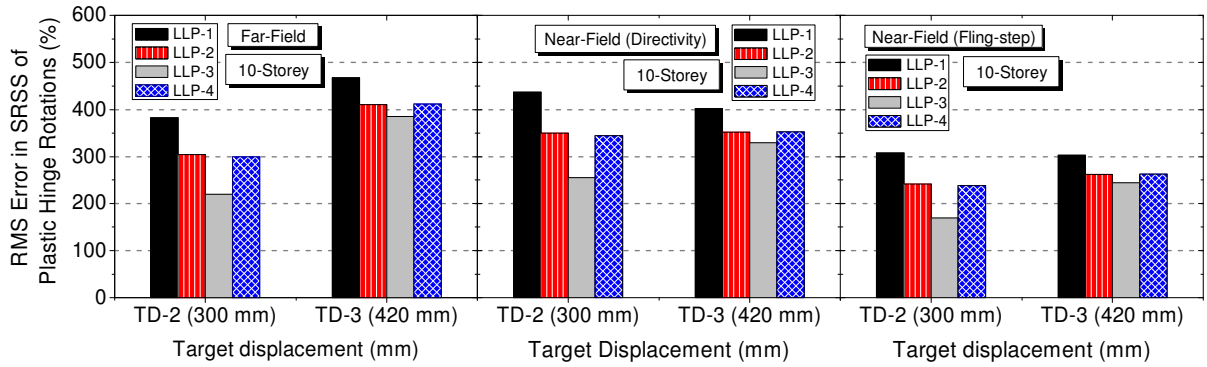

(b) RMS error in SRSS plastic hinges in 10-storey frame

Figure 5.19 RMS error exhibited by different LLPs in the prediction of SRSS of plastic hinge rotations for the far-field, near-field (directivity), and near-field (fling-step) earthquakes at TD-2 and TD-3

5.5 Conclusions

The effectiveness of four lateral load patterns (LLPs) used in the pushover analysis (POA) is evaluated using the predictions of the nonlinear time history analysis (NTHA) for the base-isolated building frames. The analyses are carried out by considering 5-storey and 10-storey base-isolated building frames installed with lead rubber bearing isolators. Further, the effect of different types of earthquakes is investigated by considering the far-field and near-field earthquakes with directivity and fling-step effects. In each type of earthquake, an ensemble of five ground motion records is used for carrying out the NTHA. The estimates of different LLPs are compared with the predictions of the NTHA at three target displacements (TD-1, TD-2, and TD-3) that lie in three different states of the frame namely, elastic, elastic to plastic and plastic. The RMS errors given by different LLPs are calculated for various response parameters namely, the peak storey displacement, the maximum inter-storey drift ratio, the maximum base shear, the maximum isolator displacement, the number of plastic hinges formed and the SRSS of plastic hinge rotations. In general, it is observed that estimations of the NTHA

predicted values of different response parameters by different LLPs differ with the target displacements, the type of earthquake and the response quantity of interest. Thus, a single LLP cannot be recommended for predicting all response quantities of interest. However, some trends of results may be concluded from the study:

1. LLP-3 turns out to be the best in estimating the maximum storey displacements for all target displacements and earthquakes considered, especially for the 5-storey frame.
2. Estimations of the base shears and the isolator displacements by all LLPs are good at TD-1 and TD-2 for all earthquakes. The errors in the estimations increase as the frames undergo excursion from elastic-plastic (TD-2) to a plastic state (TD-3); LLP3 provides the least error.
3. All LLPs provide errors in the predictions of inter-storey drift. These errors are significant in the lower stories at TD-2 and TD-3, and in upper stories at TD-1 for all earthquakes. LLP-1 and LLP-3 give least errors in the upper stories and lower stories respectively.
4. Errors in predicting the number of plastic hinges is more for the far-field earthquakes as compared to the near-field earthquakes; for the ten-storied frame, LLP-1 provides the least errors (35%-25%), while LLP-3 gives the maximum errors (of the order of 48%) for far-field earthquakes. For the five-storied frame, LLP-1 and LLP-4 provide the least errors, less than 15%, at both target displacements for both types of earthquakes.
5. Large errors in predicting SRSS of plastic hinge rotations are observed for all types of earthquakes due to the difference in the energy dissipation mechanisms between the POA and the NTHA.
6. For the specific building frames analyzed in this study, the proposed LLP-3 predictions are best with practically acceptable errors (ranges between 10% to 20%) even at the plastic state (TD-3) of both building frames, if the maximum base shears, the maximum storey displacements, and the maximum isolator displacements are considered to be the three most important response parameters in the analysis of base isolated buildings.
7. Unlike in the fixed base building frame, the POA can be used to predict the behavior of base-isolated building frame for the above three important response parameters for the design level far-field earthquakes recommended in all seismic codes and even for extreme level earthquakes, specified in some codes (i.e., Indian Code) if the proposed load pattern LLP-3 is utilized. This conclusion emerges from the observation that the average of the PGAs of far-field earthquakes which correspond to the target displacement TD-1 is about 0.65g for 10-storey frame and 0.47g for the 5-storey frame. However, further studies on

base isolated 2-D and 3-D building models having a different number of stories are required to substantiate the validity of the above findings.

Chapter 6

Seismic Fragility Analysis of Base-Isolated Building Frame Excited by Near and Far Filed Earthquakes

6.1 Introductory Remarks

The damage caused to the modern engineered structures by the past destructive earthquakes has shown the vulnerability of the buildings, especially under near-field earthquakes as they impart high seismic energy in the form of pulses in the structure. Even in the base-isolated buildings, extensive damages are possible in the near-field earthquakes. Therefore, the assessment of the existing and adequately designed base-isolated buildings in the probabilistic terms is essential in the high seismic regions (including regions in the vicinity of the faults) to check the performance of the isolation system and superstructure due to the uncertainties of earthquake occurrence, type and intensity.

The literature review presented in the chapter-2 shows that the investigations on the probabilistic evaluation of the base-isolated buildings have not been done in an exhausted manner which can bring out the effect of far-field and near-field earthquakes with directivity and fling-step effects. Moreover, it is essential to evaluate the performance by considering different response parameters which can depict the state of structure and isolation functionality. This is necessitated in order to identify the most sensitive response parameter of the building under different types of earthquakes so as to help the structural design engineers in the design of the base-isolated building with respect to the desired performance level.

With the above background in view, the present study attempts to make a contribution to the existing body of knowledge on the subject by aiming at the probabilistic seismic risk assessment of a base-isolated building frame under near and far field earthquakes by conducting a fragility analysis. For this purpose, a base-isolated reinforced concrete frame is considered with lead rubber bearing as the base isolation system. Fragility curves are developed for a suite of far-field and near-field earthquakes with directivity and fling-step effects for a number of damage measures. In the case of near-field earthquakes, the effect of its frequency contents defined by the peak ground velocity (PGV) to peak ground displacement (PGA) ratio, is considered as a variable. The incremental dynamic analysis is used to create the fragility curves assuming the different threshold values of damage states namely, non-structural, slight, moderate, and extensive for different damage measures.

6.2 Theory

The uncertainties in the earthquakes cause a seismic risk to the civil structures. The probabilistic seismic risk analysis is an estimation of the damage probability and losses occurred due to the earthquake event. Fragility functions are very useful tools for the probabilistic seismic risk assessment of the structures which can assist in the application of the retrofitting strategies, planning of the pre-earthquake event and loss estimation in the post-earthquake surveys. The fragility curves provide valuable information about the effectiveness of the different seismic control strategies by measuring the damage probability of the structure or elements which are at risk under earthquake intensity. Another way to look into the performance of the building is by the use of incremental dynamic analysis, which provides the structural response ranging from the elastic to complete inelastic state under the increasing intensity of the ground motion.

From the literature review carried out in chapter 2, it is evident that the research studies pertaining to the fragility analysis of base-isolated buildings is scanty. Towards this motivation, the present study deals with the probabilistic seismic performance of a ten-story (high rise) building frame considering the effects of near-field earthquakes. Incremental dynamics analysis and fragility analysis are carried out using real near-field and far-field earthquake records. The details of the two analyses are provided in the following subsections:

6.2.1 Incremental Dynamic Analysis

IDA is a computer analysis technique which is widely used in the comprehensive evaluation of the seismic performance of structures under the seismic loads. This concept was primarily bought up by Bertero (1977) and later comprehend and applied by Vamvatsikos and Cornell (Vamvatsikos and Cornell, 2002, 2004) in the performance-based earthquake engineering. In the IDA, numbers of NTHAs are performed under a suite of earthquake records, which are scaled by a constant scale factor to incrementally increase the intensity of the earthquake motion. The intensity is increased up to a specified level of interest or until the structure reaches to the global collapse state. Several intensity measures are prescribed to quantify the intensity of the ground motion, such as PGA, PGV, PGD, etc. Thus, in this way a curve between the ground motion intensity is plotted against the structural response parameter or damage measure (e.g., inter-storey drift or roof drift ratio), which is known as IDA curve as shown in **Figure 6.1.** The collapse capacity is reached when the IDA curve becomes flat, which means that with a small increase in the intensity of the earthquake there will be a significant amount of the response generated in the structure.

In the present study, IDA is performed to develop the fragility curves by scaling the PGA from 0.1g to 1.2g at an interval of 0.1g of earthquake records of sets 1 to 4 **(Tables 6.1 to 6.4, provided in section 6.3.1)** and the response of base-isolated frame at considered PGA levels is calculated for different damage measures which are considered in the present study as given in **section 6.3.2**

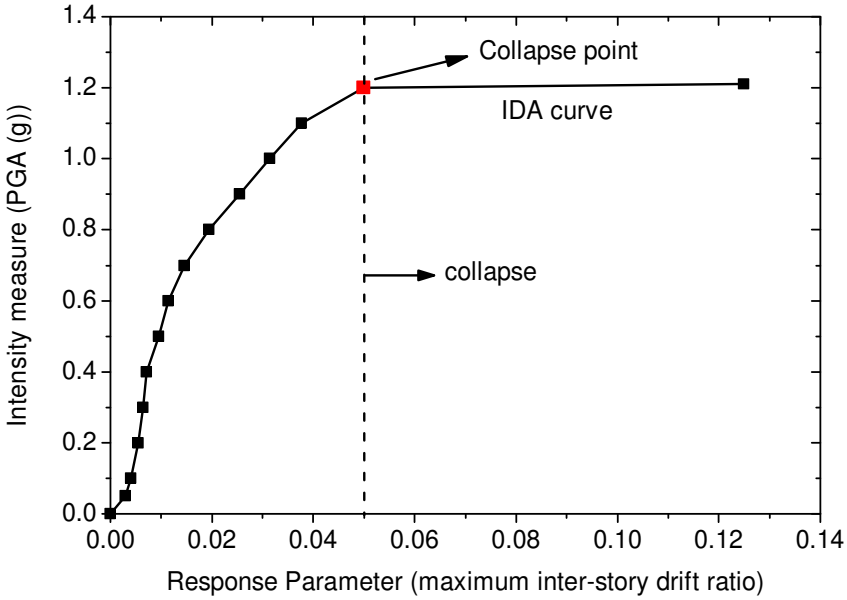

Figure 6.1 The IDA curve of a single earthquake record

6.2.2 Seismic Fragility Analysis

The concept of fragility analysis in the field of earthquake engineering is first introduced by the research work of Kennedy and his co-workers (Kennedy *et al.*, 1980) in the probabilistic seismic estimation of the nuclear power plant. With the development in the methodologies of seismic risk assessment, the fragility analysis has become an efficient tool for the risk assessment of the structures. Fragility is defined as the conditional probability of exceeding a specified limit state or threshold value of a structural member or system for a given intensity of ground shaking (Porter *et al.*, 2007; Ramamoorthy *et al.*, 2006; Reed and Kennedy, 1994). The lognormal probability distribution function is widely used to describe the fragility function, which is expressed by **Equation 6.1** (Pitilakis *et al.*, 2014).

$$P_f(ds \geq dsi \mid IM) = \Phi\left[\frac{1}{\beta_{total}} \ln\left(\frac{IM}{IM_m}\right)\right] \qquad (6.1)$$

Where, P_f = Probability of exceeding a particular damage state, DS, for a given level of intensity level, IM (e.g., PGA, PGV, Sa (T_1), and IM_m = Median threshold value of intensity measure required to cause ith damage state. Φ is standard cumulative probability function.

The uncertainty in fragility is estimated through the standard deviation, β_{total} (**Equation 6.2**), which reflects the total variability associated with seismic demand and capacity of structure in each fragility curve. The uncertainty in the structural capacity (resistance) of the element, β_C, depends on the states of the structural damage and the uncertainty due to the earthquake input motion, β_D, is depicted by the dispersion in the damage measure (DM) which is represented by structural response parameter, also known as engineering demand parameter (EDP) (Pitilakis *et al.*, 2014). The uncertainties in modeling, material properties, damping, and concrete strength variability are not considered in this present study. It is assumed that the uncertainty due to earthquake ground motions is much greater than the uncertainties as stated above.

$$\beta_{total} = \sqrt{\beta_D^2 + \beta_C^2} \tag{6.2}$$

There are several methods to develop the fragility curves namely, empirical, judgmental, analytical and hybrid (Pitilakis *et al.*, 2014). Empirical methods are based on the post-earthquake surveys and data collected due to the actual damage done by the earthquakes. The main advantage of the empirical methods is the fact that they are based on the real data, which can take into account the effects of soil structure interaction, the difference in the structural capacity for different types and group of buildings, and site effects. However, the main drawback of the empirical methods is that the fragility curves drawn gives limited information which is specific to the particular site, geotechnical and environmental conditions, earthquake parameters. Also. Due to the limited damage data for earthquake records and difficulty in defining the damage states of the structure, the use by the empirical method is limited. Judgmental methods are based on the expert judgments given by the field experts. The judgemental method leads to easy construction of the fragility curves. However, this method purely relies on the experience and expertise level of the experts which are appointed for the task. These curves lack where there is a need for the extrapolation of the results that are needed for the assessment in the other countries having different engineering design practice and construction.

Analytical methods are based on the computer simulation analysis done on the structural models under earthquake loads and are widely used due to their reliability in

estimates. The earthquake load is defined either by providing the acceleration time history records of the earthquakes or by the response spectrum. In this method, two well know analytical methods are there to derive the fragility curves. The first method is based on the static analysis of the structure, which uses capacity spectrum method (CSM) to generate the capacity curves and to arrive at a performance point. The spectral displacement corresponding to the specified damage level is obtained from the ADRS plot of the CSM. The HAZUS methodology (Kircher *et al.*, 2006), which estimates the losses of existing buildings due to earthquakes has used CSM method to generate the fragility curves. The second method is based on NTHA of the structure in which fragility curves are derived by developing the probabilistic seismic demand model (PSDM). Furthermore, there are two approaches to develop the PSDM. The first approach is the scaling approach, in which the ground motion records are scaled to the predefined levels of the earthquake intensity, and IDA is performed at each intensity level. In this method, multiple stripes of the data are generated corresponding to a particular level of ground motion intensity as shown in **Figure 6.2.** This method requires high computational efforts as a large number of analyses are required in IDA but possess more accuracy. The second approach is known as cloud approach, in which the NTHA is performed using unscaled records or unscaled records are scaled by using a constant factor if they are not capable of generating the required level of structural response. The responses generated by cloud approach is shown in **Figure 6.3**. The Hybrid methods combine any of the aforementioned methods (Bakhshi and Mostafavi, 2014; Pitilakis *et al.*, 2014).

In the present study, an analytical computer simulation method is used to develop the fragility curves by performing incremental dynamics analysis. A typical fragility curve is shown in **Figure 6.4.** According to the Cornell *et al.* (2002), the response of the building can be assumed to have a lognormal distribution, and the DM or EDP can be related to the intensity measure (IM) with power model as per **Equation 6.3**.

$$DM = aIM^{b} \tag{6.3}$$

The above equation can also be represented in the log format as given under:

$$\ln(DM) = \ln a + b\ln(IM) \tag{6.4}$$

Where a and b in the **Equations 6.3 and 6.4** are the regression coefficients obtained by performing the regression analysis of ln (DM) on the intensity measure. The uncertainty in the demand, β_D, produced by the IM corresponding to the DM is estimated by the standard error of the regression analysis (Ellingwood and Kinali, 2009).

As there is more uncertainty in the demand, β_D, the uncertainty in the capacity, β_c, is assumed to be 0.3 in the present study by following the recommendations of HAZUS, Kircher *et al.* (2006), and Wen *et al.* (2004).

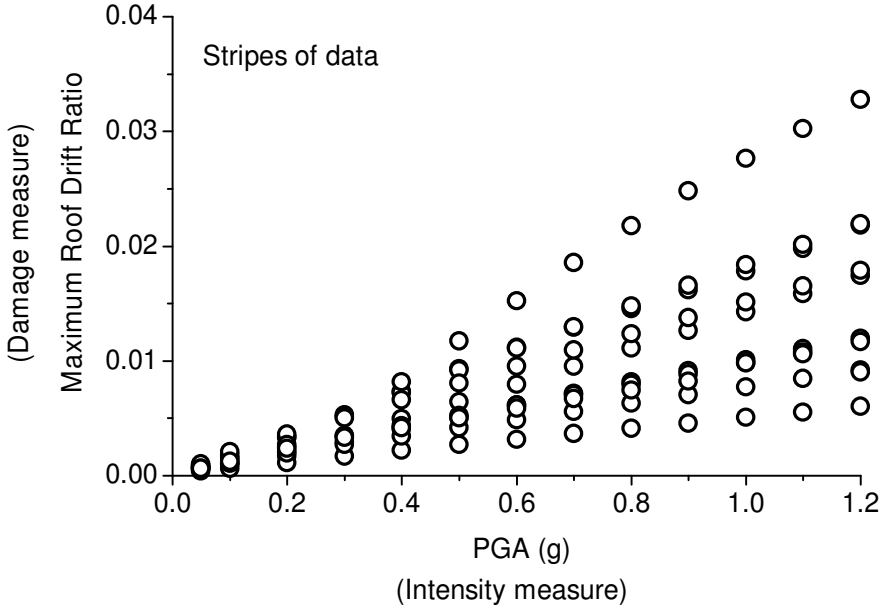

Figure 6.2 Scaling method; data is plotted in the form of multiple stripes corresponding to each level of intensity measure

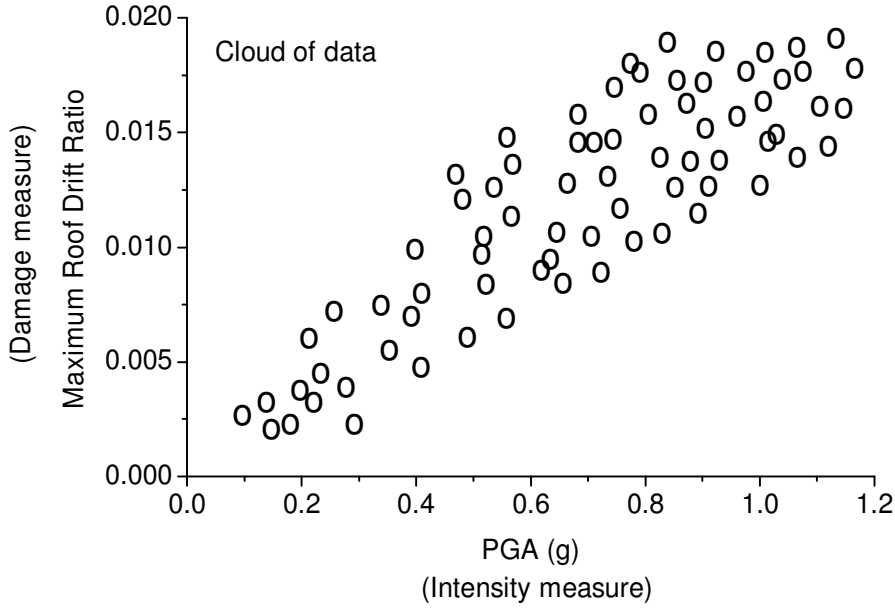

Figure 6.3 Cloud approach; data is plotted for unscaled records forming a cloud

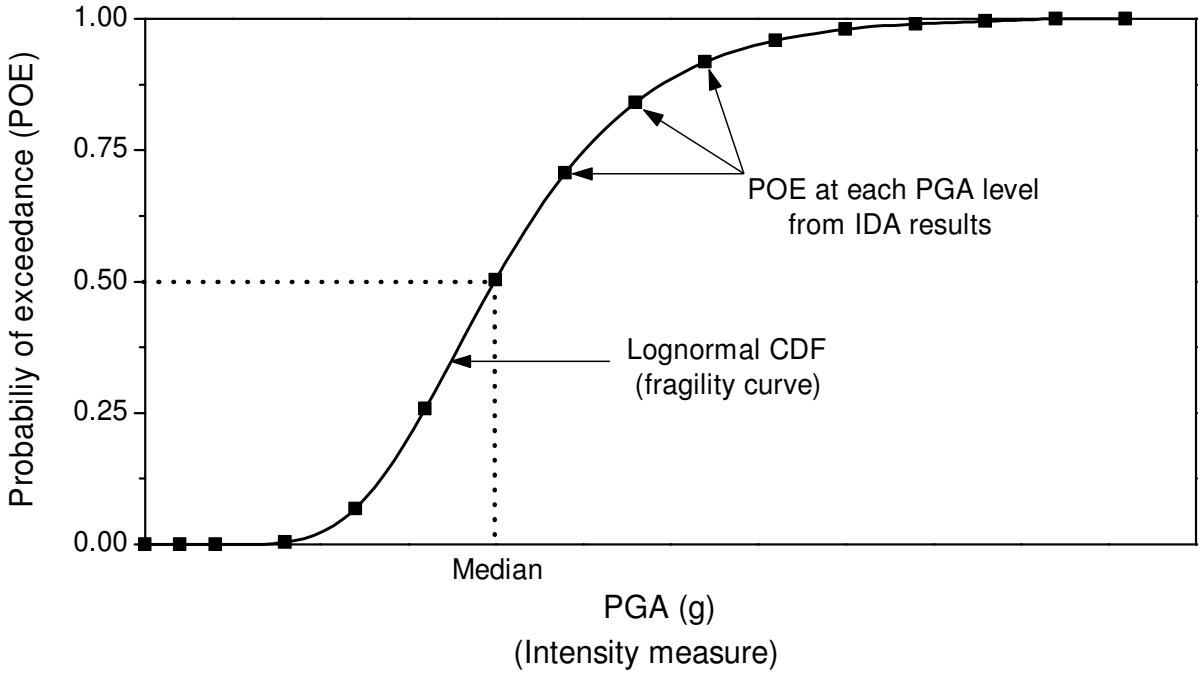

Figure 6.4 Illustration of a fragility curve

6.3. Numerical example

The numerical study is conducted with a 10-storey building frame, which is considered in the chapter-3, isolated by the medium type LRB isolators. The modeling and design of the superstructure and medium type base isolator remains same as provided in the chapters 3 and 4. Different sets of near-field and far-field earthquakes are considered for the analysis. The analysis is performed to obtain a set of demand measures which are evaluated against a set of defined damage states. The characteristics of earthquakes, the demand measures and damage states considered in the study are described in the following subsections:

6.3.1 Earthquake Records

The probabilistic seismic assessment of the frame is carried out by using different types of earthquakes: (i) far-field (FF); (ii) near-field with directivity effect having low PGV/PGA ratio (NFD-LR) i.e., PGV/PGA <150 (cm/s/g); (iii) near-field with directivity effect having high PGV/PGA (NFD-HR) i.e., PGV/PGA >150 (cm/s/g); and (iv) near-field with fling step effect (NFFS). According to the study of the Shome (1999), ten to twenty ground motion records are sufficient to estimate the seismic demand. In order to minimize the computational efforts, an ensemble of ten real earthquake records in each type of earthquake (Set 1 to 4) is considered. The far-field records are taken from Pacific Earthquake Engineering Research Center (PEER) ground motion database of Berkeley, http://ngawest2002.berkeley.edu/. The far-

field records are selected which are have Joyner Boore distance (closest distance from fault), R_{jb}, greater than 15 km and magnitude (M_w) ranging from 6 to 7.5. Set-1 contains 10 far-field records as given in **Table 6.1**.

The near-field directivity records are also taken from the PEER database, having R_{jb} less than 15 km, and magnitude (M_w) ranging from 5.7 to 7.5, and containing directivity pulses. Moreover, to investigate the effect of frequency contents of near-field earthquakes, the PGV/PGA ratio of only near-field earthquakes with directivity effect is varied, as the directivity effect is more common than the fling-step effect. Set-2 contains 10 records of near-field directivity earthquakes having low PGV/PGA ratio (PGV/PGA<150) as given in **Table 6.2** and Set-3 contains 10 records with high PGV/PGA ratio (PGV/PGA>150) as given in **Table 6.3**. The raw fling-step records need to be processed to get actual tectonic deformation and therefore, processed records are taken from the study of Kalkan and Kunnath (2006b) having high peak ground displacement ranging from 100 to 230 cm, magnitude (M_w) between 7 to 7.6, and having R_{jb} less than 15 km. Set-4 contains 10 records of near-field with fling-step effect as given in **Table 6.4**. The mean elastic acceleration spectrums of different types of earthquakes are shown in **Figure 6.5**.

Table 6.1 Characteristics of Far-field (FF) earthquake records (Set-1)

S.No.	Year	Earthquake	M_w	Station	Component	PGA (g)	PGV (cm/s)	PGD (cm)	PGV/PGA	R_{jb} (m)
1	1995	Loma Prieta	6.9	Sunol-Forest fire station	90	0.08	9.08	4.14	109	47.41
2	1992	Landers	7.3	Cool water	TR	0.42	42.35	13.84	101	19.74
3	1992	Landers	7.28	Baker fire station	50	0.12	9.25	6.54	86	87.94
4	1994	Northridge	6.69	Leona valley #5	0	0.15	14.84	2.37	102	37.47
5	1994	Northridge	6.69	Downey-co maint bldg	90	0.16	13.54	2.24	86	43.2
6	1952	Kern county	7.36	Taft lincon school	111	0.18	18.62	9.35	103	38.42
7	1987	Superstition hill	6.54	Brawley airport	225	0.14	9.72	2.84	68	17.03
8	1978	Tabas	7.35	Ferdows	L	0.09	5.4	2.24	58	89.76
9	1987	Whittier-Narrows	6	Canyon-county- W lost cany	270	0.10	7.18	0.77	73	44.88
10	1983	Coalinga	6.36	Parkfield Fault zone 14	90	0.27	28.14	4.88	103	28.11

Table 6.2 Characteristics of Near-field with Directivity effect (PGV/PGA < 150) (NFD-LR) records (Set-2)

S.No.	Year	Earthquake	M_w	Station	Component	PGA (g)	PGV (cm/s)	PGD (cm)	PGV/ PGA	R_{jb}
1	1984	Morgan Hill	6.19	Coyote Lake Dam, Southwest Abutment	195	0.72	52.9	12.75	74	0.18
2	1984	Morgan Hill	6.19	Gilroy Array #6	90	0.29	36.5	5.94	125	9.85
3	1989	Loma Prieta	6.9	Gilroy Array #3	90	0.37	45.42	24.1	123	12.23
4	1989	Loma Prieta	6.9	Saratoga - Aloha Ave	90	0.33	45.97	33.33	141	7.58
5	1989	Loma Prieta	6.9	Gilroy Array #2	90	0.32	40.37	18.45	125	10.38
6	2004	Parkfield	6	Chalome 1E	90	0.44	40.13	9.43	91	1.66
7	1995	Kobe	6.9	KJMA	0	0.84	91.1	21.11	109	0.94
8	1995	Kobe	6.9	Takarazuka	0	0.69	68.4	26.67	99	0
9	1992	Cape mendocino	7	Petrolia	90	0.66	88.51	32.22	134	0
10	1979	Coyote Lake	5.74	Gilroy Array #6	230	0.42	44.34	12.44	106	0.42

Table 6.3 Characteristics of Near-field with Directivity effect (PGV/PGA > 150) (NFD-HR) records (Set-3)

S.No.	Year	Earthquake	M_w	Station	Component	PGA (g)	PGV (cm/s)	PGD (cm)	PGV/ PGA	R_{jb}
1	1994	Northridge	6.69	Jensen filter plant adm building	22	0.41	111.47	44.63	272	0
2	1979	Imperial Valley	6.5	El Centro array #4	230	0.37	80.4	74.26	217	4.9
3	1989	Loma prieta	6.93	Saratoga W valley coll,	270	0.33	64.91	37.85	197	8.48
4	1979	Imperial valley	6.53	Brawley airport	225	0.16	36.6	25.67	226	8.54
5	1995	Kobe	6.9	Port island 0m	0	0.35	90.67	39.3	261	3.31
6	1979	Imperial Valley	6.53	Ec county center FF	2	0.21	38.44	17	181	7.31
7	1979	Imperial Valley	6.53	El centro diff. Array	270	0.35	75.58	57.15	216	5.09
8	1994	Northridge	6.69	La dam	64	0.43	74.84	19	176	0
9	1987	Superstition hill-02	6.54	Parachute test site	225	0.43	134.28	46.18	311	0.95
10	1999	Kocaeli	7.51	Gebze	270	0.14	32.64	29.76	227	7.57

Table 6.4 Characteristics of Near-field with fling-step (NFFS) effect records (Set-4)

S.No.	Year	Earthquake	M_w	Station	Component	PGA (g)	PGV (cm/s)	PGD (cm)	PGV/ PGA	R_{jb}
1	1999	Chi-Chi	7.6	TCU 072	EW	0.46	83.6	209.67	182	7.9
2	1999	Chi-Chi	7.6	TCU 065	EW	0.76	128.32	228.41	169	2.5
3	1999	Kocaeli	7.4	Sakarya	EW	0.41	82.05	205.93	200	3.2
4	1999	Chi-Chi	7.6	TCU067	EW	0.48	94.31	181.5	196	1.1
5	1999	Chi-Chi	7.6	TCU074	EW	0.59	68.9	193.22	117	13.8
6	1999	Chi-Chi	7.6	TCU084	EW	0.98	140.43	204.59	143	11.4
7	1999	Chi-Chi	7.6	TCU071	NS	0.63	79.11	126	126	4.9
8	1999	Chi-Chi	7.6	TCU089	EW	0.34	44.43	193.3	131	8.3
9	1999	Chi-Chi	7.6	TCU076	EW	0.33	65.93	101.65	200	3.2
10	1999	Chi-Chi	7.6	TCU049	EW	0.27	54.79	122	203	3.3

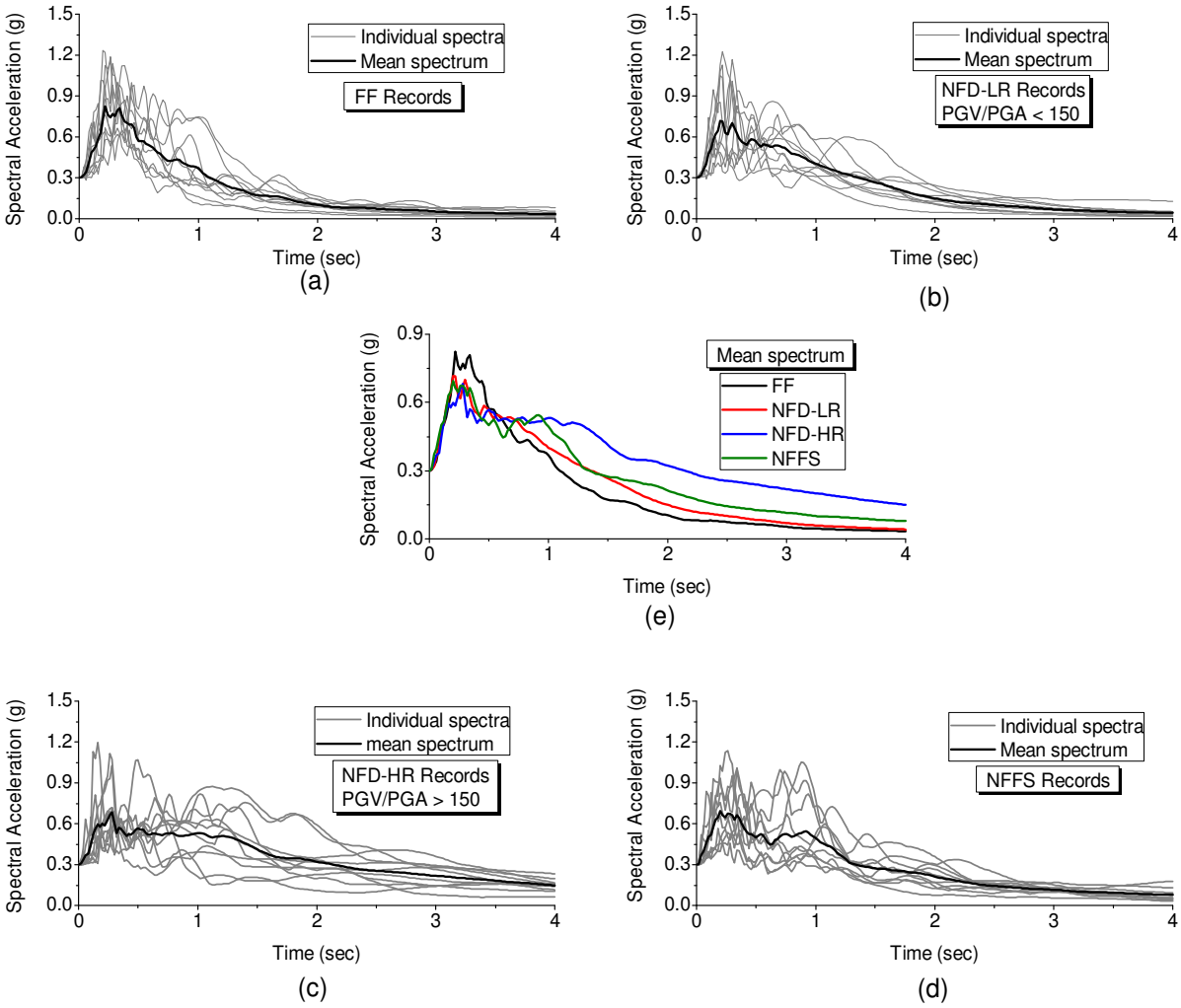

Figure 6.5 Mean acceleration response spectra (5% damping) of ten records scaled to PGA of 0.3g of different earthquakes: (a) FF; (b) NFD-LR; (c) NFD-HR; (d) NFFS; and (e) comparison of the mean spectrum of different types of earthquakes.

6.3.2. Damage Measure, Damage States, and Intensity Measure

To assess the degree of damage occurred due to the earthquake input, it is important to define the damage measures (DM) or the engineering demand parameters (EDP) which can depict the building response in the elastic and inelastic states. To estimate the damage of the base-isolated frame reasonably, five damage measures are considered including: (i) maximum inter-storey drift ratio (MIDR), which depicts the superstructure damage and architectural distortion; (ii) maximum roof drift ratio (MRDR), which indicates the possibility of pounding effect; (iii) maximum isolator displacement (MID), which depicts the safety of the isolation system, especially under near-field earthquakes; (iv) maximum top floor acceleration (MTFA), which provides the degree of discomfort felt by occupants of building and, damage caused to interior contents and machinery; and (v) maximum base shear (MBS), which is one of the important EDPs especially in the case of base isolated buildings for economic design of foundations.

In order to describe the damage condition in the base-isolated building frame, four damage states (DS) are considered namely, non-structural, slight, moderate, and extensive (Gong and Xiong, 2016) for each damage measure. The deterministic limit threshold values of damage states for different damage measures are assumed by engineering judgment (Alam *et al.*, 2012; Gong and Xiong, 2016; Zhang and Huo, 2009) as given in **Table 6.5**.

Table 6.5 Threshold values of damage states for different Damage measures.

Damage Measures	Damage States			
	Non-Structural (DS-1)	Slight (DS-2)	Moderate (DS-3)	Extensive (DS-4)
Maximum Inter-storey drift ratio (MIDR)	0.05%	0.10%	0.20%	0.70%
Maximum base shear (MBS)	5%W	10%W	15%W	20%W
Maximum roof drift ratio (MRDR)	0.10%	0.50%	1%	2%
Maximum isolator displacement (MID)	$0.2D_{max}$	$0.4D_{max}$	$0.8D_{max}$	$1.2D_{max}$
Maximum top floor acceleration (MTFA)	0.1g	0.2g	0.3g	0.4g

W = total seismic weight of the structure; D_{max} = maximum design displacement of the isolator

The choice of intensity measure (IM) is important in relation to describe the earthquake severity and to scale the earthquake records in the incremental dynamic analysis (IDA). There are various IMs which are used by researchers namely, peak ground acceleration (PGA), peak

ground velocity (PGV), spectral acceleration at the first mode period, Sa (T_1), peak ground displacement (PGD), arias intensity, etc (Mollaioli *et al.*, 2013; Shahi *et al.*, 2014). Among different IMs, PGA is widely used as IM due to its efficiency, practicality, and hazard computability (Nielson and DesRoches, 2007; Padgett *et al.*, 2008) and has been used by many researchers for analyzing the base isolated structures (Castaldo *et al.*, 2017c; Hedayati Dezfuli and Alam, 2017; Zhang and Huo, 2009). With this background, PGA is taken as the IM in the present study.

6.4. Discussion of Results

The summary of IDA curves generated by the incremental dynamic analysis (IDA) for different damage measures under different types of earthquake motions is presented in **Figures 6.6 to 6.10**. Note that the PGA values are increased from 0.1g to 1.2g with an increment of 0.1g for conducting IDA for which the base-isolated frame has not reached to the collapse limit, and hence there is no collapse point and flatness in the curves as discussed in the **section 6.2.1**. **Figures 6.6 to 6.10** are utilized to generate the mean IDA curves for different earthquakes. The mean IDA curves generated for different earthquakes are compared in **Figure 6.11** for different damage measures at the three considered PGA levels namely, low (0.2g), medium (0.4g), high (0.8g). By examining the mean IDA curves for all damage measures, it is found that the mean IDA curves for near-field earthquakes with directivity effect having low PGV/PGA < 150 (NFD-HR) provide maximum value of the damage measure for a given PGA level, which indicate that the NFD-HR earthquakes have induced the highest demand into the structure. Moreover, between the low PGA (0.2g) and medium PGA (0.4g), the mean IDA curves for NHD-HR earthquakes has crossed the third damage state (DS-3, Table 5) for all damage measures except for the maximum top floor acceleration MTFA. The fourth damage state (DS-4) is crossed at the PGA level ranging between the medium PGA (0.4g) and the high PGA (0.6g) by the NFD-HR earthquakes for all damage measure except MTFA.

On the other hand, the mean IDA curves for the FF earthquakes have the least value of damage measures expect MTFA, which show that the demands imposed by the FF earthquakes are least among all types of earthquakes considered. In order to produce the same damage level for a given damage measure, FF earthquakes require the maximum value of PGA. For the NFD-LR earthquakes, the mean IDA curves lie close to that of FF earthquakes for all damage measures. This means that the near-field directivity earthquakes with pulses can yield low responses which are compared to that of FF earthquake depending upon the ratio of PGV/PGA.

High PGV/PGA ratio has the potential of inflicting significantly high (extensive) damage in the structure.

Maximum top floor acceleration (MTFA), which is a major concern for all the base-isolated structures, is not very sensitive to the nature of earthquake up to a medium PGA level of 0.4g. Beyond this PGA level, significant difference in the MTFA is observed between different types of earthquakes; NFD-HR showing the highest value. However, the differences are less as compared to the case of other damage measures.

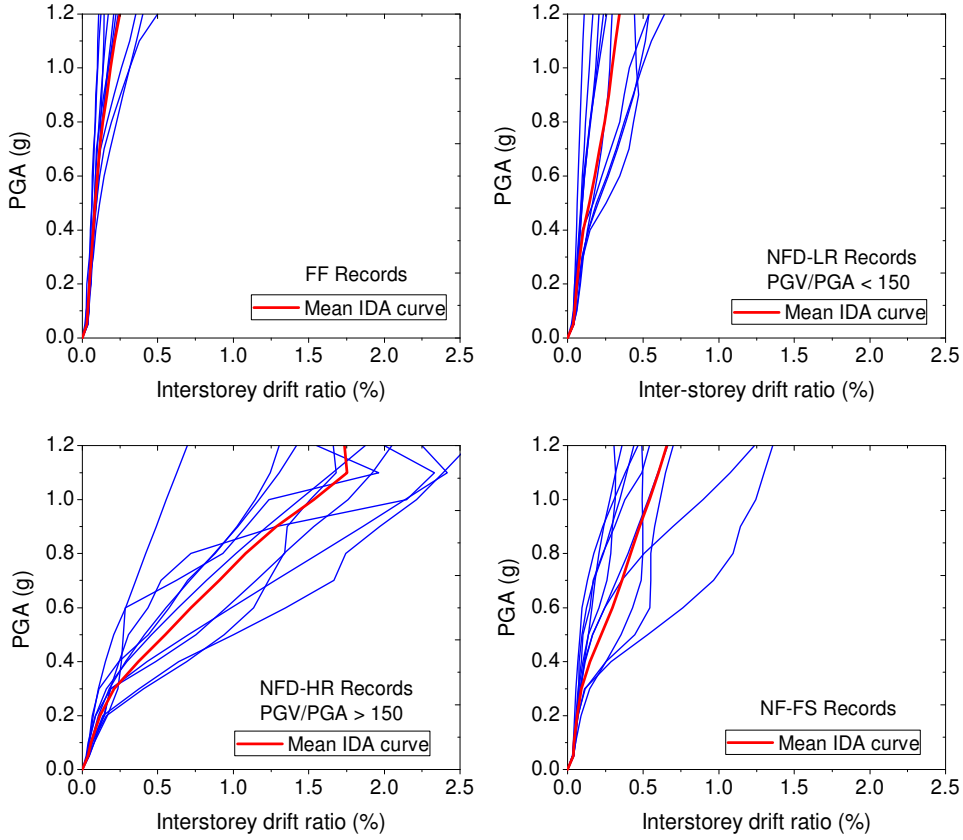

Figure 6.6 IDA curves generated for inter-storey drift ratio

The comparison of the values of different demand measures for a different type of earthquakes at the three earthquake levels, i.e., low, medium, and high are made in **Table 6.6**. It can be noted from the table that the highest and lowest values of all demand measures except for MTFA are yielded by NFD-HR and FF earthquakes respectively.

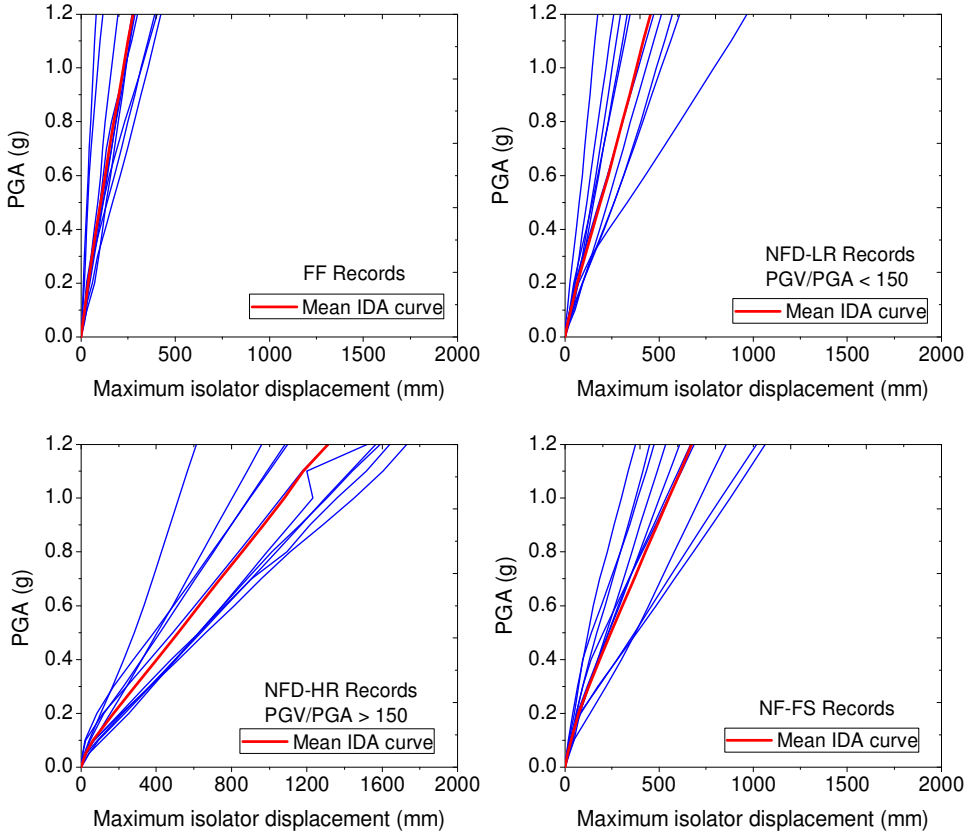

Figure 6.7 IDA curves generated for maximum isolator displacement

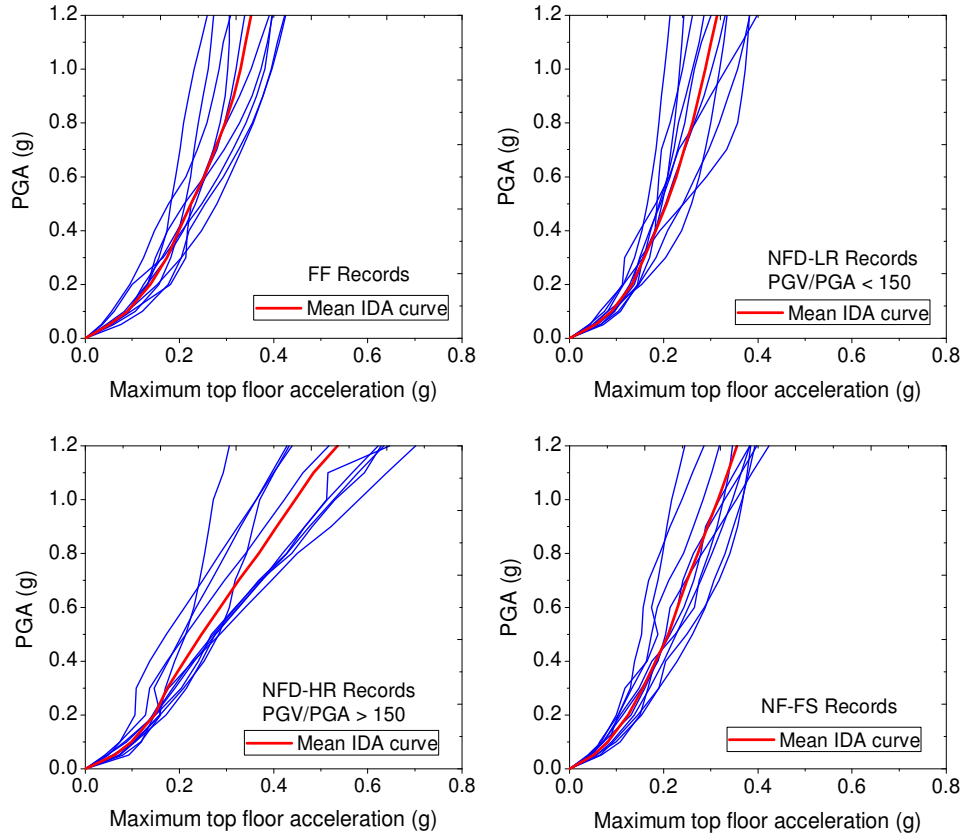

Figure 6.8 IDA curves generated for maximum top floor acceleration

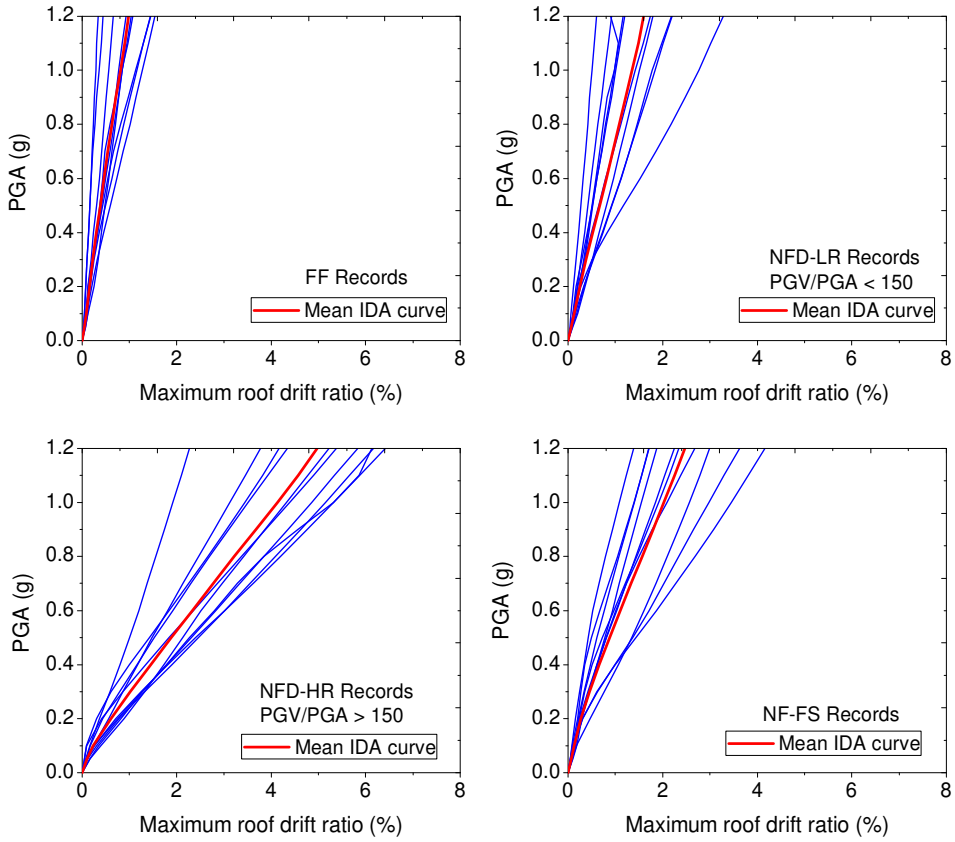

Figure 6.9 IDA curves generated for maximum roof drift ratio

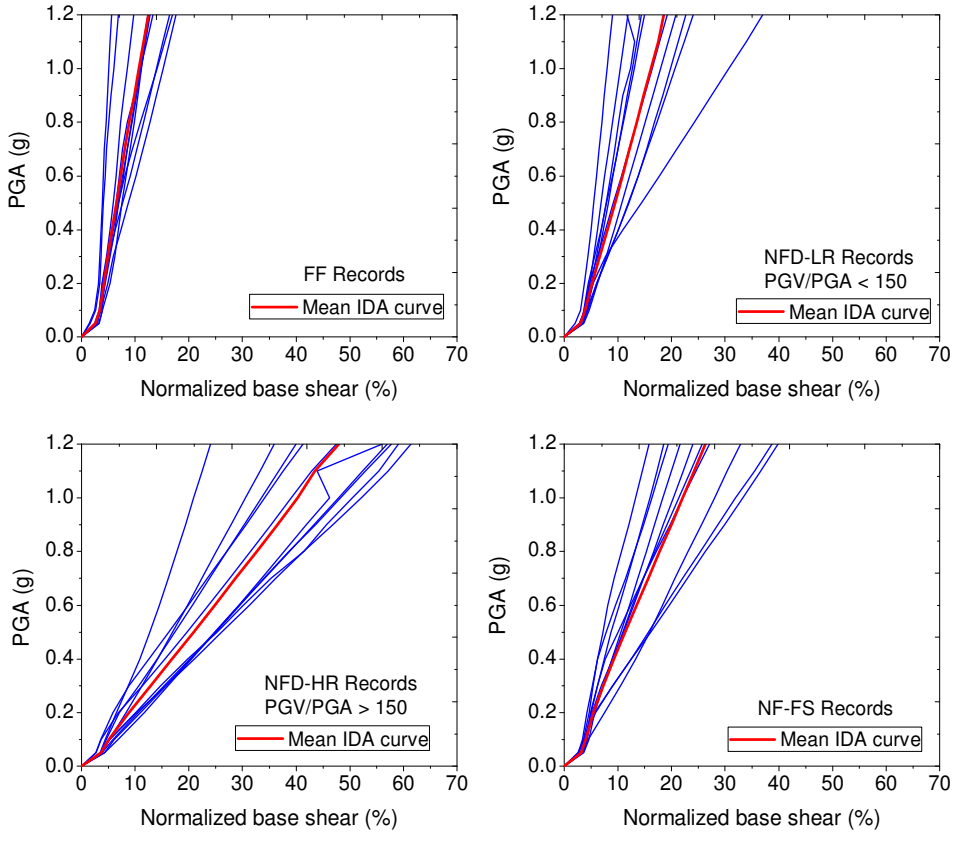

Figure 6.10 IDA curves for generated the base shear normalized by building weight

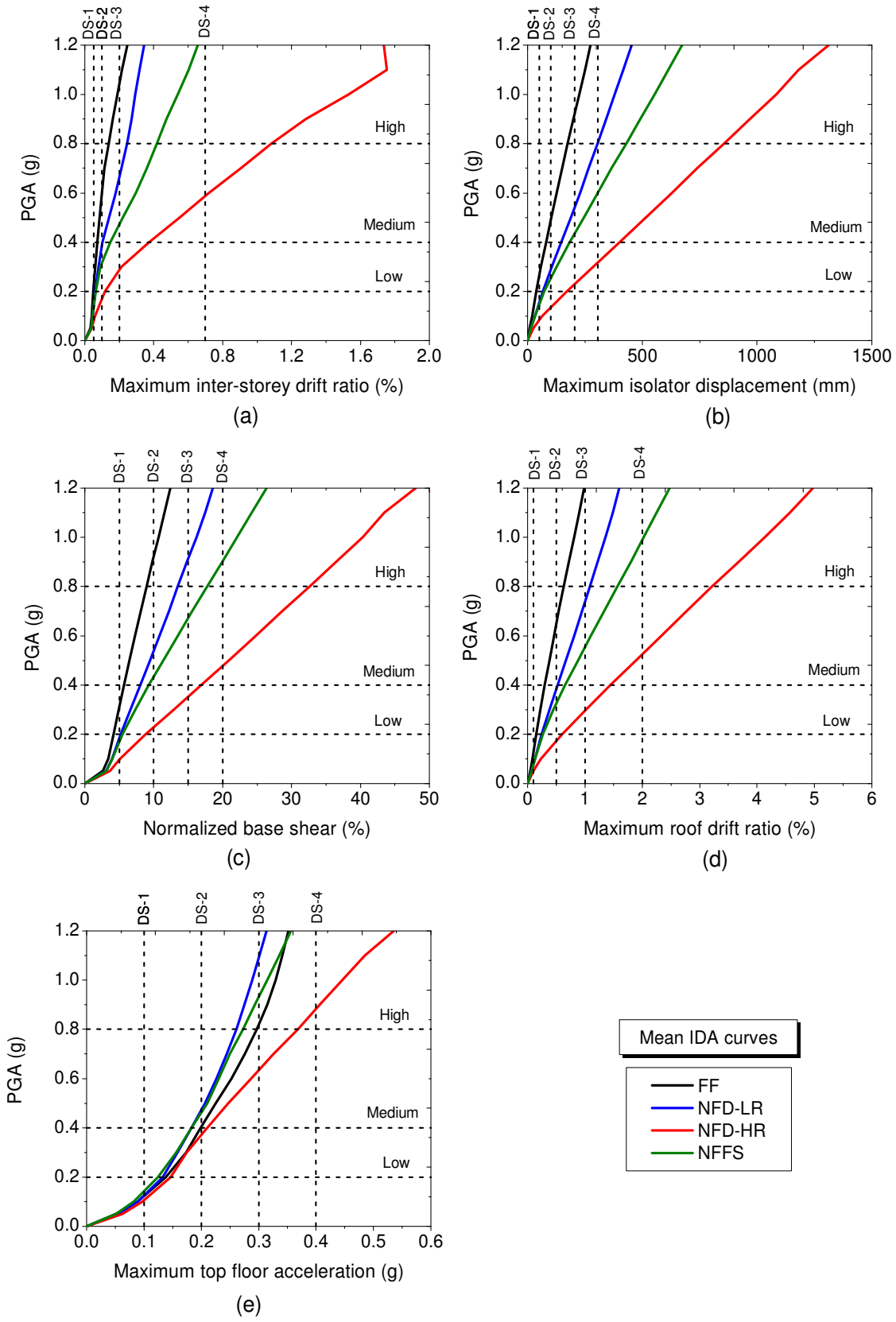

Figure 6.11 Mean IDA curves for different damage measures: (a) maximum inter-storey drift ratio; (b) maximum isolator displacement; (c) base shear; (d) maximum roof drift ratio; (e) maximum top floor acceleration

Table 6.6 Mean values of different damage measures at three considered values of PGA levels from IDA

Earthquakes	Mean values of damage measures				
	MIDR (%)	MID (mm)	MBS (%W)	MRDR (%)	MTFA (g)
	Low PGA = 0.2g				
FF	0.05	39	4.17	0.15	0.14
NFD-LR	0.06	66	5.18	0.25	0.13
NFD-HR	0.12	171	8.82	0.60	0.15
NFFS	0.06	73	5.41	0.27	0.12
	Medium PGA = 0.4g				
FF	0.07	81	5.67	0.30	0.20
NFD-LR	0.10	148	8.02	0.53	0.18
NFD-HR	0.37	402	16.88	1.45	0.21
NFFS	0.15	184	9.26	0.66	0.18
	High PGA = 0.8g				
FF	0.14	174	8.93	0.63	0.30
NFD-LR	0.24	305	13.50	1	0.26
NFD-HR	1.08	855	32.66	3.22	0.37
NFFS	0.42	429	17.8	1.57	0.27

FF = Far-field; NFD = near-field with directivity effect; LR = low ratio (PGV/PGA<150); HR = high ratio (PGV/PGA>150); NFFS = near-field with fling-step

The fragility curves of the base-isolated frame corresponding to the considered damage states are constructed by plotting the probability of exceedance of a particular damage state on the IM (PGA). The response data for different DMs generated by IDA are used to develop the probabilistic seismic demand models (PSDMs) by conducting the regression analysis. The distribution of the 10 values of the frame responses (particular for a DM) is plotted in the stripe form (Baker and Cornell, 2006; Park *et al.*, 2009) corresponding to each considered PGA level as shown in **Figure 6.12**.

The parameters which are necessary to describe the log-normal distribution (**equation 6.1**) are logarithmic mean (IM_m) and logarithmic standard deviation (β_D) which are estimated by performing the linear regression analysis of ln (DM) on ln (PGA). The logarithmic mean (IM_m) is then calculated using **Equations 6.3 or 6.4** corresponding to each threshold value of damage states. **Figure 6.13** represents the PSDMs of response data of maximum roof drift ratio (MRDR) for different types of earthquakes. The PSDMs for different demand measures and earthquake types are given in **Table 6.7**.

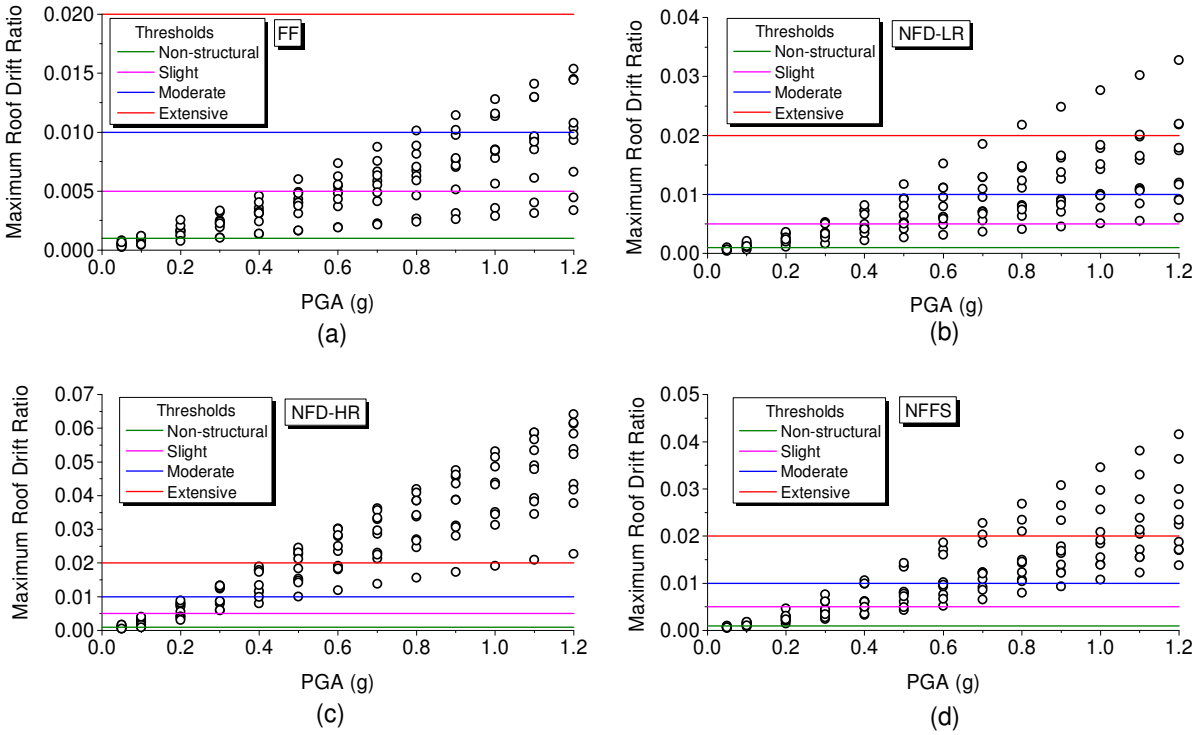

Figure 6.12 Distribution of responses of MRDR at considered PGA levels under different earthquakes: (a) FF; (b) NFD-LR; (c) NFD-HR; and (d) NFFS

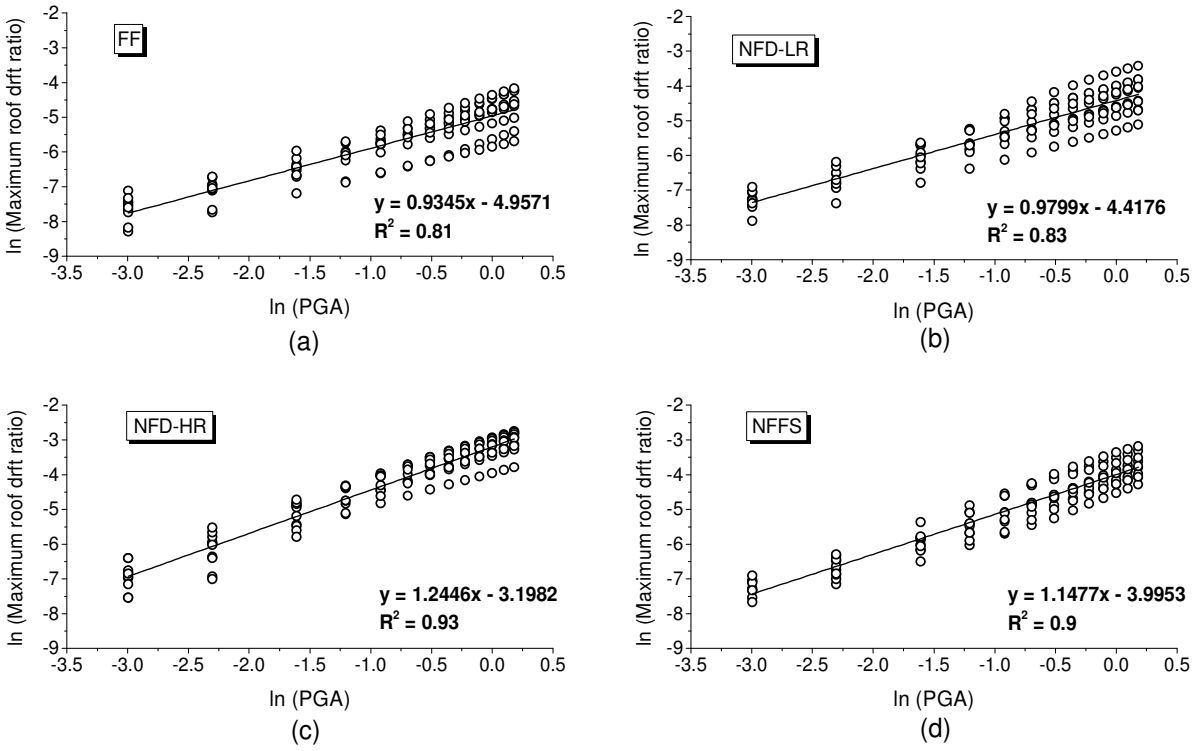

Figure 6.13 PSDMs of MRDR for different earthquakes; (a) FF; (b) NFD-LR; (c) NFD-HR; (d) NFFS

Table 6.7 Probabilistic seismic demand models (PSDM) models of various demand measures

DM	Response	PSDM	β_D	R^2
(a) Far-field earthquakes				
MIDR	ln (MIDR)	ln 0.0015 + 0.6378 ln (PGA)	0.33	0.76
MRDR	ln (MRDR)	ln 0.007 + 0.9345 ln (PGA)	0.43	0.81
MTFA	ln (MTFA)	ln 3.2543 + 0.5963 ln (PGA)	0.18	0.91
MID	ln (MID)	ln 194.7 + 1.0405 ln (PGA)	0.52	0.78
MBS	ln (MBS)	ln 614.56 + 0.4827 ln (PGA)	0.29	0.71
(b) Near-field earthquakes with directivity (low PGV/PGA ratio < 150)				
MIDR	ln (MIDR)	ln 0.002 + 0.6995 ln (PGA)	0.49	0.64
MRDR	ln (MRDR)	ln 0.0121 + 0.9799 ln (PGA)	0.42	0.83
MTFA	ln (MTFA)	ln 2.83 + 0.5284 ln (PGA)	0.17	0.9
MID	ln (MID)	ln 350 + 1.0684 ln (PGA)	0.43	0.85
MBS	ln (MBS)	ln 919.17 + 0.5667 ln (PGA)	0.31	0.75
(c) Near-field earthquakes with directivity (low PGV/PGA ratio > 150)				
MIDR	ln (MIDR)	ln 0.0126 + 1.3017 ln (PGA)	0.44	0.88
MRDR	ln (MRDR)	ln 0.0408 + 1.2446 ln (PGA)	0.33	0.93
MTFA	ln (MTFA)	ln 4.0968 + 0.6638 ln (PGA)	0.21	0.9
MID	ln (MID)	ln 1101 + 1.2635 ln (PGA)	0.35	0.92
MBS	ln (MBS)	ln 2413 + 0.8451 ln (PGA)	0.26	0.91
(d) Near-field earthquakes with fling=step effect				
MIDR	ln (MIDR)	ln 0.004 + 0.9702 ln (PGA)	0.52	0.76
MRDR	ln (MRDR)	ln 0.0184 + 1.1477 ln (PGA)	0.35	0.9
MTFA	ln (MTFA)	ln 3.047 + 0.5942 ln (PGA)	0.17	0.91
MID	ln (MID)	ln 520.4 + 1.2117 ln (PGA)	0.35	0.91
MBS	ln (MBS)	ln 1254 + 0.694 ln (PGA)	0.28	0.84

R^2 = Coefficient of determination; β_D = dispersion due to seismic demand; DM = damage measure

6.4.1 Comparison of Fragility Curves

Figures 6.14 to 6.18 present the fragility curves developed for different damage states (non-structural, slight, moderate, and extensive) which are associated with different damage measures under four types of earthquakes namely, far-field (FF), near-field with directivity effect having low PGV/PGA ratio (NFD-LR), near-field with directivity effect having high PGV/PGA ratio (NFD-HR), and near-field with fling-step effect (NFFS). It is observed from

the figures that for all damage measures and damage states considered, the base-isolated frame is most vulnerable to near-field earthquakes by having a high probability of exceeding (POE) the damage states as compared to far-field earthquakes. There is a very less variation found in the POE between different types of earthquakes in the non-structural damage state, associated with all damage measures. This variation in the POE increases from slight to extensive damage state and becomes significant, especially for moderate and extensive damage states. Furthermore, in all damage states and damage measures except maximum top floor absolute acceleration (MTFA), the probability of exceeding the damage state is highest for NFD-HR earthquakes and lowest for FF earthquakes. For the MTFA, the highest probability is given by NFD-HR, and the lowest is given by NFD-LR earthquakes.

The POE for different types of earthquakes is compared at three PGA levels, including, 0.2g (low), 0.4g (medium), and 0.8g (high). **Figure 6.14** shows the fragility curves for MIDR for different types of earthquakes. It is observed from the figure that at higher damage states like, moderate and extensive, the POE for NFD-HR and NFFS earthquakes is high even at a medium PGA value of 0.4g. The highest POE is provided by NFD-HR earthquake of the order of 35% at 0.2g, 83% at 0.4g, and 98% at 0.8g in the moderate damage state **(Fig 6.14(c))** and 19% at 0.4g, and 66% at 0.8g in the extensive damage state **(Figure 6.14(d))**.

On the other hand, it can be observed from the **Figures 6.14(c) and 6.14(d)** that the lowest POE is given by far-field earthquakes of the order of 0% at 0.2g, 0.4g and 0.8 in both moderate and extensive damage states except having very less POE of 7% at 0.8g in moderate damage state. Also, it can be clearly seen from the figures that the POE for NFFS earthquakes remains high even at moderate and extensive damage state for higher PGA levels. The POE is of the order of 38% at 0.4g and 80% at 0.8g in moderate damage state. The aforementioned trend in fragility curves shows that there exists a large variability in POE according to the type of earthquake.

Furthermore, the near-field earthquakes with directivity effect with high PGV/PGA ratio have a highest damage probability, and FF earthquakes have the least POE. The trend in the fragility curves for different types of earthquakes and demand measures is almost same and hence are not discussed again here.

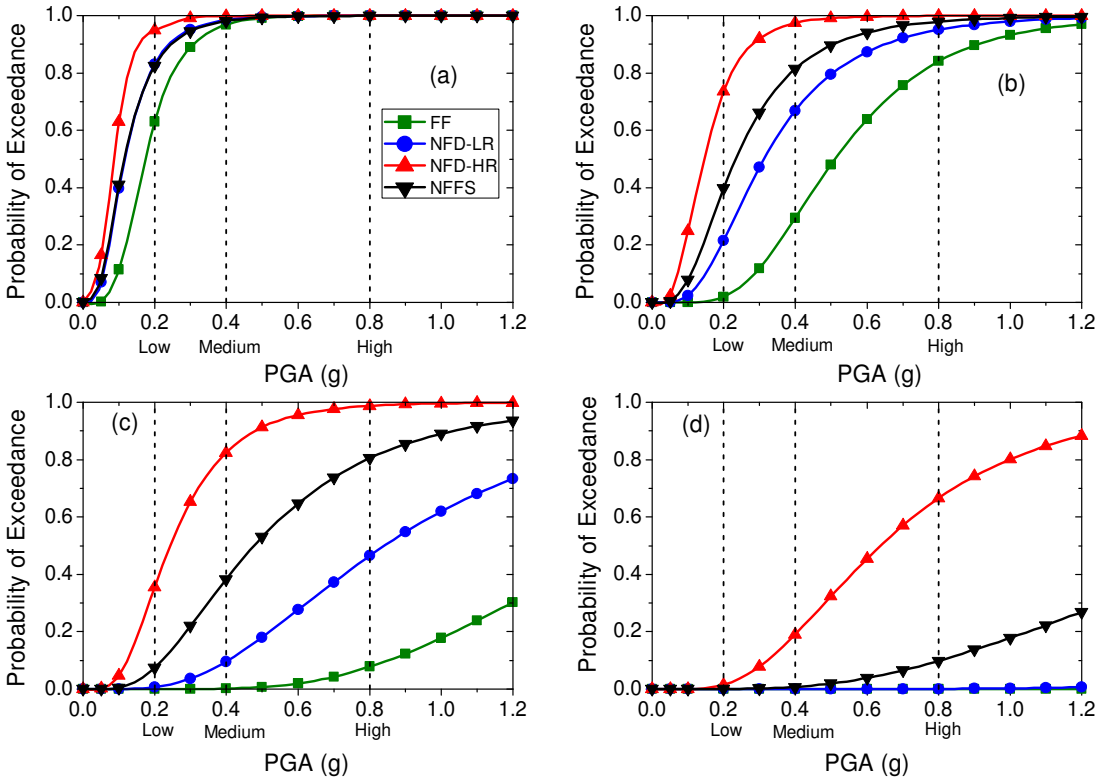

Figure 6.14 Comparison of fragility curves of MIDR under different earthquake types at four damage states: (a) non-structural; (b) slight; (c) moderate; (d) extensive

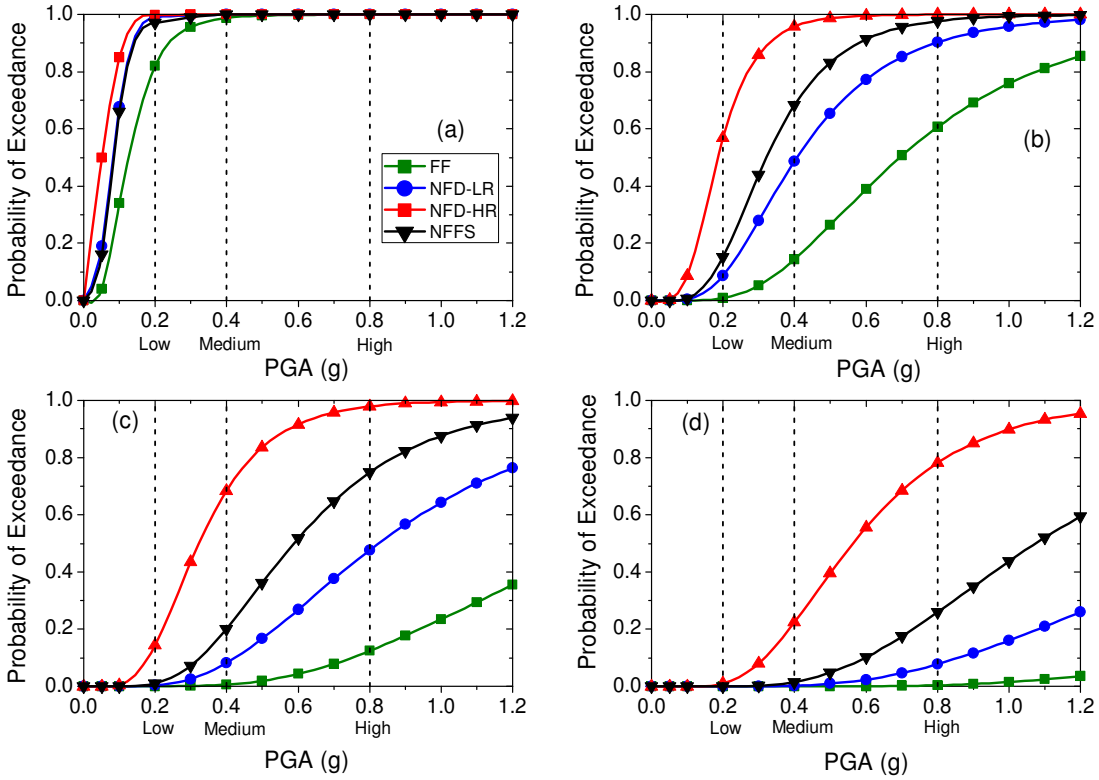

Figure 6.15 Comparison of fragility curves of MRDR under different earthquake types at four damage states: (a) non-structural; (b) slight; (c) moderate; (d) extensive

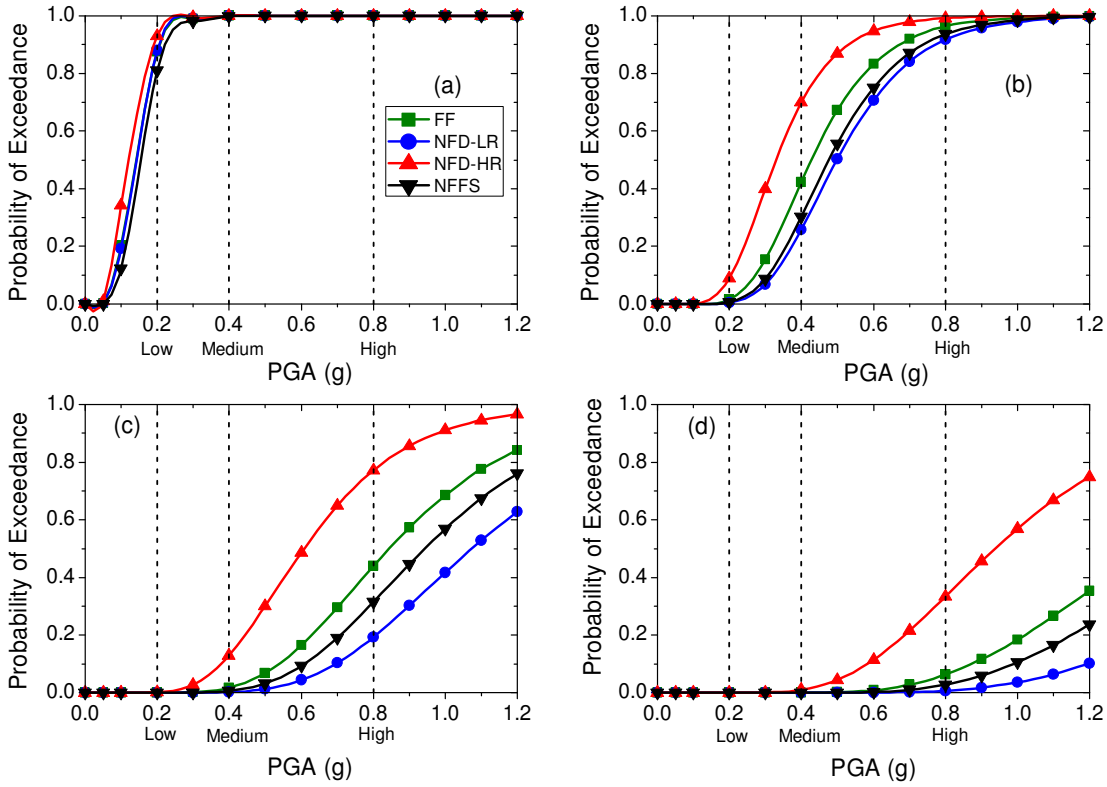

Figure 6.16 Comparison of fragility curves of MTFA under different earthquake types at four damage states: (a) non-structural; (b) slight; (c) moderate; (d) extensive

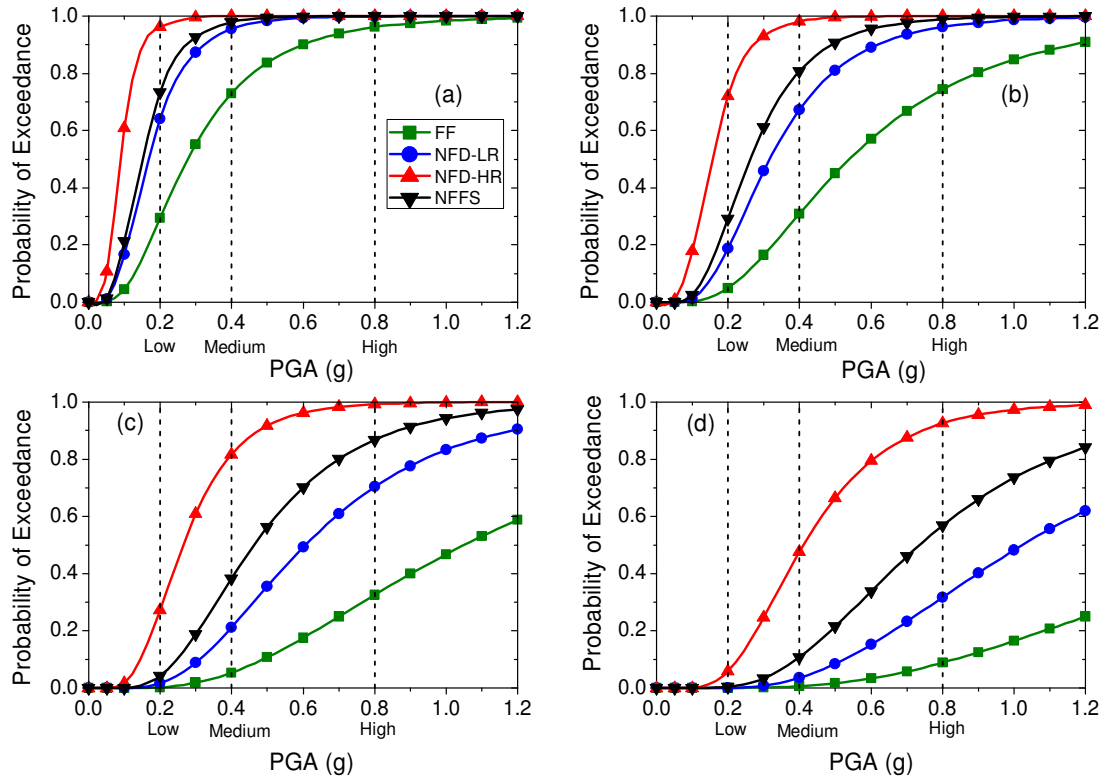

Figure 6.17 Comparison of fragility curves of MID under different earthquake types at four damage states: (a) non-structural; (b) slight; (c) moderate; (d) extensive

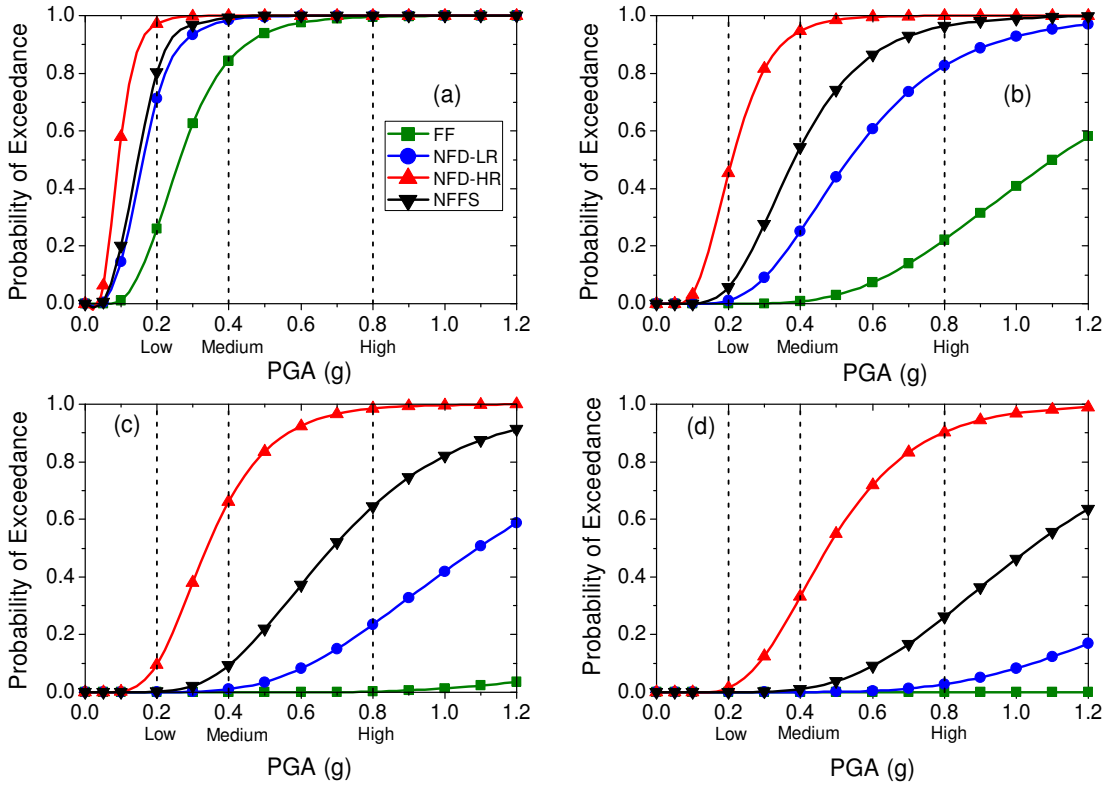

Figure 6.18 Comparison of fragility curves of MBS under different earthquake types at four damage states: (a) non-structural; (b) slight; (c) moderate; (d) extensive

6.4.2 Effect of Frequency Content (PGV/PGA ratio)

The effect of the frequency content of the near-field earthquakes with directivity effect, denoted by PGV/PGA ratio (ρ) on the exceedance probability of MIDR as DM is shown in **Figure 6.19**. The comparison is made between the POEs of NFD-LR (ρ < 150) and NFD-HR (ρ > 150) earthquakes considering three PGA levels namely, 0.2g (low), 0.4g (medium), and 0.8g (high). It is seen from the figure that for the less value of ρ (NFD-LR), the POE is less as compared to that for the higher value of ρ (NFD-HR). The difference in the POE increases with the severity of the damage level; for the moderate and extensive levels, this difference is large. As depicted in **Figure 6.19(c)**, for moderate damage, the POE is 1.6% at 0.2g, 21% at 0.4g, and 70% at 0.8g for NFD-LR earthquake as compared to 27% at 0.2g, 82% at 0.4g, and 99% at 0.8g for NFD-HR earthquakes. This difference in the POE is more pronounced in the extensive damage state, especially at 0.2g and 0.4g PGA levels as shown in the **Figure 6.19(d)**. Furthermore, the difference is found to be less for the low PGA level (0.2g) as compared to the high PGA level (0.8g). Thus, the near-field earthquakes with low ρ is less harmful and inflicts less amount of damage in the structure.

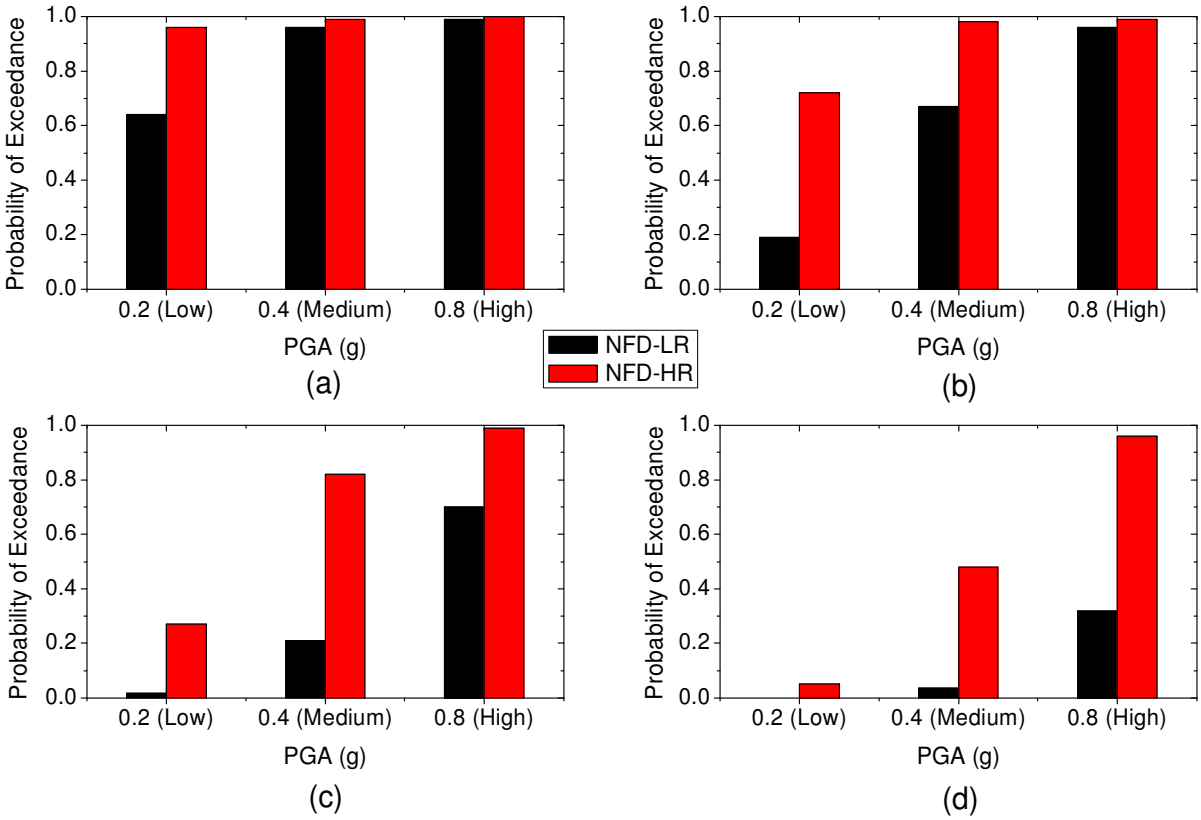

Figure 6.19 Comparison of probability of exceedance of MIDR between NFD-LR and NFD-HR at typical PGA levels for different damage states: (a) non-structural; (b) slight; (c) moderate; (d) extensive

From the present study, it is seen that the POE for NFD-LR earthquakes at moderate and extensive damage states is practically nil at the low level earthquake (PGA = 0.2g) and is very less (within 20%) at the extreme level earthquake (PGA = 0.4g) and for rare extreme level earthquake (PGA = 0.8g), only the POE of the moderate and extensive damage states are significant. Moreover, it is observed that for a value of $\rho > 150$, the POE of all damage states is nearly 1 at such a high value of PGA of 0.8g. Thus, it may be concluded that PGA/PGV ratio is an important parameter in relation to the damage assessment and highly influence the damage potential of near-field earthquakes with directivity effect. The trend of the results for other DMs remains the same, and therefore are not shown here.

6.4.3 The Effectiveness of Base Isolation System

The fragility curves for different DMs under different types of earthquakes are shown in **Figures 6.14 to 6.18**. Although these curves provide the effectiveness of base isolation in different types of earthquakes in a probabilistic sense, they cannot be readily used for designing the base isolation system for specific damage level. For this purpose, the PSDMs given in the

Table 6.7 are more useful. **Figure 6.20** shows the variation of the median PGA values of POE at different damage states under near and far field earthquakes and for different DMs.

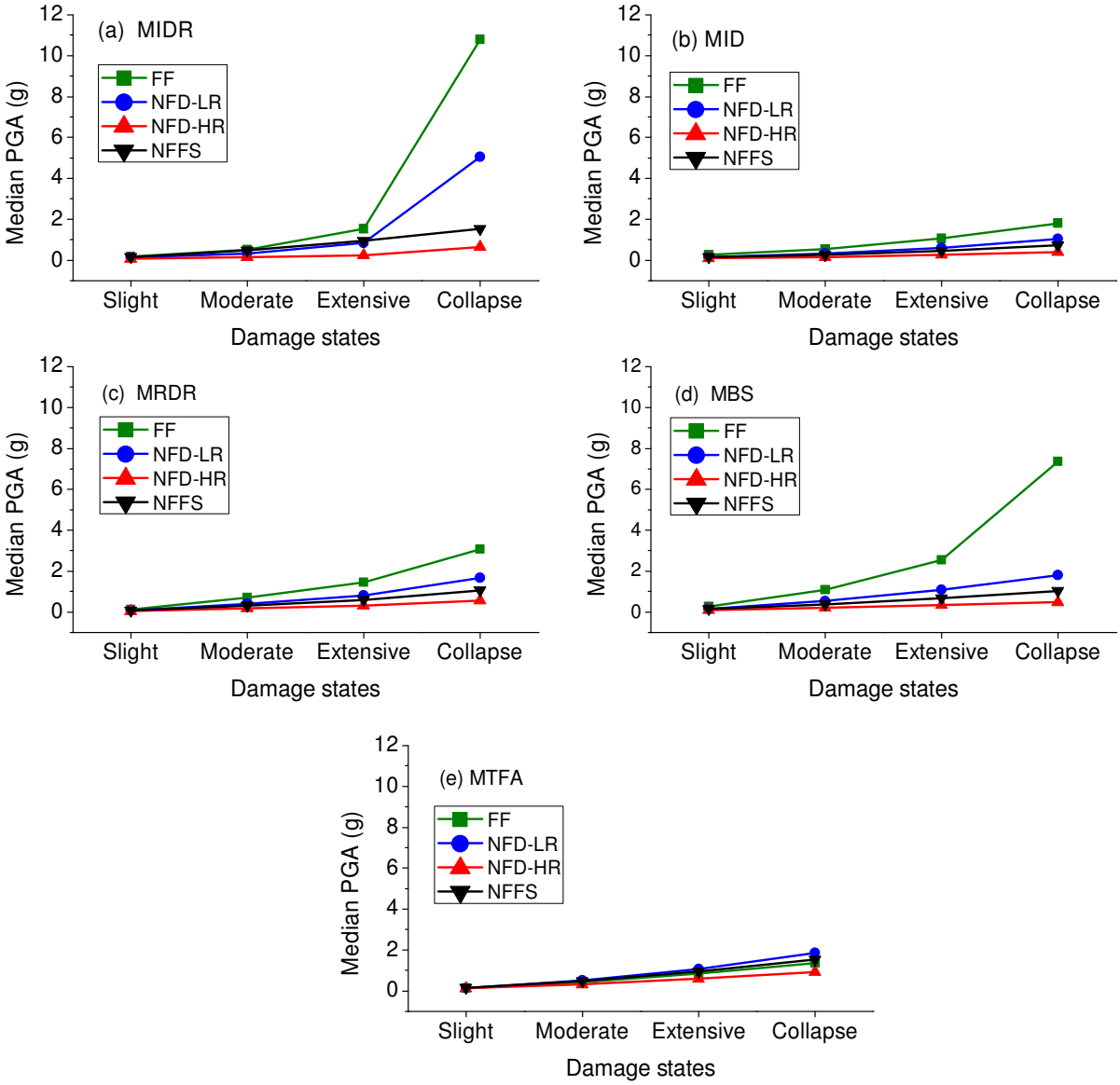

Figure 6.20 Comparison of median PGA values for different types of earthquakes considering various damage measures: (a) MIDR; (b) MID; (c) MRDR; (d) MBS; and (e) MTFA

The results interpreted by this analysis confirm the previous results which indicate that the NFD-HR is the most damaging earthquake by giving the lowest values of median PGA consistently to reach all damage states associated with all considered damage measures. On the other hand, the median PGA values are consistently the highest for the far-field earthquakes at all damage states and damage measures. The above trend in the results shows less effectiveness of base isolation system under NFD-HR and high effectiveness under FF earthquakes,

especially for MIDR and MBS by giving the largest median PGA values in these two damage measures. Furthermore, it is observed that under NFD-LR earthquakes, the performance of the base isolation is good and acceptable. Interesting, with the MTFA and MID as damage measures, the base isolation appears to be effective under FF, NFD-LR, and NFFS earthquakes as evident from **Figure 6.20(b) and 6.20(e).**

6.4.4 Sensitive Damage Measure

In the present study, five damage measures are considered to describe the damage in the structure and the isolation system. For the present study, the damage measure which gives maximum POE for a particular type of earthquake is termed as the sensitive damage measure. In order to identify it, POE of different damage states is compared at two assumed PGA levels, one is the design basis earthquake (DBE) PGA as 0.2g, and another is a maximum credible earthquake (MCE) PGA as 0.4g. This comparison is made for all damage states, excluding non-structural damage state. **Tables 6.8 and 6.9** show the POE at each damage state, for each damage measure, and for different types of earthquakes at PGA levels of 0.2g and 0.4g.

Table 6.8 POE for different damage measures and types of earthquakes at PGA of 0.2g.

Earthquakes	Damage Measures				
	MIDR	MID	MBS	MRDR	MTFA
	Slight Damage				
FF	2%	5%	0%	1%	1%
NFD-LR	22%	19%	1%	9%	0%
NFD-HR	74%	72%	45%	57%	9%
NFFS	40%	29%	6%	15%	1%
	Moderate Damage				
FF	0%	0%	0%	0%	0%
NFD-LR	1%	2%	0%	0%	0%
NFD-HR	36%	27%	9%	14%	0%
NFFS	7%	4%	0%	1%	0%
	Extensive Damage				
FF	0%	0%	0%	0%	0%
NFD-LR	0%	0%	0%	0%	0%
NFD-HR	1%	6%	2%	1%	0%
NFFS	0%	0%	0%	0%	0%

The comparison of POE at 0.2g is made in **Table 7**. It is observed from the table that in a extensive damage state, the POEs for to all earthquakes are almost zero except NFD-HR. Furthermore, MIDR and MID are the two damage measures which have the highest POE for all types of earthquakes at slight and moderate damage states. The same trend in POE is found at the PGA level of 0.4g with amplified values of POE as given in **Table 8**. Thus, it may be inferred that MIDR and MID are the two sensitive damage measures and the values of POE for the two depend upon the type of earthquake.

Table 6.9 POE for different damage measures and types of earthquakes at PGA of 0.4g.

Earthquakes	Damage Measures				
	MIDR	MID	MBS	MRDR	MTFA
	Slight Damage				
FF	29%	31%	1%	14%	42%
NFD-LR	67%	67%	25%	49%	26%
NFD-HR	97%	98%	95%	96%	70%
NFFS	81%	81%	54%	68%	30%
	Moderate Damage				
FF	0%	5%	0%	1%	2%
NFD-LR	10%	21%	1%	8%	0%
NFD-HR	83%	82%	66%	68%	13%
NFFS	38%	38%	9%	20%	1%
	Extensive Damage				
FF	0%	1%	0%	0%	0%
NFD-LR	0%	4%	0%	0%	0%
NFD-HR	19%	48%	33%	22%	1%
NFFS	1%	11%	1%	2%	0%

6.5 Conclusions

Probabilistic seismic assessment of a 10-storey base-isolated reinforced concrete frame under near and far field earthquakes is presented using fragility analysis. Two types of near-field earthquakes are considered one with directivity effect and the other with fling-step effect. For the near-field earthquake with directivity effect, the PGV/PGA ratio is varied to investigate the effect on the damage evaluation. Incremental dynamic analysis (IDA) is performed to generate the data set of seismic responses considering different demand measures namely,

maximum inter-storey drift ratio (MIDR), maximum roof drift ratio (MRDR), maximum base shear (MBS), maximum absolute top floor acceleration (MTFA), and maximum isolator displacement (MID). An ensemble of ten ground motion records is employed in the IDA for each type of earthquake, including (i) far-field (FF); (ii) near-field with directivity effect having low PGV/PGA ratio (NFD-LR), i.e., PGV/PGA <150; (iii) near-field with directivity effect having high PGV/PGA (NFD-HR), i.e., PGV/PGA >150; and (iv) near-field with fling step effect (NFFS). The probabilistic seismic demand models (PSDM) are developed by performing the regression analysis, and finally, fragility curves are constructed considering four damage states namely, slight, moderate, extensive, and complete which are associated with damage measures. The fragility curves under near and far field earthquakes are compared. For the specific building frame analyzed, the important findings inferred from the study are enumerated below:

1. The base isolated frame is highly susceptible to near-field earthquakes as compared to far-field earthquakes.
2. The near-field earthquakes with directivity effect having high PGV/PGA has high damage potential by producing the highest POE at all damage states and damage measures.
3. There is very less variability of POE in the slight damage state for different types of earthquakes, and this variability increases significantly with increases in damage states associated with all damage measures.
4. The base isolation is highly effective in reducing MIDR and MBS in FF earthquakes and less effective under near-field earthquakes, especially for the NFD-HR earthquakes. However, the effectiveness of the base isolation is improved under the NFD-LR earthquakes.
5. There is a significant effect of the PGV/PGA ratio on the POE for the near-field earthquakes with directivity effect. The significant difference of POE between NFD-LR and NFD-HR is found, and it is highly pronounced at moderate and extensive damage states even at a high PGA level, i.e., 0.8g.
6. For the specific problem analyzed, MIDR and MID are the two sensitive damage measures which have high POE in every damage state. Therefore, the design of base-isolated structure should be given due consideration on these two demand measures, MIDR and MID, especially under NFD-HR and NFFS earthquakes.

Chapter 7

Conclusions and Recommendations for Future Work

7.1 Concluding Remarks

The behavior and performance of the base-isolated building frames under far-field and near-field earthquakes are evaluated by conducting the nonlinear time history analysis (NTHA), pushover analysis (POA), and fragility analysis. The studies can be divided into four categories namely, (i) investigation of the behavior of base-isolated frame in the inelastic range for low level of PGA (0.2g) and higher level of PGA (0.4g) under far-field and near-field earthquakes. A special emphasis is paid on the evaluation of the inelastic behavior of base-isolated structure and base isolators under near-field earthquakes with directivity and fling-step effect.; (ii) performance evaluation of base-isolated building frames in the context of performance based design in which the estimates of different response parameters of interest at the different performance points obtained by the capacity spectrum method (CSM) are compared with those of benchmark estimates of the nonlinear time history analysis; (iii) evaluation of different proposed lateral load patterns (LLPs) used for performing pushover analysis by comparing the response quantities of interest between the POA with considered LLPs and NTHA at selected target displacements, which covers the entire range of elastic to inelastic excursion of the building; and (iv) probabilistic performance evaluation of the base-isolated frame under ensembles of near and far field earthquakes by constructing the fragility curves with the help of incremental dynamic analysis.

Two reinforced concrete base-isolated building frames typifying low-rise (5storey) and high-rise (10-storey) buildings are considered for the numerical study. Three types of base-isolators namely, stiff, medium, and flexible designated by the different equivalent stiffnesses are also considered in order to investigate the effect of the type of base-isolation on the seismic performance of the base-isolated buildings. A large number of response quantities or damage measures are used for assessing the performance of the BI frames; they include, maximum inter-storey drift ratio, maximum top floor displacement, maximum base shear, maximum isolator displacement, square root of sum of square (SRSS) of plastic hinge rotations, and the number of plastic hinges.

All the analyses are performed using SAP 2000 software. The major conclusion drawn from the above studies are summarized below:

1. For the two levels of the PGA of earthquake considered in the study, i.e. 0.2g and 0.4g, the percentage reductions in the 10-storey base-isolated frame with reference to fixed

base frame for response quantities like base shear, top floor absolute acceleration and maximum storey drift are higher for far-field earthquake as compared to the near-field earthquakes with directivity and fling-step effect. For reference, the maximum reduction in base shear is 75% for far-field, 60% near-field with directivity, 18% for near-field fling-step effect at a PGA level of 0.4g

2. The force-deformation loops of the isolator differ widely with the type of earthquakes; for the far-field earthquakes the hysteresis loops are wider with large number of cycles enabling high energy dissipation; for the near-field earthquake with fling-step effect, the hysteresis loop is narrow with fewer number of cycles and have large isolator displacement, especially for the higher level of PGA of 0.4g.
3. For the near-field earthquakes, the base-isolated building frame gets into the inelastic range even for the lower value of the PGA of 0.2g; for the higher level of the PGA of 0.4g, the extent of the inelastic excursion is not reduced by providing the base isolation. Thus, ductility demand is not reduced by isolating the frame at higher PGA level.
4. The effect of post to pre yield stiffness ratio (γ) of the isolator on the response behavior of the base-isolated frame differs widely with the nature of earthquake; for far-field earthquake, the effect is not very significant for both levels of PGA (0.2g and 0.4g); the effect is very pronounced for near-field earthquakes so far as the percentage reduction in responses is concerned; for near-field earthquake with fling-step effect, the formation of plastic hinges is not very sensitive to the variation of γ for upper the level of PGA.
5. At the performance point consistent with a PGA level of 0.2g, which is considered as the design level earthquake in the present study, none of the plastic hinges are formed in both base-isolated frames for both CSM and NTHA. Therefore, the inelastic effect is not introduced into the BI frames up to the design level PGA. The fixed base frame undergoes moderate damages, showing the formation of plastic hinges, at the performance point consistent with the PGA level of 0.2g.
6. No significant difference is observed between the response quantities of interest obtained by the CSM and the NTHA for performance points up to a PGA level of 0.2g for the BI frames. The same is true for the FB frames as well.
7. For all the performance points in the zone of PGA level of 0.25g – 0.4g, different degrees of differences are observed between the response quantities of interest obtained from the two analyses for both BI and FB frames; beyond the PGA level of 0.4g, differences between the responses obtained by the CSM and the NTHA significantly increases for BI frames. These differences are relatively less for the FB frames.

8. Considering the above points and specific frames analyzed in this study, it may be inferred that the CSM could be a good replacement for NTHA in predicting the peak values of the responses of the BI frames for the performance points up to a PGA level of 0.2g. Beyond this level, CSM should be cautiously used for predicting the inelastic behavior of BI buildings at different performance points up to a PGA level of 0.4g, which is considered as the extreme level earthquake in the present study.
9. The proposed LLP-3, which is the modification of uniform distribution of load pattern, turns out to be the best in estimating the maximum storey displacements for all target displacements (TDs; TD-1, TD-2, TD-3) and earthquakes considered for both base-isolated frames (5-storey and 10-storey).
10. Estimations of the base shears and the isolator displacements by all LLPs are good at TD-1(depicting the elastic state of structure) and TD-2 (depicting the elastic-plastic state of structure) for all earthquakes. The errors in the estimations increase as the frames undergo excursion from elastic-plastic (TD-2) to a plastic state (TD-3); LLP3 provides the least error.
11. All LLPs (LLP 1-4) provide errors in the predictions of inter-storey drift. These errors are significant in the lower stories at TD-2 and TD-3, and in upper stories at TD-1 for all earthquakes. LLP-1 and LLP-3 give least errors in the upper stories and lower stories respectively. Errors in predicting the number of plastic hinges is more for the far-field earthquakes as compared to the near-field earthquakes.
12. For the specific building frames analyzed in this study, the proposed LLP-3 predictions are best with practically acceptable errors even at the plastic state (TD-3) of both building frames, if the maximum base shears, the maximum storey displacements, and the maximum isolator displacements are considered to be the three most important response parameters in the analysis base isolated structures. Thus, the POA can be used to predict the behavior of base-isolated building frame for the above three important response parameters for the design level far field earthquakes recommended in all seismic codes and even for extreme level earthquakes, specified in some codes (i.e., Indian Code).
13. The base-isolated frame (10-storey) is highly susceptible to near-field earthquakes as compared to far-field earthquakes. The near-field earthquakes with directivity effect having high ratio of PGV/PGA > 150 (NFD-HR) has high damage potential by producing the highest probability of exceedance (POE) at all considered damage states and damage measures.

14. The base isolation is highly effective in reducing maximum inter-storey drift ratio (MIDR) and maximum base shear (MBS) in far-field (FF) earthquake and less effective under near-field earthquakes, especially for NFD-HR earthquakes. However, the effectiveness of the base isolation is improved under the near-field earthquakes with directivity effect having low ratio of PGV/PGA < 150 (NFD-LR) earthquakes.
15. There is a significant effect of the PGV/PGA ratio on the POE for the near-field earthquakes with directivity effect. The significant difference of POE between NFD-LR and NFD-HR is found, and it is highly pronounced at higher damage states even at a high PGA level, i.e., 0.8g.
16. For the specific problem analyzed, MIDR and maximum isolator displacement (MID) are the two sensitive damage measures which have high POE in every damage state. Therefore, the design of base-isolated structure should be given due consideration on these two demand measures, MIDR and MID, especially under NFD-HR and near-field with fling-step effect (NFFS) earthquakes.

7.2 Major Contributions of the Study

The present study leads to the following contributions:

6. In-depth investigation to study the Seismic behavior and performance of base isolated building frames in both elastic and inelastic states subjected to near field and far field earthquakes.
7. Assessment of the efficacy of the Capacity Spectrum Method in contrast with Nonlinear Time History Analysis for base-isolated frames.
8. Comparison of seismic demands for base-isolated frames and fixed base frames at different performance points ranging from the elastic to the plastic state of the structure.
9. Covers comparison of large number of demand measures which are not comprehensively looked at in other studies.
10. Reveals how Capacity Spectrum Method predicts the inelastic behaviour of base isolated frames at various PGA levels.
11. Two new lateral load patterns (LLP) are proposed to perform pushover analysis of base isolated frames for predicting inelastic seismic demands.
12. The Study reveals how considered LLPs predict the inelastic behaviour of base isolated frames at three Target displacements, considered at three different states on the capacity curve, for different response parameters.

13. The proposed lateral load pattern turns out to be best in estimating some response parameters namely, base shear, peak story displacement, and maximum isolator displacement.
14. The study shows the variation in the probability of exceedance of a specified damage state for near-field (directivity and fling-step effects) and far-field earthquakes for (10-story base isolated frame.
15. There is a significant effect of the PGV/PGA ratio on the damage probability for the near-field earthquakes with directivity effect, as the high PGV/PGA ratio has greater damage probability compared to the low PGV/PGA ratio.
16. For the specific problem analyzed, maximum inter-story drift and maximum isolator displacmenet are the two sensitive damage measures which have high probability of exceedance in every damage state.
17. The base isolation is highly effective in reducing maximum inter-story drift and maximu base shear in far-field earthquakes.

7.3 Limitations of the Study

Although the research has reached its aims, there are some limitations as appended below:

1. The investigation is conducted by considering only two-dimensional models of frames.
2. Only 5-storey and 10-storey building frames were considered.
3. Only one type of isolator, specifically lead bearing isolator, is used as a base isolation device.
4. Limited number of earthquake records are selected to perform analysis.
5. Nonlinear time history analysis is performed by applying the earthquake excitation only in one direction to the building frames.
6. The nonlinearity in the building frame is modelled only by defining default plastic hinge model.

7.4 Recommendations for Future Work

As an extension of the present study and in order to have better understanding of behavior of base-isolated buildings and base isolation system under different types of the earthquakes, the following studies may be carried out:

1. Behavior of base-isolated buildings considering 3-D building models having different numbers of stories under near-field earthquakes.
2. Development of the design response spectrum for near-field earthquakes.

3. Performing nonlinear analysis by considering multi-component ground motions.
4. Studying the effect of heating of lead core in lead rubber bearings during large inelastic excursions.
5. Development of lateral load patterns for 3-D building models, which provide close estimates of seismic demand imposed on base-isolated buildings.
6. Seismic hazard analysis of base-isolated buildings under near-field ground motions.

REFERENCES

Akkar, S., Yazgan, U., & Gülkan, P. (2005). Drift estimates in frame buildings subjected to near-fault ground motions. *Journal of Structural Engineering, 131*(7), 1014-1024.

Alam, M. S., Bhuiyan, M. R., & Billah, A. M. (2012). Seismic fragility assessment of SMA-bar restrained multi-span continuous highway bridge isolated by different laminated rubber bearings in medium to strong seismic risk zones. *Bulletin of Earthquake Engineering, 10*(6), 1885-1909.

Alavi, B., & Krawinkler, H. (2004). Behavior of moment-resisting frame structures subjected to near-fault ground motions. *Earthquake engineering & structural dynamics, 33*(6), 687-706.

Alhan, C., Gazi, H., & Kurtuluş, H. (2016). Significance of stiffening of high damping rubber bearings on the response of base-isolated buildings under near-fault earthquakes. *Mechanical Systems and Signal Processing, 79*, 297-313.

Alhan, C., & Öncü-Davas, S. (2016). Performance limits of seismically isolated buildings under near-field earthquakes. *Engineering Structures, 116*, 83-94.

Alonso-Rodríguez, A., & Miranda, E. (2015). Assessment of building behavior under near-fault pulse-like ground motions through simplified models. *Soil Dynamics and Earthquake Engineering, 79*, 47-58.

Ambraseys, N., & Menu, J. (1988). Earthquake-induced ground displacements. *Earthquake engineering & structural dynamics, 16*(7), 985-1006.

Antoniou, S., & Pinho, R. (2004a). Advantages and limitations of adaptive and non-adaptive force-based pushover procedures. *Journal of earthquake engineering, 8*(04), 497-522.

Antoniou, S., & Pinho, R. (2004b). Development and verification of a displacement-based adaptive pushover procedure. *Journal of earthquake engineering, 8*(05), 643-661.

ATC-40. (1996). Seismic evaluation and retrofit of concrete buildings. *Applied Technology Council, report ATC-40. Redwood City*.

Baker, J. W., & Cornell, C. A. (2006). *Vector-valued ground motion intensity measures for probabilistic seismic demand analysis*: Pacific Earthquake Engineering Research Center, College of Engineering, University of California, Berkeley.

Bakhshi, A., & Mostafavi, S. (2014). Development of fragility curves for base isolated RC structures. *9th international conference on structural dynamics, EURODYN*.

Banazadeh, M., Gholhaki, M., & Parvini Sani, H. (2017). Cost-benefit analysis of seismic-isolated structures with viscous damper based on loss estimation. *Structure and Infrastructure Engineering, 13*(8), 1045-1055.

Bento, R., Falcao, S., & Rodrigues, F. (2004). *Nonlinear Static Procedures in performance based seismic design.* Paper presented at the Proceedings of the 13th world conference on earthquake engineering, Vancouver, Canada.

Bertero, V. V. (1977). Strength and deformation capacities of buildings under extreme environments. *Structural engineering and structural mechanics, 53*(1), 29-79.

Bhatt, C., & Bento, R. (2014). The extended adaptive capacity spectrum method for the seismic assessment of plan-asymmetric buildings. *Earthquake spectra, 30*(2), 683-703.

Bracci, J. M., Kunnath, S. K., & Reinhorn, A. M. (1997). Seismic performance and retrofit evaluation of reinforced concrete structures. *Journal of Structural Engineering, 123*(1), 3-10.

Bray, J. D., & Rodriguez-Marek, A. (2004). Characterization of forward-directivity ground motions in the near-fault region. *Soil Dynamics and Earthquake Engineering, 24*(11), 815-828.

Burks, L. S., & Baker, J. W. (2016). A predictive model for fling-step in near-fault ground motions based on recordings and simulations. *Soil Dynamics and Earthquake Engineering, 80*, 119-126.

Cardone, D., Dolce, M., & Gesualdi, G. (2009). Lateral force distributions for the linear static analysis of base-isolated buildings. *Bulletin of Earthquake Engineering, 7*(3), 801-834.

Cardone, D., Flora, A., & Gesualdi, G. (2013). Inelastic response of RC frame buildings with seismic isolation. *Earthquake engineering & structural dynamics, 42*(6), 871-889.

Castaldo, P., Amendola, G., & Palazzo, B. (2017a). Seismic fragility and reliability of structures isolated by friction pendulum devices: seismic reliability-based design (SRBD). *Earthquake engineering & structural dynamics, 46*(3), 425-446.

Castaldo, P., Palazzo, B., & Ferrentino, T. (2017b). Seismic reliability-based ductility demand evaluation for inelastic base-isolated structures with friction pendulum devices. *Earthquake engineering & structural dynamics, 46*(8), 1245-1266.

Castaldo, P., Palazzo, B., Ferrentino, T., & Petrone, G. (2017c). Influence of the strength reduction factor on the seismic reliability of structures with FPS considering intermediate PGA/PGV ratios. *Composites Part B: Engineering, 115*, 308-315.

Chandler, A. M., & Lam, N. T. (2001). Performance-based design in earthquake engineering: a multi-disciplinary review. *Engineering Structures, 23*(12), 1525-1543.

Chopra, A. K. (2001). Dynamics of structures: Theory and applications. *Printice Hall International inc, London*.

Chopra, A. K., & Chintanapakdee, C. (2001). Comparing response of SDF systems to near-fault and far-fault earthquake motions in the context of spectral regions. *Earthquake engineering & structural dynamics, 30*(12), 1769-1789.

Chopra, A. K., & Goel, R. K. (2002). A modal pushover analysis procedure for estimating seismic demands for buildings. *Earthquake engineering & structural dynamics, 31*(3), 561-582.

Cornell, C. A., Jalayer, F., Hamburger, R. O., & Foutch, D. A. (2002). Probabilistic basis for 2000 SAC federal emergency management agency steel moment frame guidelines. *Journal of Structural Engineering, 128*(4), 526-533.

CSI. (2010). Integrated Finite Element Analysis and Design of Structures Basic Analysis Reference Manual. *Computers and Structures, Berkeley, California, USA*.

Datta, T. K. (2010). *Seismic analysis of structures*: John Wiley & Sons.

Davoodi, M., Sadjadi, M., Goljahani, P., & Kamalian, M. (2012). *Effects of Near-Field and Far-Field Earthquakes on Seismic Response of SDOF System Considering Soil Structure Interaction.* Paper presented at the 15th World Conference on Earthquake Engineering. Lisbon, Portugal.

Doudoumis, N. I., Kotanidis, C., & Doudoumis, I. N. (2006). *A comparative study on static push-over and time-history analysis methods in base isolated buildings.* Paper presented at the First European Conference on Earthquake Engineering and Seismology, Geneva, Switzerland, September, paper.

Ellingwood, B. R., & Kinali, K. (2009). Quantifying and communicating uncertainty in seismic risk assessment. *Structural Safety, 31*(2), 179-187.

Elnashai, A. (2000). Analysis of the damage potential of the Kocaeli (Turkey) earthquake of 17 August 1999. *Engineering Structures, 22*(7), 746-754.

Elnashai, A. S. (2001). Advanced inelastic static (pushover) analysis for earthquake applications. *Structural engineering and mechanics, 12*(1), 51-70.

Elnashai, A. S., & Di Sarno, L. (2008). *Fundamentals of earthquake engineering*: Wiley New York.

Faal, H. N., & Poursha, M. (2017). Applicability of the N2, extended N2 and modal pushover analysis methods for the seismic evaluation of base-isolated building frames with lead rubber bearings (LRBs). *Soil Dynamics and Earthquake Engineering, 98*, 84-100.

Fajfar, P. (2000). A nonlinear analysis method for performance-based seismic design. *Earthquake spectra, 16*(3), 573-592.

Fajfar, P., & Gaspersic, P. (1996). The N2 method for the seismic damage analysis of RC buildings. *Earthquake engineering & structural dynamics, 25*(1), 31-46.

Fajfar, P., Marusic, D., & Perus, I. (2005). Torsional effects in the pushover-based seismic analysis of buildings. *Journal of earthquake engineering, 9*(06), 831-854.

Fathi, M., Makhdoumi, A., & Parvizi, M. (2015). Effect of supplemental damping on seismic response of base isolated frames under near & far field accelerations. *KSCE Journal of Civil Engineering, 19*(5), 1359-1365.

FEMA-356. (2000). Prestandard and commentary for the seismic rehabilitation of buildings. *Washington, DC: SAC Joint Venture for the Federal Emergency Management Agency*.

FEMA-440. (2005). Improvement of nonlinear static seismic analysis procedures. *Redwood City*.

FEMA(P-695). (2009). P-695. Quantification of Building Seismic Performance Factors. *Federal Emergency Management Agency*.

Foti, D. (2014). On the seismic response of protected and unprotected middle-rise steel frames in far-field and near-field areas. *Shock and Vibration, 2014*.

Freeman, S., Nicoletti, J., & Tyrell, J. (1975). *Evaluations of existing buildings for seismic risk–A case study of Puget Sound Naval Shipyard, Bremerton, Washington.* Paper presented at the Proceedings of the 1st US National Conference on Earthquake Engineering.

Freeman, S. A. (1978). Prediction of response of concrete buildings to severe earthquake motion. *Special Publication, 55*, 589-606.

Freeman, S. A. (2004). Review of the development of the capacity spectrum method. *ISET Journal of Earthquake Technology, 41*(1), 1-13.

Ghobarah, A. (2001). Performance-based design in earthquake engineering: state of development. *Engineering Structures, 23*(8), 878-884.

Gong, W., & Xiong, S. (2016). Probabilistic seismic risk assessment of modified pseudo-negative stiffness control of a base-isolated building. *Structure and Infrastructure Engineering, 12*(10), 1295-1309.

Hall, J. F., Heaton, T. H., Halling, M. W., & Wald, D. J. (1995). Near-source ground motion and its effects on flexible buildings. *Earthquake spectra, 11*(4), 569-605.

Han, R., Li, Y., & van de Lindt, J. (2014). Seismic risk of base isolated non-ductile reinforced concrete buildings considering uncertainties and mainshock–aftershock sequences. *Structural Safety, 50*, 39-56.

Hanks, T. C. (1975). Strong ground motion of the San Fernando, California, earthquake: ground displacements. *Bulletin of the Seismological Society of America, 65*(1), 193-225.

Hasan, R., Xu, L., & Grierson, D. (2002). Push-over analysis for performance-based seismic design. *Computers & structures, 80*(31), 2483-2493.

Hatzigeorgiou, G. (2010). Behavior factors for nonlinear structures subjected to multiple near-fault earthquakes. *Computers & structures, 88*(5), 309-321.

Heaton, T. H., Hall, J. F., Wald, D. J., & Halling, M. W. (1995). Response of high-rise and base-isolated buildings to a hypothetical Mw 7.0 blind thrust earthquake. *Science, 267*(5195), 206.

Hedayati Dezfuli, F., & Alam, M. S. (2017). Effect of different steel-reinforced elastomeric isolators on the seismic fragility of a highway bridge. *Structural Control and Health Monitoring, 24*(2).

Heydari, M., & Mousavi, M. (2015). The Comparison of Seismic Effects of Near-field and Far-field Earthquakes on Relative Displacement of Seven-storey Concrete Building with Shear Wall. *Current World Environment, Vol. 10*(1), 0-46.

Huang, C.-T., & Chen, S.-S. (2000). Near-field characteristics and engineering implications of the 1999 Chi-Chi earthquake. *Earthquake Engineering and Engineering Sysmology, 2*(1), 23-41.

IS-456. (2000). *Plain and Reinforced Concrete-Code of Practice, Bureau of Indian Standards, Manak Bhawan, 9*.

IS-1893. (2016). *Criteria for earthquake resistant design of structures. Bureau of Indian Standards, Manak Bhawan*.

Iwan, W. (1997). Drift spectrum: measure of demand for earthquake ground motions. *Journal of Structural Engineering, 123*(4), 397-404.

Iwan, W. D. (1994). *Near-field considerations in specification of seismic design motions for structures.* Paper presented at the Proceedings of the 10th European Conference on Earthquake Engineering, Vienna, Austria.

Jamnani, H. H., Karbassi, A., & Lestuzzi, P. (2013). *Fling-step effect on the seismic behaviour of high-rise RC buildings during the Christchurch earthquake*. Paper presented at the 2013 NZSEE Conference.

Jan, T. S., Liu, M. W., & Kao, Y. C. (2004). An upper-bound pushover analysis procedure for estimating the seismic demands of high-rise buildings. *Engineering Structures, 26*(1), 117-128.

Jangid, R. (2007). Optimum lead–rubber isolation bearings for near-fault motions. *Engineering Structures, 29*(10), 2503-2513.

Jangid, R., & Datta, T. (1995). Seismic behaviour of base-isolated buildings: a state-of-the-art review. *Proceedings of the Institution of Civil Engineers. Structures and buildings, 110*(2), 186-203.

Jangid, R., & Kelly, J. (2001). Base isolation for near-fault motions. *Earthquake engineering & structural dynamics, 30*(5), 691-707.

Kalkan, E., & Kunnath, S. K. (2004). *Method of modal combinations for pushover analysis of buildings.* Paper presented at the Proc. of the 13th World Conference on Earthquake Engineering.

Kalkan, E., & Kunnath, S. K. (2006a). Adaptive modal combination procedure for nonlinear static analysis of building structures. *Journal of Structural Engineering, 132*(11), 1721-1731.

Kalkan, E., & Kunnath, S. K. (2006b). Effects of fling step and forward directivity on seismic response of buildings. *Earthquake spectra, 22*(2), 367-390.

Kalkan, E., & Kunnath, S. K. (2007). Assessment of current nonlinear static procedures for seismic evaluation of buildings. *Engineering Structures, 29*(3), 305-316.

Kelly, J. M. (1986). Aseismic base isolation: review and bibliography. *Soil Dynamics and Earthquake Engineering, 5*(4), 202-216.

Kelly, T. E., Skinner, R. I., & Robinson, W. H. (2010). *Seismic isolation for designers and structural engineers*: NICEE.

Kennedy, R. P., Cornell, C., Campbell, R., Kaplan, S., & Perla, H. (1980). Probabilistic seismic safety study of an existing nuclear power plant. *Nuclear Engineering and Design, 59*(2), 315-338.

Kikuchi, M., Black, C. J., & Aiken, I. D. (2008). On the response of yielding seismically isolated structures. *Earthquake engineering & structural dynamics, 37*(5), 659-679.

Kilar, V., & Fajfar, P. (1997). Simple push-over analysis of asymmetric buildings. *Earthquake engineering & structural dynamics, 26*(2), 233-249.

Kilar, V., & Koren, D. (2008). *Usage of simplified N2 method for analysis of base isolated structures.* Paper presented at the The 14th World Conference on Earthquake Engineering.

Kilar, V., & Koren, D. (2009). Seismic behaviour of asymmetric base isolated structures with various distributions of isolators. *Engineering Structures, 31*(4), 910-921.

Kilar, V., & Koren, D. (2010). Simplified inelastic seismic analysis of base-isolated structures using the N2 method. *Earthquake engineering & structural dynamics, 39*(9), 967-989.

Kilar, V., Petrovcic, S., Koren, D., & Šilih, S. (2011). Seismic analysis of an asymmetric fixed base and base-isolated high-rack steel structure. *Engineering Structures, 33*(12), 3471-3482.

Kircher, C. A., Whitman, R. V., & Holmes, W. T. (2006). HAZUS earthquake loss estimation methods. *Natural Hazards Review, 7*(2), 45-59.

Konstantinidis, D., & Nikfar, F. (2015). Seismic response of sliding equipment and contents in base-isolated buildings subjected to broadband ground motions. *Earthquake engineering & structural dynamics, 44*(6), 865-887.

Koren, D., & Kilar, V. (2011). The applicability of the N2 method to the estimation of torsional effects in asymmetric base-isolated buildings. *Earthquake engineering & structural dynamics, 40*(8), 867-886.

Krawinkler, H. (1996a). *A few basic concepts for performance based seismic design.* Paper presented at the Proceedings of 11th World Conference on Earthquake Engineering, Acapulco, Mexico. Paper.

Krawinkler, H. (1996b). *Pushover analysis: why, how, when, and when not to use it.* Paper presented at the Proceedings of the 65th Annual Convention of the Structural Engineers Association of California.

Krawinkler, H., & Seneviratna, G. (1998). Pros and cons of a pushover analysis of seismic performance evaluation. *Engineering Structures, 20*(4), 452-464.

Kreslin, M., & Fajfar, P. (2011). The extended N2 method taking into account higher mode effects in elevation. *Earthquake engineering & structural dynamics, 40*(14), 1571-1589.

Kunnath, S. K. (2004). Identification of modal combinations for nonlinear static analysis of building structures. *Computer-Aided Civil and Infrastructure Engineering, 19*(4), 246-259.

Kunnath, S. K., & Kalkan, E. (2004). Evaluation of seismic deformation demands using nonlinear procedures in multistorey steel and concrete moment frames. *ISET Journal of Earthquake Technology, 41*(1), 159-181.

Lee, D.-G., Hong, J.-M., & Kim, J. (2001). Vertical distribution of equivalent static loads for base isolated building structures. *Engineering Structures, 23*(10), 1293-1306.

Li, S., & Xie, L.-l. (2007). Progress and trend on near-field problems in civil engineering. *Acta Seismologica Sinica, 20*, 105-114.

Liossatou, E., & Fardis, M. N. (2016). Near-fault effects on residual displacements of RC structures. *Earthquake engineering & structural dynamics, 45*(9), 1391-1409.

Loh, C. H., Lee, Z. K., Wu, T. C., & Peng, S. Y. (2000). Ground motion characteristics of the Chi-Chi earthquake of 21 September 1999. *Earthquake engineering & structural dynamics, 29*(6), 867-897.

Mahdi, T., & Soltan, G. V. (2011). Plan irregular RC frames: comparison of pushover with nonlinear dynamic analysis.

Malhotra, P. K. (1999). Response of buildings to near-field pulse-like ground motions. *Earthquake Engineering and Structural Dynamics, 28*(11), 1309-1326.

Mansouri, I., Ghodrati Amiri, G., Hu, J. W., Khoshkalam, M., Soori, S., & Shahbazi, S. (2017). Seismic Fragility Estimates of LRB Base Isolated Frames Using Performance-Based Design. *Shock and Vibration*.

Martinelli, E., & Faella, C. (2015). Nonlinear static analyses based on either inelastic or elastic spectra with equivalent viscous damping: A parametric comparison. *Engineering Structures, 88*, 241-250.

Matsagar, V. A., & Jangid, R. (2004). Influence of isolator characteristics on the response of base-isolated structures. *Engineering Structures, 26*(12), 1735-1749.

Mavroeidis, G. P., & Papageorgiou, A. S. (2002). *Near-source strong ground motion: characteristics and design issues.* Paper presented at the Proc. of the Seventh US National Conf. on Earthquake Engineering (7NCEE), Boston, Massachusetts.

Mavroeidis, G. P., & Papageorgiou, A. S. (2003). A mathematical representation of near-fault ground motions. *Bulletin of the Seismological Society of America, 93*(3), 1099-1131.

Mavronicola, E., & Komodromos, P. (2014). On the response of base-isolated buildings using bilinear models for LRBs subjected to pulse-like ground motions: sharp vs. smooth behaviour. *Earthq. Struct, 7*(6), 1223-1240.

Mazza, F. (2015a). Nonlinear incremental analysis of fire-damaged rc base-isolated structures subjected to near-fault ground motions. *Soil Dynamics and Earthquake Engineering, 77*, 192-202.

Mazza, F., & Vulcano, A. (2009). Nonlinear response of RC framed buildings with isolation and supplemental damping at the base subjected to near-fault earthquakes. *Journal of earthquake engineering, 13*(5), 690-715.

Mazza, F., & Vulcano, A. (2010). Nonlinear dynamic response of rc framed structures subjected to near-fault ground motions. *Bulletin of Earthquake Engineering, 8*(6), 1331-1350.

Mazza, F., & Vulcano, A. (2012). Effects of near-fault ground motions on the nonlinear dynamic response of base-isolated rc framed buildings. *Earthquake engineering & structural dynamics, 41*(2), 211-232.

Mazza, M. (2015b). Effects of near-fault ground motions on the nonlinear behaviour of reinforced concrete framed buildings. *Earthquake Science, 28*(4), 285-302.

Mollaioli, F., Lucchini, A., Cheng, Y., & Monti, G. (2013). Intensity measures for the seismic response prediction of base-isolated buildings. *Bulletin of Earthquake Engineering, 11*(5), 1841-1866.

Mwafy, A., & Elnashai, A. (2001). Static pushover versus dynamic collapse analysis of RC buildings. *Engineering Structures, 23*(5), 407-424.

Naeim, F., & Kelly, J. M. (1999). *Design of seismic isolated structures: from theory to practice*: John Wiley & Sons.

Nielson, B. G., & DesRoches, R. (2007). Seismic fragility methodology for highway bridges using a component level approach. *Earthquake engineering & structural dynamics, 36*(6), 823-839.

Ordonez, D., Foti, D., & Bozzo, L. (2003). Comparative study of the inelastic response of base isolated buildings. *Earthquake engineering & structural dynamics, 32*(1), 151-164.

Osgooei, P. M., Tait, M. J., & Konstantinidis, D. (2015). Seismic Isolation of a Shear Wall Structure Using Rectangular Fiber-Reinforced Elastomeric Isolators. *Journal of Structural Engineering*, 04015116.

Ozdemir, G., & Akyuz, U. (2012). Dynamic analyses of isolated structures under bi-directional excitations of near-field ground motions. *Shock and Vibration, 19*(4), 505-513.

Padgett, J. E., Nielson, B. G., & DesRoches, R. (2008). Selection of optimal intensity measures in probabilistic seismic demand models of highway bridge portfolios. *Earthquake engineering & structural dynamics, 37*(5), 711-725.

Park, J., Towashiraporn, P., Craig, J. I., & Goodno, B. J. (2009). Seismic fragility analysis of low-rise unreinforced masonry structures. *Engineering Structures, 31*(1), 125-137.

Park, Y., Wen, Y., & Ang, A. (1986). Random vibration of hysteretic systems under bi-directional ground motions. *Earthquake engineering & structural dynamics, 14*(4), 543-557.

Perotti, F., Domaneschi, M., & De Grandis, S. (2013). The numerical computation of seismic fragility of base-isolated Nuclear Power Plants buildings. *Nuclear Engineering and Design, 262*, 189-200.

Petrovcic, S., & Kilar, V. (2015). *Modelling and analysis of seismic base-isolated masonry heritage structures.* Paper presented at the Proc. SECED 2015 Conf.: Earthquake risk and engineering towards a resilient world.

Pitilakis, K., Crowley, H., & Kaynia, A. (2014). SYNER-G: typology definition and fragility functions for physical elements at seismic risk. *Geotechnical, Geological and Earthquake Engineering, 27*.

Porter, K., Kennedy, R., & Bachman, R. (2007). Creating fragility functions for performance-based earthquake engineering. *Earthquake spectra, 23*(2), 471-489.

Poursha, M., Khoshnoudian, F., & Moghadam, A. (2009). A consecutive modal pushover procedure for estimating the seismic demands of tall buildings. *Engineering Structures, 31*(2), 591-599.

Providakis, C. (2008a). Effect of LRB isolators and supplemental viscous dampers on seismic isolated buildings under near-fault excitations. *Engineering Structures, 30*(5), 1187-1198.

Providakis, C. (2008b). Pushover analysis of base-isolated steel–concrete composite structures under near-fault excitations. *Soil Dynamics and Earthquake Engineering, 28*(4), 293-304.

Ramamoorthy, S. K., Gardoni, P., & Bracci, J. M. (2006). Probabilistic demand models and fragility curves for reinforced concrete frames. *Journal of Structural Engineering, 132*(10), 1563-1572.

Rao, P. B., & Jangid, R. (2001). Experimental study of baseisolated structures. *ISET Journal of Earthquake Technology, 38*(1), 1-15.

Reed, J. W., & Kennedy, R. P. (1994). Methodology for developing seismic fragilities. *Final Report TR-103959, EPRI*.

Ryan, K. L., & Chopra, A. K. (2004). Estimation of seismic demands on isolators based on nonlinear analysis. *Journal of Structural Engineering, 130*(3), 392-402.

Ryan, K. L., & Chopra, A. K. (2006). Estimating seismic demands for isolation bearings with building overturning effects. *Journal of Structural Engineering, 132*(7), 1118-1128.

Saiidi, M., & Sozen, M. A. (1981). Simple nonlinear seismic analysis of R/C structures. *Journal of the Structural Division, 107*(5), 937-953.

SAP. (2000). Integrated software for structural analysis and design. *Computers and Structures*.

Sasani, M., & Bertero, V. (2000). *Importance of severe pulse-type ground motions in performance-based engineering: historical and critical review.* Paper presented at the 12th world conference on earthquake engineering.

SEAONC. (1986). *Tentative Seismic Isolation Design Requirements*: Structural Engineers Association Of Northern California. Seismology Committee. Base Isolation Subcommittee.

SeismoArtif. (2016). Computer program for generation of artificial earthquake accelerograms. *Siesmosignal*.

Shahi, R., Lam, N. T., Gad, E. F., Saifullah, I., Wilson, J. L., & Watson, K. (2014). Choice of Intensity Measure in Incremental Dynamic Analysis.

Sharma, A., & Jangid, R. (2009). Behaviour of Base-Isolated Structures with High Initial Isolator Stiffness. *World Academy of Science, Engineering and Technology, International Journal of Civil, Environmental, Structural, Construction and Architectural Engineering, 3*(2), 49-54.

Shome, N. (1999). *Probabilistic seismic demand analysis of nonlinear structures*: Stanford University.

Somerville, P., & Graves, R. (1993). Conditions that give rise to unusually large long period ground motions. *The Structural Design of Tall and Special Buildings, 2*(3), 211-232.

Somerville, P. G. (2002). *Characterizing near fault ground motion for the design and evaluation of bridges.* Paper presented at the Third National Conference and Workshop on Bridges and Highways. Portland, Oregon.

Somerville, P. G. (2005). *Engineering characterization of near fault ground motions.* Paper presented at the Proc., NZSEE 2005 Conf.

Somerville, P. G., Smith, N. F., Graves, R. W., & Abrahamson, N. A. (1997). Modification of empirical strong ground motion attenuation relations to include the amplitude and duration effects of rupture directivity. *Seismological Research Letters, 68*(1), 199-222.

Takeda, T., Sozen, M. A., & Nielsen, N. N. (1970). Reinforced concrete response to simulated earthquakes. *Journal of the Structural Division, 96*(12), 2557-2573.

Tavakoli, H., Naghavi, F., & Goltabar, A. (2014). Dynamic responses of the base-fixed and isolated building frames under far-and near-fault earthquakes. *Arabian Journal for Science and Engineering, 39*(4), 2573-2585.

Tsiavos, A., Mackie, K. R., Vassiliou, M. F., & Stojadinović, B. (2017). Dynamics of inelastic base-isolated structures subjected to recorded ground motions. *Bulletin of Earthquake Engineering, 15*(4), 1807-1830.

Vamvatsikos, D., & Cornell, C. A. (2002). Incremental dynamic analysis. *Earthquake engineering & structural dynamics, 31*(3), 491-514.

Vamvatsikos, D., & Cornell, C. A. (2004). Applied incremental dynamic analysis. *Earthquake spectra, 20*(2), 523-553.

Ventura, C. E., Archila, M., Bebamzadeh, A., & Liam Finn, W. (2011). Large coseismic displacements and tall buildings. *The Structural Design of Tall and Special Buildings, 20*(S1), 85-99.

Warn, G. P., & Ryan, K. L. (2012). A review of seismic isolation for buildings: historical development and research needs. *Buildings, 2*(3), 300-325.

Wei, T., Zhao, F.-x., & Zhang, Y.-s. (2006). Characteristics of near-fault ground motion containing velocity pulses. *Acta Seismologica Sinica, 19*(6), 677-686.

Wen, Y.-K. (1976). Method for random vibration of hysteretic systems. *Journal of the engineering mechanics division, 102*(2), 249-263.

Wen, Y., Ellingwood, B. R., & Bracci, J. M. (2004). Vulnerability function framework for consequence-based engineering. *MAE Center Report 04-04*.

Xie, L., Xu, L., & Adrian, R.-M. (2005). Representation of near-fault pulse-type ground motions. *Earthquake Engineering and Engineering Vibration, 4*(2), 191-199.

Yadav, K. K., & Gupta, V. K. (2017). Near-fault fling-step ground motions: Characteristics and simulation. *Soil Dynamics and Earthquake Engineering, 101*, 90-104.

Yang, D., Pan, J., & Li, G. (2010). Interstorey drift ratio of building structures subjected to near-fault ground motions based on generalized drift spectral analysis. *Soil Dynamics and Earthquake Engineering, 30*(11), 1182-1197.

Yang, D., & Zhao, Y. (2010). Effects of rupture forward directivity and fling step of near-fault ground motions on seismic performance of base-isolated building structure. *Acta Seismologica Sinica, 5*, 007.

York, K., & Ryan, K. L. (2008). Distribution of lateral forces in base-isolated buildings considering isolation system nonlinearity. *Journal of earthquake engineering, 12*(7), 1185-1204.

Zamora, M., & Riddell, R. (2011). Elastic and inelastic response spectra considering near-fault effects. *Journal of earthquake engineering, 15*(5), 775-808.

Zhang, J., & Huo, Y. (2009). Evaluating effectiveness and optimum design of isolation devices for highway bridges using the fragility function method. *Engineering Structures, 31*(8), 1648-1660.

BIO-DATA

The author is a regular PhD Research Scholar at Malaviya National Institute of Technology Jaipur, Jaipur (Rajasthan) since 2015. He obtained his Bachelor's Degree in Civil Engineering (B.Tech) from D.A.V Institute of Engineering and Technology (DAVIET), Jalandhar (Punjab) in 2011. He completed his Master's Degree (M.Tech) in Structural and Construction Engineering from Dr. B. R. Ambedkar National Institute of Technology, Jalandhar (Punjab) in 2013. His area of specialization is "Earthquake Engineering".

Following is the list of the publications from his Doctoral work

List of publications

Journals

1. Bhandari M, Bharti S D, Shrimali M K, Datta T K. The Numerical Study of Base-Isolated Buildings Under Near-Field and Far-Field Earthquakes. *Journal of Earthquake Engineering*. 22(6), 2017:989-1007. **(Published)**
2. Bhandari M, Bharti S D, Shrimali M K, Datta T K. Applicability of Capacity Spectrum Method for Base-Isolated Building Frames at different Performance Points. *Journal of Earthquake Engineering*. **(Accepted)**
3. Bhandari M, Bharti S D, Shrimali M K, Datta T K. Assessment of Proposed Lateral Load Patterns in Pushover Analysis for Base-Isolated Frames. *Engineering Structures. 175, 531-548.* **(Published)**
4. Bhandari M, Bharti S, Shrimali M K, Datta T K. Seismic Fragility Analysis of Base-Isolated Building Frame Excited by Near and Far Field Earthquakes. *Journal of Performance of constructed Facilities (ASCE).* **(Accepted)**

International Conferences

1. M Bhandari, S D Bharti and M K Shrimali (2017), "Behavior of Base Isolated Buildings Subjected to Near Field Earthquakes", *16th World Conference on Earthquake, 16WCEE 2017 (*9-13 January2017) *Santiago, CHILE.*
2. Bhandari M, Bharti S D, Shrimali M K, Datta T K. Performance of base isolated building for extreme earthquakes. *Structural Engineering Convention (SEC-2016). Chennai, INDIA 2016.*

3. Bhandari M, Bharti S D, Shrimali M K, Datta T K. Pushover analysis of base isolated building. 2nd *International Conference on Advances in Concrete, Structural, and Geotechnical Engineering (ACSGE-2018). Pilani, INDIA.*
4. Bhandari M, Bharti S D, Shrimali M K, Datta T K. *Assessment of seismic performance of base isolated building frame under near and far field earthquakes using fragility curves*. The 16th Symposium on Earthquake Engineering, to be held on December 20-22, 2018, IIT Roorkee, India.